Geothermal energy piles design, sizing and modelling

Jevgeni Fadejev

Aalto University

Aalto University publication series
Doctoral Theses 228/2025

Geothermal energy piles design, sizing and modelling

Jevgeni Fadejev

A doctoral thesis completed for the degree of Doctor of Science (Technology) to be defended, with the permission of the Aalto University School of Engineering, at a public examination held at the lecture hall R001/H304 of the school on 20 November 2025 at 12:00.

Aalto University
School of Engineering
Department of Civil Engineering

Supervising professor
Prof. Heidi Salonen, Aalto University, Finland

Thesis advisors
Prof. Jarek Kurnitski, Aalto University, Finland
Prof. Ergo Pikas, Tallinn University of Technology, Estonia
Prof. Andrea Ferrantelli, Tallinn University of Technology, Estonia

Preliminary examiners
Prof. Alireza Afshari, Aalborg University, Denmark
Prof. Enrico Fabrizio, Politecnico di Torino, Italy

Opponents
Prof. Alireza Afshari, Aalborg University, Denmark
Prof. Enrico Fabrizio, Politecnico di Torino, Italy

Aalto University publication series
Doctoral Theses 228/2025

ISBN 978-952-64-2829-1 (soft cover)
ISBN 978-952-64-2828-4 (PDF)
ISSN 1799-4934 (printed)
ISSN 1799-4942 (PDF)

https://urn.fi/URN:ISBN:978-952-64-2828-4

Unigrafia Oy
Helsinki 2025

Aalto University

ABSTRACT

Author Jevgeni Fadejev

Name of the doctoral thesis Geothermal energy piles design, sizing and modelling

Article-based thesis

Number of pages 131

Keywords Activated pile foundations; Seasonal Thermal Storage; GSHP; GEP sizing guide

This thesis addresses the challenges associated with the design, sizing, and modelling of geothermal energy piles (GEPs), the lack of validated methods for their use as a renewable heating and cooling solution for nearly zero-energy buildings (NZEBs). GEPs provide both load-bearing and ground heat exchange functions, making them well-suited for use with ground source heat pumps (GSHPs). However, their designs have often relied on assumptions originating from borehole heat exchangers (BHEs), which differ considerably from GEPs in geometry, thermal boundary conditions, and placement, as the layout of GEPs is dictated by the building's foundation plan.

This research aimed to develop and validate a modelling method for assessing the performance of GEPs with thermal storage coupled with a detailed whole building simulation model for a parametric study. The method was developed in IDA ICE and validated using COMSOL Multiphysics and real-world measurement data. The research methodology combined a systematic literature review, model development, validation, and demonstration of the modelling method's performance using an as-built calibrated model with measured performance data from a commercial NZEB in Finland for energy analysis. A parametric study was conducted to support the development of a tabulated GEPs sizing method for early-stage design, considering factors such as heat pump sizing power, pile spacing and depth, soil type, and the presence of a thermal storage.

The findings confirmed that conventional BHE-based modelling approaches are unsuitable for GEP systems due to major differences in thermal boundary conditions, particularly the influence of building floor slabs on ground temperature distribution. The validated GEP modelling method, implemented in IDA ICE and verified with COMSOL simulations, accurately captured these effects and showed strong agreement with measured data from a monitored NZEB in Finland. The model calibration procedure revealed unexpected plant operation due to improper control algorithms, highlighting the importance of monitoring and logging systems in buildings with unconventional plant designs to ensure proper operation and maintain long-term efficiency. According to parametric study results, seasonal thermal storage demonstrated notable improvements in energy efficiency and enabled a reduction in required pile length by over 50% in a specific case. A tabulated GEP sizing guide was developed to support early-stage design, enabling engineers to estimate system configurations effectively without relying on complex simulation tools. The method demonstrated in this thesis can be extended to any climate region and building type.

TALLINN UNIVERSITY OF TECHNOLOGY
DOCTORAL THESIS
81/2025

Geothermal energy piles design, sizing and modelling

JEVGENI FADEJEV

TALLINN UNIVERSITY OF TECHNOLOGY
School of Engineering
Department of Civil Engineering and Architecture

This dissertation was accepted for the defense of the degree of Doctor of Philosophy in Engineering on October 27th, 2025.

Supervisor:
Prof. Jarek Kurnitski
Department of Civil Engineering and Architecture
Tallinn University of Technology
Tallinn, Estonia

Co-Supervisors:
Prof. Ergo Pikas
Department of Civil Engineering and Architecture
Tallinn University of Technology
Tallinn, Estonia

Prof. Heidi Salonen
Department of Civil Engineering
Aalto University
Espoo, Finland

Prof. Andrea Ferrantelli
Department of Civil Engineering and Architecture
Tallinn University of Technology
Tallinn, Estonia
Department of Energy and Mechanical Engineering
Aalto University
Espoo, Finland

Opponents:
Prof. Alireza Afshari
Department of the Built Environment
Aalborg University, Denmark

Prof. Enrico Fabrizio
Department of Energy of Politecnico di Torino
Politecnico di Torino, Italy

Defense of the thesis: 20.11.2025, Espoo

Declaration:
Hereby I declare that this doctoral thesis, my original investigation and achievement, submitted for the doctoral degree at Tallinn University of Technology and at Aalto University School of Engineering, has not been submitted for doctoral or equivalent academic degree.

Jevgeni Fadejev:

signature

European Union
European Regional
Development Fund

Investing
in your future

ISSN 2585-6898(publication)
ISSN 2585-6901(PDF)

TALLINNA TEHNIKAÜLIKOOL
DOKTORITÖÖ
81/2025

Energiavaiade projekteerimine, dimensioneerimine ja modelleerimine

JEVGENI FADEJEV

Kokkuvõtte

Käesolev töö käsitleb energiavaiade projekteerimise, dimensioneerimise ja modelleerimisega seotud väljakutseid adresseerides valideeritud meetodite puudumist nende kasutamiseks kütte- ja jahutuslahendusena liginullenergiahoonetes. Energiavaiad täidavad nii kande- kui ka maasoojusvaheti funktsiooni, mis teeb neist hästi sobiva lahenduse maasoojuspumpadega kasutamiseks. Siiski on nende projekteerimisel sageli tuginenud eeldustele, mis pärinevad puuraugu soojusvahetitest, mis erinevad energiavaiadest oluliselt nii geomeetria, soojuslevi ääretingimuste kui ka paigutuse poolest, kuna energiavaiade asukohad määratakse hoone vundamendiplaani järgi.

Käesoleva uurimistöö eesmärk oli välja töötada ja valideerida modelleerimismeetod hoajalise soojussalvestusega energiavaiade jõudluse hindamiseks, ühendades selle detailse kogu hoone simulatsioonimudeliga parameetrilise analüüsi läbiviimiseks. Meetod töötati välja ja valideeriti simulatsioonitarkvarade IDA ICE ja COMSOL Multiphysics abil, kasutades tegelikke mõõtmisandmeid. Uurimismetoodika koosnes süstemaatilise kirjanduse ülevaatest, mudeli arendamisest, valideerimisest ning modelleerimismeetodi jõudluse demonstreerimisest, kasutades tegeliku hoone järgi kalibreeritud mudelit ja Soomes asuva liginullenergiahoone mõõtmisandmeid energiakasutuse analüüsimiseks. Parameetriline analüüs viidi läbi, et võimaldada tabelipõhise energiavaiade dimensioonimismeetodi väljatöötamist hoone projekteerimise varases etapis, arvestades selliseid tegureid nagu soojuspumba võimsus, vaiade vahekaugus ja sügavus, pinnase tüüp ning hooajalsie soojussalvestuse olemasolu.

Tulemused kinnitasid, et traditsioonilistel puuraugu soojusvahetitel põhinevad modelleerimislähenemised ei sobi energiavaiasüsteemide jaoks suurte erinevuste tõttu soojuslevi ääretingimustes, eriti seoses hoone põrandaplaadi mõjuga pinnase temperatuuri jaotumisele. Valideeritud energiavaiade modelleerimise meetod, mis implementeeriti simulatsioonitarkvaras IDA ICE ja verifitseeriti COMSOLi simulatsioonidega, kirjeldas neid mõjusid täpselt ning näitas tugevat vastavust Soomes välja ehitatud liginullenergiahoone mõõtmisandmetega. Mudeli kalibreerimine paljastas ootamatu süsteemi töö, mis oli põhjustatud ebaõigetest juhtimisalgoritmidest, rõhutades seeläbi seire- ja logimissüsteemide tähtsust ebastandardsete tehnosüsteemilahendustega hoonetes, et tagada korrektne toimimine ja pikaajaline energiatõhusus. Parameetrilise analüüsi tulemuste kohaselt parandas hooajaline soojussalvestus märkimisväärselt

energiatõhusust ning võimaldas konkreetsel juhul vähendada vajalikku vaiapikkust üle 50%. Tabelipõhine energiavaiade dimensioonimisjuhend töötati välja toetamaks projekteerimise varajasi etappe, võimaldades inseneridel hinnata süsteemi konfiguratsiooni tõhusalt ka ilma keerukaid simulatsioonitarkvarasid kasutamata. Käesolevas töös demonstreeritud meetodit saab rakendada igas kliimas ja erinevat tüüpi hoonete puhul.

Acknowledgements

I would like to express my deepest gratitude to all those who supported me and provided encouragement throughout the long journey of my doctoral studies.

My greatest thanks go to my wise thesis advisor, Professor Jarek Kurnitski, for his immense patience, constant support in both my work and life, the vast experience I gained through working with him, the opportunities he opened up for me in academics, and his trust and sincerity.

I would also like to thank my thesis advisor, Professor Ergo Pikas, for motivating me, providing sound advice, and actively supporting me in the writing and revising of my doctoral thesis. I would also like to express my gratitude to my supervising professors, Heidi Salonen and Jari Puttonen, whose support made my studies at Aalto University possible.

I am also immensely grateful to my good friend and colleague, Anti Hamburg, for introducing me to the Tallinn University of Technology family and inspiring me to pursue an academic career.

I extend my thanks also to my colleagues and friends from the Nearly Zero Energy Buildings Research Group at the Tallinn University of Technology – Professor Targo Kalamees, Professor Martin Thalfeldt, Raimo Simson, Alo Mikola, Andrea Ferrantelli, Martin Kiil, Tuule Mall Parts, Endrik Arumägi, Jaanus Hallik, Karl-Villem Võsa, Paul Klõšeiko, Laura Kadaru, Villu Kukk, Francesco De Luca, Simo Ilomets, Mikk Maivel, Ülar Palmiste, Erkki Seinre, Kristo Kalbe, and Ene Pähn. I am deeply grateful to all of you for your support and willingness to share your expertise.

I am sincerely grateful also to Mika Voulle and the EQUA Simulations OY team for their readiness to answer IDA ICE modelling questions.

I would like to give special thanks to my mentor and wonderful colleague, Teet Tark, for the vast engineering experience I gained through my collaboration with Hevac OÜ, for the constant support and consultations related to complex HVAC matters and for Teet's sincerity and honesty. My gratitude also goes to the entire Hevac OÜ team (Albert Rodin, Ulvi Kundla, Piret Raud, Kaia Hannus) for their warm reception and the wonderful working atmosphere during my time with their organization.

I also want to thank my closest friends, Vitali Davidenko and Vitali Romanov—brothers, thank you for your support during difficult times and for believing in me!

Finally, I want to sincerely thank my family for their endless love, support, patience, and wise advice, especially my mom and dad, Irina Fadejeva and Alexandre Fadeev; my brother, Deniss Fadejev; my faithful and loving wife, Julia Fadejeva; and my amazing children, Kolya and Misha. I succeeded only with your help—thank you!

My research was supported by the Estonian Centre of Excellence in Zero Energy and Resource Efficient Smart Buildings and Districts, ZEBE, grant 2014-2020.4.01.15-0016 funded by the European Regional Development Fund; Estonian Research Council with Institutional research funding grant IUT1–15; Estonian Science Foundation under the Grant MTT74; European Commission under the Grant VIE647.

Helsinki, Finland, 13 April 2025,

Jevgeni Fadejev

Contents

List of Abbreviations

AHU	Air handling unit
BHE	Borehole heat exchanger
BMS	Building monitoring system
COP	Coefficient of performance
DAT	Design ambient temperature [°C]
DST	Duct ground heat storage model
DHW	Domestic hot water
EU	European union
EPBD	Energy performance of building directive
EPV	Energy performance value
FDM	Finite Difference Model
FEM	Finite Element Method
GSHP	Ground-source heat pump
GHE	Ground heat exchanger
GEP	Geothermal energy pile
NZEB	Nearly zero-energy building
NTU	Number of transfer units
PHC	Prestressed high-strength concrete
SCOP	Seasonal coefficient of performance
SFP	Specific fan power [kW/(m^3/s)]
TRY	Test Reference Year
TRT	Thermal response test
NMBE	Normalized Mean Bias Error (ASHRAE Guideline 14 parameter)
CV(RMSE)	Coefficient of Variation of the Root Mean Squared Error

List of Symbols

C_p	Specific heat [W/(m K)]
d_b	Borehole diameter [m]
d_p	Pipe diameter [m]
D	Demand covered by the heat pump
E	Annual heat demand [kWh]
g	Dimensionless temperature response
h	Convection heat transfer coefficient [W/(m² K)]
H	Borehole length [m]
k	Thermal conductivity [W/(m K)]
k_g	Grout thermal conductivity [W/(m K)]
L	Energy piles length [m]
m	Mass flow [kg/s]
n	Number of U-pipes
Pr	Prandtl number
r_b	Borehole radius [m]
Rb	Pile thermal resistance [(m K)/W]
t_b	Temperature at borehole wall [°C]
T	Temperature [°C]
T_0	Far field (initial soil) temperature [°C]
T_f	Fluid outlet temperature [°C]
Ts	Ground surface temperature [°C]
T_{inlet}	Brine inlet temperature [°C]

T_{outlet}	Brine outlet temperature [°C]
V_{in}	Inlet velocity [m/s]
q	Heat flux along borehole length [W/m]
Q	Building design heat load [kW]
Q_{evap}	Evaporator load [W]
Q_{cond}	Condenser load [W]
ΔT	Temperature difference [°C]

List of Greek Symbols

a	Soil diffusivity [m^2/s]
γ	Euler constant
μ	Dynamic viscosity [Pa s]
λ	Thermal conductivity [W/m K]
ρ	Density [kg/m^3]

List of Publications

This doctoral dissertation includes details from the following publications, which are referenced in the text by number.

1. Fadejev J, Simson R, Kurnitski J, Haghighat F. A review on energy piles design, sizing and modelling. *Energy*, Volume 122, pp.390-407, January 2017.

2. Fadejev J, Kurnitski J. Geothermal energy piles and boreholes design with heat pump in a whole building simulation software. *Energy and Buildings*, Volume 106, pp.23-34, June 2015.

3. Ferrantelli A, Fadejev J, Kurnitski J. Energy pile field simulation in large buildings: Validation of surface boundary assumptions. *Energies*, Volume 12, Art.No. 770, pp.1-20, February 2019.

4. Fadejev J, Simson R, Kesti J, Kurnitski J. Measured and simulated energy performance of OLK NZEB with heat pump and energy piles in Hämeenlinna. *E3S Web of Conferences, NSB 2020 – 12th Nordic Symposium on Building Physics*, Volume 172, Art.No. 16012, pp.1-11, June 2020.

5. Ferrantelli A, Fadejev J, Kurnitski J. A tabulated sizing method for the early stage design of geothermal energy piles including thermal storage. *Energy and Buildings*, Volume 223, Art.No. 110178, pp.1-16, June 2020.

Author's Contribution

Publication 1: A review on energy piles design, sizing and modelling

The author of this thesis was responsible for the literature review, preparation of tables and figures, the structuring of the manuscript, and the writing of the final manuscript under the supervision of Prof. Jarek Kurnitski and Prof. Fariborz Haghighat.

Publication 2: Geothermal energy piles and boreholes design with heat pump in a whole building simulation software

The author of this thesis was responsible for a detailed modelling of a geothermal heat pump plant with energy piles using IDA ICE, numerical simulations, the analysis of results, and the writing of the final manuscript under the supervision of Prof. Jarek Kurnitski.

Publication 3: Energy pile field simulation in large buildings: Validation of surface boundary assumptions

The author of this thesis was responsible for modelling and simulations using IDA ICE, validation methods and the analysis of COMSOL results in collaboration with DSc. Andrea Ferrantelli, and the writing of the final manuscript with collaboration with DSc. Andrea Ferrantelli under the supervision of Prof. Jarek Kurnitski.

Publication 4: Measured and simulated energy performance of OLK NZEB with heat pump and energy piles in Hämeenlinna.

The author of this thesis was responsible for the analysis and processing of measurement data for input to IDA ICE, numerical simulations using the measurement data, the comparison of measured performance with simulated performance, the analysis of results and validation, and the writing of the final manuscript in collaboration with Ph.D. Raimo Simson under the supervision of Prof. Jarek Kurnitski.

Publication 5: A tabulated sizing method for the early stage design of geothermal energy piles including thermal storage.

The author of this thesis was responsible for the modelling of the benchmark IDA ICE model based on input files, the processing of input files and their coupling with the benchmark model, numerical simulations, the analysis of results, the preparation of tables and figures, the preparation of a GEP sizing

method for early design stages, and the writing of the final manuscript in collaboration with DSc. Andrea Ferrantelli under the supervision of Prof. Jarek Kurnitski.

1. Introduction

1.1 Research background and gaps

Building stock accounts for approximately 43% of total final energy consumption [1] and 36% of greenhouse gas emissions in the EU [2]. The EU's 2030 climate and energy framework [3] targeted an improvement in energy efficiency by 32.5%, an increase in the share of renewable energy by 32%, and a reduction in greenhouse gas emissions by at least 40% below 1990 levels. The recast European Parliament directive 2010/31/EU [4] on the energy performance of buildings (EPBD) required all new buildings constructed after January 2021 to comply with national requirements for nearly zero-energy buildings (NZEB). Compliance with NZEB requirements assumes the wide availability and use of renewable energy sources. This ambition demands validated modelling and simulation of and design methods for heating and cooling systems using renewable energy sources.

A widely used renewable energy source is geothermal energy, which can be harnessed using a ground-source heat pump (GSHP) and a ground heat exchanger (GHE). A most recent review of the global usage of geothermal energy [5] revealed that the installed capacity of GSHPs worldwide grew by 69.8% from 2015 to 2020, at an annual compound growth rate of 11.7%, and are being used in at least 54 different countries. GHEs are typically classified by their installation method, e.g., horizontal or vertical installation. A common vertical GHE solution is a borehole heat exchanger (BHE) installed individually or in a group to form a BHE field [6].

More than 40 years ago, the use of building pile foundations as GHEs was introduced in Austria [7]. Such GHEs eventually came to be known as geothermal energy piles (GEPs). Today, the popularity of GEPs is still growing. They are considered cost-effective because they combine structural load-bearing and thermal energy transfer in a single structure. GEPs have also become an important research topic due to the complexity of their thermal behavior. The structural foundation plan with its piling specifications typically determines the installation layout of the GEPs, and this unfortunately often leads to thermal interference between closely located GEPs. In ground heat extraction mode (the building's heating season), the temperature of the soil surrounding the GEPs decreases relative to that of the ground, pile, and circulating fluid, while in heat rejection mode (the building's cooling season) it increases. Unbalanced heat extraction and rejection in GEPs can significantly decrease the long-term energy

performance of the designed system. Seasonal thermal storage must, therefore, be considered in the modelling and designing of GEPs for long-term stable operation.

It is often assumed that GEPs operate under conditions like those under which BHEs operate. Boundary conditions are, however, different: while BHEs are directly exposed to outdoor climate conditions and solar radiation, the building's floor-on-ground structure is the boundary surface for GEPs. Heat loss through the building floor warms the ground in cold climates, producing a thermal storage effect, which can enhance the thermal performance of GEPs. Given this fact and the effect of such variables as the thermal properties of the ground, grout, pipe, and fluid, temperature boundary conditions, different possible GEP configurations, the distance between piles, and pile length, the design and optimal sizing of GEPs and/or GSHPs (systems with GEPs) require dynamic numerical modelling. Unfortunately, there is not currently a validated method for determining the optimal size of a GEP/GSHP system that takes into account the thermal storage effect.

1.2 Research aim, objectives, and questions

The primary aim of this thesis consists of two parts:

1. to identify and justify the need for the research undertaken and develop and validate a modelling method for assessing the performance of geothermal energy piles with thermal storage coupled with a detailed whole building simulation model for a parametric study;
2. to demonstrate the accuracy and utility of the proposed geothermal energy pile modelling method and use this model to propose a tabulated GEPs sizing method that can be used in the early stages of design.

This thesis consists of a descriptive (theoretical) part and a prescriptive (practical) part. The descriptive part focuses first on the identification of and justification for the development of the modelling method for GEPs with thermal storage, relying on a systematic literature review (Publication 1) and a comparison of BHE and the proposed modelling method for GEPs (Publication 2). The focus then shifts to the development and validation of the proposed modelling method for GEPs with thermal storage coupled with a detailed whole-building simulation model for a parametric study (Publication 3). The prescriptive part first demonstrates the utility and accuracy of the proposed GEPs modelling method using a Finnish case study (Publication 4). This part ends with a parametric study of GEPs and the proposal of a tabulated GEPs sizing method for use in the early stages of design by building engineers when assessing the feasibility of the use of GEP technology as a renewable energy alternative (Publication 5).

The following measurable objectives were defined as the criteria for meeting the abovementioned aims and evaluating the success of the research:

- identification of the need for GEPs design, modelling, and sizing methods, based on a systematic literature review (Publication 1);

- justification of the need for the GEP modelling method on the basis of a comparison of BHE with the proposed GEP method taking into account the differences in ground surface boundary conditions (Publication 2);
- further development and validation of the proposed GEP modelling method using the IDA-ICE borehole model and measurement data for the GEPs using the FEM modelling environment COMSOL (Publication 3);
- demonstration of the utility of the developed GEP modelling method using a case study of its application to NZEB in Finland with accuracy gauged against the as-built calibrated model using 1-hour time step measurement data (Publication 4);
- proposal of a tabulated GEP sizing method that can be used in the early stages of design with input parameters including thermal storage values, pile spacing, pile length, and ground thermal conductivity (Publication 5).

The following research questions were posed to operationalize and achieve the main research aim and five related objectives:

- What are the main concepts, approaches, and methods involved in the design, modelling, and sizing of GEPs?
- What are the key differences between BHE and GEP modelling?
- What are the variables required for GEP modelling, how are they related, and how are they validated?
- How useful and accurate is the proposed GEP modelling method when applied to the design of NZEB in Finland, and what are the main lessons learned?
- How can the work of engineers be facilitated in the early stages of design when GEP systems are being sized?

1.3 Research scope, approach, and methods

This dissertation, based on five publications, is focused on the modelling, sizing, and design of Geothermal Energy Piles (GEPs). GEP technology harnesses renewable solar energy stored in the ground. This research can contribute to achieving EPBD targets for reducing CO2 emissions from the heating and cooling of buildings.

Publication 1, the systematic literature review, showed that GEPs are often misinterpreted as BHEs, leading to the over- or undersizing of GEP systems. The paper looked at typical schemes for building geothermal energy systems and considered different BHE/GEP configurations and models, expected performance, software applications and capabilities, and available design guidelines. It also looked at available modelling and simulation environments suitable for the designing of GEPs.

Publication 2 demonstrated a significant difference in GEP performance when using the proposed GEP modelling methods instead of BHE methods when there are variations in ground surface boundary conditions. Long-term simulation results showed that the natural thermal storage effect due to heat losses through the floor structure provided a more stable energy yield for GEPs

than the BHE field-based model. This finding highlighted the need for a dedicated GEP modelling method.

Publication 3 validated the proposed GEP modelling method using the IDA ICE borehole model (Publication 2). For the validation, GEP data for 20 energy piles was analyzed in the Finite Element Method (FEM) modelling environment COMSOL Multiphysics. Measurement data and modelled results were well-aligned. The same measurement data was also compared with refined IDA ICE borehole model results, which also showed a good agreement.

Publication 4 quantified the performance of the GEP modelling method developed by validating the operation of a Nearly Zero-Energy Building (NZEB) over a one-year period. A NZEB was designed in Finland using the sizing results derived using the method developed in this thesis. The paper detailed the model calibration procedure using 1-hour timestep measurement data. Modelling results agreed with the measurement data and highlighted the need to develop a building performance monitoring system.

Publication 5 proposed a new tabulated GEP sizing method that could be used in the early stages of design. It is expected to facilitate the work of engineers in the early stages of designing GSHP systems with GEPs for commercial hall-type buildings in countries with cold climates, such as Finland. The application of this method could, in fact, be extended to the design of any building type in any climate.

To operationalize and achieve the main research aim and related objectives and answer the questions posed, the research for this thesis was divided into the following four methodology phases:

1. **Identification and justification of the need for the research (Publication 1 and 2):** This phase was covered in Publication 1 and 2. It included the systematic literature review on GEP modelling methods, their application and design, and system sizing. Further justification was provided in Publication 2, which demonstrated a significant difference in the modelled performance of BHE and GEPs due to the difference in ground surface boundary conditions. The following research methods were applied in this phase:

    - A scientific literature review;
    - A study of design standards and guidelines;
    - The collection and processing of measurement data;
    - Dynamic simulations and numerical modelling in IDA-ICE.

2. **Development and validation of a GEP modelling method (Publication 3):** Publication 3 focused on the validation of the proposed GEP modelling method using the IDA-ICE borehole model and GEP measurement data in COMSOL Multiphysics using FEM, and it showed that there

was good agreement with a refined IDA ICE borehole model. The following methods were applied:

- Collection, processing, and analysis of measurement data;
- Dynamic simulations and numerical modelling in IDA ICE and COMSOL Multiphysics.

3. **Demonstration and evaluation of the utility and accuracy of the GEP method (Publication 4):** Publication 4 reported on the performance of the developed GEP modelling method using measurement data for NZEBs over the course of a year (Publication 4), and it also showed that there was good agreement. The following two methods were applied in this phase:
    - The collection and processing of measurement data;
    - Dynamic simulations and numerical modelling in IDA ICE.

4. **Proposal of a tabulated GEP sizing method (Publication 5):** Publication 5 focused on a GEP parametric study and proposed a GEP sizing guide for use in the early stages of design. The following three methods were applied:

    - Dynamic simulations and numerical modelling in IDA ICE;
    - Parametric study and sensitivity analysis;
    - Preparation of a sizing guide.

Table 1 summarizes the knowledge gap, main aim, objectives, research questions, and research methods and aligns them with the main outcomes and publications.

Table 1. Summary of thesis structure.

Research gap	Research Aims	Research Objective	Research Question	Methods	Outcomes and Publications
Modelling, design, and sizing of GEPs	(1) Research gap identification and justification; detailed modelling method for GEPs	Identification of need for GEP modelling	What are the main concepts, approaches, and methods involved in the modelling, design, and sizing of GEPs?	Systematic literature review, study of design standards and guidelines	Research Gap and Aim (Publication 1)
		Justification of need	What are the key differences between the modelling of BHEs and GEPs?	Numerical simulations in IDA ICE	Justification of Research Gap (Publication 2)
		Proposed validation of modelling method	What are the variables required for GEP modelling, how are they related, and how are they validated?	Numerical simulations in COMSOL and IDA ICE using measurement data	Validated Method (Publication 2 and 3)
	(2) Demonstration of the accuracy and utility through a case study; parametric study; sizing guide for GEPs	Demonstration of the utility of modelling method	How useful and accurate is the proposed GEP modelling method when applied to the design of NZEB in Finland, and what are the main lessons learned?	Numerical simulations in IDA ICE using measurement data and a calibrated model	Demonstration (Publication 4)
		Development of a sizing method that can be used in the early stages of design	How can the work of engineers be facilitated in the early stages of design when GEP systems are being sized?	Parametric study based on results of IDA ICE numerical simulations	Sizing guide (Publication 5)

1.4 Theoretical and practical novelty

The novelty of this research rests on the following:

- **The Systematic Literature Review on GEPs and BHEs:** The research provides a comprehensive and systematic literature review that differentiates geothermal energy piles (GEPs) from borehole heat exchangers (BHEs). This review addresses misconceptions and highlights the unique characteristics and performance metrics of GEPs when compared with BHEs.

- **The Comparison of Software Tools:** The research compares the modelling functionalities of different simulation software tools used for modelling GEPs. This comparison provides insights into the suitability of various tools for specific applications and underscores the importance of selecting the tool that would yield the most accurate simulations.

- **The Validated Modelling Method:** The development and validation of a novel method for modelling GEPs with thermal storage, coupled with a detailed whole-building simulation model, represents a significant advancement. This method takes into account specific boundary conditions and thermal storage effects unique to GEPs, both often overlooked in existing models.

- **The Long-term Performance Analysis:** The research introduces long-term (20-year) performance simulations that incorporate detailed thermal storage modelling. This long-term analysis is crucial for understanding the sustainability and efficiency of GEPs systems over time, a relatively unexplored topic in existing literature.

- **The Boundary Condition Analysis:** The investigation into the impact of different boundary conditions on numerical estimates for GEP performance adds a new dimension to the theoretical understanding of geothermal systems. The findings demonstrate that simplified boundary condition models can provide sufficient accuracy, challenging the need for more complex multiregional models.

This research has the following practical utility:

- **Practical Validation with Real-World Data:** The research validates the proposed method for modelling GEPs using real-world data from a nearly zero-energy building (NZEB) in Finland. This practical validation bridges the gap between theoretical models and actual performance, providing a robust foundation for future research and application.

- **Guidelines for Plant Automation and Control:** The research highlights the importance of proper plant automation and control in the achievement of expected performance levels. Recommendations

for adjustments and optimization of plant control systems include practical guidelines for improving the efficiency and reliability of GEP installations.

- **Recommendations for System Improvement:** The research provides actionable recommendations for improving the design, control, and monitoring of GEP systems. These recommendations are based on empirical data and simulation results, offering practitioners concrete steps to enhance system performance and reliability.

- **Practical Design and Sizing Tool:** The development of a tabulated GEP sizing method that can be used in the early stages of design offers engineers a practical, user-friendly tool. This tool simplifies the initial design process, allowing for quick and reasonably accurate estimates of required pile length and system performance, while taking into account the specific building type and climate conditions. The tool's adaptability to different contexts enhances its practical utility.

1.5 Limitations

The following are known limitations of this research:

- Water advection and phase change effects due to freezing in soil are not addressed in the proposed method for modelling GEPs;

- Data for missing intervals in the measurement data was interpolated in the calibration model of the as-built NZEB;

- Modelled SCOP results may vary significantly, depending on proper sizing of GSHP with GEPs and thermal storage, specific building type, secondary side temperature curves, indoor temperature conditions, outdoor climate conditions, and building usage profiles.

2. Background

This section is based on Publication 1, which reviewed applications for energy piles and their potential use as a renewable energy source. Four topics are addressed (see Table 1 in Publication 1): (1) Fundamental schemes for heat pump plants with geothermal energy piles, (2) geothermal energy pile configuration types and their performance, (3) modelling applications, and (4) approaches to sizing and design. Despite known differences in boundary conditions, borehole research for energy piles is also considered because the operation of energy piles and boreholes [8] is conceptually similar.

More specifically, research reviewing common basic schemes for GSHP plants with GEPs and examples of plant performance are covered in Section 2.1. Since there is not much in the literature concerning the performance of GEPs, this includes the performance of borehole field plants. Section 2.2 summarizes studies on the performance of different energy pile configurations assessed using the thermal response test (TRT). Sections 2.3 and 2.4 review the categories of energy pile modelling and sizing.

2.1 Basic schemes for GEP plants

This section reviews basic schemes for GEP plants and their benefits and challenges. All the schemes described support different ground heat exchangers, including energy piles and boreholes.

In scheme no. 1 (Figure 1), energy piles are used in buildings primarily for heating, to maintain indoor climate conditions. When there is a heating demand, the heat pump activates, warming the fluid in the buffer tank. If the heat pump alone is unable to meet demand and the tank's temperature drops below the set point, an electrical heating coil or alternative heating source will raise the temperature to the desired level. When cooling is required, the fluid in the energy piles is redirected through a "free cooling" heat exchanger, cooling the fluid in the secondary circuit. An optional cooling circuit, connected using three-way valves, makes it possible to switch the direction of the fluid flowing through the heat pump to allow either the heating or cooling of the buffer tank. When "free cooling" fails to meet cooling demand, an additional cooling circuit is an option, though at this point, simultaneous heating and cooling of a building is impossible.

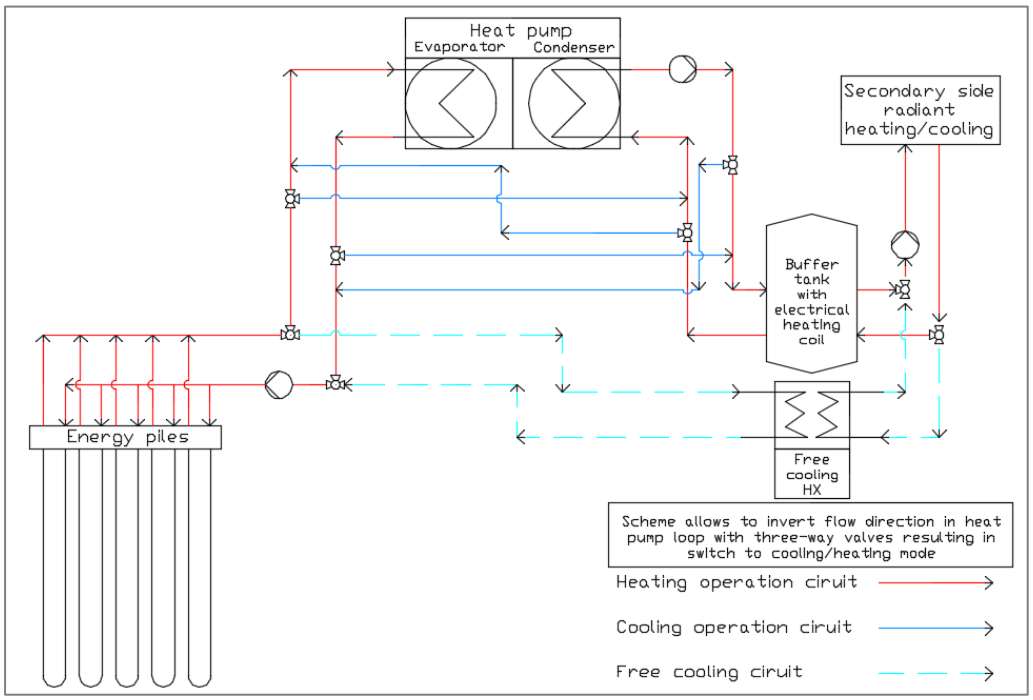

Figure 1. Hybrid heat pump plant with energy piles and “free cooling” option (Publication 2).

There is a case study [9] of a two-story house in Hokkaido, Japan, using the same system with 26 energy piles, each 9 meters deep, that in total generated 18.3 MWh of heat, equivalent to 78 kWh per meter of pile, over a five month period (December to April). During these five months, the minimum outdoor temperature was -17°C, the heat pump's average coefficient of performance (COP) was 3.9, and the system's seasonal coefficient of performance (SCOP), taking into account the energy consumed by the pumps and control system, was 3.2.

Plant scheme no. 2 (Figure 2) is optimized for buildings with simultaneous heating and cooling demands. This design expands on the first scheme by introducing an extra cooling unit and a cold buffer tank.

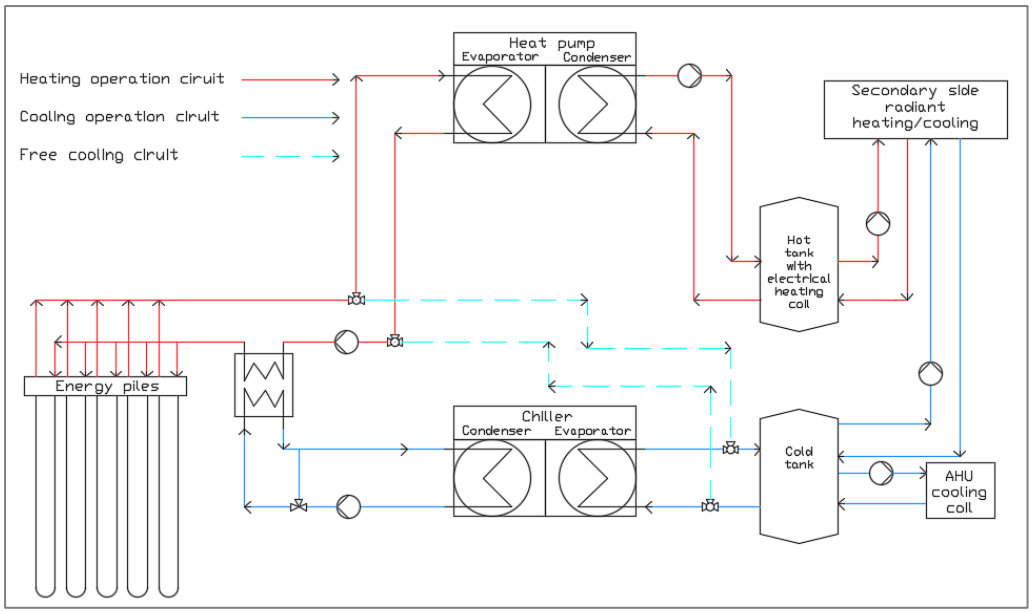

Figure 2. Heat pump plant with energy piles and active cooling (Publication 2).

This type of scheme was followed in the construction in 2003 of Terminal E of the Zurich Airport [10], where the ground heat exchanger (GHE) uses 306 concrete energy piles for efficient heating and cooling. The plant was designed and sized using PILESIM software, which uses a finite difference method to produce a duct ground heat storage model (DST) [11]. The system is powered by a 630 kW heat pump, which covers 85% of heating needs and is supplemented by district heating under peak loads. This design scheme relies on "free cooling" from energy piles to meet cooling demands, with additional cooling activated when it is not otherwise possible to maintain the supplied coolant at 14°C. The piles, having diameters ranging between 900 to 1500 mm and installed at a depth of 26.8 m, were each fitted with five U-pipes. Over a year, the heat pump provided 2210 MWh for heating (73% of demand) and 620 MWh for cooling (53% of demand), demonstrating significant energy efficiency with a projected payback period of eight years. The system had on average a COP of 4.5 and SCOP of 3.9, with the heat pump's evaporator capacity at about 59.7 W/m per meter of pile length, indicating an effectiveness much greater than that of traditional district heating and cooling solutions.

While the unbalanced heat extraction/rejection in energy piles can cause a significant drop in a system's long-term performance, thermal storage can be used to enhance the long-term stability of Ground Heat Exchanger (GHE) systems. Scheme no. 3 (Figure 3), intended for cold climates, incorporates thermal storage options such as solar collectors, dry coolers, and exhaust air heat exchangers provided by air handling units.

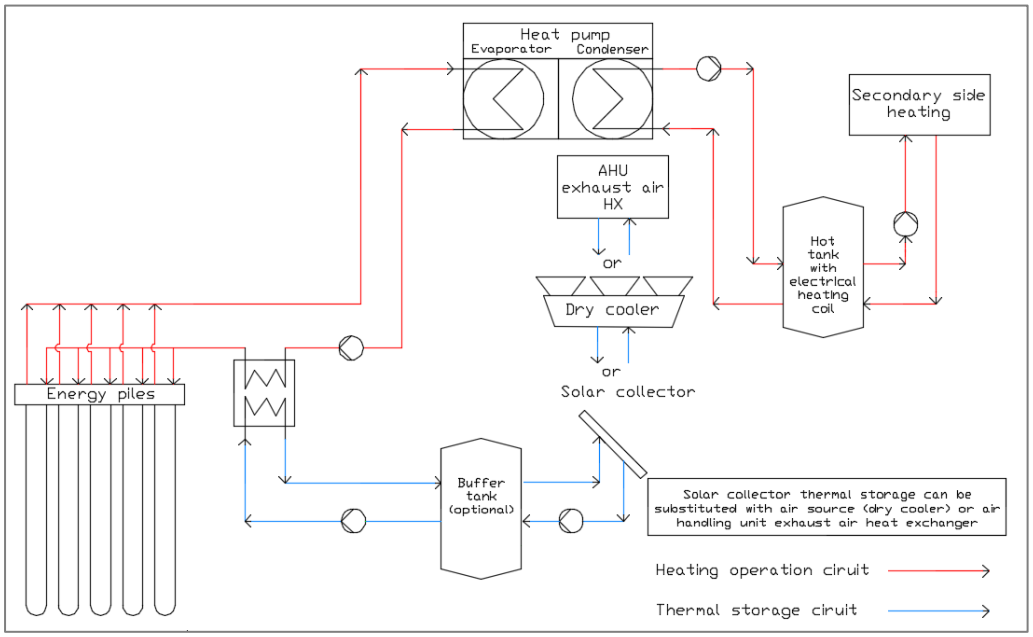

Figure 3. Heat pump plant with energy piles and solar/air source/AHU exhaust air HX thermal storage (Publication 2).

Reda [12] studied the integration of solar thermal storage in a ground source heat pump (GSHP) system with a borehole field (not energy piles) in Finland's

cold climate and showed that this resulted in significant improvements in system efficiency. Using TRNSYS simulation software with the DST model, it was shown that without thermal storage, the GSHP would have a SCOP of 1.6, satisfying 53% of heating demand, with the remaining demand met by auxiliary heating. Introducing a 46.8 m² solar collector resulted in a SCOP of 2.5, with the heat pump satisfying 84% of heating demand. Doubling the solar collector area to 93.6 m² led to a SCOP of 3.0, with the heat pump fulfilling 94% of heating demand. These results demonstrated that solar thermal storage can significantly boost GSHP performance. While average annual heat capacity for boreholes without thermal storage was 93 kWh per borehole meter, it was approximately 153 kWh and 171 kWh, respectively, for plants equipped with flat plate solar collectors having total areas of 46.8 m² and 93.6 m².

Plant scheme no. 4 (Figure 4) incorporates seasonal thermal storage using warm and cold air sources. In winter, the heat pump extracts heat from an energy pile field for heating, while in summer, heat is injected into a cold energy pile field for cooling, with a dry cooler facilitating heat exchange with the warm pile field.

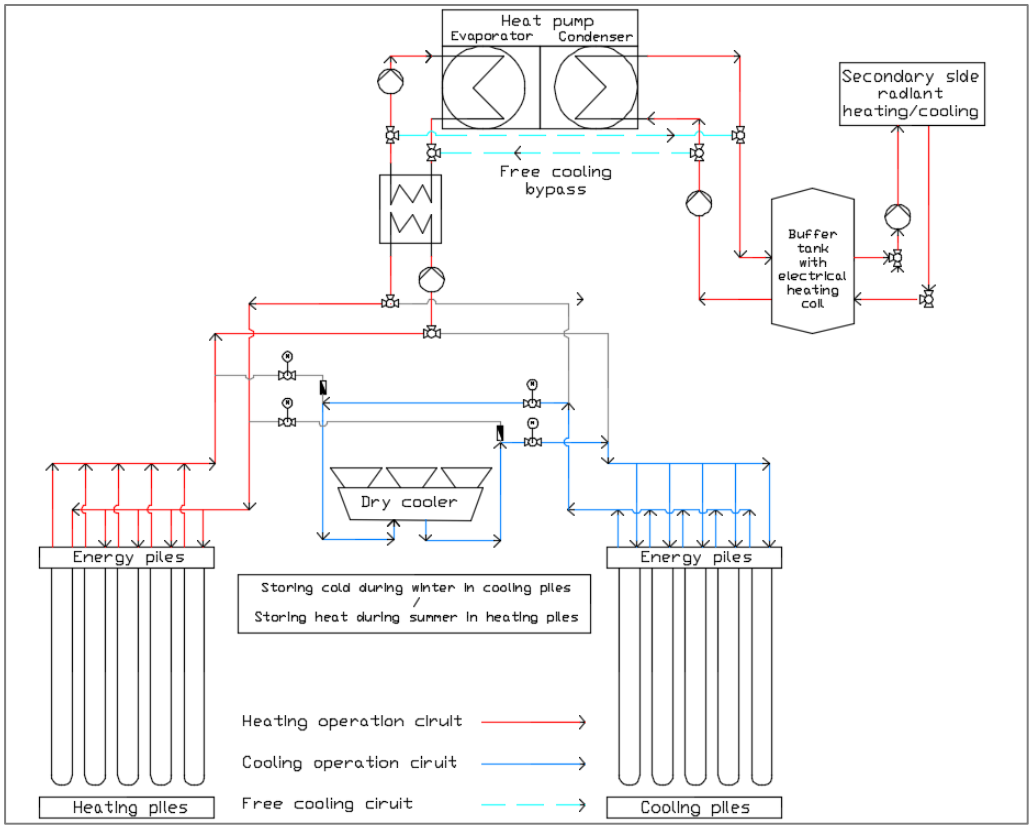

Figure 4. Heat pump plant with separated energy pile field for cooling and heating with air source thermal storage (Publication 2).

Allaerts et al. [13] used the TRNSYS simulation environment to numerically model the performance of a Belgian office building employing a dual borehole field (distinct from energy piles) with active air source storage. The borehole field was simulated using a DST model employing the finite difference method. Their results indicated a 47% reduction in the required borehole field size when

compared to that of a conventional single-borehole setup with equivalent thermal storage capacity, thus demonstrating the improved performance and space-saving benefits of their innovative system.

Four basic GEP design schemes effective in both cold and hot climates have been identified. These design schemes have demonstrated high system efficiency, with SCOP values exceeding 4.5 in some cases [14]. Advanced software like TRNSYS and PILESIM, both employing DST models based on the finite difference method, and PILESIM2, with a modified DST model, were used to design the plants reviewed and analyze their performance. The addition of thermal storage proved to enhance plant efficiency, potentially also reducing the overall length of the ground heat exchanger.

Table 2 summarizes a comparison of the four different plant schemes.

Table 2. Comparison of basic plant schemes (Publication 1).

Basic scheme no. **Reference**	1. Hybrid heat pump plant with energy piles (Figure 1) [15]	2. Energy pile heat pump plant with active cooling (Figure 2) [9]	3. Energy pile heat pump plant with thermal storage (Figure 3) [15]	4. Heat pump plant with separate heating/cooling pile fields (Figure 4) [13]
Heating	✓	✓	✓	✓
Free cooling	✓	✓	✓	✓
Active cooling	✓[1]	✓		
Simultaneous heating/cooling		✓		
Thermal storage			✓	✓
Heating SCOP (HP SCOP)	2.0 (4.62)[3]	3.9 (4.5)[2]	2.0 (4.62)[3]	-
Cooling SEER	-	2.7[2]	-	-
Free cooling SEER (demand covered)	40 (49%)[3]	61 (78%)[2]	40 (7%)[3]	-
Cost category	energy pile heat pump	energy pile heat pump chiller	energy pile heat pump solar collectors or exhaust air heat exchanger	energy pile heat pump dry cooler

[1]Three-way valves reverse the flow in heat pump loop
[2]Measured value
[3]Numerically calculated value

Plant scheme no. 1 is most suitable for buildings where heating needs predominate and cooling needs are minor, i.e., where the ratio of heating demand to cooling demand approaches 1 to 0.1. With a Seasonal Energy Efficiency Ratio (SEER) of 40, this scheme only covers 49% of cooling needs through "free cooling" [15]. This scheme has a heating SCOP of 2.0, reaching 4.62 with the heat pump alone, without factoring in electrical top-up heating. Its application in structures like office buildings is limited due to its inability to provide simultaneous heating and cooling.

Plant scheme nr 2, with a measured heating SCOP of 3.9, is, however, a good choice in environments requiring simultaneous heating and cooling [10]. On the negative side, the initial investment required by such a system is higher than that for the use of conventional district heating with an active cooling system, up to 5.2 times the annual operating costs, and it has a payback period of up to 8 years.

Plant scheme no. 3 benefits from thermal storage. By integrating exhaust air heat exchangers and solar collectors into the system, energy pile field size can be reduced by up to 50% [11]. This approach was used to store 28.3 MWh of heat and allowed the system to extract 12 MWh more heat than was possible without storage, enabling a 42% utilization rate of stored heat. At the same time, the system's "free cooling" capability diminished with increased thermal storage, so that it satisfied only 7% of cooling demands [11].

Lastly, plant scheme nr 4 is an advanced solution, enabling both heating and cooling energy storage and significantly improving "free cooling" efficiency. This scheme represents an adaptive approach that accommodates a broader range of climate control needs while optimizing energy use.

2.2 Geothermal energy pile configurations

Energy piles can be differentiated by material (cast in-situ concrete, prestressed high-strength concrete (PHC), or steel) and the configuration of their heat exchange loops. Common configurations include single U-pipe (or U-tube), double U-pipe, multitube, W-tube, coiled designs with known pitch, and indirect double-pipe systems (Figure 5). In piles with larger diameters, the configuration often extends beyond two U-loops. Although spiral and helical designs are popular in academic studies, these are less common in practice.

An on-site Thermal Response Test (TRT) [16] can be used to evaluate the thermal conductivity and diffusivity of the soil and the thermal resistance of energy piles at a specific location. The TRT could also be used to assess the thermal performance or capacity in watts per meter (W/m) of different pile configurations. To ensure accuracy, the analysis model must account for the short-term thermal behavior of energy piles and the thermal properties of their internal components.

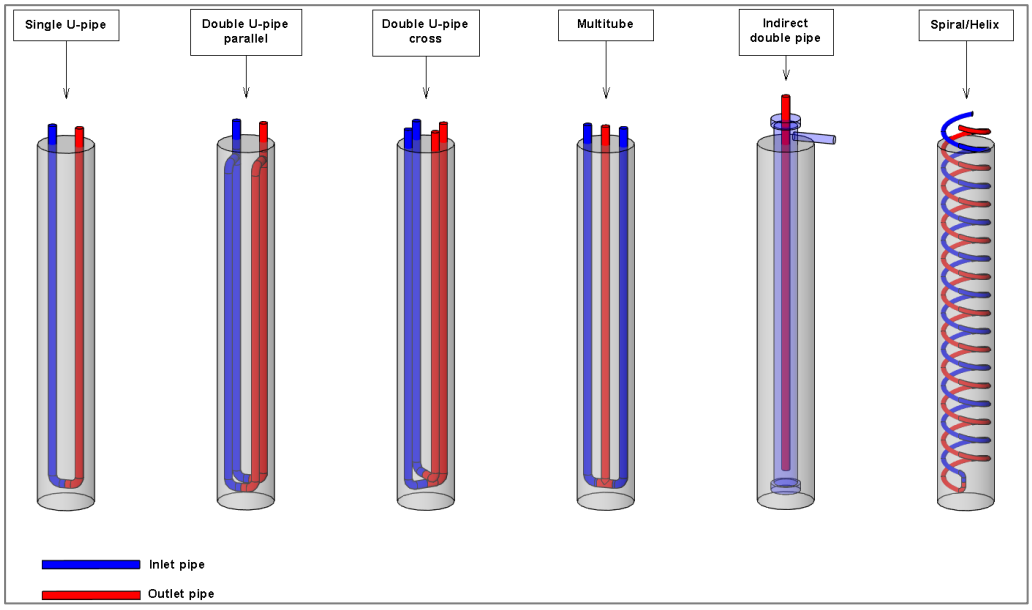

Figure 5. Energy pile configurations (Publication 2).

During the TRT, a constant temperature is maintained in the energy pile by connecting it to a heat source, while the flow and temperature of the outgoing fluid are monitored to ensure stability. The test, which typically takes 72 hours, also necessitates maintaining a constant heat flux in the pile's ground loop for the determination of the thermal characteristics of the soil.

Before installation, the undisturbed ground temperature is measured to facilitate the calculation of average heat extraction and rejection rates using an analytical model. TRT results offer a basis for rating the thermal performance of various pile configurations. The comprehensive literature review on energy pile configurations and thermal response test performance is summarized in Table 3.

Table 3. Thermal response test performance of different energy pile configurations (Publication 1).

Reference	Pile material	Pile configurations	Soil thermal properties	Test type	TRT Performance
Y. Hamada et al. [9]	PHC	single U-pipe double U-pipe indirect double-pipe o_d = 302 mm	-	constant inlet temp	single U = 54 W/m double U = 55 W/m double-pipe = 69 W/m
J. Gao et al. [17]	cast in-situ concrete	W-pipe single U-pipe double U-pipe triple U-pipe o_d = 600 mm	λ= 1.3 W/(mK)	constant inlet temp	W-pipe = 83 W/m single U-pipe = 58 W/m double U-pipe[1] = 89 W/m triple U-pipe[1] = 108 W/m
Miyara et al. [18]	Steel	single U-pipe double-tube multi-tube o_d = 139.8 mm	λ= 1.1…2.1 W/(mK)	constant inlet temp	single U-pipe = 30 W/m double-tube = 50 W/m multi-tube = 35 W/m
A. Zarrella et al. [19]	cast in-situ concrete	coil-type pitch 75 mm coil-type pitch 150 mm coil-type pitch 350 mm triple U-pipe o_d = 500 mm	λ_{trt}= 1.8 W/(mK) cp_{trt}= 2.4 MJ/(m^{3}K)	constant inlet temp (simulated TRT)	75 mm = 123 W/m 150 mm = 120 W/m 350 mm = 113 W/m triple U-pipe = 107 W/m
S. Park et al. [20]	cast in-situ concrete	coil-type pitch 200 mm coil-type pitch 500 mm o_d = 1350 mm	λ_{trt}= 3.3 W/(mK) α_{trt}= 4.45 x 10^{-6} m^2/s	constant inlet temp (intermittent)	200 mm = 285 W/m 500 mm = 248 W/m

[1]flow in double and triple U-pipe was twice and trice higher respectively compared to single U-pipe and W-pipe

To determine the thermal properties of the soil, the following equation derived from an infinite line source model is often used to process measurement data from the TRT for the boreholes (not energy piles) [21]:

$$T_f(t) = \frac{q}{4\pi t} \cdot \left(\ln\left(\frac{4at}{{r_b}^2}\right) - \gamma \right) + q \cdot R_b + T_0 \qquad (1)$$

where T_f is the fluid outlet temperature (°C), T_0 is the far field or initial soil temperature (°C), q is the heat flux along the length of the borehole (W/m), t is time (s), R_b is the thermal resistance of the borehole (W/mK), γ is the Euler constant, a is the soil diffusivity (m²/s), and r_b the is borehole radius (m).

Review of the TRT results for different energy pile configurations showed that the amount of pipe surface area grouted into the pile structure significantly impacted the short-term specific heat extraction/rejection rate. Coil-type heat exchangers produced the highest heat rejection rates. High heat extraction/rejection potential, however, might not always be the most important consideration since the amount of potential ground energy extracted also depends on the initial temperature of the ground and the intended use of the ground source system

(heating/cooling). For example, the use of a dense coil-type heat exchanger for heating (heat extraction) in cold climate regions with soil temperatures of around 5 °C may not be practical. Similarly, a double U-tube configuration may yield the same amount of ground heat if the ground temperature eventually drops below 0 °C and shuts off the heat pump. Thus, systems with shorter heat exchange pipes may sometimes be more feasible.

2.3 Geothermal energy pile modelling

While borehole modelling has been studied extensively, little research has been carried out on the modelling of energy piles. Boreholes and energy piles may seem to operate under very similar conditions, but these conditions in fact differ significantly.

Due to their load-bearing function, energy piles are typically shorter and radially thicker than boreholes. The length of boreholes typically ranges from 50 to 300 meters, while their diameter is typically smaller because they are not required to bear weight. Boreholes are typically modelled as line sources. The borehole structure, including grout, pipe legs, and fluid thermal capacitances, is ignored because the diameter of the borehole is so small relative to its length. In the case of the energy pile, however, thermal capacitance of the grout material significantly impacts the short-term thermal behavior of the pile and must be considered.

Further, due to the length of boreholes, the ground surface boundary is typically modelled as adiabatic because fluctuations in ambient surface temperature only penetrate to a small depth near the ground surface. The length of an energy pile, however, may only be a few meters, making it necessary to model the surface boundary since it will then significantly impact heat extraction and rejection. Thus, borehole models should only be used to analyze the performance of energy piles after due consideration of all of the abovementioned differences.

The literature review of the borehole models presented in this section may prove a useful reference aid during the selection of a suitable borehole model solution for an energy pile simulation. The two types of published models are analytical and numerical. Analytical models, which typically incorporate many assumptions to simplify the problem, are mainly used to evaluate a pile's soil properties and thermal resistance based on TRT results. It should be remembered that overcoming the thermal capacitance of an energy pile requires TRT tests to be conducted much longer than in the case of boreholes. Some of the analytical models are appropriate for transient simulations.

Numerical models, on the other hand, can be extremely detailed, accounting for phase changes in soil caused by freezing, modelling a pile’s internal components, variable boundary temperature conditions, the thermal capacitance of pile’s internal materials, etc. Numerical simulation also offers the opportunity to quantify the differences between 2D, 3D, and quasi-3D models. This detail, however, all comes at a cost in high computation time and modelling complexity, going against typical design practice in engineering.

Table 4 presents the findings of the literature review on available energy pile models, summarizing and presenting their key characteristics in chronological order.

Table 4. Comparison of models (Publication 1).

Reference	Model	Solution			Domain			Pile type			Features											
		Analytical	Numerical	Response factor	1D	2D	3D	Single U-tube	Double U-tube	Coil-type	Surface boundary variable temp	Adjacent pile interactions	Interactions between pipe legs	Water advection	Phase change in soil	Pile thermal capacitance	Fluid thermal capacitance	Short time-step	Multilayered ground	Pile incline	Finite pile length
H.S. Carslaw, J.C. Jaeger [21]	ILSM[3]	✓			✓																	
L.R. Ingersoll et al. [22]	CSM[3]	✓			✓																	
P. Eskilson [28]	FDM/g-funct		✓	✓	✓	✓		✓	✓			✓		✓								✓
G. Hellstrom [11]	FDM DST		✓			✓		✓	✓[2]			✓	✓				✓	✓	✓			✓
T.K. Lei [25]	FDM		✓			✓		✓			✓		✓				✓	✓				✓
N.K. Muraya [27]	FEM		✓			✓		✓			✓		✓	✓		✓	✓	✓	✓			✓
T. Kohl, R. J. Hopkirk [49]	FEM		✓				✓		✓		✓		✓	✓		✓	✓	✓	✓			✓
S.P. Rottmayer et al. [44]	FDM		✓				✓	✓					✓				✓	✓				✓
C. Yavuzturk et al. [29,45]	FDM/FVM/g-funct		✓	✓		✓		✓				✓	✓			✓	✓	✓				✓
H. Y.Zeng et al. [23]	FLSM	✓				✓		✓				✓										✓
S. He et al. [26,48]	FVM		✓			✓	✓	✓			✓		✓			✓	✓	✓	✓			✓
Y. Man et al. [24]	ISCSM/FSCSM[3]	✓			✓	✓						✓				✓[5]		✓				✓
S. Javed, J. Claesson [31]	Short-term response	✓	✓			✓		✓								✓	✓	✓				✓
P. Eslami-Nejad, M. Bernier [41]	2U2ICM[4]	✓	✓[1]		✓[1]	✓			✓				✓		✓			-				✓
C.K. Lee, H.N. Lam [46]	FDM		✓				✓	✓	✓[2]				✓			✓	✓	✓	✓			✓
O. Ghasemi-Fare, P. Basu [47]	FDM		✓				✓	✓			✓					✓	✓	✓	✓			✓
A. Zarrella et al. [19]	CARM		✓			✓	✓	✓	✓	✓	✓	✓	✓			✓	✓	✓				✓
P. Hu et al. [35]	CCSM	✓			✓			✓	✓[2]			✓				✓		✓				
E.H.N. Gashti et al. [52]	FEM (Comsol)		✓				✓		✓		✓		✓	✓		✓	✓	✓	✓			✓
W. Zhang et al. [32,33]	Solid CSM	✓			✓					✓		✓		✓		✓[5]		✓				✓
T.V. Bandos et al. [38]	FCSM[3]	✓				✓						✓				✓[5]		✓				✓
F. Dupray et al. [54]	FEM (Lagamine)[3]		✓			✓					✓	✓		✓				✓	✓			✓
J. Fadejev, J. Kurnitski [8]	Equa borehole FDM		✓				✓	✓	✓[2]		✓	✓	✓			✓	✓	✓			✓	✓

[1]ground model with phase change
[2]supports multiple U-tube configurations
[3]pile interior was not modeled,
[4]double U-tube with two independent circuits
[5]pile is modelled as cylinder filled with soil material

Figure 6 shows the key feature of the models as reported in the scientific literature. The soil and pile are the two regions where heat transfer is typically modelled. Analytical models treat the soil and pile regions as single homogeneous mediums (if present). Most numerical models, however, can take the ground's multi-layered structure into account. Some numerical and analytical models can account for water advection in the soil region. The literature review revealed only one numerical model that can simulate the phase change of water vapor caused by freezing in a porous soil medium.

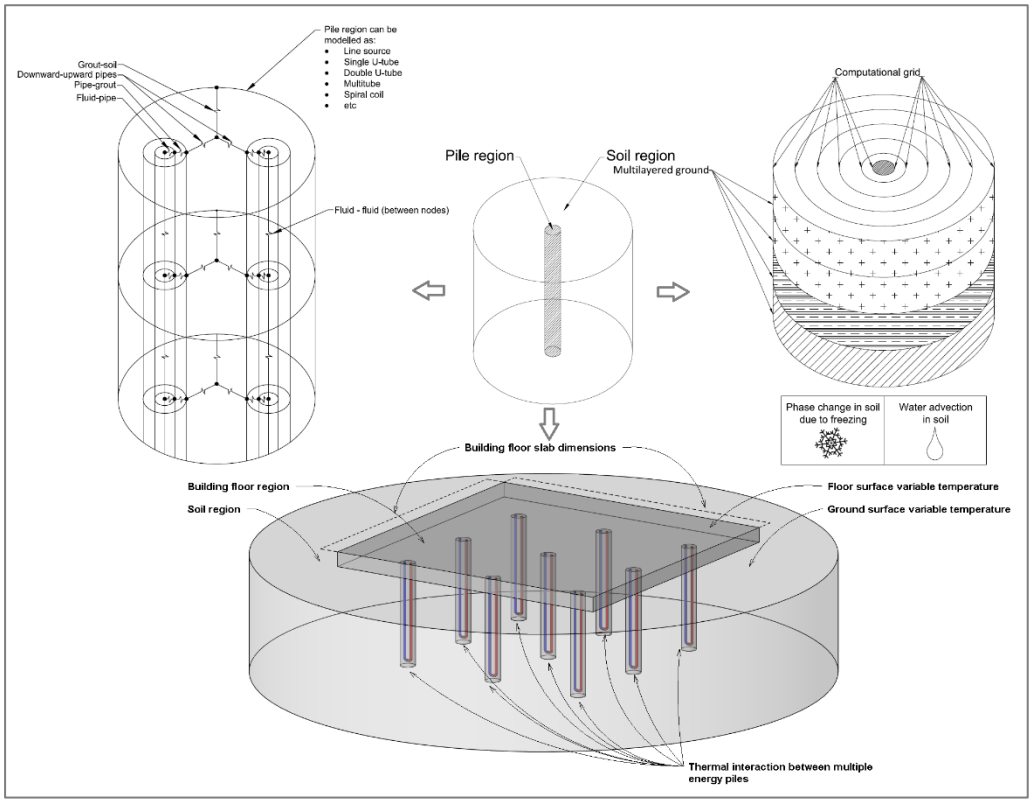

Figure 6. Energy pile modelling variables and boundary conditions (Publication 2).

In analytical models, temperature development is typically modelled as a line source, ignoring the thermal capacitance of the inner components of the pile. Some analytical models can take into account the internal pipe layout of a pile by using the thermal resistance *Rb* of the pile as an input. Some also consider the thermal capacitance of a pile (Table 4). These models can simulate short time steps, yielding precise results for time steps of less than an hour.

Models are available specifically for single U-tube, double U-tube, multi U-tube, and coil-type pile configurations. Internal pile components are generally modelled numerically. These models take into account axial heat transfer, upward/downward fluid flow, thermal capacitance of the fluid and grout, as well as the geometry of the pipe legs and the thermal interactions between them.

Table 5 summarizes the main applications of the models described in Table 4, their suitability given practical design considerations, and their limitations when applied.

Table 5. Borehole model applications and limitations in the analysis of energy piles (Publication 1).

Modelling method	Application	Limitations
Analytical infinite heat source models [21],[22]	Processing of TRT results (suitable for longer measuring periods due to lack of thermal capacitance)	Temperature rise tends to infinity due to infinite length, single pile analysis in original form (without superposition), constant heat flux, adiabatic ground surface boundary,
Analytical finite heat source models [23],[24]	Processing of TRT results	Single pile analysis in original form (without superposition), constant heat flux, adiabatic ground surface boundary
Numerical finite difference models [11],[25]	Dynamic annual simulation of boreholes/energy piles with custom plant and whole building modelling capability	Long computational time, limitations in boundary conditions depending on the model (non-homogenous ground, no water advection, etc.), simulation environment modelling knowledge requirements
Numerical finite element/volume models [26],[27]	Detailed heat/moisture transfer analysis of any modelled geometry with soil freezing and fluid dynamics capabilities	Extremely long computational time, high requirements for modelling and boundary condition knowledge, impractical for engineering purposes
Response factor models [28],[29]	Annual simulation of boreholes based on the input of building load data (small time steps can be applied, but there may be loss of accuracy at very small time steps)	Only accurate for borehole simulations due to adiabatic ground surface boundary, limited to precalculated borefield configurations, no coupling with whole building simulation, no detailed thermal storage modelling capabilities

The thermal interaction between multiple piles can be modelled both analytically and numerically. Analytical models commonly make use of the superposition method, which involves summing up the thermal impact of all piles at the temperature of the ground. In numerical models, which account for the geometry of the pile field, thermal interactions between piles are modelled by solving heat balance equations.

Ground surface temperature and far field temperature (the initial ground temperature) are constant boundary conditions in analytical models. Some numerical models, however, allow for variable ground surface temperature, which is crucial when modelling energy piles. Additionally, while most analytical models in their original form can only simulate constant heat flux along the length of the pile, numerical models can handle varying heat flux.

One of the goals of the literature review was to find a model capable of simulating the thermal performance of energy pile fields, where ground surface boundary conditions determine building floor slab geometry and soil region geometry surrounding the building (Figure 6), heat transfer through the floor slab to the soil beneath is modelled in the building region, and heat transfer between the soil and outdoor air (and solar radiation) is modelled in the surrounding soil region. Unfortunately, no such model was discovered.

The effect of heat loss from a heated floor slab on soil temperatures for buildings without energy piles was modelled by Chuangchid and Krarti [30]. According to the results of a simulation in winter conditions with an uninsulated heated slab, the temperature under the building was 10 K higher at a depth of about 2 meters and 5 K higher at a depth of about 4 meters. In theory then, if floor slab heat loss is taken into account when designing a geothermal heat exchanger in a system with short piles, the performance of the geothermal plant can be increased, and the cumulative length of the energy pile field can be shortened. An additional consideration is the fact that the amount of heat loss in the slab region also varies due to the exposure of the floor slab surface to indoor conditions, while the floor slab edge is exposed to outdoor conditions. The results of the case study carried out by Chuangchid and Krarti [30] show that soil temperature in a building section view begins to decline sharply at about 2 m from the edge of the floor slab, where it reaches its lowest values. As a consequence, piles that are less than 2 m from the edge of the slab would operate under completely different temperature conditions than piles that are closer to the center of the building. Even though these problems can be modelled using numerical finite element 2D or 3D software such as COMSOL, more practicable transient solutions are yet to be developed.

2.3.1 Analytical models

The most widely known (1-D) analytical solution for modelling a vertical borehole GHE is the infinite line source model, which is based on Kelvin's line source theory [21]. This model neglects the physical dimensions of the borehole, while an initial uniform ground temperature is given, a grouted borehole with piping is assumed to be a line heat source of infinite length, and the ground in which it is located is considered to be an infinite homogeneous medium. A line source model can calculate temperature response at a given distance perpendicular to the axis of the line heat source at a given time based on heat output per length of line source and ground thermal conductivity and diffusivity.

A cylindrical source model [21]-[22] is a 1-D analytical solution that can estimate the temperature response at the borehole wall while taking the size of the borehole into account. In addition to the input parameters of the line source model, the outer diameter of the borehole is a required input of the cylindrical source model. Both models are primarily used to describe heat transfer outside the borehole. In both models, ground surface boundary conditions and the heat capacity of borehole materials are neglected. After first calculating the temperature at the borehole wall, temperature development inside the borehole can be derived, e.g., by using thermal resistances.

Eskilson [28] developed an analytical model that took into account the finite length of a borehole. It is worth noting that the heat capacity of the borehole itself was neglected. The boundary and initial conditions in Eskilson's model were assumed to be constant and the ground homogenous. Eskilson introduced a dimensionless temperature response at the borehole wall, the g-function, which is defined as:

$$t_b - t_0 = -\frac{q}{2\pi k} g(\tau/(\frac{H^2}{9a}), r_b/H) \quad (2)$$

where g is the dimensionless temperature response, t_b is the temperature at borehole wall (°C), t_0 is the far field temperature (°C) (initial ground temperature), q is the heat flux along the length of the borehole (W/m), H is the borehole length (m), a is soil diffusivity (m²/s), and r_b is the radius of the borehole (m).

Thermal interactions between multiple boreholes were modelled using the superposition method. G-functions were calculated for many different energy pile field configurations using a numerical finite difference model. The values of these g-functions can be used to simulate the performance of borehole fields analytically. The results of such modelling are, however, accurate only for a time greater than $\frac{5{r_b}^2}{a}$ due to the neglecting of the heat capacity of the borehole. For this reason, this model is classified as a long time-step model.

A short time-step model for transient simulations was introduced by Yavuztzuk and Spitler [29]. This analytical model can produce accurate results with a time step of less than one hour. It follows a logic similar to that of the g-function, while a two-dimensional finite volume model was applied to calculate g-functions values.

On the basis of Eskilson's model, Zeng et al. [23] developed a finite line source model, an analytical solution that shows good agreement with a numerical solution. The main advantage of this model is its fast computational times. While the Kelvin line source model has temperature rising during a long simulation period and tending towards infinity, the finite line source model temperature tends toward the initial ground temperature, which is constant over the calculation period.

Man et al. [24] developed infinite and finite “solid” cylindrical source models for pile heat exchangers on the basis of the existing “hollow” cylindrical source model [22]. In this new analytical solution, the modelling of the thermal capacitance of a pile is simplified by filling its "hollow" interior with a homogeneous material having thermal characteristics identical to those of the ground, also assumed to be homogeneous. In effect, the internal geometry of the pile is neglected, and for an accurate analysis, the thermal properties of the grout must be the same as those of the soil. These models were created in one and two dimensions and were validated against numerical models. When compared to the outcomes of numerical models, the predictions of these models proved accurate for short time steps. It should be noted that the ground surface boundary temperature remains constant throughout the simulation period, as it does in most analytical models.

In order to determine the average borehole fluid temperature for time steps under an hour, Javed and Claesson [31] developed an analytical short-term response borehole model that takes into account the thermal capacitances of the circulating fluid and grout in the borehole. A single equivalent-diameter pipe is used to represent each pipe leg of a single U-tube, with a fluid temperature equal to the average of the temperatures of the supply and return pipe legs. Heat transfer is modelled as radial and solved with help of Laplace transforms. Javed

and Claesson achieved good agreement by validating their analytical model using actual measurement data and their own developed numerical solution.

Zhang et al. [32] developed a conduction-advection equation for heat transfer in porous media for an infinite line source model to account for ground water advection. The groundwater is assumed to flow over an infinite homogenous porous medium in the x direction at a specific velocity. Water advection in a field of boreholes was also studied by Zhang et al. [32], revealing that groundwater flow leads to a steady state in heat transfer much more rapidly than if there were no water advection. To make it possible to quickly estimate the potential impact of water advection on the thermal performance of energy piles, they also provided a summary of the thermal and hydraulic properties of various rocks and soils.

Man's [24] infinite and finite solid cylindrical source models were modified by Zhang et al. [33] to account for groundwater advection. The model was developed under the same assumptions as the infinite line source water advection model by Zhang et al. [33]. According to the study, with groundwater advection the heat exchange performance of energy piles can be as much as 5 times higher than it would have been without it. With the aim of creating an analytical model with greater accuracy when ground water velocities exceed 1e-5 m/s, Wang et al. [34] evaluated the performance of the Zhang et al. [33] model in the finite element modelling environment ANSYS CFX.

Using a composite line source model as a foundation, Hu et al. [35] created a composite cylindrical model as well as a cylindrical source model [36]. Validation of the composite cylindrical model using a 3D numerical model and TRT measurement data indicated good agreement. The proposed analytical model has the advantage of allowing simulations with short time steps while also taking into account the heat capacitance of the pile. The model assumes the ground is homogenous and neglects heat transfer in the pile's axial direction. The layout of pipes in the borehole/energy pile are modelled using borehole thermal resistance Rb. Thermal resistance Rb can be calculated using equations that were proposed for single U-tube [37] and double and triple U-tube configurations [11]. Volumetric heat capacity and soil heat conductivity were calculated using TRT with the proposed composite cylindrical model, and these results were compared to the results of the same calculations using a line-source model. The soil thermal conductivity and volumetric heat capacity obtained were both about 20% less than that obtained using the line-source model. The composite cylindrical model demonstrated excellent agreement at even the very early stages of TRT.

Bandos et al. [38] presented a finite cylinder-source analytical model, which was modified from a double to a single integral form to reduce computation time [24].

Seeking an analytical solution covering the typical geometry of energy piles, Loveridge and Powrie [39] developed additional g-functions for Eskilson's [28] analytical response factor model for piles with an aspect ratio of 1000. They investigated how connecting piles in parallel or serially affected thermal performance. They also provided g-function graphs with the locations of upper and

lower bond U-pipes as well as a technique for calculating nearly any g-function for an energy pile field. In one case, where nine piles were placed very close to one another, they showed that their performance was only 16 percent of that of an individual pile isolated from the group, demonstrating the importance of accounting for thermal interactions between adjacent piles. Eskilson's theory that thermal interactions between piles occur when the distance between adjacent piles is at least equal to the length of a pile in the field was confirmed by their findings. They also suggested that it might not be practical to activate all of the piles in a foundation and that it might be more effective to leave some piles that are too close to one another inactive. Using a 2-D numerical model in COMSOL, Loveridge and Powrie [40] investigated heat transfer within the pile region. They proposed an empirical equation that could be used to determine the borehole resistance for pile configurations with different conductivity ratios and pipe counts.

Eslami-Nejad and Bernier [41] developed a ground model that captures phase change effects using the effective heat capacity method. They combined it with an analytical borehole model that they had also developed [42]. The borehole model, which only considers fluid heat capacitance, was used to analyze two U-loops to account for thermal interactions between the U-pipe legs. Fluid axial temperature variation and borehole depth were also taken into account by the borehole model. It was assumed that the temperature of the borehole wall remained constant along the borehole depth. Heat transfer in the soil region was modelled using the ground model, while heat transfer within the borehole (in the fluid) was modelled using the borehole model. On the basis of small-scale experimental measurements, Eslami-Nejad and Bernier validated the ground model, discovering good agreement between model performance and experimental findings. Phase change is modelled according to Bonacina et al. [43] and is described with three phases: liquid, solid, and transition. In the Eslami-Nejad and Bernier ground model, natural convection and moisture transfer in saturated soil regions were neglected because once the water has frozen it maintains a constant density. It is important to remember, however, that ground loop outlet temperature is frequently restricted so that it doesn't fall below 0 °C (to prevent frost heave). As a consequence, common design allowances eliminate the need for a ground model with phase changes in the case of applications involving energy piles.

2.3.2 Numerical models

Numerical energy pile/borehole models have been grouped by modelling approach into three different categories: finite difference, finite volume, and finite element. A literature review, however, also uncovered a quasi-numerical approach that does not fit into any of these modelling categories. Just such a model is the capacity resistance model (CaRM) developed by Zarella et al. [19] for analyzing and designing boreholes. There are two versions of this model: one takes the thermal capacitances of the internal components of the pile into account, and the other one does not. Ground surface thermal convection, short- and long-wave solar radiation, and axial heat transfer in the grout are all modelled

by the former. Theoretically, the model could be used to design energy piles and evaluate their performance if the initial data on solar radiation is ignored and replaced with the variable temperature above the pile foundation structure. The model takes into account the geometries of coaxial pipes and single, double, and triple U-tubes. The model is capable of accounting for the thermal interaction among multiple piles and calculating variable outlet temperatures. Validation against both the HEAT2 finite difference model and field data showed very good agreement. While a comparison of the outlet temperatures of piles with and without thermal capacitances showed a fluid temperature difference of approximately 0.6...2 °C, the authors also demonstrated the importance of accounting for the thermal capacitances of the internal components of piles.

2.3.3 Finite difference method

Eskilson [28] developed a two-dimensional finite difference model with constant boundary conditions that ignored the thermal capacitance of the fluid and pile. G-functions for his analytical solution (described in section 2.3.1) were then calculated using the model.

A model for simulating multiple boreholes intended for seasonal thermal storage operation was developed by Hellstrom [11]. The temperature distribution in the ground was modelled using the finite difference method and the so-called duct storage model (DST). The DST model is a TRNSYS library component that supports variable surface boundary conditions and short time-step transient simulations.

Lei [25] proposed a 2-D finite difference numerical model to simulate radial-axial borehole ground heat exchange. The inner and outer regions of the borehole cross section are separated. Heat transfer between the ground and fluid is modelled in the outer region, while heat transfer between adjacent U-pipe legs is modelled in the inner region. The model neglects heat transfer in the ground, grout, and pipes and only analyzes axial heat transfer of fluid.

To simulate heat transfer processes occurring inside the borehole region, Rottmayer et al. [44] developed a quasi-three-dimensional finite difference method. The model looks at axial heat transfer in the fluid, while axial heat transfer in the grout is ignored. The heat capacitance of the pipe wall and grout is also neglected. The borehole section is divided into a cylinder-shaped grid of nodes and then analyzed using the finite difference method to model radial heat transfer. Due to the specifics of the calculation grid, the U-pipe cross-section in Rottmayer's model is trapezoidal rather than circular. The area of the trapezoidal section is generated on a circular grid so that it corresponds to the actual area of the U-pipe section. Rottmayer introduced a geometric factor based on empirical data to model circular thermal resistance in a portion of the cylindrical grid since thermal resistance in trapezoidal and circular domains differs.

Yavuzturk and Spitler [45] introduced a two-dimensional finite difference transient borehole model that analyzed the heat capacitance of the grout, U-pipes, and circulating fluid. While the circular pipe section's grid is generated as an equivalent U-pipe area "pie sector," the cylindrical grid in Yavuzturk and Spitler's model is generated in way similar to how the model that Rottmayer et

al. [44] developed. The major benefit of this model is its ability to simulate short-term responses, for example, in a year-long simulation coupled with a ground-source heat pump model.

Lee and Lam [46] developed a three-dimensional finite difference model of a single energy pile. The two different soil regions in the model are the bedrock layer on which the tip of the pile rests and the soil that radially surrounds the pile. In addition to the soil and bedrock, pile grout and fluid are also modelled, and the heat capacitances of these components are taken into account in the equations for the heat balance. The heat capacitance of the pipe wall is ignored. The model can take into account different pipe connection arrangements and multiple U-pipes. The distance between pipes can vary, but modelled pipes must be spaced equally apart from the center of the pile. The ground surface and pipe boundaries are assumed to have constant temperatures, and each pipe, an identical fluid flow rate. The model was initially validated over a period of ten years against a finite line source model in which the pipe legs were treated as separate line sources of heat. The model and analytical solution showed excellent agreement, with the largest difference being just 0.11 °C. The steady-state thermal resistance of one pile configuration was also calculated using the same model, and the results were validated using Hellstrom's [11] steady-state methodology, showing good agreement with just a 3.6% difference in results. Numerous studies using a validated model showed that the thermal conductivity of the bedrock layer beneath the pile has very little impact on the pile's ability to reject or extract heat because there is so little heat conduction there. However, changes in the thermal conductivity of the soil radially surrounding the pile have a significant impact on performance. The study also found that connecting four U-pipes in parallel instead of in series had little effect on the pile's thermal performance, resulting in a temperature difference of only 0.02 °C. The pile's ability to extract/reject heat was, however, significantly reduced when the distance between the U-pipe legs was reduced.

Ghasemi-Fare and Basu [47] developed an annular cylinder heat source model for a single geothermal pile that uses the explicit finite difference method to calculate the change of temperature within the radial and axial pile/soil regions. At the pile's center, a symmetry condition is applied, and only one U-pipe leg is modelled. To preclude thermal interference, adjacent U-pipe leg interactions are ignored. Because the pipe wall thickness is assumed to be negligible, heat transfer through the pipe wall is also not modelled. The model does, however, take into account the heat capacities of the fluid, grout, and soil, performing accurately when using a short-time step. Heat transfer within the fluid is only modelled in the axial direction. Ground water flow is also neglected. The authors stated that the model showed good agreement during field testing, but the duration of the validation period was only 3 hours and the resulting circulation tube vicinity temperature was about 1 °C lower than the reference temperature. The model is capable of accounting for non-homogenous pipe/soil material conditions. When applying the finite difference scheme, initial boundary conditions, such as ground surface (top boundary), bottom boundary, and far-field

(radial boundary) temperatures, are given as node temperature values. As a consequence, variable surface temperatures can be used in the model, and this is very important when modelling the thermal interface between the energy pile and floor structure. A sensitivity analysis of this model revealed that the energy output of the modelled pile depends primarily on the temperature difference between the inlet fluid temperature and soil temperature, soil thermal conductivity, and the size of the circulation tube/pipe.

A number of temperature fields are calculated using the finite difference method in the Equa IDA-ICE borehole model [8] before being superimposed to create the three-dimensional field. The model supports temperature gradient and borehole inclination inputs. Each borehole's thermal behavior is first calculated in multiple borehole configurations. The separate impacts of the boreholes on the ground's temperature are then combined by superposition. While ignoring the thermal mass of the pipe material, the model is capable of performing short time-step calculations and accounting for thermal interference between adjacent boreholes, and the thermal capacitance of the ground, borehole fluid, and filling material. The model also accounts for heat transfer between the U-pipe, the upward and downward flowing liquid, the grout, the ground, the ground surface, and the ambient air. The boundary condition of the ground surface can change over time. Only the U-pipe configuration of GHE is supported by the model, but the user can specify the precise number of U-pipes to be placed inside a borehole. The length of each pile is assumed to be equal and the ground, uniform, while ground water movement is neglected.

2.3.4 Finite volume method

Yavuzturk and Spitler [29] developed a finite volume model in two dimensions. Based on internal components and borehole geometry, their model automatically creates a computational grid. G-function values for the analytical solutions of Yavuzturk and Spitler were computed using this model.

In both two and three dimensions, He et al. [26] used the finite volume approach to model a borehole heat exchanger. The two-dimensional model represented a one meter deep cell in a three-dimensional model. These models were created in an environment known as the general elliptical multi-block solver in two or three dimensions [48] (GEMS2D/3D). Boundary fitted grids in GEMS2D can conform to complex geometry without further simplifications, in contrast to the grids used in finite difference models. The ability to model fluid dynamics and fluid transport along the pipe loop are two benefits of using a three-dimensional model. It is also possible to model the variation in fluid, borehole, and ground temperature along the borehole depth. Different soil and rock layers can be described using their thermal properties. Boundary conditions at the surface dependent on the climate can be applied. Finally, it is possible to explicitly consider heat transfer below the borehole and to apply initial vertical gradients in the ground temperature. The potentially long computational time demanded by this highly detailed model is, however, a significant drawback.

2.3.5 Finite element method

To simulate transient heat and mass transfer in the soil surrounding boreholes coupled with a ground source heat pump, Muraya [27] introduced a two-dimensional finite element model for a borehole heat exchanger. The model analyzes water advection heat transfer as well as the effects of soil moisture content and grout type on pile thermal performance.

Kohl et al. developed a three-dimensional finite element model [49]-[50] for a borehole heat exchanger using the 3D Finite Element Program FRACTure. According to Signorelli et al. [51], this model is capable of accounting for hydraulic, thermal, and elastic processes in transient conditions.

While finite element models are well-known for their lengthy computation times, they can nevertheless take into account complex configurations of fluid circulation piping, the uneven thermal loading of different U-pipe legs, and non-homogenous ground and backfill due to the specifics of the grid scheme.

Using the finite element method in COMSOL software, Gashti et al. [52] numerically modelled five different single energy pile cases. The model demonstrated satisfactory agreement when validated against 28 days of experimental measurement data. COMSOL makes it possible to model ground water advection, but there was no significant ground water flow in the measurement area. The study's objective was to assess thermal regimes generated by pile operation in heating/cooling mode during the investigation of mechanical behavior, where the pile operates in the cooling mode as a heat sink for a solar collector. Since heat is typically extracted from the ground for heating purposes, lowering system performance over time, solar collectors are used with a ground source heat pump with energy piles in Finland's cold climate to maintain an energy balance between heat extraction and rejection [53]. Research showed that some minor temperature differences of up to 1.5 °C appeared in the heating mode of an energy pile. In the cooling mode, however, there were temperature variations of up to 15 °C in the pile shaft's first meter and about 11 °C in the pile's lower end beneath the U-curve spot. This indicated the necessity for additional research into the mechanical behavior of the pile. Given that most finite element analysis software produces results that are typically displayed graphically, this type of modelling is useful for in-depth examination of individual elements over shorter time periods despite the high modelling effort and lengthy simulation times.

Using the finite element program Lagamine, Dupray et al. [54] modelled a field of energy piles in contact with a floor slab. They reduced a complex three-dimensional problem to a two-dimensional one, modelling the thermo-hydro-mechanical behavior of energy piles while ignoring their internal components. The initial boundary conditions for the temperature of the ground and floor were constant. The clayey soil had no water flux and was completely saturated. The change in water pressure in soil pores was modelled. Each modelled pile was subjected to a mechanical load of 3 MPa, which is equivalent to the mechanical system of an average building. To further investigate the effects of high temperature thermal storage on the thermal and mechanical performance of energy piles, they carried out a parametric study using different heat extraction/rejection scenarios over the course of a five-year simulation period. According to the

study, the initial ground temperature rose by about 13 °C with an injection rate of 245 W/m and an extraction rate of 225 W/m. The efficiency loss per extra °C in the average storage temperature was only 1.4%. It was also discovered that it is important to look at a pile group and not just a single pile when studying thermo-mechanical behavior. From a mechanical perspective, use of high temperature thermal storage may impact a pile's bearing function. For this reason, thermal stresses should be accounted for in pile design, since both heating and cooling trigger measurable changes in soil conditions.

2.4 Sizing and design of geothermal energy piles

Design and installation guidelines, sizing manuals, and major available literature are related to boreholes and not energy piles. The design and installation guidelines frequently refer to a standard or sizing manual or suggest using specialized software to perform a detailed numerical calculation to size the GSHP system. While manuals use more intricate analytical sizing procedures, standards use simplified graphical/tabular data. Most simplified methods have very strict limitations and are mainly suitable for small scale systems, ensuring heating with design loads of up to 45 kW. Standards from Austria [55], Germany [56], Switzerland [57], and the UK [58] all employ similar techniques. The German VDI 4640 [56] gives an example of the limitations of standards, stating that precise sizing is only possible for individual borehole lengths between 40 and 100 m, while the UK standard MCS MIS 3005 [58] requires a minimum spacing between adjacent boreholes of at least 6 m. Sizing is performed for a fixed number of heat pump operation hours (e.g. in VDI 4640 for 1800 or 2400 h/y) based on established heat extraction rates that vary with soil/rock type and its thermal conductivity. As a result, sizing data in standards is bound to local climate conditions and in most cases may only be applicable in the country of origin.

The GSHPA [59] energy pile design and installation guide suggests using MCS MIS 3005 as a guide to sizing energy pile systems up to 45 kW or else hiring a GSHP designer, who would use special software. Similarly, Brandl [7], [60] highlights how important it is to use sizing software to perform calculations when evaluating the performance of specific energy pile fields.

The IGSHPA [61] borehole design and installation guide suggests following the ASHRAE [62]-[63] sizing manual when designing borehole heat exchangers. The IGSHPA [61] and ASHRAE [62]-[63] manuals provide instructions for the analytical sizing of boreholes based on the cylindrical source model (CSM). These are useful in the preliminary design phase when sizing larger complex borehole systems, but they recommend carrying out further more detailed simulations using sizing software.

One important factor that is rarely addressed in manuals and standards is the heat pump sizing ratio. MCS MIS 3005 proposes sizing the heat pump to 100% of the design heat load. However, it is common practice in some countries, such as Finland or Estonia, to size the heat pump to account for 50–60% of peak heat demand, with auxiliary heating covering the remaining peak load. This minimizes the investment cost of the heat pump, as a heat pump sized for 60% of the

design heat load is still capable of covering more than 90% of the annual heating need for a building during the test reference year (TRY) [64].

The abovementioned constraints make it difficult to apply existing borehole-related standards and manuals when sizing energy piles because of the differences in the geometry and boundary conditions of piles and boreholes. However, a new sizing procedure tailored specifically to energy piles may be developed in future research using the ASHRAE analytical sizing procedure as a template.

The equations and a more thorough explanation and comparison of the standards and manuals are provided in [65]. A hypothetical (ca 70 m²) UK home was used by Sailer et al. [65] to compare the abovementioned sizing techniques. Results showed that use of the standard/manual method can lead to a variation in sized borehole length of over 40%. Simplified methods based on the standards used very limited input data to describe the system, and Sailer preferred the ASHRAE analytical sizing procedure, which is capable of accounting for more detailed borehole geometry, borefield layout, the thermal properties of materials, and multiple U-pipe configurations. Use of the ASHRAE analytical sizing procedure with the same initial input data as MCS MIS 3005 resulted in a calculated borehole length of 173 m, almost the same as that calculated using the latter standard, 168 m.

Most sizing and design software currently on the market focuses specifically on boreholes, though some may also be used as a tool for the design and sizing energy piles. Table 6 compares the features of different software solutions.

Table 6. Sizing and design software (Publication 1).

Product	Model	Variable floor surface temperature boundary	Coupling with whole building simulation	Loads input		Thermal storage				Heat pump		Pile location by (X,Y)
				Hourly	Monthly	Solar	Cooling tower	Exhaust air	Simplified[6]	Fixed SCOP	Dynamic	
EED [66],[67]	g-funct				✓[3]				✓	✓		
GLHEPro [68],[69]	g-funct		✓[5]		✓[3]				✓		✓[4]	
TRNSYS DST [11]	DST	✓	✓	✓		✓	✓	✓			✓	
TRNSYS EWS[7] [70]	FDM	✓	✓	✓		✓	✓	✓			✓	
Program EWS [71]	FDM	✓		✓					✓	✓		✓
GLD [72]	CSM+g-funct				✓[3]				✓		✓	✓
PILESIM2 [73],[74]	modified DST	✓[1]		✓					✓		✓	
IDA borehole [8]	FDM	✓	✓	✓[2]		✓	✓	✓			✓	✓

[1]building floor domain is separated from outdoor ground surface domain by the input of different variable temperatures
[2]calculation step can be less than an hour
[3]peak load value and duration during each month can be defined
[4]curve fitting is applied to describe heat pump performance
[5]g-function export to HVACSIM+
[6]simplified accountancy for thermal storage in the form of additional heat extraction/rejection load data
[7]single pile only

Depending on the model used, the commercial software shown in Table 6 falls into one of two primary categories - analytical and numerical. The GLD, GLHEPro, and EED software packages use analytical models, while the rest, EWS, IDA ICE with borehole model extension, TRNSYS with DST model extension, TRNSYS with EWS model extension, and PILESIM2, use numerical models.

The analytical response factor models used by EED, GLHEPro, and GLD support the fewest of the features highlighted in Table 6. This response factor, also

known as the g-function, is typically calculated numerically and used to describe the temperature response of a particular borefield configuration. Precalculated g-functions of various borefield configurations are stored in software databases. As a consequence, EED and GLHEPro software databases may not, for example, have the g-function characterizing the pile field configuration for a building with a pile foundation where the piles are arranged chaotically, according to the foundation plan. The response factor-based software GLD, on the other hand, offers the ability to compute and apply the g-function based on the user-specified location of the piles in a two-dimensional Cartesian coordinate system. The precise pile location in relation to the foundation plan can only be defined in IDA ICE and EWS when using numerical model-based software.

Software that cannot be coupled with whole building simulation software requires the user to enter data on building heating and cooling demand in either an hourly or monthly time-step resolution, according to the capabilities of the software. Building heating and cooling demand data can only be handled by analytical response factor software packages with a monthly time-step resolution, while peak loads are defined as hours per chosen month. Unlike the analytical model-based software, all of the numerical model-based software packages in Table 6 can accept a time-step of an hour or less. GLHEPro is the only response factor-based software that can be integrated with a whole building simulation, while the g-function can be exported to HVACSIM+. Both TRNSYS and IDA ICE support whole-building simulation. Thus, numerical component models for IDA ICE and IDA borehole and for TRNSYS - EWS and DST can be coupled with a whole building simulation model.

Heat pump load data is generated by the software from user-defined or whole building simulation heating/cooling demand data. Heat pump performance can be expressed using a fixed SCOP value or the dynamic heat pump model, depending on the software package. The heat pump model can be based on a performance map and include a physical heat exchanger model, or it may even be the result of simple curve fitting. A heat pump in most software packages operates as an ideal capacity-controlled heat pump with a part load in the range of 0...100%, which is comparable to that of a real-world inverter-controlled heat pump, which can operate at part loads as low as 20%. Many large heating/cooling plants are, in fact, not built to run at part load but rather at full load exclusively, i.e., with ON/OFF control. The duration of each heat pump operation cycle depends mainly on actual heat demand and fluid volume in the system. As a result, the efficiency of capacity-controlled heat pump operation can vary significantly from that of ON/OFF heat pump operation. Both IDA ICE and TRNSYS software packages are capable of modelling ON/OFF operation.

Thermal interference between adjacent piles is due to the restricting of the quantity and arrangement of the energy piles by the foundation plan. Thermal storage is typically used in GSHP plants to boost yields and stabilize long-term performance. To accommodate different thermal storage sources or combinations of them, the software has to provide an option to use component models and allow custom plant modelling. Custom plant modelling is supported by the

numerical model-based software packages IDA ICE and TRNSYS, which provide component models for different thermal storage sources. The rest of the software listed in Table 6 only allows a more basic accounting of thermal storage through the manipulation of heat extraction/rejection load data, e.g., by assuming that storage will produce a specific amount of energy each month and then adding this amount of energy to the heating/cooling demand input data. Wood et al. [66] examined the mean fluid temperatures of an energy pile field during a heating season using both measured temperatures and the temperatures that were computed using EED response factor software. The measured mean fluid temperature was consistently about 2 °C higher than that predicted by the EED software since pile thermal capacitance is not considered by g-functions. This underestimation of mean fluid temperature would lead to a roughly 40% reduction in the actual system heat extraction potential for climate regions with a low mean annual soil temperature (e.g., 5 °C). As a consequence, using response factor-based borehole sizing software for energy piles seems less advantageous than using the numerical model-based software discussed in this section.

Using the IDA ICE software package and the IDA borehole model extension, Fadejev and Kurnitski [8] modelled the geothermal plant of a commercial hall-type building coupled with boreholes and energy piles. There were differences in the ground surface boundary conditions of the energy piles and boreholes. The soil surface of the energy piles was beneath the floor slab, while the borehole field was left open to the surrounding air. The initial soil temperature in both cases was 8 °C. The dimensions of the pile and borehole fields were the same - 115 mm in diameter, 15 m in depth, 4.5 m spacing, and 196 units overall. The energy piles were modelled without taking into account the actual geometry of the building floor since the entire ground surface domain was considered to be the floor. The validity of these assumptions is supported by Chuangchid and Krarti's study of a simulated winter case where the building had an uninsulated slab [30]. Results showed that the soil temperature in the building section view started to decrease drastically at about 2 m from the edge of the floor slab, reaching its lowest values at the edge of the floor slab. The energy pile modelling approach of Fadejev and Kurnitski [8] is suitable for piles located further than 2 m from the edge of the floor slab, as the initial temperature conditions of such piles are roughly the same as those at the center of the slab. According to the findings of the study, temperature variations in the soil affected the intensity of floor heat loss, and simulation results revealed that a geothermal plant with energy piles performed about 23% more efficiently than plants with boreholes. In the case of energy piles, soil temperatures greater than the initial 8 °C were observed during the winter below the soil surface (floor slab) boundary, down to a depth of about 12 m. However, due to direct exposure to the cold winter air, soil temperatures near the soil surface boundary in the borehole case were lower than the initial 8 °C soil temperature. As soil surface temperature has a significant impact on plant performance, it is important to account for heat transfer through the floor structure when sizing GSHP systems with energy piles. Software that supports variable surface temperatures makes this more practicable. The software based on numerical models named in this thesis all support this

feature. This makes response factor-based software then the least effective in sizing energy piles, as numerically determined g-functions are obtained using adiabatic ground surface boundary conditions, neglecting heat transfer through the floor structure and variability in floor surface temperature.

PILESIM2 software has two variable surface temperatures due to the building floor domain being separated from the ground surface domain, which is exposed to ambient air. However, according to the software manual [74], the precise geometry of the building floor cannot be defined. Building floor geometry in PILESIM2 is determined by the number of piles and the distance between them. In PILESIM2, piles are located in a circular storage volume, and their exact location cannot be defined. According to the software manual [74], PILESIM2 is not intended for the simulation of a single pile or piles arranged in a line, but rather the simulation of systems that have a relatively large number of energy piles in a square or circular field. An older version of PILESIM was used in the design of the geothermal plant of the E-terminal of the Zürich Airport. The current version of PILESIM2 was developed using field measurement data for built energy pile systems [10], with changes principally affecting the geocooling module of the software.

Numerical and analytical modelling software differ in modelling accuracy, required computational time, ability to define the exact location of piles, and dynamic heating/cooling plant modelling capabilities. When it comes to very large energy pile fields, response factor-based software can plot the results of a 25-year period simulation instantly, while numerical software might take days to complete the same simulation [53]. Nevertheless, most numerical model-based software is generally more accurate and able to take into account sub-hourly time steps and the exact locations of energy piles, and it can be coupled with whole building simulation software, allowing the modelling of more complex dynamic heating/cooling plants. At the same time, the learning curve for numerical model-based software with custom plant modelling capabilities such as IDA ICE and TRNSYS is considerably longer.

3. Methods

This chapter presents the research methodology. As a first task, the systematic literature review (Publication 1) in the preceding chapter was carried out to address the research question on the main concepts, approaches, and methods involved in the design, modelling, and sizing of GEPs. This literature review identified the need for validated modelling and sizing methods for GEPs.

To justify this need, the next step, covered in Section 3.1, was to develop a detailed modelling method for GEPs (Publication 2) and investigate the key differences between borehole and GEP modelling.

This leads to validation of the developed GEP modelling method (Publication 3) in Section 3.2, to address the research question related to the validation of variables and their relationships.

Section 3.3 looks at the designing of an actual commercial NZEB hall-type building and the use of its measurement data for as-built model calibration and energy analysis, with the aim of demonstrating the performance of the proposed GEP modelling method, answering the research question related to its usefulness and accuracy when designing an NZEB in Finland, and highlighting the main lessons learned (Publication 4).

Finally, Section 3.4 presents a parametric study of GEPs and a GEP sizing method for use in the early stages of design (Publication 5), to address the research question on how to facilitate the work of engineers in the early stages of design when sizing GEP systems.

3.1 Detailed modelling of GEPs and boreholes

This section addresses the key differences between GEP and borehole modelling. The methods involved in the proposed GEP modelling method (Publication 2) are presented here.

A commercial hall-type building coupled with a heat pump plant using GEPs or boreholes as a GHE was modelled using IDA ICE. The modelling in IDA ICE was performed using an advanced interface which allows the user to manually edit the connections between the model's components, modify and log its unique parameters, and view the model's source code. In total, two plant variants were modelled, one for buildings with GEPs and one for buildings with a BHE field (see Figure 7).

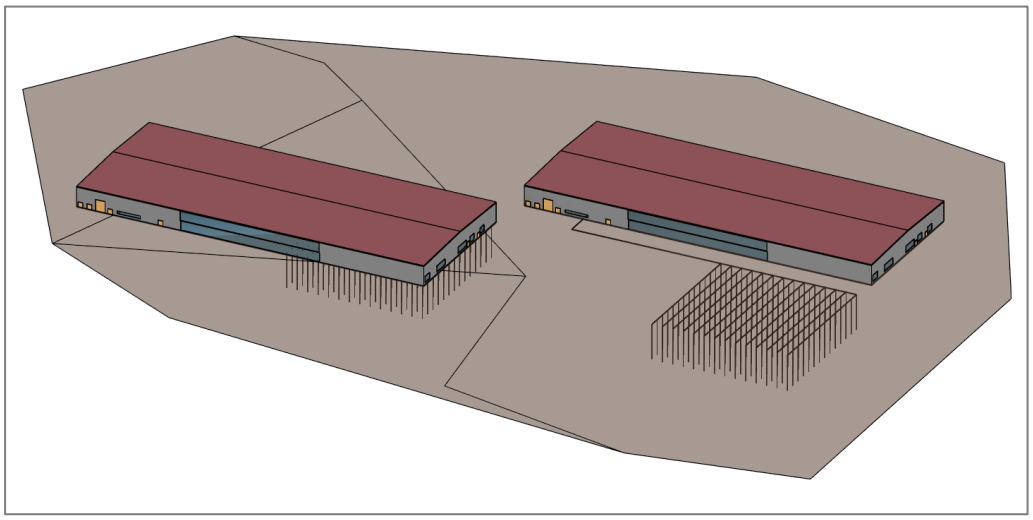

Figure 7. A building with GEPs (left) and a building with a BHE field (right) (Publication 2).

3.1.1 Building model description

The commercial hall-type building that was modelled was located in the cold climate of Helsinki, Finland. The climate data used in the simulation was obtained from the Helsinki TRY climate file [64].

The building's heating and cooling demands were met using radiant heating/cooling panels, which are standard components in the IDA ICE model library. The performance of radiant heating/cooling panels is characterized using the power law coefficient and exponent values. Table 7 provides a complete overview of the parameters used to characterize the building model.

Table 7. Overview of building model parameters (Publication 2).

Descriptive parameter	Value
Location	Finland
Net floor area, m^2	9119.5
External walls area, U = 0.16 W/(m^2 K), m^2	2552
Roof area, U = 0.15 W/(m^2 K), m^2	9123
External floor area, U = 0.09 W/(m^2 K), m^2	9120
Window area, SHGC = 0.51, U = 0.97 W/(m^2 K), m^2	726
External doors, U = 0.97 W/(m^2 K), m^2	89
Heating set point, °C	18
Cooling set point, °C	25
Occupancy/lighting schedule	8:00-21:00
AHU operation schedule	7:00-22:00
Occupants, 1.2 met, 0.8 clo, no	213
Lights load, kW	72.9
AHU air flow, m^3/s	10.1
AHU heat recovery, %	80
Air tightness, ACH	0.3 @50 Pa
Supply air temperature, °C	18
Radiant heating/cooling panels, b = 1.2m, m	750
Heat load design temperature, °C	-26
Design heat load, kW	463
Heat pump capacity, kW	172

3.1.2 Heat pump model description

The heat pump was sized to cover 40% of the building's design heat load at a design ambient air temperature of -26°C. The remaining peak load was expected to be covered by electrical top-up heating. The heat pump was modelled using a brine-to-brine heat pump model from the standard IDA ICE component library. This model consists of a compressor performance model and a heat exchanger model [75]. The condenser and evaporator of the heat pump are included in the heat exchanger model, which is based on the NTU-method. The heat pump model can operate under full or partial load. The use of an "ON/OFF" heat pump was considered. A detailed mathematical model including equations describing the heat pump are presented in Publication 2.

The values of the parameters used as settings in the heat pump model, to ensure it performs according to the manufacturer's performance map, are presented in Table 8.

Table 8. Overview of heat pump model parameters (Publication 2).

Descriptive parameter	Value
Nominal capacity at rating, kW	171.2
Coefficient of performance at rating, COP	4.65
Evaporator LMTD at rating, $\Delta Tlogevapdim$, °C	3
Condenser LMTD at rating, $\Delta Tlogconddim$, °C	5
Evaporator inlet temperature at rating, T_{evapin}, °C	0
Evaporator outlet temperature at rating, $T_{evapout}$, °C	-3
Condenser inlet temperature at rating, T_{condin}, °C	30
Condenser outlet temperature at rating, $T_{condout}$, °C	35
Calibration parameter B, %	3.21
Calibration parameter C, %	-1.6
Calibration parameter E, %	0.72
Calibration parameter F, %	1.97

A total of eight parameters are used to describe the performance of the heat pump at rating. These can be taken from the heat pump performance map (Figure 8). The user must calculate the B, C, E, and F calibration parameters for the heat pump model so they match the values in the manufacturer's performance map.

The equations used to calculate the heat pump model calibration parameters were derived from the open-source code of the IDA ICE heat pump model. A calculation example is presented in Publication 2.

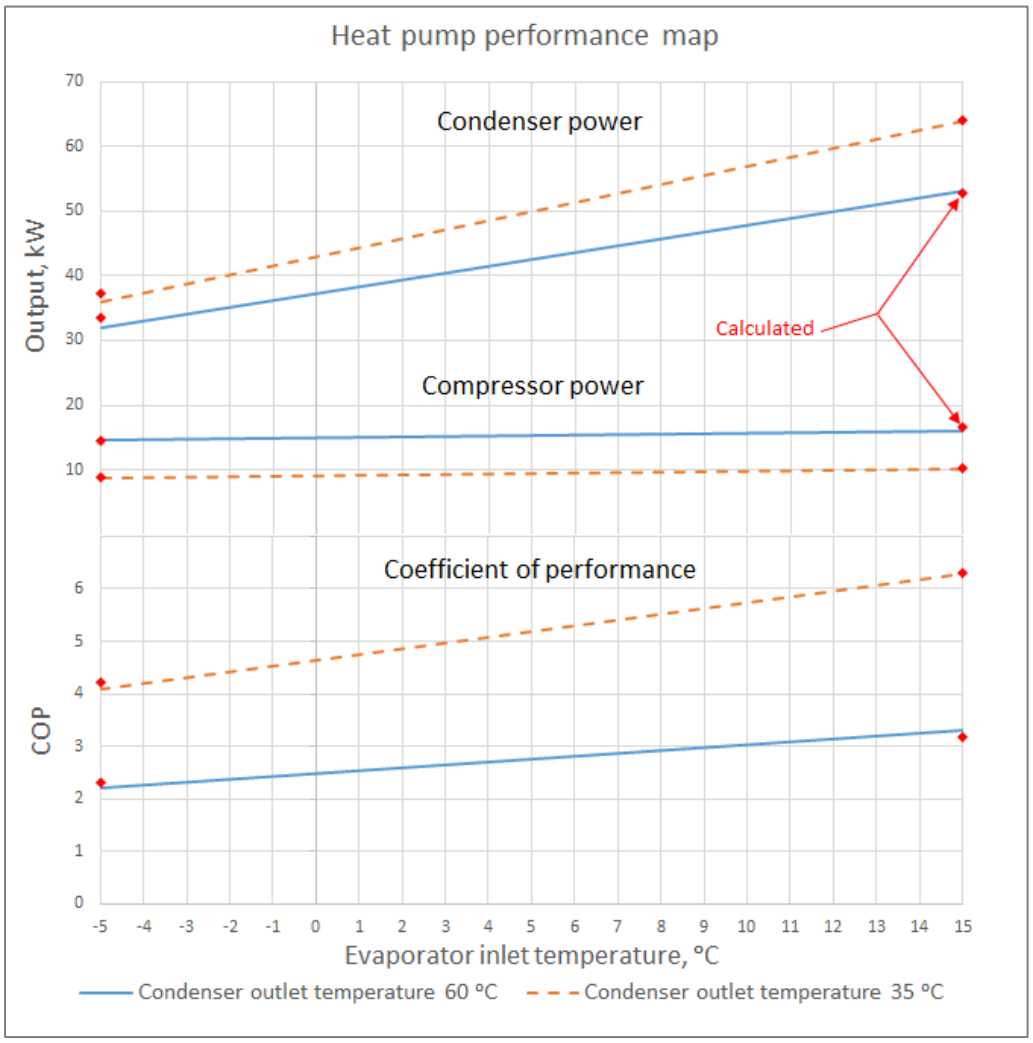

Figure 8. Heat pump performance map. Solid and dashed lines show manufacturer specifications. IDA-ICE heat pump model output is shown with markers for selected points (Publication 2).

3.1.3 Borehole model description

The IDA ICE borehole model extension was used to model the boreholes in the GEP and BHE field plant variants [76]. In both cases, a total of 196 boreholes (Figure 9) were modelled. The three-dimensional field was created by superimposing a number of temperature fields calculated using the finite difference method in the borehole model [77]. For each borehole, the following temperature fields were calculated [76]:

- One-dimensional heat transfer for both upward and downward liquid flow in a U-pipe;
- One-dimensional heat transfer between grout, liquid, and ground;
- Two-dimensional heat transfer between grout and liquid in cylindrical coordinates around the borehole.

A one-dimensional heat transfer equation was also used to compute an undisturbed ground temperature field by using the heat transfer coefficient with the

ambient temperature at the ground surface. The model supports inputs for temperature gradient and borehole inclination. The actual ground temperature at the borehole wall is calculated using superposition. In multiple borehole configurations, the thermal behavior of each individual borehole is first calculated. The impact of each borehole on ground temperature is then combined using superposition [76].

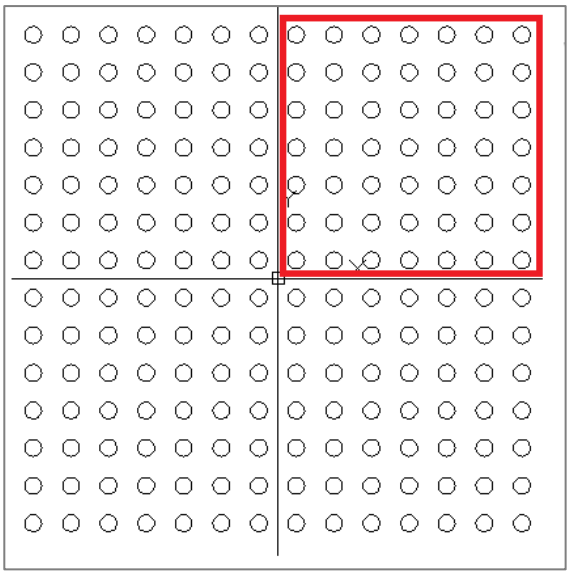

Figure 9. GEP/BHE field layout, dimensions are 58.5 x 58.5 m and the distance between piles, 4.5 m (Publication 2).

The model can operate with a short time step and take into account thermal interference between adjacent boreholes and the thermal capacitance of the ground, borehole fluid, and filling material, while ignoring thermal mass of the pipe material. Heat transfer between the U-pipe, upward and downward flowing liquid, the grout, the ground, the ground surface, and ambient air are all considered in the model. It also allows for change in the boundary conditions of the ground surface over time. Only the U-pipe configuration of the GHE is supported by the model, and it allows the arrangement of a user-specified number of U-pipes inside a borehole. The ground is considered to be homogeneous, the length of each pile, equal, and ground water movement is not taken into account. A detailed mathematical model and the equations used in the IDA ICE borehole model [76] are presented in Publication 2.

The model offers an option to mirror (Figure 10) a portion of the domain results to shorten the simulation's runtime in case there are many boreholes. By using mirror option 2 (Figure 10), only 49 of 196 boreholes had to be defined in the borehole model.

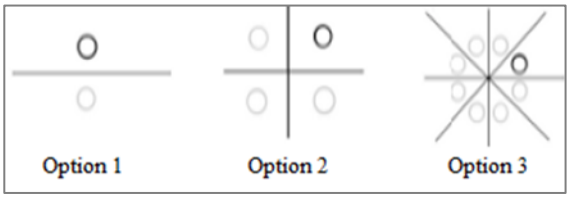

Figure 10. Borehole field mirroring (Publication 2).

The parameters characterizing the thermal and physical characteristics of the ground, pipe, grout, and brine (Table 9) must be provided by the user.

Table 9. Overview of borehole model parameters (Publication 2).

Parameter	Value
Borehole number, pcs	196
Borehole depth, m	15
Borehole diameter, mm	115
Distance between boreholes, m	4.5
Pipes outside walls distance, mm	52.4
U-pipe outer diameter, mm	25
U-pipe inner diameter, mm	20.4
Ground heat conductivity, W/(m K)	1.1
Ground volumetric heat capacity, kJ/(m^3 K)	2019
Ground average annual temperature, °C	8
Borehole grouting heat conductivity, W/(m K)	1.8
Grout volumetric heat capacity, kJ/(m^3 K)	2160
Pipe material heat conductivity, W/(m K)	0.3895
Pipe volumetric heat capacity, kJ/(m^3 K)	1542
Brine ethanol concentration, %	25
Brine freezing temperature, °C	-15
Brine heat conductivity, W/(m K)	0.43
Brine volumetric heat capacity, kJ/(m^3 K)	4023
Brine density, kg/m^3	969
Brine viscosity, Pa s	0.006
Borehole thermal resistance, (m K)/W	0.1
Heat transfer coefficient at ground surface, W/(m^2 K)	0.15
Prandtl number	58

In the BHE field plant variant, because the ground surface is exposed to the ambient air, a ground surface temperature variable was combined with an outside air variable in the borehole model. The ground surface heat transfer coefficient describes the rate of heat transfer between the ground surface and the ambient air.

In the GEP plant variant, however, the ground surface above the energy piles was covered by the floor slab. The modelled building is located in the cold Finnish climate, where the average annual ground temperature is about 8 °C and the set point for indoor air temperature during the heating season is 18 °C. Large temperature differences between the ground and surface of the floor slab cause natural heat loss from the floor to the ground, raising the temperature of the ground.

When using GEPs in a building, the GSHP extracts heat from the ground during the heating season until the fluid entering the evaporator reaches a temperature below 0 °C. The heat pump can operate for longer periods and energy piles can extract more heat thanks to the rise in ground temperature brought on by the floor's heat loss to the ground. Because the GSHP cools the ground during the heating season, the average ground temperature is significantly lower than for a building without GEPs, resulting in higher annual floor heat loss than in a building without GEPs.

The performance of the BHE field and the GEP plants will thus differ significantly. Therefore, it is crucial to model the connection between the floor slab and borehole model in the GEP plant. Given that the IDA ICE borehole model

was created primarily for the simulation of borehole fields rather than GEPs, some additional known modeling limitations cannot be ignored.

To model the GEP plant variant, the ground surface temperature variable in the borehole model was combined with the surface temperature variable in the 58.5 x 58.5 m zone slab model. Both the slab and borehole models define the slab structure. The slab model defines the floor structure as layers of material with thermal properties. In the borehole model, the definition of an insulated slab is represented by a ground surface heat transfer coefficient with a value equivalent to the slab's thermal transmittance.

Using the difference between the two temperatures, that of the floor surface and that of the ground surface, the zone slab finite difference model in IDA ICE calculates the heat flux. By default, the IDA ICE ground model, which is not connected to the borehole model, calculates the ground surface temperature. As a consequence, a connection between the slab model the borehole model is required.

However, the version of the borehole model implemented at the time of the study was not capable of calculating the ground surface temperature, which was an input variable. Therefore, the ground surface temperature variable in the zone slab model was linked to the borehole outlet temperature parameter. In this way, the effects of heat conduction through the floor structure on the ground temperature and vice versa were modelled. The connections between the zone floor structure model and the borehole in the plant variant with GEPs are shown in Figure 11.

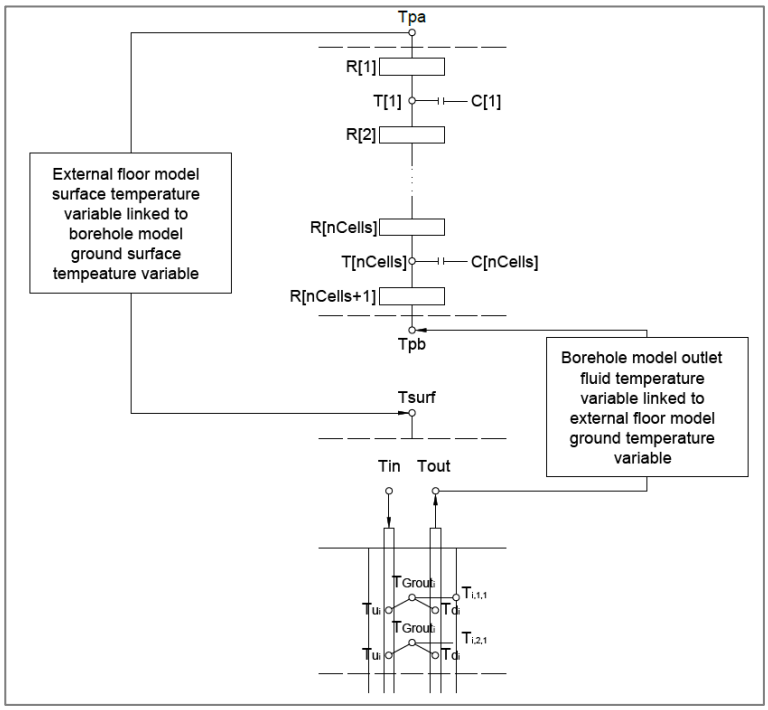

Figure 11. Scheme of links between borehole model and external floor model (Publication 2).

It should be noted that the rough estimation of the intensity of heat conduction through the floor structure is a known limitation of the GEP plant variant. This is due to the fact that the borehole outlet fluid temperature is used as the

ground surface temperature. Another known limitation is that the floor surface temperature is assumed to be constant throughout the domain of the energy piles. In reality, the temperature at the slab edges in contact with the soil is different from the temperature at the center of the floor. As a consequence, the model will overestimate the natural thermal storage effect caused by heat conduction through the floor structure when simulating a case where the energy pile field is located close to the perimeter of the building.

To reduce this effect, energy piles must not only be placed near the center of the floor but also have a relatively short length compared to the slab's width. The error caused by these conditions is further quantified in Sections 3.2 and 4.2, respectively.

Model input values that must be calculated by the user are borehole thermal resistance and the Prandtl number. Thermal resistance is calculated using equation [78] as follows:

$$R_b = \frac{1}{2\pi k_g} \ln\left(\frac{d_b}{d_p\sqrt{n}}\right) \quad (3)$$

The Prandtl number is calculated using the following equation:

$$Pr = \frac{C_p \mu}{k} \quad (4)$$

More information about borehole model input parameters and values used in the modelling is provided in Table 9.

3.1.4 Geothermal heat pump plant modelling

The detailed heating/cooling plant model (Figure 12) includes a brine-to-brine heat pump coupled with a GEP or BHE field. The heat pump's condenser side is connected to the stratification tank (hot). To meet the peak heating loads of the building, an additional electric boiler, known as top-up heating, is connected to the same tank. The heat pump model uses the performance map data for manufacturer-specific products.

Plant cooling equipment consists of the stratification tank (cold) and a “free cooling” heat exchanger connected to the ground loop to meet the building's cooling demand as required. The plant does not include an active chiller. For the plant to operate optimally according to design intent, several conditions must be fulfilled. The value for the secondary side supply water temperature value will depend on the value for outdoor air temperature, i.e., according to the heating curve (upper left corner of Figure 12).

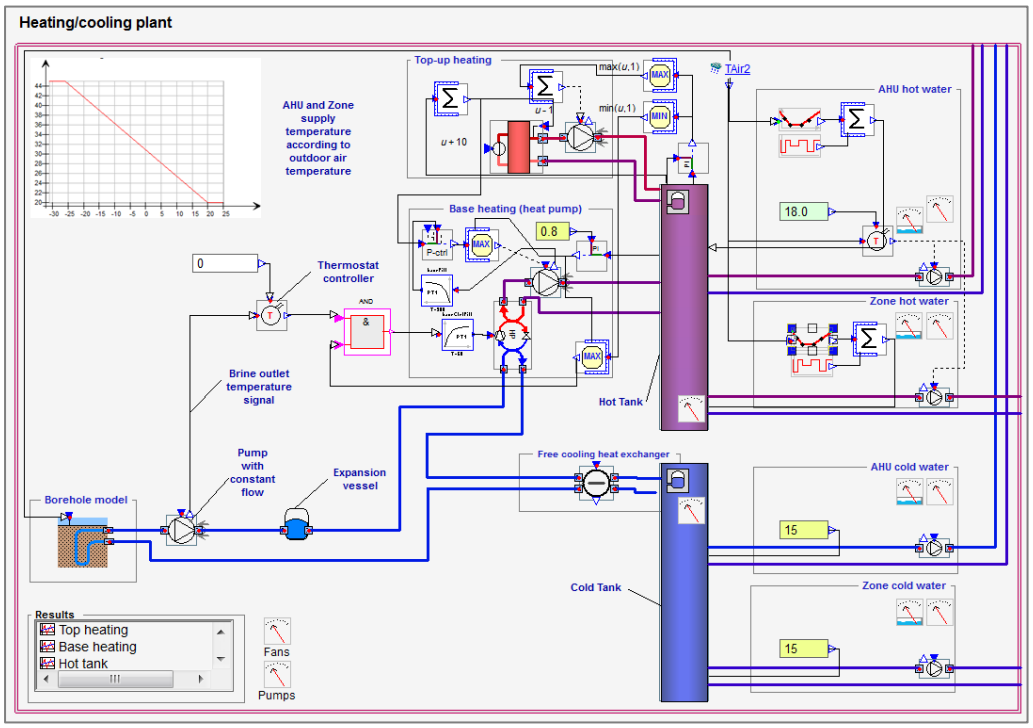

Figure 12. Detailed heating/cooling plant modelled in IDA-ICE (Publication 2).

To prevent ice formation in the underground layers, a thermostat model was applied to switch off the heat pump when the temperature of the brine supplied from the borehole drops below 0 °C. As high-capacity ground-source heat pumps usually lack compressor inverters, a logical on-off controller model was employed to allow heat pump on-off operation (with no part-load capability).

The operation of a plant with the described control logic is presented in Figure 13. The heat pump starts to operate at full load whenever the temperature in the hot tank drops below the set point, according to the heating curve. Whenever the temperature in the hot tank reaches the desired set point or the borehole outlet temperature drops below 0 °C, the heat pump ceases operation.

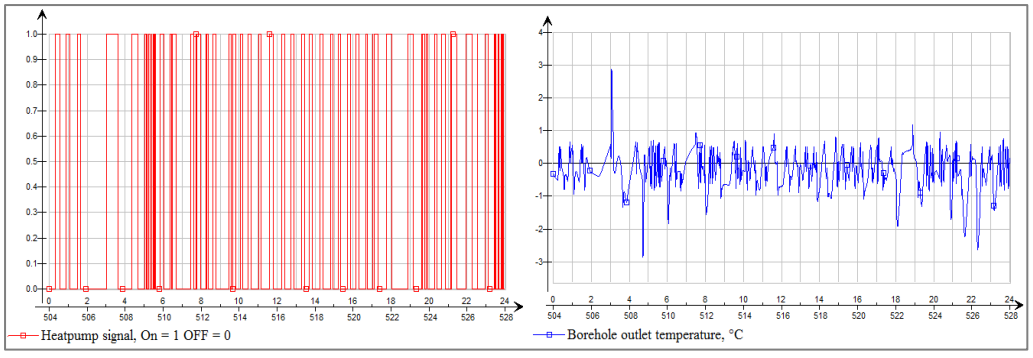

Figure 13. Heat pump modelled operation (Publication 2).

Due to a thermostat deadband of 1 K, the delivered brine temperature occasionally fell below the desired set point. To prevent numerical issues and errors that could prevent the simulation from running, a signal smoother was applied to the control signal. Because of the signal smoother's long integration time, the heat pump continued to operate even when the thermostat controller signaled

an "off" state. As a result, the delivered brine temperature sometimes dropped below the thermostat's deadband, as illustrated in Figure 13.

3.2 Validation of the GEP modelling method

This section addresses the research question related to the validation of variables and their relationships in the GEP modelling method. The methods for validating the developed GEP modelling method (Publication 2 and 3) are presented here.

First, the IDA ICE borehole model was validated against measurement data for a single borehole to assess its performance and suitability for ground heat exchange modelling (see Section 3.2.1). Next, a single pile model was created using the FEM software package COMSOL and validated against measurement data to make it possible to use COMSOL for further validation of the limitations identified in the proposed GEP modelling method (see Section 3.2.2). Then, the limitation of having to assume a constant floor surface temperature throughout the domain of the energy piles was validated using the COMSOL 2D model (see Section 3.2.3). After that, the IDA ICE borehole model was validated against a COMSOL 3D model with multiple energy piles (see Section 3.2.4) to ensure accuracy. Finally, the impact of boundary conditions, where borehole outlet temperature was used in place of the ground surface temperature to model the floor heat losses imposed by the GEP location beneath the floor slab, was quantified (see Section 3.2.5).

3.2.1 Validation of the IDA ICE borehole model

The IDA ICE borehole model was validated in Publication 2 using field measurement data from the energy pile test station located in Hämeenlinna, Finland. The following measurements were taken at the energy pile station and recorded at ten-minute intervals:

- inlet brine temperature;
- outlet brine temperature;
- brine flow rate in the borehole.

Apart from the aforementioned data, ambient air temperature was measured and recorded near the station at one-hour intervals. The validated results apply only to the modeled BHE field case, as the measured borehole was not part of the building foundation, and the ground surface was exposed to ambient air. The validation results may be applied in the GEP case only when bearing in mind the known limitations described in Section 3.1.4.

The measured borehole had a total length of 20.6 meters and was composed of two U-pipes grouted into a steel casing. Using the inlet flow and temperature input variables, the borehole model calculates the brine's outlet temperature. To account for heat exchange between the ground surface and the surrounding air, the model can also be linked to an ambient air temperature variable.

A simple validation environment (Figure 14) was created in IDA ICE to validate the borehole model using measurement data as input for the variables mentioned earlier. The validation process comprised two stages: parameter identification and validation.

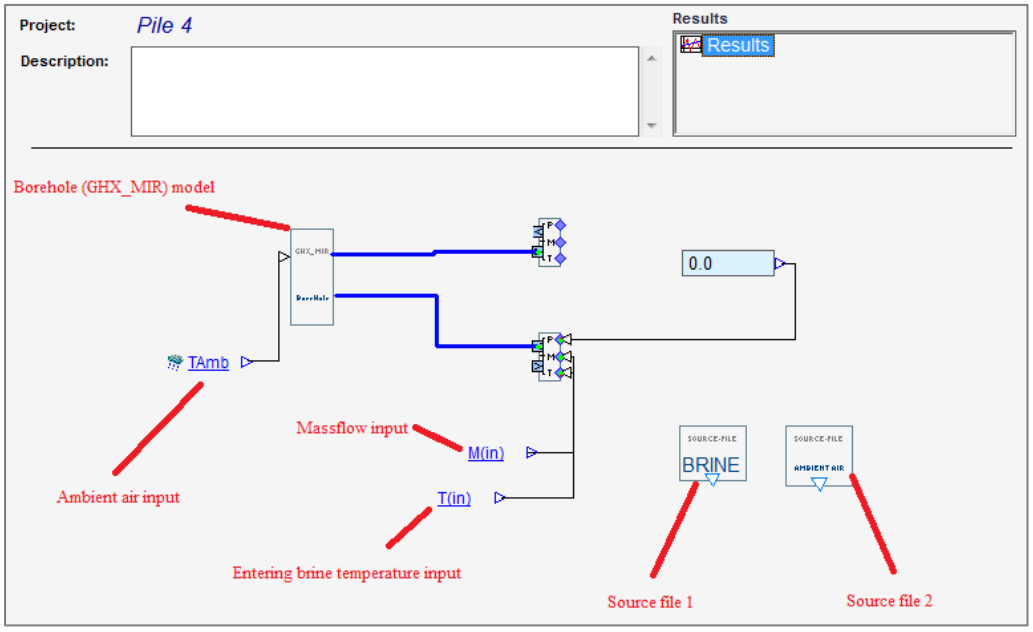

Figure 14. Validation model (Publication 2).

Both the heat extraction (heating) and rejection (cooling) phases of borehole operation were included in the 5000-hour measurement dataset (Figure 15). Because some data were inaccurate due to the fact that the measurement sensors could not record temperatures below 0 °C, error-free intervals had to be selected for the validation procedure. Data on heat rejection was used as input during the parameter identification phase, while data on heat extraction was used as input during the validation phase.

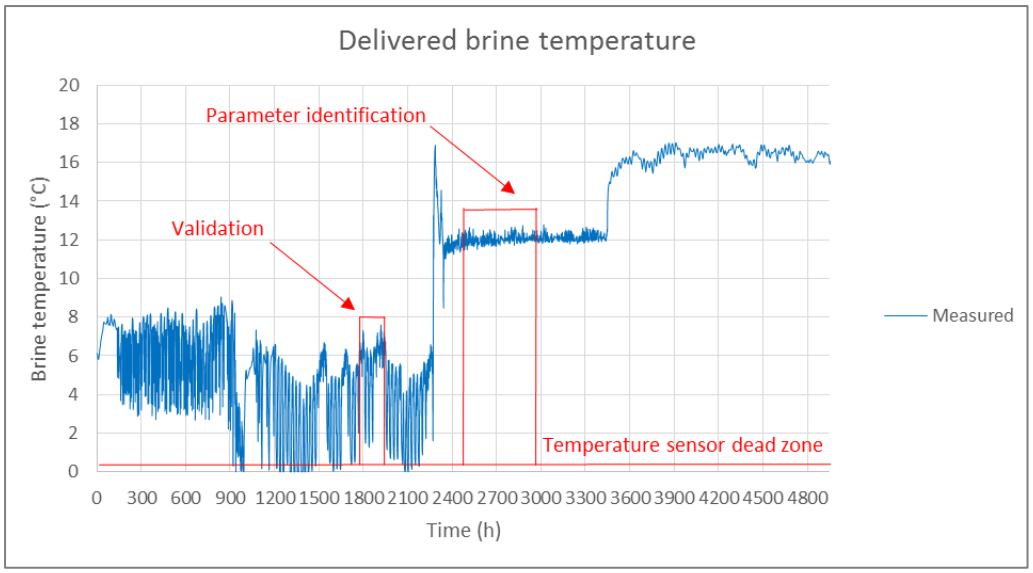

Figure 15. Borehole measurement data (Publication 2).

Measured physical and thermal properties of the ground and borehole (Table 10) were set as constants in the borehole model. Equation 3 was used to calculate the overall resistance of the borehole and to determine the in-situ heat conductivity of the ground using a thermal resistance test. The borehole was not affected by groundwater.

Table 10. Validation settings for borehole model (Publication 2).

Descriptive parameter	Value
Borehole depth, m	20.6
Borehole diameter, mm	170
U-pipe outer diameter, mm	25
U-pipe inner diameter, mm	20.4
U-pipe amount, pcs	2
Ground heat conductivity, W/(m K)	1.8
Ground volumetric heat capacity, kJ/(K m^3)	1488
Borehole grouting heat conductivity, W/(m K)	1.8
Grout volumetric heat capacity, kJ/(K m^3)	2160
Pipe material heat conductivity, W/(m K)	0.3895
Pipe volumetric heat capacity, kJ/(K m^3)	1542
Brine ethanol concentration, %	28
Brine heat conductivity, W/(m K)	0.43
Brine volumetric heat capacity, kJ/(K m^3)	3533
Brine viscosity, Pa s	0.006
Borehole thermal resistance, (m K)/W	0.1
Ground average annual temperature, °C	8.5

The only unknown constant required for validation of the IDA ICE borehole model was the “annual mean ground temperature.” This parameter was identified during the parameter identification phase by applying different values in the IDA ICE borehole model until the simulated rejected heat agreed with the measured value. The resulting “annual mean ground temperature” was then used in the subsequent validation phase. Validation results are presented in Section 4.2.1.

3.2.2 Validation of the COMSOL single pile model

The proposed GEP modelling method in Section 3.1 has known limitations whose impact on calculation accuracy must be assessed to reduce the discrepancies between the simulations and reality. The FEM software package COMSOL Multiphysics can model different limitation scenarios and, when used with actual measurement data, is suitable for performing the validation. For this reason, the validation of the FEM-based numerical simulation of a single energy pile created using the software package COMSOL Multiphysics was necessary and is discussed here.

The first building in Finland to use a pile foundation as a geothermal heat exchanger (GHE) is an office building known as Innova 2, which was built in the summer of 2012 in Jyväskylä. The geothermal heat pump plant is equipped with energy meters, and two out of the 40 energy piles in the foundation (Figure 16) are equipped with temperature sensors along their depth (see [79] for more detailed information on pile construction and plant description).

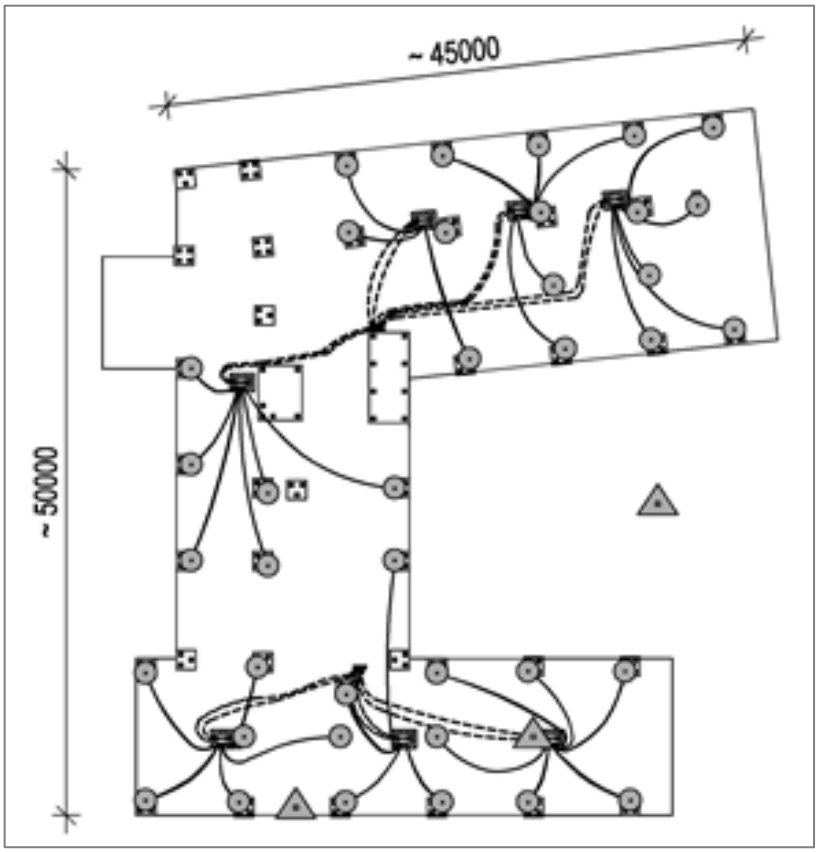

Figure 16. Energy piles (circles) and monitoring layout (undisturbed *T* monitored at the isolated triangle) (Publication 3).

Additionally, a reference energy pile near the building, equipped with 11 sensors along its depth, measured the undisturbed soil temperature, as detailed in Table 11. This isolated energy pile was modelled in COMSOL together with its surrounding soil layers. Temperature was logged according to the locations of sensors on the reference pile. The depth, density (ρ), and thermal conductivity (λ) of each layer were measured on-site [80].

Table 11. Temperature sensor locations on the reference energy pile (Publication 3).

Temperature sensor	Depth, m
Ground surface	0
Pile top	-0.5
T28	-0.5
T29	-2.5
T30	-4.5
T31	-6.5
T32	-8.5
T33	-10.5
T34	-12.5
T35	-14.5
T36	-16.5

As shown in Figure 17, the reference pile was modeled as a 22-m-long concrete cylinder having a diameter of 170 mm, with λ = 1.8 W/mK, ρ = 2400 kg/m³, and c_p = 900 kJ/kgK.

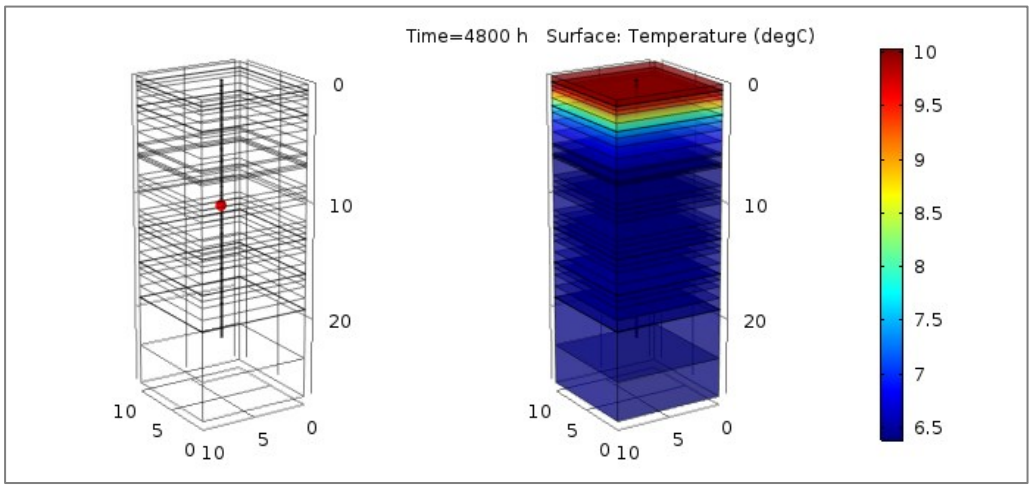

Figure 17. The COMSOL model of the Innova office building reference pile. (**Left**) Pile geometry (sensor T31 in red). (**Right**) Result of t = 4800 h (Publication 3).

The pile was embedded in a 10 m × 10 m, 26.7 m deep multilayer block with the material properties listed in Table 12. The specific heat *cp* was obtained by combining dry specific heat values from reference sources [81] and [82] with the measured humidity content of each soil layer obtained from reference source [80], assuming a value 4.2 kJ/kgK for the specific heat of water.

Table 12. Soil layer properties for the single pile simulation (Publication 3).

Layer nr	Depth, m	p , t/m3	c_p , kJ/kgK	λ , W/mK
1	3.73	1.4	1.8	0.87
2	5.67	1.72	1.82	1.24
3	5.84	1.66	1.78	1.08
4	6.5	1.8	1.71	1.25
5	6.67	1.83	1.72	1.39
6	6.84	1.91	1.57	1.42
7	12.9	2.03	1.4	1.89
8	12.91	2.01	1.39	1.81
9	15.9	2.06	2.32	1.92
10	15.91	2.05	2.33	1.91
11	19	1.99	2.39	1.53
12	19.01	1.95	2.41	1.5
13	23.3	2.28	2.1	2.52
14	26.7	2.21	2.16	2.44

COMSOL Multiphysics version 5.3a was used with the Heat Transfer in Solids module. The FEM method solves the time-dependent heat conduction equation in three dimensions with no heat source, as shown in Equation 5.

$$\rho C_p \frac{\partial T}{\partial t} - \nabla \cdot \mathrm{k}\nabla \mathrm{T} = 0, \tag{5}$$

where $q = -\mathrm{k}\nabla \mathrm{T}$ is the heat flux through each layer of the medium.

According to the large scale of the simulation, the mesh was defined as follows (a few tests performed using finer meshes showed a negligible impact of the resolution on temperature profiles): maximum and minimum element sizes were 2.67 m and 0.481 m, respectively, maximum element grow rate was 1.5, the curvature factor was 0.6, and resolution of narrow regions was 0.5.

The actual pile temperatures were measured using sensors placed in the soil at the edge of the pile, at the depths listed in Table 11, as shown in Figure 17. The temperatures of all the soil layers at $t = 0$ were defined as initial conditions in the COMSOL simulation according to the measurement data. The upper boundary condition, defined as the temperature at ground level, was determined from the measurement data received from the sensor located at the top of the pile for the period 7 March 2014–2 October 2014 (i.e., for a period of 4800 h). The transient study was performed with a constant time step $\Delta t = 1$ h.

Though the setup and the physical phenomenon being studied are straightforward, the accurate reproduction of the measurements was not trivial due to the inherent inhomogeneity of the soil. The soil's composition and thermophysical properties might be approximated globally using Table 12, but this approximation becomes less accurate at smaller scales. For example, an initial specific heat of 2.5 kJ/kgK was computed for Layer 1, but this value led to incorrect initial temperatures for sensors T28 and T29 (see Table 11). It was thus necessary to reset specific heat to 1.8 kJ/kgK in the COMSOL simulation to obtain the correct initial temperature for T28 (at 0.5 m depth) and be consistent with the properties of Layer 2 located beneath it (see Figure 38 in Section 4.2.2).

The initial temperature of each pile section was set to match that of the surrounding soil layer, and the measured surface temperature was interpolated and used as a boundary condition. The main difficulty in validating the simulation involved matching the initial conditions across all sensors, not just T28, since several layers contained sensors with different initial temperatures, and uniform conditions were required by the software.

To increase accuracy, soil stratification around the pile was refined. As illustrated in Figure 17, the original 14 layers were split into 36 layers, to allow for a finer initial temperature profile. This refinement meant that 36 different initial temperatures were set in the model, without changing the thermophysical properties listed in Table 12. The end result would be a more accurate initial temperature profile in the soil, preventing significant differences at the interfaces of contiguous layers. The results of COMSOL single pile model validation are presented in Section 4.2.2.

3.2.3 Validation of ground surface boundary in COMSOL

The first limitation of the proposed GEP modelling method (see Section 3.1) that required validation was the assumption of a constant floor surface temperature throughout the domain of the energy piles. After validating the simulation setup discussed in Section 3.2.2, an analogous COMSOL model, a 2D reduction of the 3D model extended to a multiple-pile layout, was used to perform a 2D heat transfer analysis in energy piles with two different surface boundary conditions. Case (a) uses the ground surface boundary condition for a uniform floor slab, while case (b), corresponding to a real-case scenario, takes into account the soil region surrounding the building floor slab.

The 2D COMSOL model in Figure 18 shows the heat transfer processes occurring between five 15 m-long energy piles beneath the building and surrounded by homogeneous soil. In case (a), the surface temperature of the floor alone was

set at 20°C, which is accepted here as the average annual indoor air temperature of a commercial hall-type building. In case (b), the floor and surrounding soil were both taken into account, with the soil exposed to the outdoor air and extending 5 meters from each floor edge.

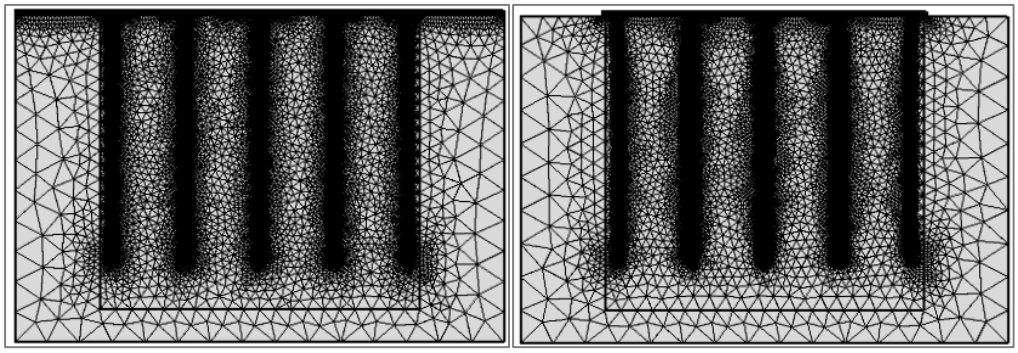

Figure 18. COMSOL mesh for (**left**) (a) the floor only and (**right**) (b) floor + soil (Publication 3).

The 20 m-long floor slab consisted of two layers: a lower 20 cm-thick EPS layer with k = 0.034 W/mK, ρ = 20 kg/m^3 and c_p = 750 kJ/kgK, and an upper 10 cm-thick concrete slab with k = 1.8 W/mK, ρ = 2400 kg/m3 and c_p = 880 kJ/kgK. Each pile was modelled as 15 m-long concrete grout with a diameter of 115 mm surrounding a U-pipe with an external diameter of 25 mm. Pile spacing was 4.5 m, and they were buried in a soil medium where k = 1.1 W/mK, ρ = 1800 kg/m^3 and c_p = 1800 kJ/kgK.

The soil surface temperature (T) was set at 5.67 °C, which corresponds to the average annual outdoor air temperature in Southern Finland. The same temperature value was used as the initial temperature for both the soil layer and the grout. The U-pipes were maintained at a constant T = 0 °C (with constant heat pump operation), the floor was kept at 20 °C in both cases (a) and (b), and the soil surface was set at 5.67 °C for case (b).

A 2D heat conduction module, defined by an equation analogous to (5), was used to take into account the thermal interaction between adjacent piles. The mesh was tetrahedral and physics-controlled and had a finer resolution at the soil/pile interface and a coarser resolution near the boundaries (see Figure 18), with minimum element size of 9 mm and maximum of 2 m. The simulation was carried out for 2400 h, with a time interval Δt = 1 h.

The brine flow in the U-pipes inside the energy piles was neglected in this COMSOL simulation due to the large geometry and time scales (Δt = 1 h, t_{tot} = 2400h). This decision was supported by the literature [83],[84], which showed how models of transient fluid transport inside the tubes would be justified only for much smaller time scales. To quantify the error induced by neglecting the fluid flow, the system shown in Figure 18 considered only heat conduction, and the U-pipes were modelled as being made of concrete at a constant temperature of 0 °C. The surrounding grout was initially set at 5.67 °C at t = 0 and was then subjected to heat transfer for 2400 h. Another simulation was created based on the exact same setup, but this time the U-pipes were modelled as containing water flowing at 0 °C, with inlet velocity V_{in} = 0.45 m/s, but neglecting pipe thickness.

The results are plotted in Figure 19, where the average temperatures in the soil area surrounding the piles, which are active for heat extraction, are compared.

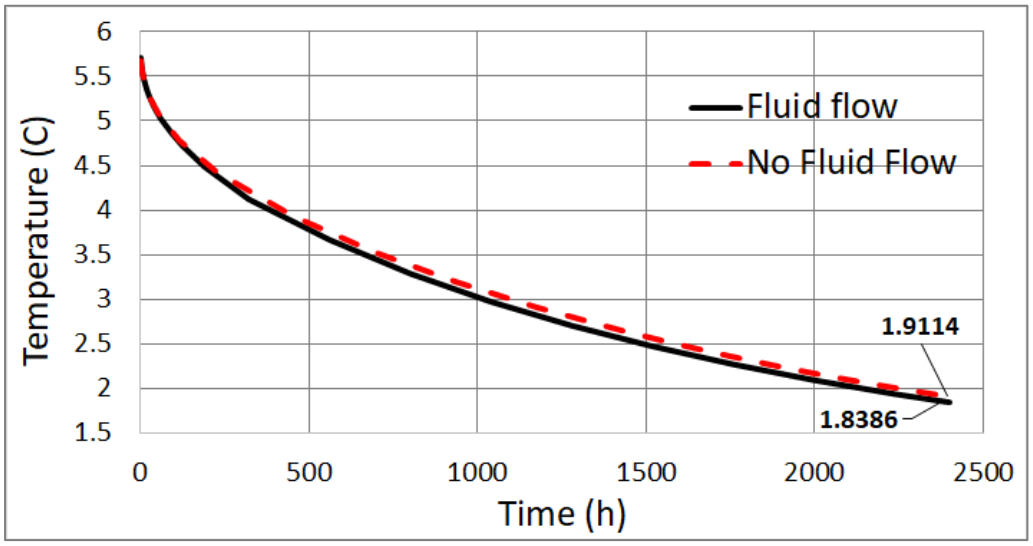

Figure 19. Average temperature in the highlighted area of **Figure 18**. Modelling with fluid flow (solid) compared with modelling without fluid flow (dashed) (Publication 3).

The observed negligible difference confirms that ignoring fluid flow was justified. Consequently, the U-pipes are modeled as concrete with a constant temperature in both the 2D and full 3D simulations presented in Sections 3.2.4 and 3.2.5. It should be noted, however, that this consideration applies only to COMSOL simulations. In IDA ICE, fluid turbulence is accounted for by default when computing the convection heat transfer coefficient h. Results of the ground surface boundary validation are presented in Section 4.2.3.

3.2.4 IDA-ICE borehole model validation against COMSOL model

To assess the accuracy of the 3D IDA ICE finite difference borehole model, a direct 3D extension of the 2D COMSOL model with multiple energy piles (see Section 3.2.3) is used for comparison. Both models compute the outlet temperatures at different depths along the edges of 20 energy piles buried in soil beneath a multilayer floor.

The 3D FEM COMSOL extension of the 2D model consists of 20 identical energy piles, each 15 m in length and all spaced 4.5 m apart. The same geometry is employed in both COMSOL (Figure 20) and IDA ICE, in the former using a 3D finite element model and in the latter, a finite difference borehole model, to take into account the thermal interaction between adjacent piles.

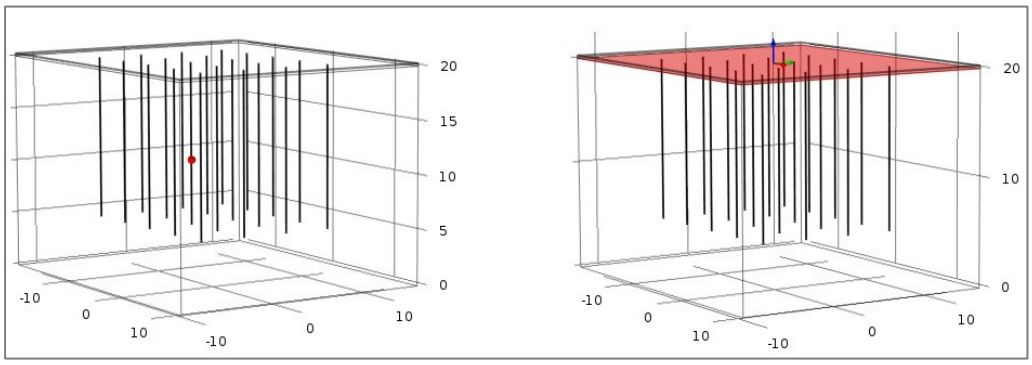

Figure 20. Floor slab with 20 energy piles in COMSOL. Data point at 9 m shown as a red dot (Publication 3).

The piles were buried in a soil medium measuring 25 m × 25 m × 20 m (layout in Table 13), beneath the same type of multilayer floor (a concrete slab over an EPS layer) described in Section 3.2.3 as the upper boundary condition.

Table 13. Spatial arrangement (view from above) of the energy piles for both the IDA ICE and COMSOL models (Publication 3).

17	18	19	20
13	14	15	16
9	10	11	12
5	6	7	8
1	2	3	4

Temperature loggers were placed on a center pile (#10), a center-edge pile (#12), and a corner pile (#20) to quantify the impact of surrounding piles on the temperature fields. Temperatures were logged at depths of 1.5 m, 3 m, 6 m, and 12 m, with the loggers positioned on the pile edge in contact with the soil.

In the COMSOL simulation, piles, floor, and soil were modelled exactly as described in Section 3.2.3, and they had the same material properties. The exact same setup was used in the IDA ICE borehole model. In the COMSOL model, the concrete floor was maintained at a constant 20 °C, and the U-pipes were kept at a steady T = 0 °C (with constant heat pump operation). To decrease the simulation time, fluid flow was not modelled, as explained in Section 3.2.3. In the IDA-ICE model, however, the fluid, at a constant T = 0 °C, entered the energy piles at a very high flow rate. Simulations in COMSOL and IDA-ICE were run for 2400 h, with a time step Δt = 1 h. The results of these simulations are presented in Section 3.2.4.

3.2.5 Impact of boundary conditions on calculation accuracy

In the proposed GEP modelling method (see Section 3.1), the IDA ICE borehole model (version released prior to November 2017) had a limitation that prevented the use of the calculated ground surface temperature as an input variable when calculating floor heat loss above the GEP region. As a workaround, the borehole outlet temperature was used in the floor heat loss calculation, as illustrated in Figure 11 (see Section 3.1.3). This limitation was addressed in a new version of the IDA ICE borehole model released in November 2017.

To assess the error introduced by this limitation, a 3D COMSOL FEM model was used to calculate the ground surface temperature and compare it with both the outdated 'outlet' solution used in the older IDA ICE model (Publication 2) and the updated 'slab' solution used in the revised IDA ICE model.

Geothermal energy piles with a heat pump in a whole building were modelled in IDA ICE according to the design proposed in Section 3.1 and based on the same commercial hall-type building (Figure 21). The total number of energy piles was 192, each with a length of 15 m, and the initial soil temperature was set at 5.67 °C. Soil properties were set as follows: k = 1.1 W/mK, ρ = 1800 kg/m^3 and c_p = 1800 kJ/kgK.

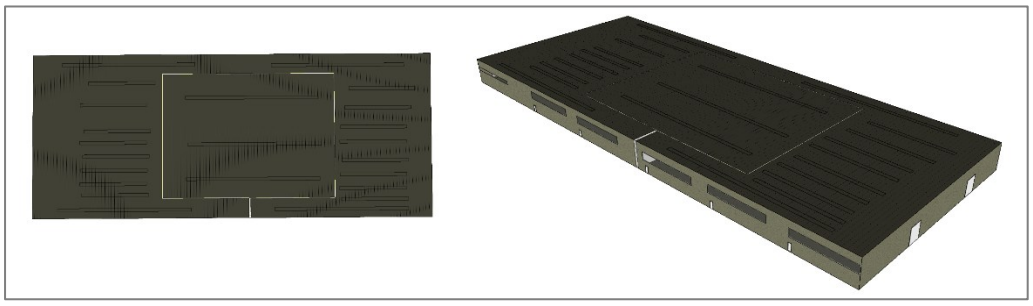

Figure 21. Building model with a separate zone (center) above the energy piles modelled using IDA ICE (Publication 3).

In the proposed GEP modelling method (see Section 3.1), a full-year IDA-ICE simulation was performed based on this design. Inlet and outlet temperatures of the energy piles, obtained with hourly resolution, were used to calculate the average fluid temperature of the energy piles. These values were then used in COMSOL as boundary conditions so a fluid dynamics module would not have to be included, thus helping to decrease computational time. In effect, the COMSOL simulation involves only heat conduction, and the IDA-ICE values are used to increase accuracy.

To compute the yearly energy demand for this building, the model was divided into two zones—one with energy piles and one without. The building floor slab above the energy piles accounted for about 33% of the total floor slab area. In the original “outlet” approach (Publication 2), the variable temperature beneath this surface is roughly estimated using the energy pile outlet temperature, as shown in the connection scheme in Figure 11 (see Section 3.1.3).

This was necessary because, before November 2017, IDA-ICE could not calculate the exact ground surface temperature above the piles. This limitation was addressed with the new 'slab' solution.

The full-year simulation with hourly resolution performed in COMSOL provided the average ground surface temperature Ts beneath the floor slab, which was then compared with the same Ts calculated using the new “slab” borehole model. Finally, the discrepancy between COMSOL and the two IDA-ICE models, “outlet” and “slab”, was quantified in terms of the yearly energy demand for the building.

3.3 Calibration of as-built model and energy analysis

This section addresses the research question related to the usefulness and accuracy of the proposed GEP modelling method when applied to the design of an NZEB in Finland and highlights the main lessons learned. It presents the methods used to demonstrate the performance of the proposed GEP modelling method, methods which involved the calibration of the as-built model and an energy analysis (Publication 4).

The GEP modelling method proposed in this thesis (see Section 3.1) was used in previous research [15] on the design and energy performance modelling of a geothermal heat pump plant for the OLK NZEB, a commercial hall-type building located in Hämeenlinna, Finland. On the basis of the results of the geothermal heat pump plant sizing using the proposed GEP modelling method, the OLK NZEB was constructed, put into operation, and then subjected to data monitoring and measurement. Whole-year building operational data is used in the analysis of measured energy use, which also takes into account the impact of free cooling on the indoor climate and the energy performance assessment of the geothermal heat pump plant.

Simulated energy use for case 14 from [15], corresponding to the energy use of the as-built initial design case, is compared with the measured energy use for room unit heating, the air handling unit (AHU) heating coil, lighting, and other equipment. Since measured outdoor climate conditions differed from the test reference year (TRY) climate [64] and actual building use differed from the initial design building use, a building model calibration was conducted in IDA ICE using detailed hourly-based measurement data and as-built documentation parameters. The building model was calibrated on a monthly basis with reference to TRY climate conditions to assess its impact on building energy performance and to quantify modelling accuracy.

The calibrated building model offers possibilities for further research. For example, it could be coupled with a detailed geothermal plant model, and the impact of different parameters, such as indoor temperature setpoints and AHU setpoints, on building energy performance could be assessed.

The results presented in Section 4.3 provide insight into the seasonal coefficient of performance (SCOP) for the geothermal heat pump plant in both the simulated and measured cases. Conditions in the measured case are compared with the initial design intent, and recommendations for improving energy performance are provided. The energy performance values (EPVs) for each case are presented, and compliance with Finland's NZEB requirements is assessed. The SCOP for the measured heat pump is compared with the SCOP estimated in post-processing using the heat pump manufacturer's performance map. Findings on the operation of the geothermal heat pump plant, suggestions for improving its energy performance, and a quantification of expected performance increases are presented.

3.3.1 Data processing and workflow

Measurement data for the period 01.02.18-01.31.19, with an hourly timestep resolution, was obtained from the monitoring/logging system in the OLK NZEB building, processed, and then analyzed in Excel. There were gaps in the measurement data that had to be filled with interpolated data. Ambient climate conditions were defined in the IDA ICE climate file using measured outdoor air temperature, relative humidity, wind direction, wind velocity, and direct and diffusive solar radiation. For the building model calibration, the measurement data was converted into input files compatible with the IDA ICE simulation environment. Modeling in IDA ICE was performed using the advanced interface, where the user can manually edit connections between model components, edit and log model-specific parameters, and inspect the model's code.

A detailed OLK NZEB building model (Figure 22) was prepared in IDA ICE on the basis of the as-built documentation, taking into account available measurement data. Building model calibration was performed on a monthly basis with the aim of achieving a perfect fit for the measured AHU heat and room unit heat.

Figure 22. (a) Initial design model in IDA ICE. (b) OLK NZEB in Hämeenlinna. (c) Building calibration model in IDA ICE (Publication 4).

While outdoor climate conditions corresponded with measured climate conditions, indoor air temperatures and AHU setpoints were set on the basis of hourly-based measurement data. Internal gains and AHU operation schedules had to be modified due to the fact that some data was not measured or did not include electricity usage for additional separately cooled equipment.

A simplified heat pump SCOP calculation model, based on the actual heat pump performance map and measured evaporator/condenser inlet/outlet temperatures, was completed in Excel using mostly second-degree polynomial equations.

3.3.2 Building model data

Figure 22 shows the initial design model of the OLK NZEB (a) as well as a more detailed room-based model (c), which was created in IDA ICE according to the as-built documentation for calibration of the building model.

Table 14 provides a detailed overview of the general parameters characterizing the building model.

Table 14. Building parameters (Publication 4).

Parameter	Value
Location	Finland
Net floor area, m^2	1496.5
External walls area, U = 0.16 W/(m^2 K), m^2	1201
Roof area, U = 0.12 W/(m2 K), m^2	1467
External floor area, U = 0.14 W/(m2 K), m2	1496.5
Windows area, SHGC = 0.33, U = 0.79 W/(m^2 K), m^2	158
External doors, U = 1.0 W/(m^2 K), m^2	67
Initial design heating set point, °C	18
Initial design cooling set point, °C	25
AHUs heat recovery, % (TK01/TK02)	75/78
Measured air tightness, m^3/m^2 h	0.76 @50 Pa
Heating/cooling room units	radiant panels
Heat load design temperature, °C	-26
Design heat load, kW	84
Heat pump capacity, kW	40

Figure 23 shows the thermal bridges used in the calibration model. They were defined using the calculated values obtained during the design process.

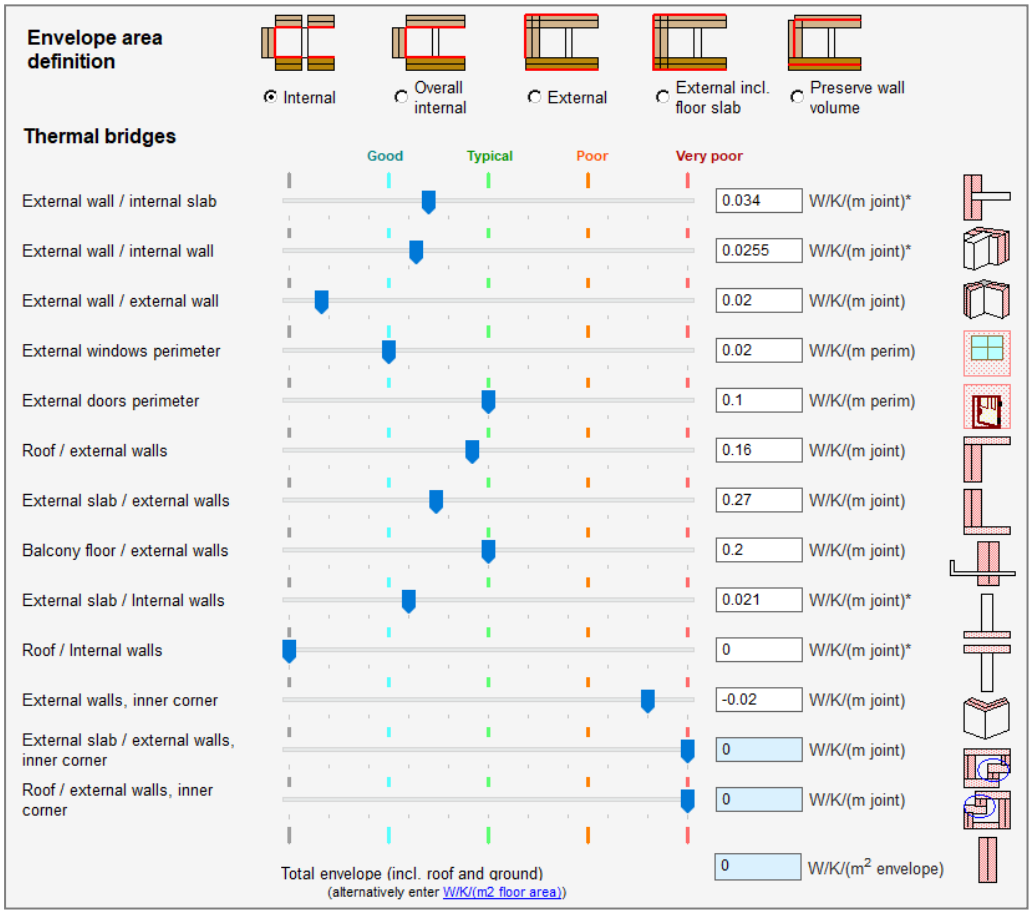

Figure 23. Thermal bridge values for the building calibration model (Publication 4).

It is worth noting that the thermal bridges were modeled as internal components given that it was a room-based calibration model.

3.3.3 Heating system modelling

There are two secondary heating systems in the OLK NZEB calibration model: floor heating and radiant ceiling heating panels. Both were modelled as ideal heaters. The floor heating was modeled with a design power of 40 W/m². The radiant ceiling heating panels had a total design power of approximately 40 kW, which was distributed across the building model according to the design documentation.

3.3.4 Modelling of air handling units

In the OLK NZEB, two main air handling units had been installed: TK01 and TK02, both equipped with rotary heat exchangers and water heating coils. In the actual installation, the supply air temperature setpoint was controlled by the exhaust air temperature. This feature was, however, neglected in the modelling because the supply air temperatures, measured with an hourly time step resolution and varying for each AHU, were used to match the measured AHU heat values. The technical parameters for the AHUs were obtained from design and commissioning documentation, while the initial operational schedules (discussed in the results section) were provided by OLK NZEB staff.

AHU TK01 serviced high hall-type rooms, while TK02 serviced all other rooms. AHU TK02 operated with a design airflow of 0.7 m³/s, while TK01 operated at 1 m³/s (the part load of the design airflow). Part load was calculated using a coefficient of 0.625 for the AHU airflow, as the actual design airflow was 1.6 m³/s. This modeling approach was applied to accurately calculate the electricity consumption of the fans. As a consequence, the exact fan pressure and efficiency values had to be set to match the design documentation's specific fan power (SFP).

3.3.5 Modelling of internal gains

The internal gains of a building consist of the following components: occupancy gains, lighting gains, equipment gains, and solar gains. Solar gains are calculated in IDA ICE on the basis of the climate description and building geometry/envelope properties. Occupancy, lighting, and equipment gains were both measured and estimated.

In the OLK NZEB, lighting and equipment consumption were not measured separately. There were four electricity measuring points in each room, and the total annual consumption for the entire building was approximately 91.3 MWh for the period 01.02.2018-31.01.2019.

One of the measuring points includes heavy machinery that is cooled by a separate active cooling system. This machinery cannot, therefore, be included in the internal gains and will not then contribute to the building's overall heat balance. Since the machinery's electricity consumption was not measured separately, these internal gains had to be estimated. The estimation method proposed by the building constructor involved summing total consumption at that measuring point on an hourly basis and limiting the maximum consumption

value to 8.71 kW, during working hours only and excluding weekends. This adjustment reduced the initial electricity consumption of 71 MWh to approximately 23.9 MWh through the omission of the heavy machinery's electricity consumption. The measured electricity consumption for the other measuring points remained unchanged, amounting to approximately 20.2 MWh. The final internal heat gain for lighting and equipment applied in the first calibration case was 44.1 MWh.

Since the measured electricity consumption was available with hourly resolution, three control signal input files were created based on the measured and estimated data. The data was first sorted to align it with the IDA ICE date structure. The starting date of the measured data in Excel was 00:00 01.02.18, which corresponded to hour 744 in the IDA input file. Input files were created accordingly. The IDA ICE model zones were further grouped into three separate categories to allow the lighting signal to be controlled according to the input file data.

Occupancy was modeled on the basis of the estimates provided by OLK NZEB staff. The model assumed a total of 10 occupants distributed across the building's heated spaces. Two different occupancy profiles were prepared based on this data.

3.3.6 Modelling of opening of cargo gates

A total of three cargo gate opening phases were measured. However, the measurement data appeared inconsistent and unreliable and was therefore excluded from the modelling. In the final calibration (see the results section), some cargo gate openings were estimated.

3.3.7 Modelling of indoor air temperature setpoints

In the OLK NZEB, indoor air temperatures and actual setpoints at specific times in particular rooms were measured and exported from the building monitoring system with a one-hour resolution for 11 rooms. Attempts were made to use both the measured indoor air temperatures and the measured setpoints in each room. However, due to wide variations in the measured indoor air temperature, it was decided to calculate a weighted average building-wide temperature to use as a heating system setpoint input for all zones in the building calibration model. The building weighted average temperature (BWAT) was calculated based on the specific heat loss of each room and the room’s measured indoor air temperature.

3.3.8 Geothermal heat pump plant concept

The fundamental scheme for the OLK NZEB geothermal heat pump plant is shown in Figure 24. The plant design includes an option to separate the energy pile loop from the borehole loop by closing the motorized valve (V-3) during the summer thermal storage cycle. This allows the boreholes to provide "free cooling" while the energy piles are being charged with heat from the thermal storage

source. To prevent ice formation in the ground and possible frost heave, the brine outlet temperature of the geothermal loops could not drop below 0 to -1 °C. Therefore, circulation pumps in each loop (V-2 and V-3) would cease operation when the measured brine outlet temperature (T2 and T3) dropped below the 0 °C setpoint.

The condenser side of the heat pump is connected to a hot buffer tank, where the heat carrier temperature is maintained according to a supply schedule dependent on the outdoor air temperature. The maximum supply temperature is +50 °C with a design outdoor air temperature of -26 °C. The heat pump operates as long as the temperature in at least one of the loops is above the 0 °C setpoint. Conversely, the heat pump stops operating when there is no flow in the system (i.e., both loops are below the setpoint).

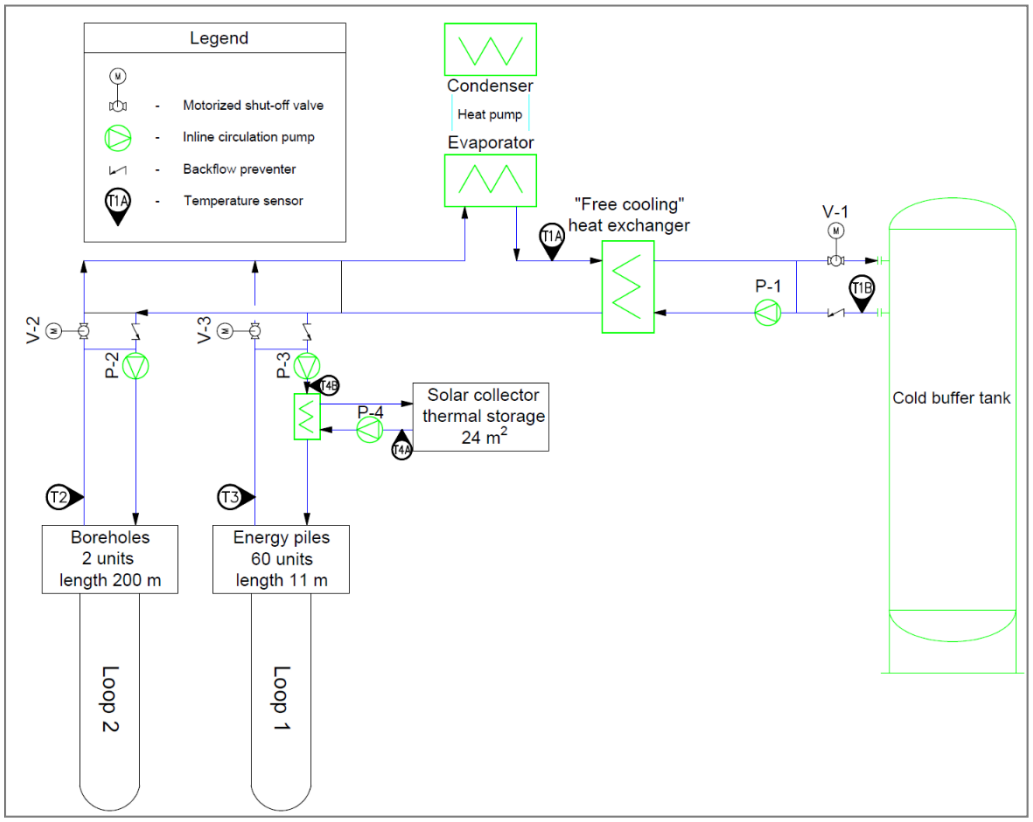

Figure 24. Schematic diagram of geothermal heat pump plant (Publication 4).

This control logic ensures that all the available geothermal energy will be absorbed. If the cooling cycle starts and there is no heat demand in the system, the heat pump will not operate. When the heat pump is inactive, the energy pile loop should be isolated from the evaporator circuit, for example, using a three-way valve. In this case, only the boreholes (heat wells) will be active, and the flow in their circuit will pass through the “free cooling” heat exchanger.

The two loops have separate thermal storage sources. For the boreholes (heat wells), the required amount of heat is supplied during their free cooling operation. A solar collector (with or without a buffer tank) is used as a thermal storage source in the energy pile loop. The thermal storage source is connected via a heat exchanger to the inlet pipe of the energy pile loop. When the heat pump is inactive, the energy pile loop should be isolated using a three-way valve, but

while still maintaining the design flow in the energy piles, now separate from the flow in the energy wells.

Solar thermal storage is controlled according to a temperature difference (ΔT) setpoint logic, where two temperatures are measured and the desired ΔT value is maintained. In the solar thermal storage loop, ΔT = 6 K. The temperatures measured in the solar thermal storage loops, as shown in Fig. 3, are T4A and T4B. When the temperature of T4A is higher than 6 K above the temperature of T4B, pump P-4 starts and stays in operation until the temperature T4A falls and the desired ΔT of 6 K is reached. The “free cooling” loop goes into operation “when beneficial,” meaning pump P-1 starts whenever the temperature T1B is higher than T1A.

Performance results for the proposed GEP modelling method for designing NZEBs are presented in Section 4.3.

3.4 GEP parametric study and sizing guide

This section addresses the research question on how the work of engineers can be facilitated in the early stages of design when GEP systems are being sized. The methods used in the GEP parametric study and the GEP sizing method developed for use in the early stages of design (Publication 5) are presented here.

The performance of the energy piles serving a commercial hall-type building was evaluated by simulating approximately 120 different energy pile configurations with IDA-ICE, using a custom-made benchmark model. This parametric study examined many different factors, including the power rating for the heat pump, pile separation distance and installation depth, soil type, and thermal storage source. The results of the GEP parametric study (see Section 4.4) were used to develop the GEP sizing method for use in the early stages of design (see Section 4.5 for an example).

3.4.1 Building model and case study parameters

Building geometry and envelope parameters used in the case study are shown in Table 15. The design heating load at temperature T = -26 °C is plotted in Figure 25 . It had a total value of about 465 kW, which is the sum of the Air Handling Unit (AHU) heating coil power (290 kW) and the heat pump condenser power (175 kW). Domestic hot water production by the heat pump is not considered.

Table 15. Building model parameters for the reference simulation (Publication 5).

Descriptive parameter	Value
Building size	66 x 137.4 m
Roof (310mm) U	0.12 W/(m^2 K)
Floor (EPS100) U	0.09 W/(m^2 K)
Walls (sandwich panel 230mm) U	0.16 W/(m^2 K)
Windows (SHGC 0.51) U	1.0 W/(m^2 K)
Air tightness q_{50}[1]	2 m^3/(m^2 h)
Heating setpoint[1]	18 °C
Cooling setpoint[1]	25 °C
Fresh air flow[2]	1.1 l/(s m^2)
Occupants[1]	2 W/m^2
Lighting[2]	8 W/m^2
Equipment[1]	1 W/m^2
Occupancy period[1]	8:00-21:00 (6d/7d)
Occupancy rate[1]	1.0
AHU heat recovery	80 %
Plant type	Heat pump with energy piles
Room unit type	Radiant heating/cooling panels

The operational performance of energy piles and boreholes is typically assessed over a simulation period of 20 years [85],[86].

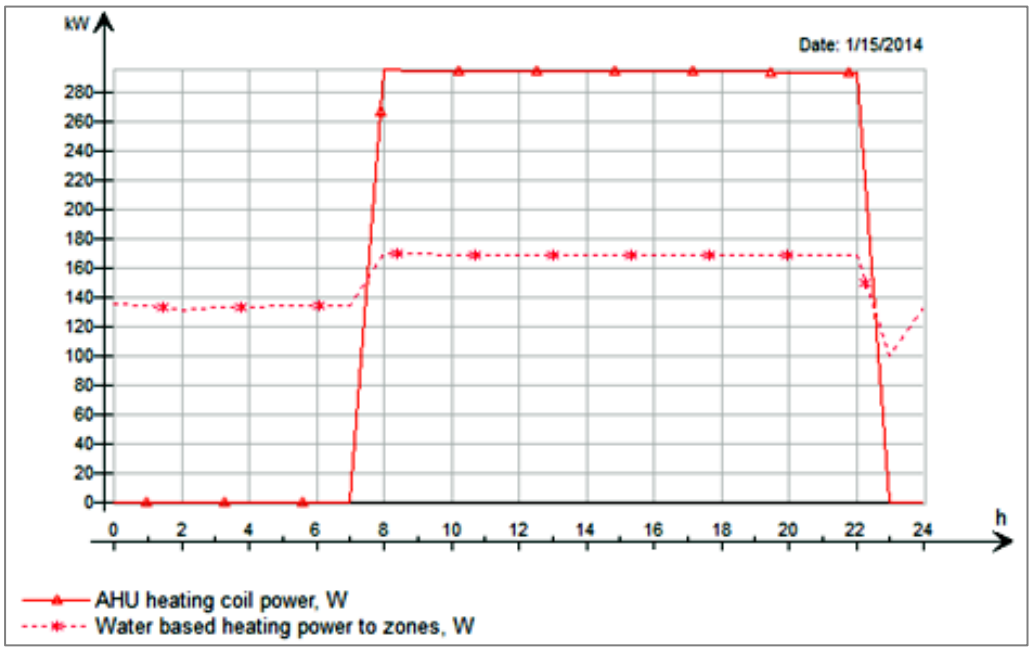

Figure 25. Building heating load for a design temperature T = -26 **°C** (Publication 5).

The weather data source for the location and the input parameters for the energy pile field are listed in Table 16 (an average annual ground temperature of 5.62 °C is assumed). To ensure comparability among all considered cases, the envelope size was varied according to the heat pump power, which was fixed at 50% of the total heating demand (physical dimensions of the modelled building were scaled so that its heat load is proportional to the heat pump capacity). 15 different building models were also created to be able to take into account different energy pile depths and specific heat extraction rates [W/m].

Since a detailed IDA ICE simulation for a single case could take up to 3 days, the GHE was isolated by replacing the heat pump and building with hourly time step data, according to the heat pump evaporator load data used as pile input. In theory, such data is dependent on the annual operational profile for each specific heat pump size.

Table 16. Input parameters for the energy pile field (Publication 5).

Parameter	Value
Field size	30 m x 30 m
Pipe size	DN 20
Pile diameter	170mm (Double U-pipe), (125mm special cases)
Depth in the ground	15 m, 30 m
Distance between piles	3 m, 4.5 m, 6 m
Ground heat conductivity	Clay 1.1 W/(m K), Silt 2 W/(m K)
Ground volumetric heat capacity	Clay 3343 kJ/(m3 K), Silt 4259 kJ/(m3 K)
Fluid type	Ethanol
Thermal storage ratio	0%, 50 %, 100 %
Heat pump design power (evaporator)	20 W/m, 40 W/m, 60 W/m, 80 W/m, 100+ W/m
Heat pump power to heat demand ratio	50%
Climate file	Helsinki-Vantaa 2012

The building's instantaneous energy demand determines this profile. Running a simulation for the model defined by the parameters in Table 15 (benchmark

case), the annual building load profile shown in Figure 26 was thus generated, and in turn, the hourly time step load data for the heat pump evaporator. This profile data was then used for each simulation, where the upper limit (1.0) in Figure 26 corresponds to the building's design heat load at -26 °C. In other words, only one input parameter – the design heat load – was used to generate each case.

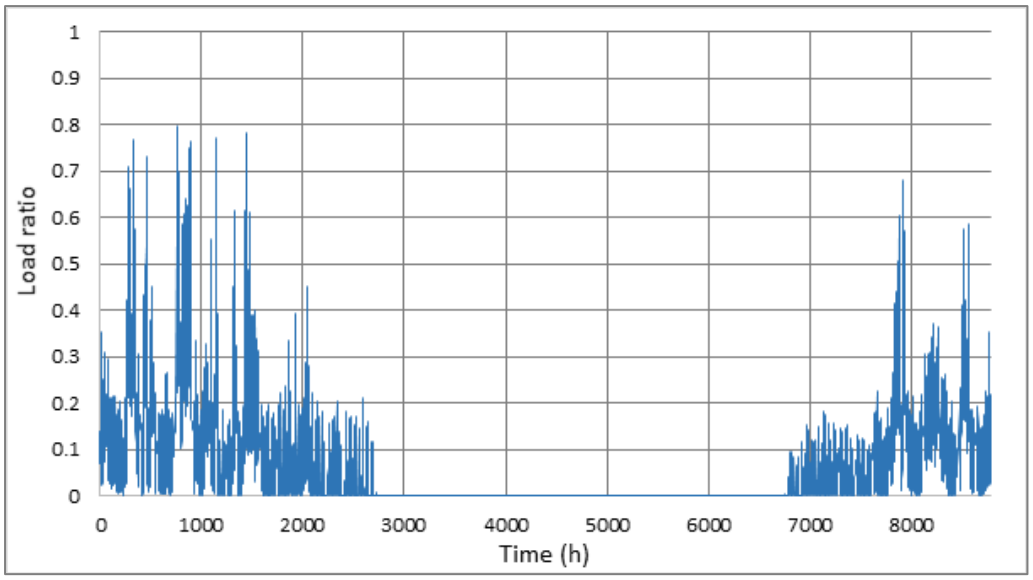

Figure 26. Building heating load profile for the benchmark simulation (Publication 5).

The benchmark model (Figure 27) is based on an analogous three-dimensional borehole field simulation that was introduced and experimentally validated in Publication 2 and Publication 3. No cooling season operation was modelled. The results of this validation are presented in Section 4.2.

3.4.2 Heat pump load profile and operation

The heat pump model is illustrated on Figure 27. The evaporator load Q_{evap} [W] is described using Equation 6.

$$Q_{evap} = mc\Delta T \tag{6}$$

where m [kg/s] is the mass flow, c [J/kgK] is the brine specific heat capacity, and ΔT [K] is the temperature difference between borehole outlet and inlet. The benchmark model operates at a partial load of 0–100% (effectively, a design limitation, since an actual heat pump operates at ~30–100%).

Heat pumps can be operated in two modalities - at constant (on/off) load or with partial (inverter) load. In the case of constant load operation, the heat pump is turned ON and operated at full load under heat demand. In contrast, partial load operation is managed by the inverter heat pump, which can adjust its output to be between approximately 30% and 100% of its maximum capacity. Since hourly average (dynamic) data generated from the benchmark profile is used as input, partial load operation is enabled for the heat pump. As a consequence, the results are applicable only to plants equipped with inverter heat pumps. The thermal storage operation in this model is presented in Section 3.4.4.

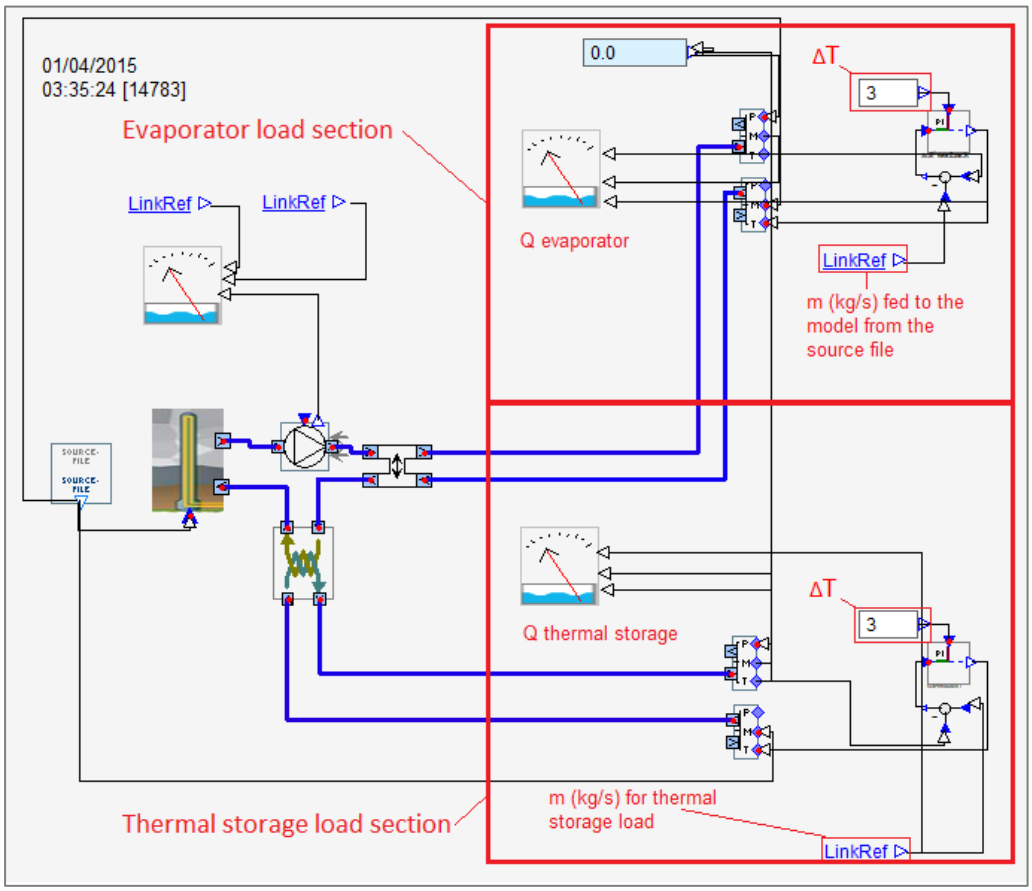

Figure 27. Benchmark simulation model based on the source files (Publication 5).

The heat pump evaporator load data was generated from the building load data, which was based on the annual average COP of the heat pump. The mean annual ground temperature *T* and the resulting average brine temperature were assumed to stay in the 0 °C to 10 °C range during operation. An annual average heat pump COP of 4.5 was assumed, on the basis of the heat pump performance map data (Figure 28), with a condenser side outlet temperature of 45 °C.

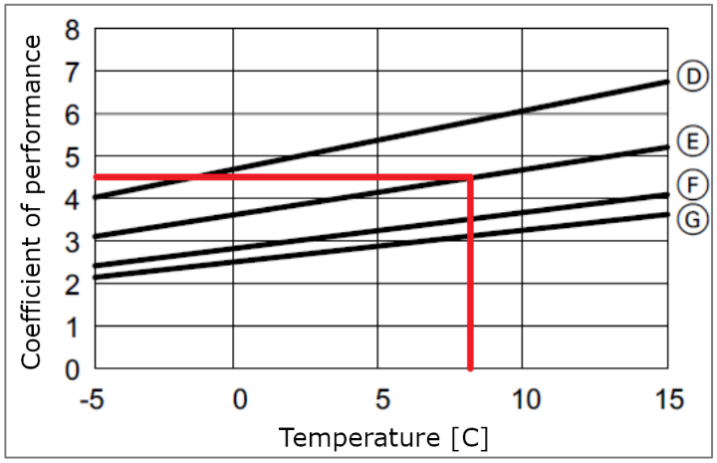

Figure 28. Heat pump performance graph (Publication 4).

This assumption is justified by the long simulation period, which compensates for small fluctuations in soil temperature and deviations from the average COP value.

In Figure 29, the evaporator load profile is shown in green, the heat pump condenser load, in yellow, and the top-up heating covering the rest of the load, in red.

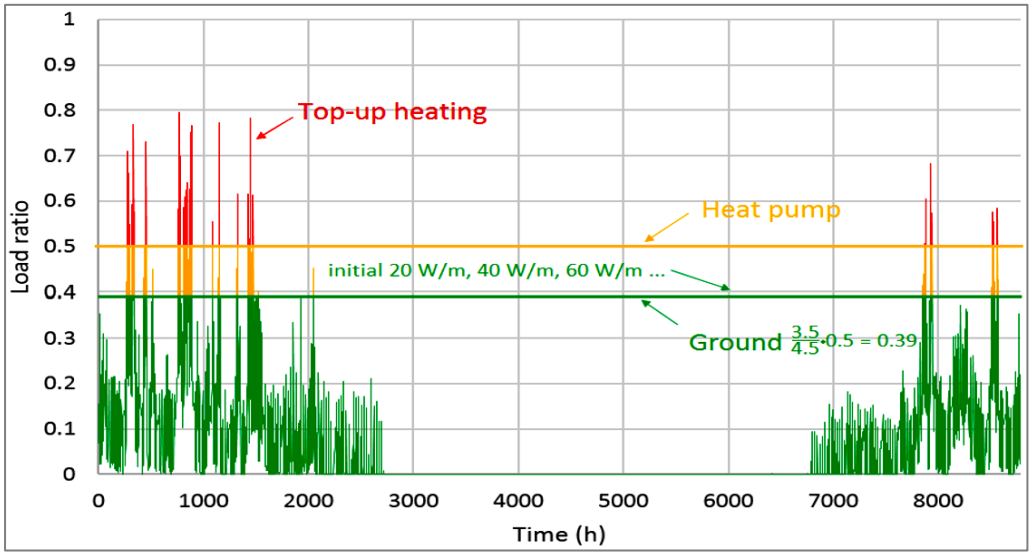

Figure 29. Annual building heat demand profile (Publication 5).

The generated evaporator load data was fed to the simulation model as a source file, as illustrated in Figure 27. This required input of annual hourly time-step data (8784 h) for both the liquid mass flow [kg/s] of the heat pump evaporator load and the eventual thermal storage load. Because hourly loads cannot be fed directly in units of power [kW] in IDA ICE, a specific control was developed to maintain a predefined temperature difference ΔT with a variable mass flow [kg/s] provided by the source file.

The control logic in the model is as follows. The borehole outlet temperature is determined by the inlet temperature, flow, and thermal processes occurring in the fluid-borehole-soil system, which are all computed by the borehole model. To prevent frost heave, soil temperatures cannot be allowed to drop below 0 °C, though a borehole inlet temperature of -1 °C is tolerated for short periods as a preset limit. To test this limitation, a simulation was carried out where the heat pump is turned off when the evaporator inlet fluid temperature is low.

As the liquid mass flow data entered the energy pile model, a feedback controller measured the brine outlet temperature and supplied a new inlet temperature T, which was computed according to a pre-set $\Delta T = T_{outlet} - T_{inlet} = 3$ °C. The source file provided, at intervals $\Delta T = 1\ h$, a mass flow m corresponding to the building heating demand. The outlet temperature was then calculated by the borehole model using the inlet temperature and brine flow. The inlet temperature, T_{inlet}, was calculated by the model using the preset ΔT for most of the time (exceptions are explained in the paragraph below). For a given mass flow and inlet temperature, the new outlet temperature was calculated by the borehole model before starting a new cycle. Source files were created using Equation 6, which used the mass flow [kg/s] as its only parameter once the building heat load had been converted into evaporator load using Equation 7 for the heat pump evaporator sizing.

$$Q_{evap} = \frac{Q_{cond} \times (COP-1)}{COP} \quad (7)$$

The $\Delta T = 3$ °C value is effectively "semi-constant" to ensure that frost heave does not occur. In cases where $T_{inlet} \leq -1$°C , two extremal scenarios can be considered to illustrate this functionality: an extremely large and an extremely small energy pile field.

- Very large energy pile field case. The initial soil temperature is 5 °C. When it is very cold outdoors and the heat pump starts working, the source file feeds the brine flow into the model. The last known outlet temperature (5 °C, the initial soil temperature) is then used to calculate the inlet temperature, which is 5 °C - $\Delta T = 2$ °C. Since the borehole field is virtually infinitely long, it is possible that locally $T_{outlet} < 5$°C, depending on the thermal resistances between the fluid, energy pile, and soil. For example, if $T_{outlet} = 3$°C, which represents a significant drop, then $T_{inlet} = 0$°C. This approach accounts for local drops in soil temperature and still prevents frost heave, ensuring that the heat pump can operate continuously and meet the building's heat demand as designed.

- Extremely small pile field case. It has the same boundary conditions given above. The field would be very sensitive to thermal inhomogeneities in the soil. As the heat pump starts, the building heat demand cools down the soil due to the small heat exchange area of the pile field. With $T_{outlet} = 2$°C and $T_{inlet} = -1$°C, the threshold value that blocks the pump is reached. As a consequence, while the flow continues from the source file, the inlet temperature is fixed at -1 °C. The borehole model then calculates the outlet temperature based on these conditions, potentially resulting in T_{outlet} being lower than 2 °C. If T_{outlet} is assumed to be 1 °C, then $\Delta T = 1\ °C - (-1\ °C) = 2\ °C < 3\ °C$. Since 2°C is now less than the original pre-set value, the heat pump would be unable to meet the heat load for the entire building, covering only about 66% of the actual load (2 °C / ΔT).

Once the simulation is complete, the calculated value is compared to the initial evaporator load used in the source file, allowing for the determination of the amount of top-up energy required to meet the building's heating demand.

3.4.3 Floor surface temperature assumption

In buildings with energy piles, heat loss from the floor to the ground creates a so-called "free thermal storage" effect, which can significantly enhance the performance of the piles. This effect was easily incorporated into IDA ICE by using the floor surface temperature as the ground surface temperature in the GHE model, as shown in Figure 30. The thermal properties of the floor are defined in the energy pile model, as detailed in Table 15.

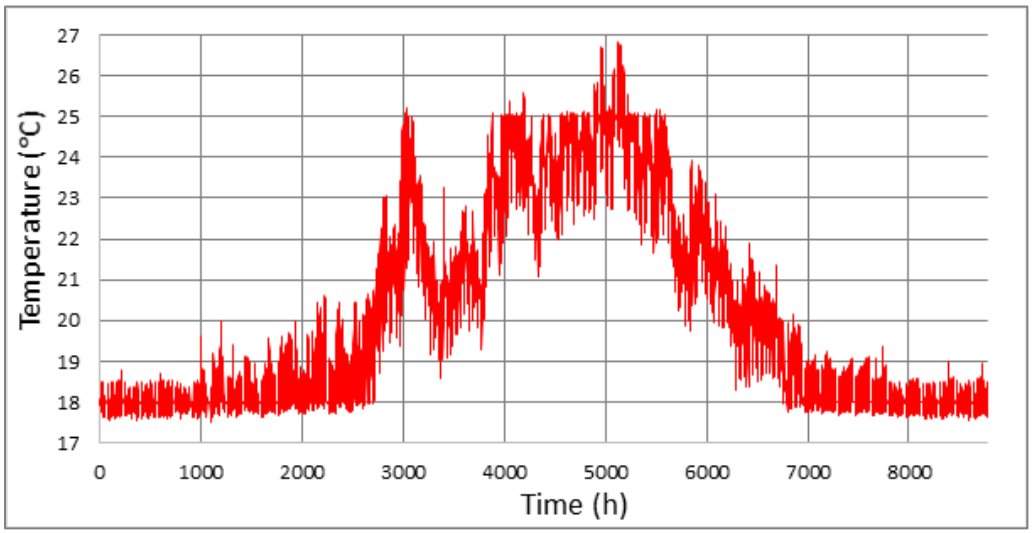

Figure 30. Annual floor surface temperature profile (Publication 5).

The "free thermal storage" effect estimation is based on the average ground temperature over a period of 20 years, calculated annually by assessing the floor heat loss induced by the volumetric heat capacity of the energy pile field's ground mass. As the floor heat loss over time warms the ground beneath the building, the annual heat loss through the ground will vary from year to year.

3.4.4 Thermal storage profile

The hourly load data for solar thermal storage (50% or 100%) was logged in much the same way the heat pump evaporator load data was logged (see Section 2.2). The data was generated from a benchmark solar storage profile (Figure 31), which was obtained by using IDA ICE to model a solar collector with an orientation of 300° and an angle of 40° that was connected to the inlet pipe of the energy piles via a heat exchanger.

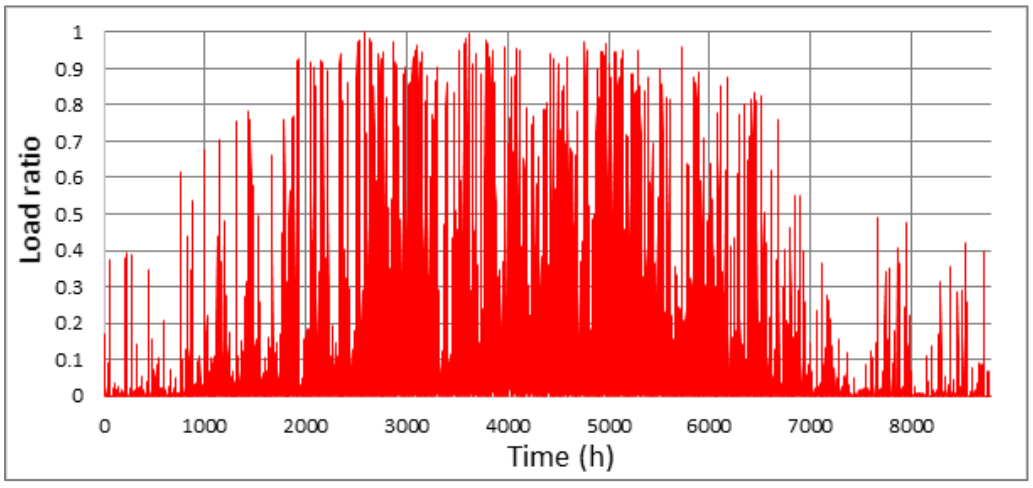

Figure 31. Annual thermal storage profile (Publication 5).

In the cases with thermal storage, the total annual amount of stored energy equaled the sum of solar storage and floor heat loss (i.e., the "free storage" energy plotted in Figure 30).

The latter was estimated in MS Excel by using a 20-year average for the ground temperature. This temperature was computed annually on the basis of the volumetric heat capacity of the soil surrounding the GHE and the floor heat losses, which gradually warmed the ground beneath the building. Annual heat loss through the ground varied from year to year.

Once the 20-year average ground temperature was obtained, the energy provided annually by floor heat loss could be calculated using standard heat conduction equations. The thermophysical properties of the soil surrounding the building floor slab are listed in Table 17.

Table 17. Soil thermal properties (Publication 5).

Material	λ, W/mK	Porosity, %	Saturation, %	Bulk density, kg/m^3	Wet density, kg/m^3	Volumetric heat capacity, kJ/m^{3}K	Heat capacity, J/kg K
Clay	1.1	56	100	1250	1812	3343	1845
Silt	2	31	100	1529	1835	4259	2321

3.4.5 Description of top-up sizing simulation

The inverter heat pump was sized at 50% of the building design load, while top-up heating would be expected to cover the remaining peak load. Due to the unsteady performance of the energy piles, full load operation of the inverter heat pump could be maintained only for a limited amount of time, specifically until the fluid in the evaporator circuit dropped below approximately -3 °C, at which point the heat pump stopped.

When this occurs, top-up heating sized at, for example, 50% may not be sufficient to fully meet the building's heat demand. To determine the optimal size for top-up heating, a sizing scenario was developed for critical conditions. An additional building load profile was created and converted into a heat pump evaporator load profile. The first three years of operation were computed based on a Test Reference Year (TRY), while for the fourth year, temperatures between -20 °C and -26 °C were set for two weeks in January. The heat pump output power was logged on the 14th day of operation under these extreme conditions, and the minimal output was compared to the sized value. The sizing of top-up heating for specific cases was then calculated.

4. Results and Analysis

This chapter reports on the main research results and findings. First, the research gap identified in Chapter 2 is addressed in light of the results obtained from numerical simulations using the proposed GEP modelling method in IDA ICE (Publication 2). The impact of different ground surface boundary conditions on the performance of a heating/cooling plant with GEPs and a BHE field in a commercial hall-type building is shown.

Second, the proposed detailed GEP modelling method is validated against measurement data and data simulated in COMSOL Multiphysics (Publications 2 and 3). The impact of the limitations of the proposed GEP modelling method on calculation accuracy is quantified.

Third, the performance of the proposed GEP modelling method is demonstrated using a commercial hall-type building, the OLK NZEB (Publication 4) in Hämeenlinna, Finland. Performance is quantified on the basis of the results of the analysis of measured and simulated energy use.

Fourth, the results of the GEP parametric study (Publication 5) are presented. The study covers many different factors, such as heat pump evaporator sizing power, pile separation and installation depth, soil types, and thermal storage implementation.

Finally, the GEP parametric study results are used to develop a method for the preliminary sizing of a geothermal heat pump plant.

4.1 GEP and BHE field plant simulation results

The results related to the research question on the key differences between GEP and borehole modelling are presented here. The numerical simulations were carried out for a period of 20 years, and the results are presented in the form of annual average data. Main difference between the two simulated cases with 196 boreholes/geothermal energy piles was in ground surface boundary condition. In the BHE field case, the ground surface was exposed to outdoor air. In the GEP case, the building floor structure was modelled as a ground surface boundary condition with exposure to simulated room indoor air temperature. The heating season in the simulation started in October and lasted until the end of April, the cooling season started in June and lasted until the end of August

Results of the detailed modelling of GEP and BHE field heating/cooling plant performance in a commercial hall-type building are compared in Table 18.

Table 18. Simulation results for BHE field plant and GEP plant (Publication 2).

Calculated results	BHE field	GEPs
Evaporator absorbed heat, MWh/a	66.4	112.2
Compressor electricity, MWh/a	15.3	27.2
Condenser rejected heat, MWh/a	81.7	139.4
Top-up heating energy, MWh/a	106.4	64.6
Circulation pumps, MWh/a	8.2	8.2
Thermal storage heat through floor structure, MWh/a	0.0	32.2
Heat pump seasonal coefficient of performance	5.3	5.1
Heating system seasonal coefficient of performance	1.4	2.0
Heat pump operation duration, h	477	804
Borehole specific heat extraction rate, W/m	47.3	47.5
Borehole average annual yield at condenser, kWh/(m a)	28	47
Specific electricity usage for building heating, kWh/(m^2 a)	14.2	11.0
Average annual ground temperature, °C	2.9	6.7

The plant with the BHE field absorbed about 40% less ground heat on the evaporator side than the plant with the GEPs. However, due to increased heat losses through the structural floor in the GEP case, annual heat demand (sum of top-up and condenser heat) amounted to 204 MWh/a, compared to 188.1 MWh/a in the BHE field case. The initial ground temperature in both cases was 8 °C. The average annual ground temperature over 20 years of plant operation was 6.7 °C in the GEP case and 2.9 °C in BHE field case. Regarding the scale of electricity demand for building heating purposes, the GEP plant consumed 100 MWh/a, while the BHE field consumed 129.9 MWh/a, the former showing an approximately 23% increase in efficiency.

The seasonal coefficient of performance for the entire heating system (SCOP), which takes into account top-up heating and circulation pump energy consumption, was 2.0 for the GEPs and 1.4 for the BHE field. Considered separately, the heat pump coefficient of performance (COP) was 5.1 in the GEP case and 5.3 in the BHE field case. Comparatively low overall system SCOP in both cases can be attributed to either an insufficient number of installed boreholes/geothermal energy piles or a lack of seasonal thermal storage. According to results, the heat pump in GEP case was able to cover only about 68% of overall building heat demand, and in BHE field case, about 44%, while the rest of the heat was supplied by electrical top-up heating. Regarding total operation time, the heat pump was in operation for a total of 804 hours in the GEP case, and 477 hours in the BHE case. The circulation pumps operation was modelled simply as “always ON” in both cases, this resulted in the maximum possible circulation pumps energy consumption.

The significant difference in long-term performance of the GEPs and BHE field is illustrated in Figure 32. In the case of the BHE field plant, where the ground surface boundary was exposed to outdoor air, the long-term performance decreased over the years, with a reduction of about 30% after the first year of operation. In the case of the GEP plant, the ground surface boundary was connected to the floor structure and exposed to indoor air. As a consequence, performance remained more stable over the years. This can be explained by heat conductance through the structural floor to the ground, resulting in a natural thermal storage effect.

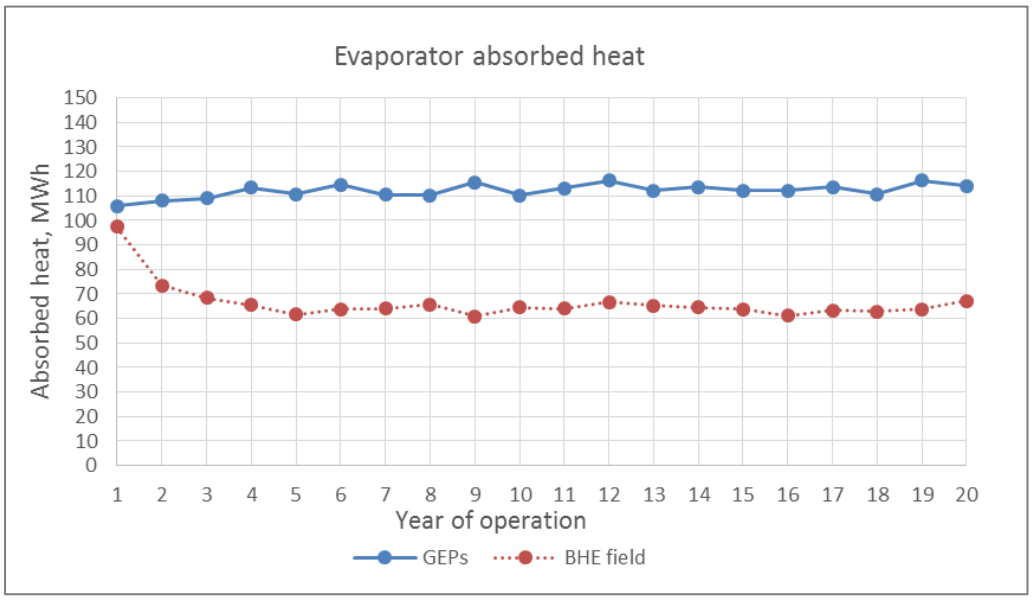

Figure 32. Long-term simulation results for GEPs and BHE field (Publication 2).

Simulated monthly average temperatures of brine delivered for both cases are shown on Figure 33. In BHE field case, as expected, the average temperature of the delivered brine during the winter operation of the heat pump was about 0 °C due to the control logic of the heat pump. In the GEP case, the average temperature of the delivered brine in the winter period was about 2...3 °C higher than in the BHE field case due to the difference in the ground surface boundary condition.

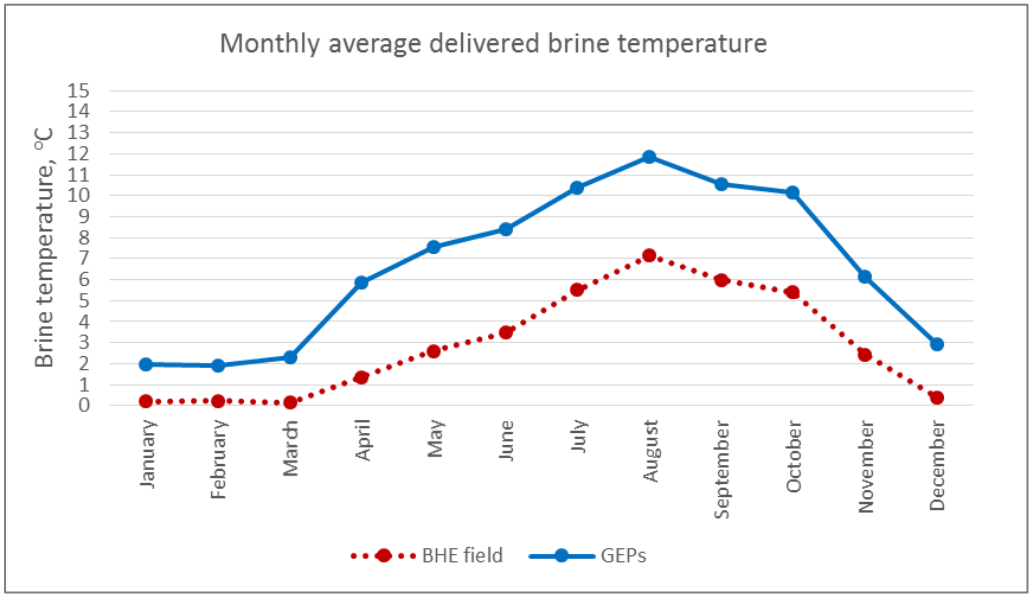

Figure 33. Monthly average brine temperature delivered (Publication 2).

From a building cooling perspective, the temperature of the delivered brine during the summer period peaked at +15 °C in BHE field case and +17 °C in the GEP case. In neither case had an active cooling system been implemented, and the delivered brine reached the cooling tank via a free cooling heat exchanger. The simulated indoor air temperature (Figure 34) was below the set point of +25

°C most of the time, and when it exceeded it, it was mainly due to the limited cooling capacity of the installed radiant cooling ceiling panels.

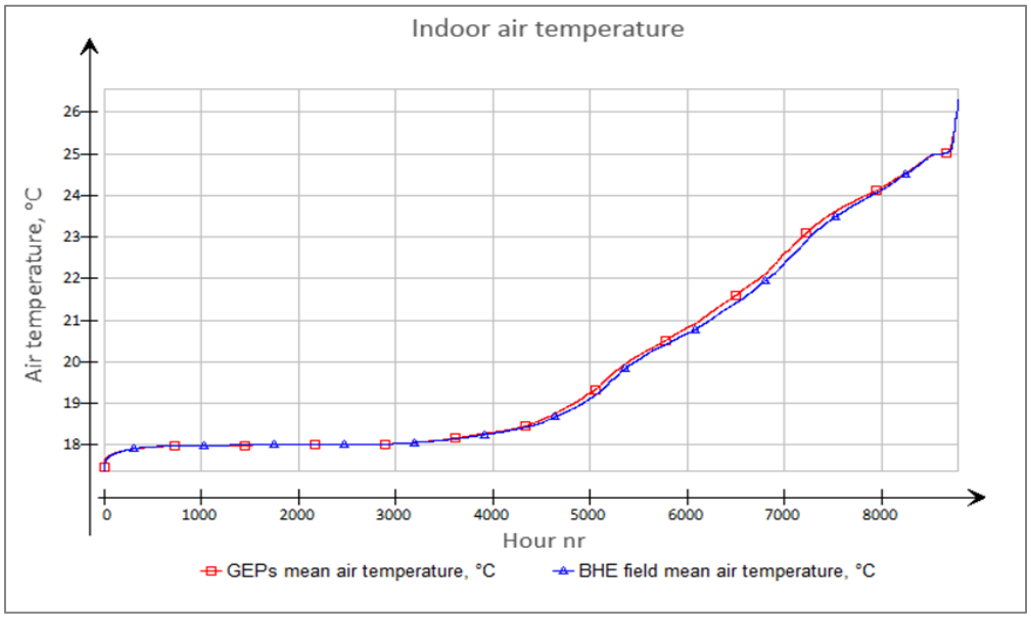

Figure 34. Cumulative graph of indoor air temperature (Publication 2).

The impact of borehole thermal resistance on absorbed evaporator heat is quantified in Figure 35. A lower Rb means more efficient heat transfer between the fluid and the ground, which is desirable for system performance. Borehole thermal resistance in the two simulations differed by nearly a factor of 2.

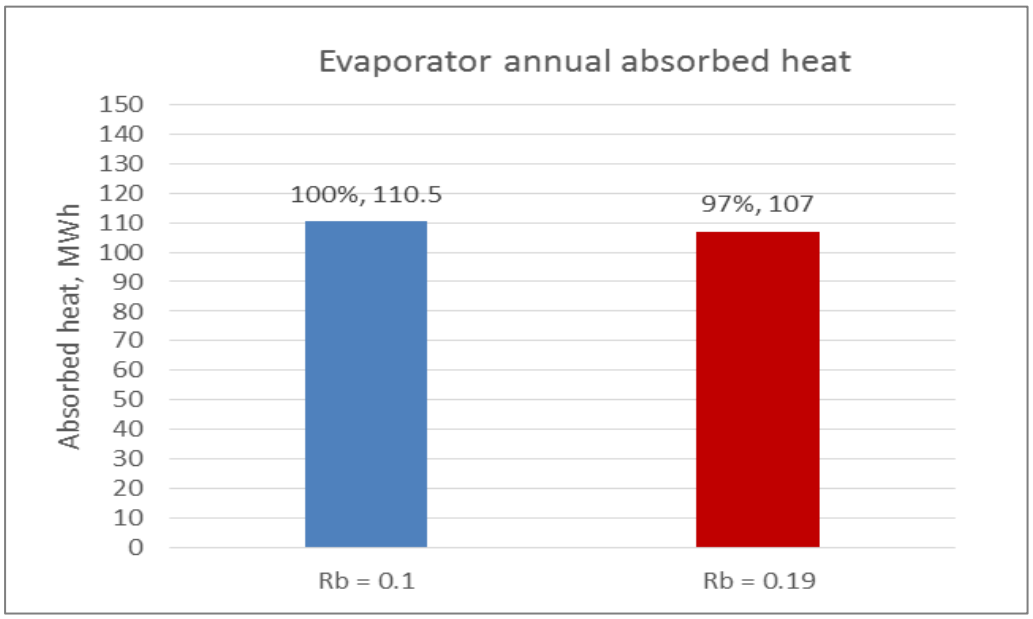

Figure 35. Impact of borehole thermal resistance on absorbed evaporator heat (Publication 2).

With a borehole thermal resistance of Rb = 0.19 (mK)/W, there was a 3% decrease in annual heat absorption from what it was with a borehole thermal resistance of Rb = 0.1 (mK)/W.

According to the results presented in this section, ground surface boundary conditions are a key difference between GEP and borehole modelling. One of

the conclusions of this research is that GEPs, when compared with boreholes, are expected to perform with more stability in the long term due to the natural thermal storage effect induced by the exposure of the ground surface of the GEPs to indoor air. GEPs should not be modeled as standard boreholes if the ground free surface is not present.

4.2 Results of validation of GEP plant modelling method

This section addresses the validation of the IDA ICE borehole model, which was modified to account for GEP ground surface boundary conditions in the GEP plant modelling method proposed in this thesis. IDA ICE borehole model validation was performed against energy pile measurement data (Publication 2) using the finite element analysis software COMSOL Multiphysics (Publication 3). The impact of boundary conditions on calculation accuracy was quantified.

4.2.1 Validation of IDA ICE borehole model using measurement data

The validation of the IDA ICE borehole model against single borehole measurement data was divided into two phases, a parameter identification phase and a validation phase. The goal of the parameter identification phase was to obtain the unknown value of the „annual mean ground temperature" input parameter required by the IDA ICE borehole model. Parameter identification simulations were conducted using measurement data from the period 14.06.2012 - 11.07.2012 (i.e., 650 hours). Measured mass flow rate fluctuated within the 0.09...0.14 kg/s range. An "annual mean ground temperature" input parameter value of 8.5 °C in IDA ICE borehole model yielded 120.7 kWh of simulated rejected heat compared to 120.6 kWh of measured rejected heat during the same period. The measured and simulated outlet brine temperatures for the IDA ICE borehole model during the parameter identification phase are compared below in Figure 36.

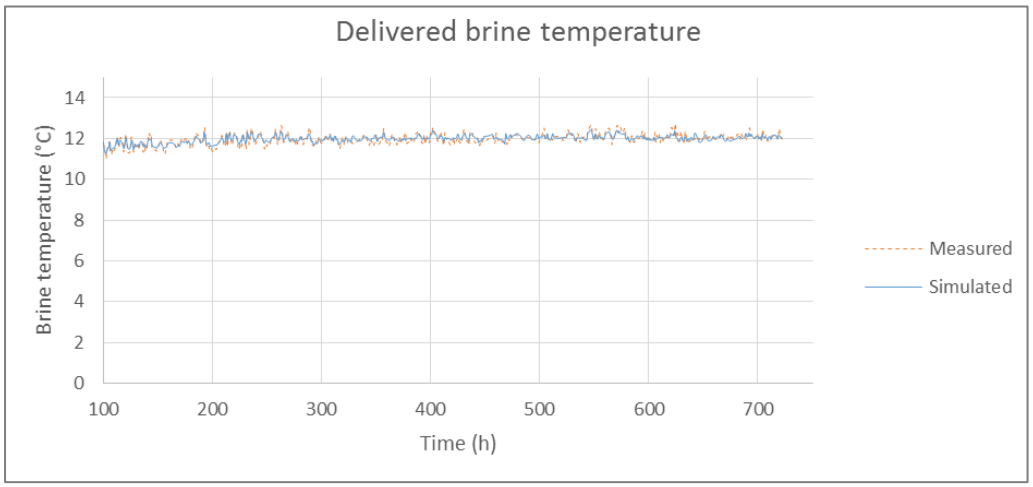

Figure 36. Results of the IDA ICE borehole model parameter identification phase (Publication 2).

The obtained "annual mean ground temperature" input parameter of IDA ICE borehole model was then used in the validation phase using measurement data from the period 20.05.2012 - 28.05.2012. The results of the validation of the IDA ICE borehole model are shown in Figure 37. In the validation phase simulation, the mass flow rate fluctuated from 0.15 to 0.19 kg/s over a span of 192 hours.

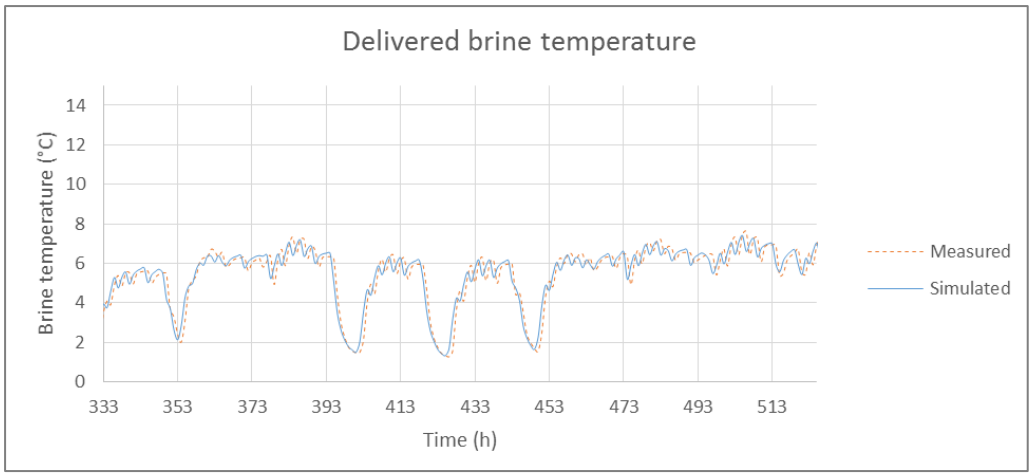

Figure 37. Results of DA ICE borehole model validation phase (Publication 2).

The extracted ground heat in the simulation had a value of 387.1 kWh, which showed exact agreement with the measured value. NMBE resulted in -0.45% within the +-10% tolerance and CV(RMSE) resulted in 16.65% within the tolerance of <30% required by ASHRAE Guideline 14.

4.2.2 Single pile model in COMSOL against measurement data

The plot displayed in Figure 38 compares the single borehole temperature profiles for sensors positioned at a depth of 0.5 m and 4.5 m over a 4800 hour period computed by COMSOL with the actual temperatures measured. Good agreement was found between measured and simulated borehole temperatures for all sensors.

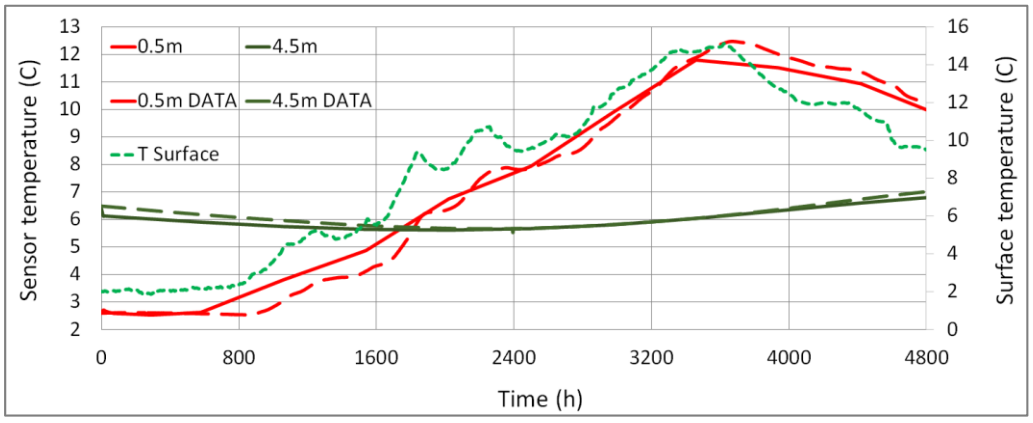

Figure 38. Measured temperatures (dashed) vs. temperatures simulated in COMSOL (solid) for a single pile, with sensors at depths of 0.5 m and 4.5 m. Surface temperature also shown (small dashes) (Publication 3).

The temperature profiles in Figure 39 show outstanding agreement at 4.5 m, 10.5 m and 16.5 m, with differences well below 5% at 4.5 m and at about 0.2°C (3%) at the other depths. This is significant, considering that the specific heat of the soil layers was initially unknown and had to be calculated.

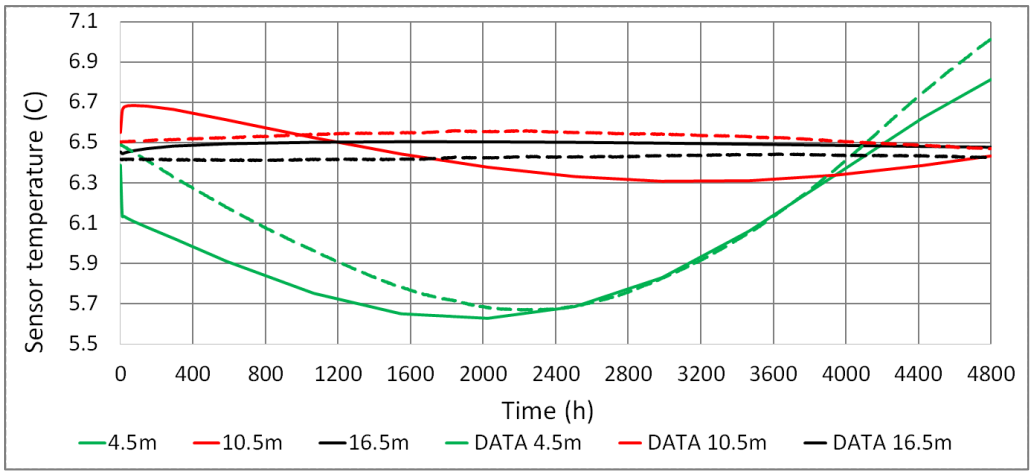

Figure 39. Measured temperatures (dashed) vs. temperatures simulated in COMSOL (solid) for sensors at depths of 4.5 m, 10.5 m and 16.5 m (Publication 3).

Though more accurate initial soil properties would provide even more precise validation, the accuracy of the agreement achieved using the COMSOL simulation environment suffices for the validation of the proposed GEP modelling method in this thesis.

4.2.3 Ground surface boundary analysis in COMSOL

Figure 40 shows the 2D thermal profiles generated in COMSOL over a 2400-hour simulation period for two different surface boundary conditions. Case (a) corresponds to the uniform floor slab ground surface boundary condition applied in the proposed GEP modelling method to take into account IDA ICE borehole model limitations. Case (b) corresponds to the real-life scenario, where a soil region surrounds the building floor slab.

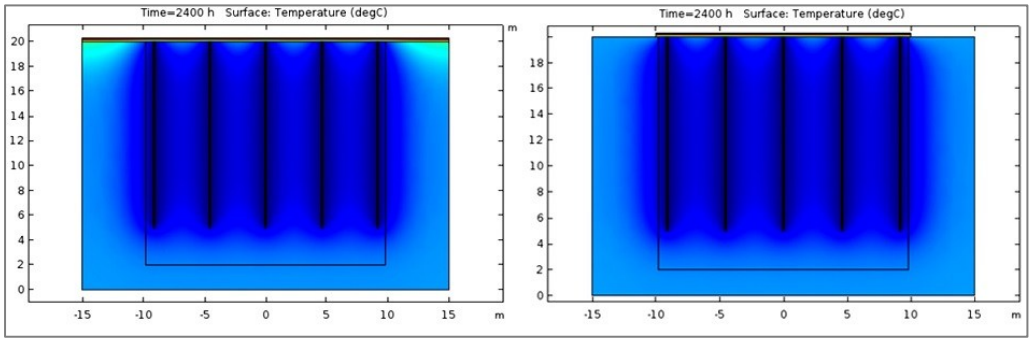

Figure 40. Results of 2400-hour simulation in 2D COMSOL for (**left**) (a) the floor only and (**right**) (b) the floor + soil as the upper boundary (Publication 3).

The average temperature of the rectangular region highlighted in Figure 40 was computed for both cases to quantify temperature differences in the soil region active for heat extraction. This region extends for 1.5 m from the piles located at the edges and 1 m from the bottoms of the piles. The active heat extraction region was employed to mitigate the impact of excessive soil surrounding that region on modelling accuracy in COMSOL. The different ground surface boundary conditions are compared in Figure 41.

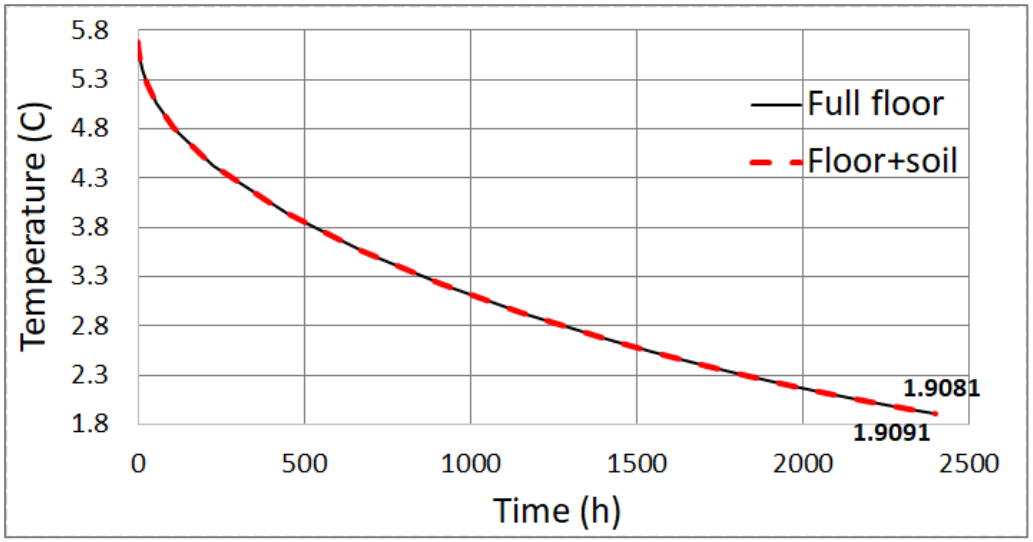

Figure 41. Average temperature in the active heat extraction region, in (a) the floor case (dashed) vs. (b) the floor + soil case (solid). *T* [°C] values for the last point are in bold (Publication 3).

According to the COMSOL simulation results, even after many hours of heat pump operation at full load, the difference was negligible, at most about 0.015 °C. Therefore, the one known limitation of the proposed GEP modelling method, i.e., the uniform floor slab boundary condition used in the IDA ICE borehole model, could be neglected without compromising the accuracy of the results, and thus the method had been validated.

4.2.4 IDA ICE borehole model against COMSOL

In this section, the results of the validation of the IDA ICE 3D finite difference borehole model against the COMSOL model are presented. Temperatures on the edges of 20 energy piles at different depths were computed in both models and compared to estimate the accuracy of the IDA ICE calculations. Figure 42 shows, as expected, that central pile #10 exhibits a slightly lower temperature compared to the and corner pile #20 due to thermal interactions between adjacent piles.

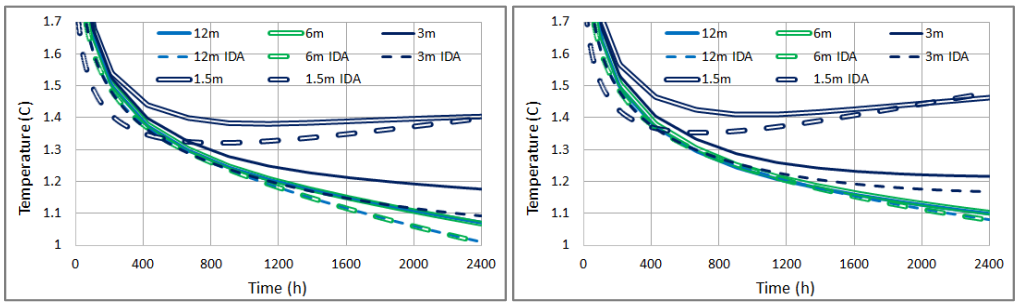

Figure 42. Temperatures of central pile #10 (**left**) and corner pile #20 (**right**) at different depths in IDA ICE vs. COMSOL (Publication 3).

COMSOL and IDA ICE simulation results are very similar, with an average difference of only about 0.05 °C. The difference in the calculated temperature decreases as depth increases, while the 6 m and 12 m curves overlap almost perfectly, showing excellent agreement.

4.2.5 Impact of boundary condition on calculation accuracy

Due to the fact that the IDA ICE borehole model (the pre-November 2017 version) did not allow the use of the calculated ground surface temperature as an input variable for the calculation of floor heat loss above the GEP region, it was decided to use the borehole outlet temperature in the floor heat loss calculation (Publication 2), as shown in Figure 11. In November 2017, an updated version of the IDA ICE borehole model was released, and the abovementioned limitation was mitigated by the introduction of the IDA ICE “slab” method.

To quantify the error resulting from this choice, the results plotted in Figure 43 compare the ground surface temperatures calculated in COMSOL with those obtained using the outdated "outlet" solution in the IDA ICE borehole model (Publication 2) and those calculated using the “slab solution” in the updated IDA ICE borehole model.

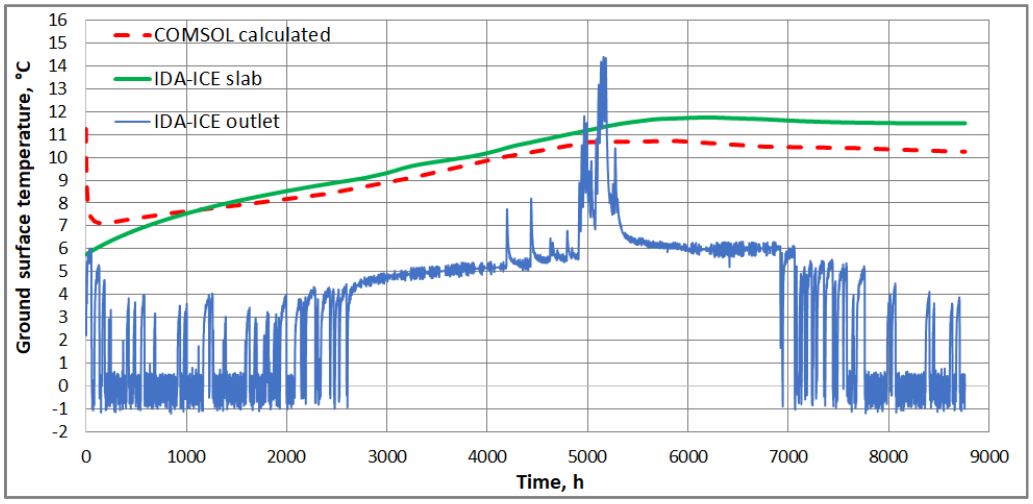

Figure 43. Ground surface temperature estimated in IDA-ICE vs. calculated (Publication 3).

The new "slab" implementation demonstrated a remarkable improvement over the "outlet" method in the assessment of energy consumption. A significant difference of 5.8 °C between the new “slab” and old “outlet” versions over the

year-long simulation period could be observed. Results for the new "slab" implementation of the IDA ICE borehole model and the COMSOL results differed by only 0.6 °C.

Validation results (Table 19) show how improper modelling of the ground surface temperature affects the value of the floor slab heat flux over the energy piles and thus the calculation of the annual heat demand of the building.

In terms of annual heat flux difference, using the outlet temperature of the energy piles as the ground surface boundary condition results in a difference of about 54%, which leads to almost a 5% overestimation of building annual heating need.

Table 19. Results of validation of ground surface temperatures estimated in IDA ICE (Publication 3).

Case	Floor Slab Heat Flux, kWh/a	Heating Need, kWh/a	Heat Flux, % Difference	Heating Need, % Difference
COMSOL	24066	142900	-	-
IDA ICE slab	24073	142580	0.03%	0.20%
IDA ICE outlet	37127	150196	54%	5%

In contrast, the new "slab" version of the IDA ICE borehole model performed well and was in a very good agreement with COMSOL, with acceptable differences in heat flux difference and heating need, 0.03% and 0.2%, respectively.

4.3 Demonstration of application of GEP modelling method

This section looks at the performance of the GEP modelling method in the OLK NZEB, a commercial hall-type building constructed in Hämeenlinna, Finland (Publication 4). The performance of the proposed GEP modelling method was quantified on the basis of the analysis of measured and simulated energy use. Building measurement data for a period of one year was used as input for an as-built calibration model. The results of the building model calibration are presented in Section 4.3.1, and the results of the analysis of the measured and simulated energy performance are presented in Section 4.3.2.

4.3.1 Building model calibration results

Figure 44 shows the monthly results of the building model calibration in IDA ICE for the OLK NZEB for the operation period 01.02.18-01.31.19. A total of four cases were considered. The first used measurement data obtained from a building monitoring system (BMS), while the other three were simulations. In each case, delivered energy had three components – heat provided by room units, heat provided by the AHU heating coil, and lighting/equipment electricity, all representing the building's internal heat gains.

In the measured case, the lighting/equipment energy component (green in Figure 44) included not only the electricity usage of lighting and equipment but also the electricity consumption of heavy machinery, since they were measured together on a room basis and could not be separated at the source of consumption. Heavy machinery had, however, a separate cooling system and its electricity use did not contribute to an internal heat gain in the building heat balance.

Consequently, the heavy machinery's electricity use had to be deducted from the electricity consumption of the lights and equipment in the calibrated model. This adjustment led to the simulation of three additional cases (see Section 3.3.5).

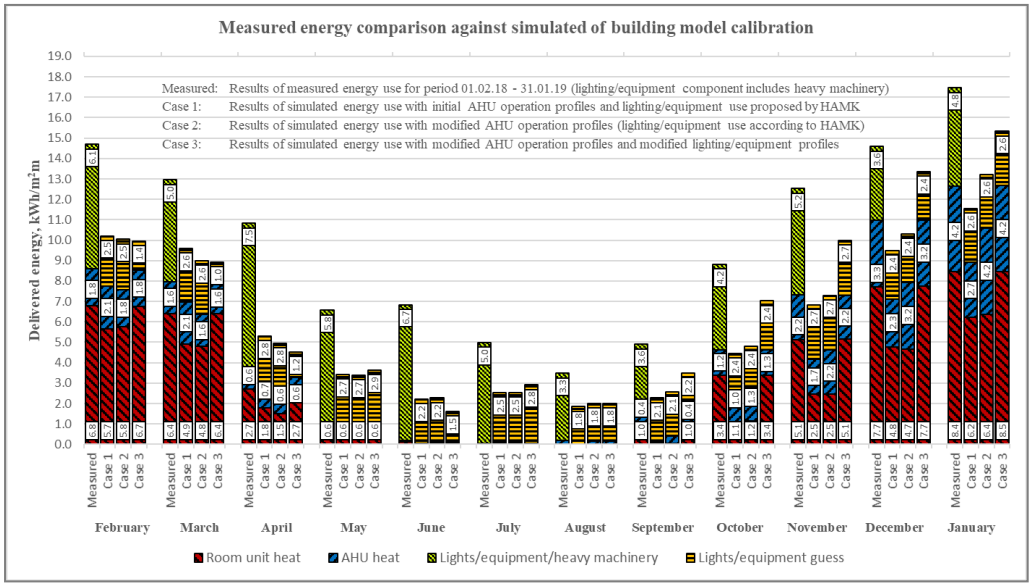

Figure 44. Building model calibration results (Publication 4).

In Figure 44, Case 1 results correspond to a simulation with the initial settings, where AHU operational profiles were defined according to the proposal of the Building Owner, since AHU electricity was not measured separately (see Table 20), and internal gains from lights/electricity were modified to meet the maximal internal light load in order to exclude heavy machinery from the building's heat balance (see Section 3.3). Results showed that the simulated room unit heat (41.4 MWh/a) was about 35% less than the measured room unit heat (63.3 MWh/a) and AHU heat (18.9 MWh/a) was about 19% less than the measured AHU heat (23.3 MWh/a).

Table 20. AHU working hour results (Publication 4).

Month	AHU operational time					
	Case 1		Case 2		Case 3	
	hours/week					
	TK01	TK02	TK01	TK02	TK01	TK02
February	64	77	35	59	40	58
March	64	77	35	38	35	38
April	64	77	30	28	28	25
May	64	77	55	64	54	60
June	64	77	64	93	64	93
July	64	77	63	98	63	101
August	64	77	160	168	116	140
September	64	77	110	94	65	71
October	64	77	64	78	64	66
November	64	77	64	85	64	70
December	64	77	68	89	63	76
January	64	77	105	86	100	83
Average	**64**	**77**	**71**	**82**	**63**	**73**

During the heating period from Feb - May, the simulated AHU heat exceeded the measured AHU heat, while during the heating period from Sep - Jan, the simulated AHU heat fell dramatically below the measured heat. The modelled AHU supply temperature matched the measured one, while modelled heat recovery performance matched that in the design documentation. Given the significant difference between measured and simulated AHU heat, it can be assumed that the AHU operational profiles proposed by HAMK in case 1 do not match the measured case scenario.

The generation of Case 2 proceeded from the abovementioned assumption involving the monthly modification of initial AHU profiles to align with the measured AHU heat. Figure 44 reveals that a perfect match between simulated AHU heat (23.3 MWh/a) and measured AHU heat (23.3 MWh/a) was obtained by using AHU operational hours in Case 2 (Table 20). Despite the match achieved between simulated and measured AHU heat, the simulated room unit heat (41.1 MWh/a) was 35% less than the measured room unit heat, essentially mirroring the results seen in Case 1. Assuming that the thermodynamic properties of the building envelope were defined in compliance with building as-built design documentation, and indoor air temperature setpoints were defined according to measurement data with an hourly resolution, significant differences between simulated and measured room unit heat would have arisen from inaccurate (overestimated) internal heat gains, i.e., the electricity usage of lighting/equipment, and/or additional sources of heat loss. The former would be due to the absence of separate monitoring of the electricity usage of heavy machinery. While an initial estimation of internal gains from lighting/equipment was based on a measured value of 90.9 MWh/a (including heavy machinery), it was then reduced to 44 MWh/a (excluding heavy machinery) in the first two simulated cases, representing a 52% decrease. An additional source of heat loss can be attributed to the systematic opening of the cargo doors. This was logged by the BMS, but due to a monitoring system failure, it could not be included in the modelling of the first two cases. The operation of the exhaust fans in the laboratory section of the building was also not monitored separately and as a consequence, was also neglected in the modelling.

Table 21. Cargo gate opening results (Publication 4).

Month	Cargo gate opening		
	Case 1	Case 2	Case 3
	min/day		
February	0	0	0
March	0	0	0
April	0	0	0
May	0	0	0
June	0	0	0
July	0	0	0
August	0	0	20
September	0	0	43
October	0	0	32
November	0	0	42
December	0	0	30
January	0	0	12
Average	**0**	**0**	**15**

To complete the building model calibration, either lighting/equipment electricity usage had to be decreased and/or additional sources of heat loss had be included in the model to achieve better agreement between simulated and measured room unit heat.

In Case 3, the last considerations were all taken into account. In Figure 44, for the period Feb-July, the input data for lighting/equipment electricity was scaled on a monthly basis, resulting in the aligning of simulated room unit heat values with the measured values. In the same case, the cargo gate openings were included in the model for the period Aug – Jan with opening shown in Table 21.

With these adjustments, internal gains from lighting/equipment were 37.3 MWh/a, less than the initial estimate of 44 MWh/a, while the cargo doors were opened for an average of 15 minutes per day throughout the year. After a perfect match between simulated and measured room unit heat had been achieved, further adjustments were made to AHU operational profiles to match AHU heat values as well (see Table 20) to complete the building model calibration. According to calibration results NMBE resulted in 0.17% and CV(RMSE) resulted in 1.05%, which is well within the ASHRAE Guideline 14 tolerances for monthly data (≤±5% for NMBE and ≤15% for CV(RMSE)).

Simulations were performed using the measured building weighted average (BWA) temperature (highlighted in red in Figure 45) as a heating system setpoint for each zone in the building calibration model in IDA ICE. BWA temperature was calculated on the basis of zone-specific heat loss and measured hourly indoor air temperature (see Section 3.3). Figure 45 shows a comparison of measured BWA temperatures with initial design indoor temperatures from simulations conducted in [15]. In the heating periods Feb - May and Oct – Jan, the measured BWA temperature was on average about 1.54 °C higher than the initial design indoor temperature.

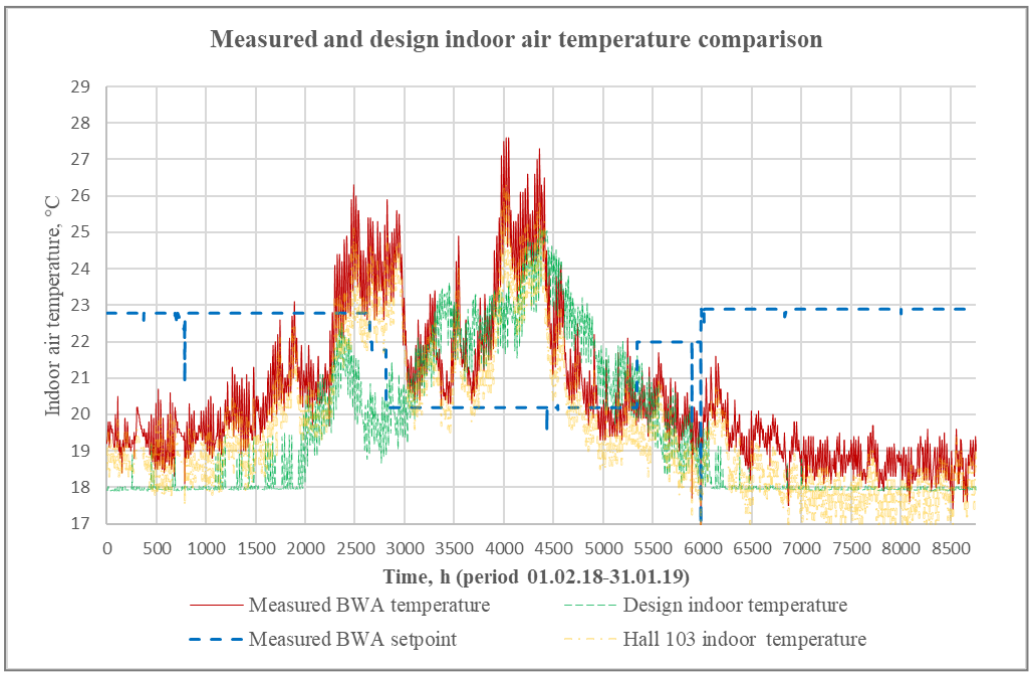

Figure 45. Measured and design indoor air temperatures (Publication 4).

When analyzing room overheating, the measured BWA temperature exceeded the cooling setpoint of 25 °C between 08:00-17:00 (working hours) by 135 °Ch. However, only the rooms serviced by the radiant ceiling panels were cooled, and this was done via the connection to the geothermal "free cooling" heat exchanger, while the other rooms were not cooled at all. The measured indoor air temperature for Hall 103, one of the cooled rooms, is shown in yellow in Figure 45. In Hall 103, indoor air temperature peaked at +26.3 °C, exceeding the cooling setpoint of 22 °Ch for working hours during the measuring period. This aligns well with Finnish regulations, as indoor air temperature should not exceed 100 °Ch during the summer period (01.06 – 31.08) in test reference year (TRY).

Comparison of measured AHU supply air temperatures (TK01/TK02) with initial design AHU supply temperatures applied in the simulations is shown in Figure 46. On average, during the heating period, the measured supply air temperature was about 1 °C higher than the initial design AHU supply air temperature for both AHUs.

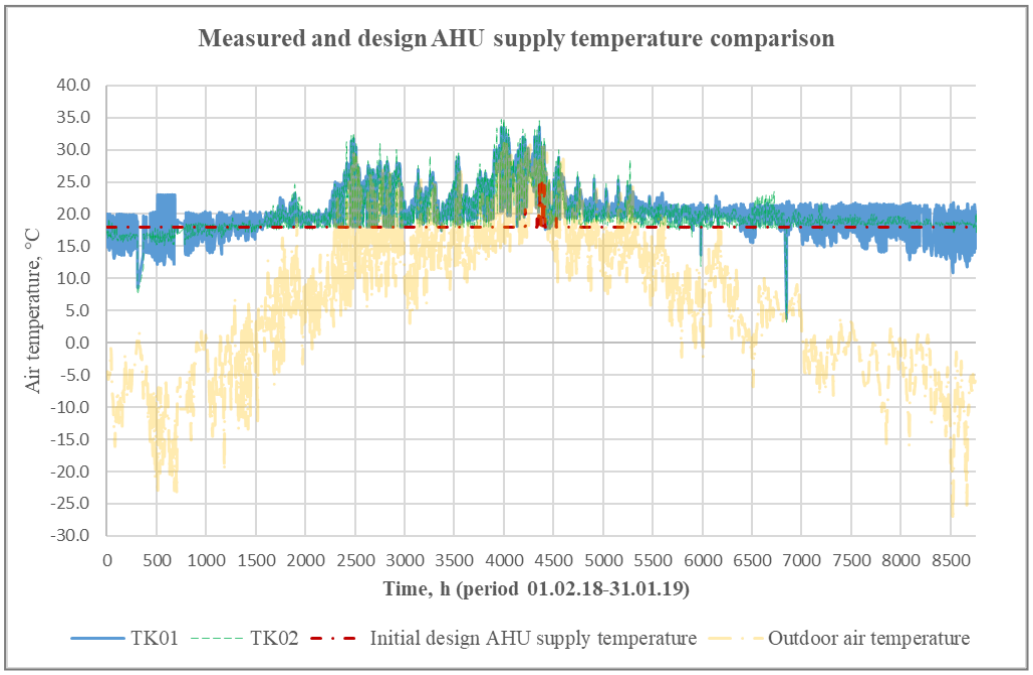

Figure 46. Measured and initial design AHU temperatures (Publication 4).

According to the as-built design, the AHUs lacked a "free cooling" connection. As a consequence, during the cooling period the measured supply air temperature was much higher than the initial design AHU supply air temperature.

4.3.2 Analysis of measured and simulated energy performance

Table 22 shows the results of the analysis of the measured and simulated energy performance of the OLK NZEB, a commercial hall-type building (Publication 4) for the period 01.02.18 – 31.01.19. Four cases in total are shown, the first corresponding to a reference initial design case from [15]. The second case shows measured energy performance. The third case shows the energy performance of

the calibrated model, with heat pump operation modelled in Excel. Heat pump modelling relied on polynomial equations involving performance map data for the installed heat pump and the measurement data for evaporator/condenser inlet/outlet fluid temperature. The fourth case shows the energy performance of the calibrated model under TRY climate conditions using the SCOP calculated in Excel in the previous case. Energy usage components are shown as delivered energy values that include the efficiencies and distribution losses in the operation of the heating/cooling system.

The measured heat consumption of the hydronic heating system (room unit heat in Table 22) is about 32% higher than in the design case, and that of the AHU heating coil, about 63% higher. Domestic hot water (DHW) heat consumption, in contrast, is about 12% lower than in the initial design case. In terms of heat consumption, indoor climate conditions in the measured case were less favorable due to a 1.54 °C higher average heating system setpoint temperature and 1 °C higher average AHU supply air temperature during the heating period. AHU heat recovery temperature efficiency in the initial design was slightly better (n = 0.8) than that of the as-built AHUs (n = 0.78). In terms of internal gains, the energy delivered by appliances (lighting and equipment electricity in Table 22) was 92% higher than in the initial design case.

Table 22. Measured and simulated annual energy performance of the OLK NZEB (Publication 4).

Case		Initial design (simulated SCOP)	Measured data (actual SCOP)	Calibrated model (Excel SCOP)	Calibrated model in TRY climate (Excel SCOP)
Units		Specific annual energy consumption per floor area (kWh/m²a)			
Building	Delivered room unit heat	32.1	42.3	42.3	41.8
	Delivered AHU heat	9.5	15.5	15.5	15.5
	Delivered DHW heat	4.1	3.6	3.6	3.6
Plant	Top-up heating	2.8	14.9	0.3	0.3
	Heat pump compressor	9.2	20.1	13	12.9
	Cooling electricity	0	0	0	0
	Fan electricity	9.2	9.51	9.5	9.5
	Pump electricity	2	2.01	2.01	2.01
	Lighting/equipment electricity	13	24.9	24.9	24.9
	DHW electricity	1.5	4.5	4.5	4.5
EPV[2]		**45**	**91**	**65**	**65**
Seasonal coefficient of performance value (SCOP)					
Heat pump SCOP		**4.68**	**2.88**	**4.46**	**4.46**
Whole plant heating SCOP		**3.28**	**1.97**	**3.8**	**3.8**
Whole plant SCOP with DHW		**2.95**	**1.56**	**3.45**	**3.45**

[1]Pump/fan electricity in the measured case are estimated values, where BMS/automation electricity was deducted.

[2]Energy performance value (EPV) is calculated using an electricity primary energy factor of 1.2.

However, the expected decrease in heat consumption resulting from the higher internal gains of appliances was significantly reduced by additional heat losses due to the opening of the cargo gates and lower overall solar radiation in the measured case than in the initial design case. In the initial design case, the opening of the cargo gates was not modelled. In the measured case, as mentioned in Section 4.3.1, the opening of the cargo gates had to be estimated due to a malfunction in the monitoring system. Moreover, the inability of the log-

ging/monitoring system to differentiate the electricity consumption of lighting/equipment/cooled heavy machinery also made it necessary to estimate electricity consumption by appliances. The impact of the opening of the cargo gates on the heating needs of the OLK NZEB in the calibrated case is 32%. The impact of climate conditions on heating needs can be quantified by comparing the room unit heat in the measured case (42.3 kWh/m²a) with the room unit heat in the TRY climate calibration case (41.8 kWh/m²a). This is a difference of just 1.2%. Conversely, the comparison of measured climate data with reference climate data showed 3803 °Cd in measured degree days verses 3661 °Cd in reference degree days at a balance point temperature of +15 °C. During the heating period, the sum of diffuse and direct solar radiation was 2.8% (23.4 MWh/a) less in the measured climate case than in the TRY climate case.

For electricity consumption by fans, there was good agreement between the measured consumption (9.5 kWh/m²a) and the reference consumption (9.2 kWh/m²a). The specific fan power (SFP) in the measured case was slightly lower than in the reference case, and the operation duration of AHUs was 13% higher than in the reference case. The measured and simulated delivered heat for room units and AHUs, shown in the form of 24h moving averages in Figure 47, showed good agreement.

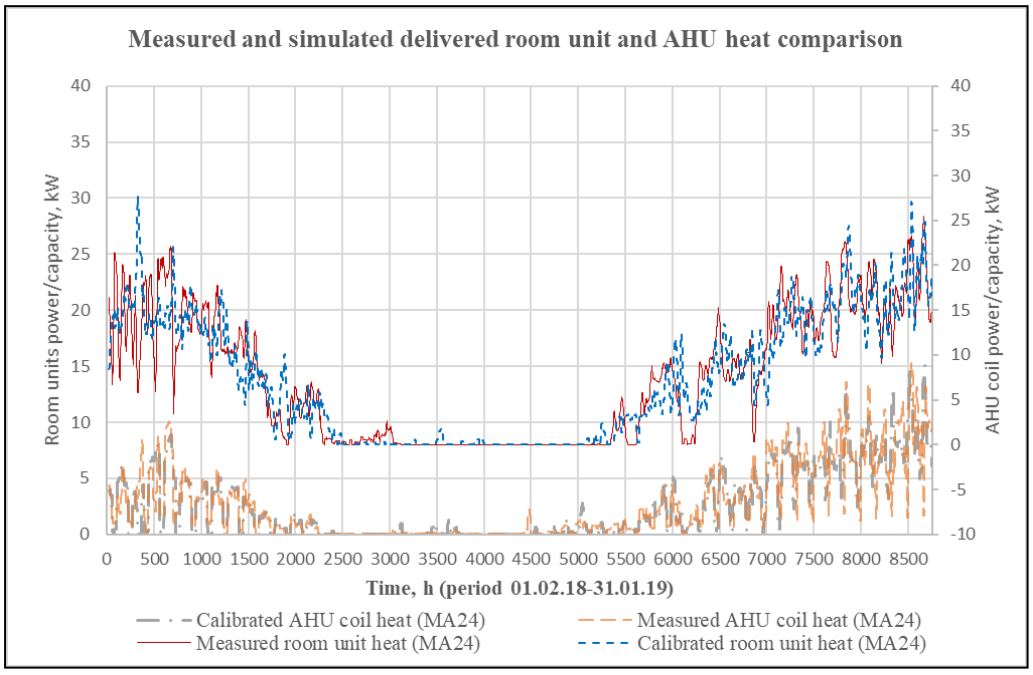

Figure 47. Measured and calibrated delivered heat (Publication 4).

The results for the seasonal coefficient of performance (SCOP) are categorized into three groups (see Table 22). The first group, “heat pump SCOP”, only considers AHU and room unit heat. The second group, “whole plant heating SCOP”, also considers top-up heating and electricity for pumps. The final category also takes DHW heat into account. According to the results, the geothermal heat pump plant in the measured case significantly underperformed, yielding an overall plant SCOP of 1.56. This is about 47% lower than the whole plant SCOP of 2.95 expected by the simulated initial design. Without taking top-up heating

into account, the heat pump SCOP in the measured case was 2.88, compared with 4.68 for the initial design, representing an underperformance of 38%.

The electricity value for top-up heating represents the energy consumption when the ON/OFF heat pump was unable to meet the building's heat demand, typically due to the temperature of the evaporator reaching the 0°C limit. At these times, top-up heating would provide additional energy to maintain the temperature in the hot buffer tank at the desired setpoint. In the measured case, the electricity consumption for top-up heating (14.9 kWh/m²a) was about five times higher than that in the initial design case (2.8 kWh/m²a). Poor monthly performance of the measured geothermal plant can also be observed in Table 23, where the average plant COP for July was recorded as 0.26. The low measured overall plant SCOP was in fact caused by improper operation of the geothermal plant due to incorrect control algorithms and/or a faulty automation system.

Table 23. Measured and calculated COP results for heating (Publication 4).

Month	Measured cond. outlet	Measured evap. inlet	Calculated COP[1]	Measured COP[1]
Feb	46	7	4.82	1.26
Mart	49	5	4.19	2.01
April	48	12	4.68	1.99
May	55	13	3.53	1.52
June	55	15	3.24	0.94
July	55	17	2.9	0.26
August	55	15	3.24	0.78
Sept	55	12	3.8	1.77
Oct	54	9	3.86	2.32
Nov	54	8	4.12	2.73
Dec	50	4	4.21	2.26
Jan	48	3	4.16	2.67
Average	**52**	**10**	**3.9**	**1.71**

[1]DHW production is taken into an account

As consequence, top-up heating became the dominant heat source in place of the heat pump. This can be observed in Figure 48. For example, at the beginning of February (0 – 200 h), the evaporator inlet fluid temperature was approximately +12.5 °C, which falls within the heat pump's operation range. However, the measured heat pump compressor power ranged from 0 to 1 kW, indicating minimal operation, while the top-up heating system operated at a power ranging from 20 to 55 kW. Similar observations can be made at the beginning of April (1400 – 1500 h) and November (6700 – 7000 h). Additionally, during the cooling period (2500 – 5000 h), when DHW consumption was high and geothermal loop fluid temperatures ranged from +10 to +18 °C, top-up heating remained operational, contrary to initial design expectations.

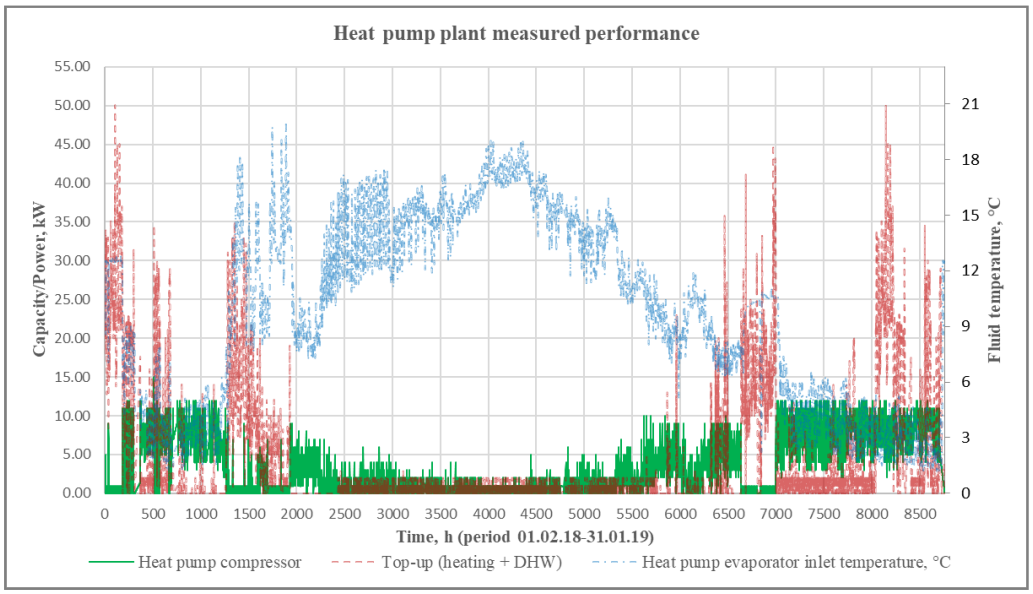

Figure 48. Measured heat pump plant performance (Publication 4).

According to the results of the measured case, the plant did not operate according to design intent. To quantify the performance potential of the geothermal plant under measured conditions, the heat pump was modelled in Excel using second-degree polynomial equations with an hourly time step. These equations were based on the heat pump performance map data and calculated evaporator inlet and condenser outlet fluid temperatures.

This simplified modelling approach has known assumptions and limitations. It neglects all thermodynamic processes in the soil and geothermal heat exchanger (GHX), assuming that the GHX and heat source are infinite. Additionally, the heat pump evaporator inlet temperature corresponds to the measured one and is not influenced by the operation of the modelled heat pump. Hypothetically, the results of this case correspond roughly to the highest achievable SCOP under the measured GHX temperature conditions, based on the heat pump performance map data and measured secondary side temperatures. The SCOP for the whole plant (3.45), including DHW, modelled in Excel on the basis of the measurement data, was 17% higher than that in the simulated initial design case (2.95) and about 2.2 times higher than the measured SCOP. It is worth noting, that the installed heat pump model differed from the one simulated in the initial design case. However, in the initial design case [15], the SCOP was obtained through a detailed numerical simulation, which was far more accurate than the simplified approach used in Publication 4 for estimating the SCOP. Nevertheless, due to the poor plant performance in the measured case, it was decided that a simplified SCOP estimation was sufficient to quantify the best possible performance of the as-built plant. Additional deviations in measured plant operation from the initial design case (see section 3.3.8) can be observed on Figure 49.

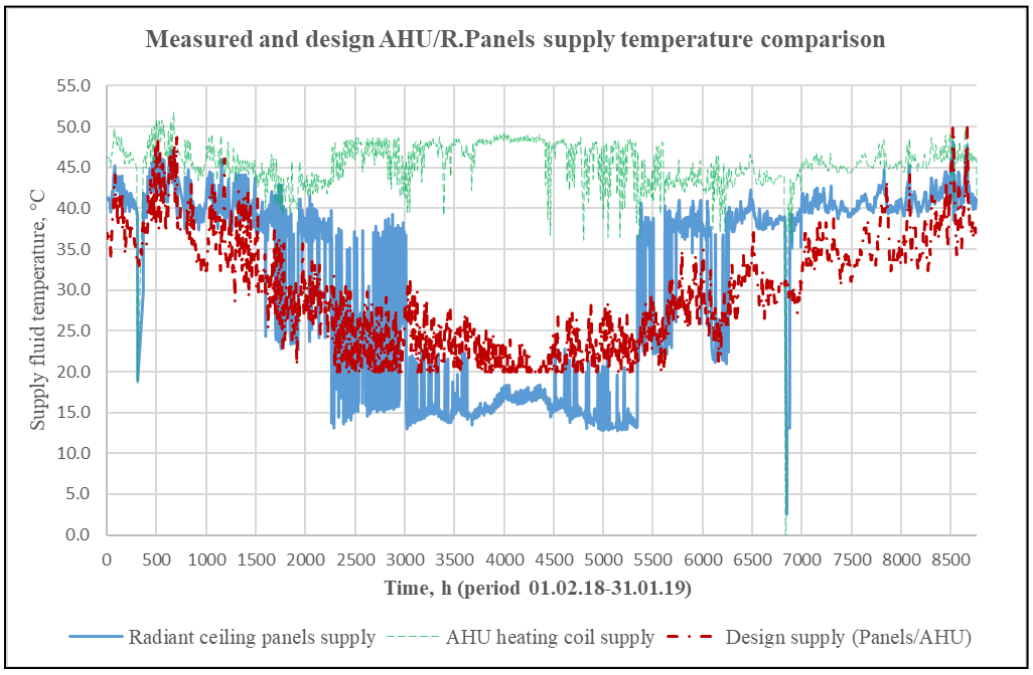

Figure 49. Measured and design plant supply temperatures (Publication 4).

According to the initial design case, the secondary side supply fluid temperatures for both the AHU and radiant ceiling panels were supposed to follow the heating curve presented in Figure 50. According to the heating curve, at an outdoor air temperature of -26°C the supply side temperature should be at its maximum value of +50°C. This temperature should gradually decrease as the outdoor air temperature increases, reaching +20°C when the outdoor air temperature reaches +20°C.

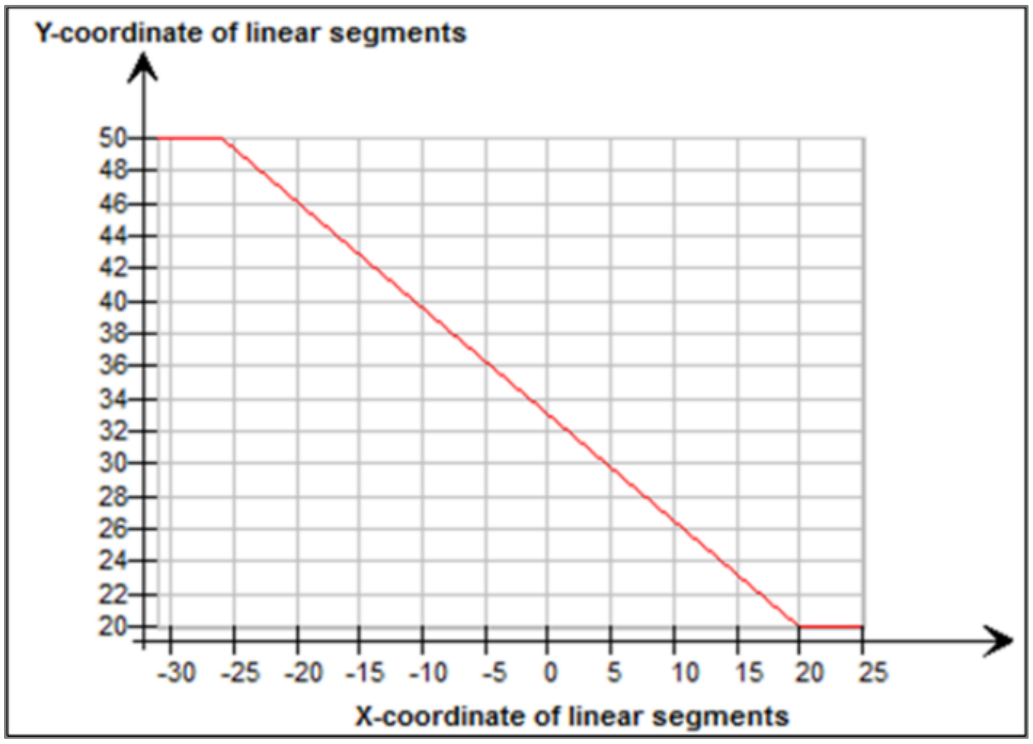

Figure 50. Secondary side supply temperature schedule. Y-coordinate corresponds to supply temperature and X-coordinate corresponds to outdoor air temperature (Publication 4).

However, according to Figure 49, the measured supply fluid temperature for the AHUs is not dependent on the heating curve, while the supply temperature for the radiant ceiling panels shows signs of dependency, though is still higher than that expected in the design case. The latter might be explained by the inability of the radiant ceiling panels to maintain the desired setpoint temperature (see Figure 45), while this in turn could result in an increase in plant supply temperature. This negatively impacts the COP of the heat pump, decreasing overall plant energy performance. According to the modelling of heat pump performance in Excel, the installed heat pump, with a rated capacity of about 40 kW, was capable of meeting about 99.5% of the heat demand under the measured climate conditions.

The overall goal of the design and construction of the OLK NZEB was to achieve the Finland NZEB target [87], which is 135 kWh/m2a of primary energy consumption for commercial hall-type buildings. The energy performance values (EPV) for each case are presented in Table 22. The EPV was calculated using the energy factor for electricity (1.2) for the year 2018, according to Finland regulations [87].

The simulated EPV in the initial design case was 45 kWh/m²a, exceeding the Finland NZEB target by a factor of 3, while the EPV in the measured case was 91 kWh/m2a, which is twice as high as the initial design result. Nevertheless, the EPV in the measured case complies with Finland NZEB commercial hall-type building requirements and confers the official status of a nearly zero-energy building. However, there is room for improvement, as the EPV in the calibrated case for the geothermal plant SCOP modelled in Excel was 65 kWh/m²a, representing a 29% improvement on the EPV in the measured case. As already discussed in this section, the operation of the plant automation system should be checked and adjusted/tuned so the plant will operate in accordance with the initial plant design intent/control logic.

The procedure for calibrating the building model confirmed that it is possible to achieve good agreement between measured and simulated results in the IDA ICE simulation environment. It also showed that this environment is capable of processing a large amount of measurement data via source files and allows for highly detailed modelling.

Despite some challenges, such as the lack of separation between the measured electricity usage of lighting, equipment, and heavy machinery, issues with monitoring cargo gate opening times, missing measurement data, and the fact that electricity usage of the AHUs and fans was not measured, the study successfully produced a monthly calibration model. Good agreement was achieved by making a considerable effort to use most of the available hourly-based measurement data as input, making well-considered assumptions, and carefully modifying the input data.

To improve the energy performance of the building studied, it was suggested to the Building Owner to lower the indoor air temperature by approximately 1.5 °C to meet the design intent, as the weighted average measured indoor air tem-

perature was found to be about 1.54 °C higher. Additionally, it was recommended to reduce the supply air temperature of the AHUs by 1 °C to align it with the initial design intent.

As an outcome of this research, the importance of a proper building monitoring/logging system has been shown, particularly in buildings with unconventional custom heating/cooling plant designs. In actual operation, such plants may dramatically underperform. To ensure that the heating/cooling plants and systems operate as designed, it is crucial to have a well-designed building monitoring/logging system that aligns with building model calibration needs.

Based on this research, the following measured parameters, covering a complete year with an hourly resolution, should be used in the building monitoring/logging system to carry out a successful detailed building model calibration in IDA ICE:

- Outdoor climate data (outdoor air temperature, relative humidity, wind velocity, wind direction, direct and diffuse solar radiation);
- Indoor air temperatures, setpoints;
- The plant's primary and secondary side temperatures (including heat pump evaporator/condenser inlet/outlet, thermal storage components etc.);
- Plant energy consumption by component (heat pump compressor/condenser/evaporator, cooling equipment, top-up heating/cooling/DHW, circulation pumps, AHU heating/cooling coils, buffer tank primary and secondary side energies, chillers, etc.);
- Internal gain data by component (lighting, equipment, cooled equipment);
- AHU energy and operation by component (supply/return air flows, fan electricity, supply/return air temperatures, energies/temperatures of air conditioning components);
- Opening data for cargo gates/large windows.

4.4 Results of GEP parametric study

This section covers the results of the GEP parametric study (Publication 5), which was carried out using benchmark simulations (see Section 3.4). This study looked at the sizing power of the heat pump evaporator, pile separation and installation depth, soil types, and the implementation of thermal storage. The total number of simulated cases was 120. For easy reference, the results of the parametric study are summarized in Table 24, Table 25, and Table 26. Results related to borehole outlet temperature in the 20th year of operation of the GEP plant are shown in Figure 51, Figure 52, and Figure 53. The impact of the outer diameter of the borehole on geothermal plant performance is discussed. Results for the sizing of electrical top-up heating are presented.

4.4.1 Performance of GEPs without thermal storage

This section investigates the impact of GEP spacing on different simulated initial design loads of the evaporator when there is no thermal storage (see Table 24). The energy piles, either 15 m or 30 m long, were buried in clay or silt. Separations of 3 m, 4.5 m, and 6 m correspond, respectively, to cases with 121, 48, and 36 piles, while each case was rescaled according to the building load profile in Figure 26 (see Section 3.4.1).

When the evaporator sizing power was 60 W/m (three times greater than 20 W/m), the condenser yield at a smaller spacing (3 m) with deeper installation (30 m) in silt soil only doubled (39 kWh/m vs 21 kWh/m). The same comparison in clay soil shows a minor increase by a factor of 1.35 (27 kWh/m vs 20 kWh/m), showing that increase in sizing power does not result in a linear increase in geothermal system output.

From a soil type perspective, silt performed better than clay for GEP installations. Shallower installations (15 m) in silt soil with evaporator sizing power at 60 W/m produced about 44% more condenser yield (56 kWh/m) when piles were spaced 3 m apart and 9% more condenser yield (62 kWh/m) when piles were 6 m apart than in the case of deeper installations (30 m). This shows that shallower installations and higher spacing without thermal storage are more effective. This conclusion is supported by the proximity of the building floor boundary, while a larger portion of its surface provides free thermal storage via floor heat losses.

Regarding the yield per ground surface area, closer distances between piles are strongly favored. Shallower installations (15 m) at low or high evaporator power (20 W/m or 60 W/m) can indeed return more than three times the yield per ground surface area with 3 m spacing instead of 6 m spacing. In contrast, deeper installations (30 m) return roughly double the yield per ground surface area with 15 m-deep piles at both 20 W/m and 60 W/m.

In Table 24, the demand covered by the heat pump corresponds to that of the specific case simulated in the benchmark, calculated using Equation 8.

$$D = 100\% - \left(E_{required} - E_{produced}\right)\% \quad (8)$$

Heat pump demand coverage is highest at lower power inputs (20 W/m), achieving near-full coverage (97%) in both soils, but silt soil supports higher coverage at higher power inputs.

However, this value may be increased by increasing the number of energy piles in the system, thus improving geothermal plant performance.

Table 24. Summary of the study results, 20 W/m – 60 W/m, no thermal storage (Publication 5).

			Silt						Clay					
			step 3m		step 4.5m		step 6m		step 3m		step 4.5m		step 6m	
			15m	30m	15m	30m	15m	30m	15m	30m	15m	30m	15m	30m
No thermal storage	20 W/m	power, W/m	20	20	20	20	-	20	20	18	20	19	-	20
		condenser yield, kWh/m	21	21	22	22		21	21	20	22	22		21
		ground area yield, kWh/m^{2}a	34	67	14	27		20	34	62	14	27		20
		demand covered by the heat pump[2]	97%	97%	97%	97%		97%	97%	90%	97%	96%		97%
	40 W/m	power, W/m	39	32	39	38	39	38	33	22	37	31	38	34
		condenser yield, kWh/m	42	35	43	42	42	42	37	25	41	35	41	37
		ground area yield, kWh/m^{2}a	66	110	27	52	20	39	57	77	26	43	19	35
		demand covered by the heat pump	95%	80%	96%	93%	96%	95%	83%	56%	92%	76%	94%	84%
	60 W/m	power, W/m	51	36	55	48	56	52	38	24	47	35	50	40
		condenser yield, kWh/m	56	39	62	53	62	57	42	27	52	39	55	44
		ground area yield, kWh/m^{2}a	87	122	38	66	29	53	65	83	32	48	26	41
		demand covered by the heat pump[2]	84%	59%	91%	79%	93%	85%	63%	40%	77%	57%	83%	66%

[1]thermal storage ratio of 100%

[2]amount of heat demand met by the heat pump in initial simulation (20 W/m, 40 W/m, 60 W/m, etc.), ideal case is 98.9%, the rest is met by natural thermal storage from heat loss exceeds storage ratio %

4.4.3 Performance of GEPs with 50% thermal storage

Table 25 shows benchmark simulation results when thermal storage was 50% of the expected condenser yield together with the exact value of the thermal storage (solar thermal storage according to profile in Section 3.4.4) required to achieve the reported yields.

Table 25. Summary of the study results, 20 W/m – 80 W/m, thermal storage 50% (Publication 5).

Thermal storage 50%			Silt						Clay					
			step 3m		step 4.5m		step 6m		step 3m		step 4.5m		step 6m	
			15m	30m	15m	30m	15m	30m	15m	30m	15m	30m	15m	30m
20 W/m	power, W/m		20	20					20	19		20		
	condenser yield, kWh/m a		21	21					21	21		22		
	ground area yield, kWh/m²a		34	67	-	-	-	-	34	67	-	27	-	-
	required thermal storage, kWh/m a		3.3	4.9					3.3	5.2		0		
	demand covered by the heat pump²		97%	97%					97%	96%		97%		
40 W/m	power, W/m		39	37	39	38		39	37	32	38	34	38	35
	condenser yield, kWh/m a		43	41	43	43		42	41	35	42	38	42	39
	ground area yield, kWh/m²a		67	128	27	53	-	39	64	110	26	48	19	36
	required thermal storage, kWh/m a		12	13	4	8		5	12	14	6	9	2	6
	demand covered by the heat pump²		96%	93%	96%	95%		95%	92%	79%	93%	85%	94%	88%
60 W/m	power, W/m		56	49	56	53	57	54	49	41	51	44	52	46
	condenser yield, kWh/m a		61	54	63	59	62	59	53	45	57	49	57	50
	ground area yield, kWh/m²a		95	169	39	73	29	55	83	141	35	61	26	47
	required thermal storage, kWh/m a		20	22	13	17	8	14	20	22	15	18	11	15
	demand covered by the heat pump²		92%	81%	93%	87%	94%	89%	80%	68%	84%	72%	86%	75%
80 W/m	power, W/m		68	59	70	64	72	67	58	69.8*	60	66.5*	62	65.3*
	condenser yield, kWh/m a		75	65	79	72	78	73	64	76.2*	67	72.7*	68	71.4*
	ground area yield, kWh/m²a		117	204	49	89	37	68	100	239*	42	92.3*	32	66.7*
	required thermal storage, kWh/m a		29	30	22	26	17	22	30	64.6	23	59.9	19	57.1
	demand covered by the heat pump²		84%	73%	87%	80%	89%	83%	72%	86%*	75%	82%*	77%	81%*

[1]thermal storage ratio of 100%

[2]amount of heat demand met by the heat pump in initial simulation (20 W/m, 40 W/m, 60 W/m, etc.), ideal case is 98.9%, the rest is met by -natural thermal storage from heat loss exceeds storage ratio %

According to Table 25, the demand covered by the heat pump decreases roughly linearly with increasing evaporator power for all pile lengths. As expected, thermal storage provides a significant amount of energy that should not be ignored.

Comparing Table 24 (with no thermal storage) with Table 25 (with 50% thermal storage), when the spacing is 3 m and the evaporator power, 60 W/m, the heat pump covers 8% more with 15 m-long piles and an impressive 22% more with 30 m piles. This is expected since longer piles penetrate deeper into the ground and exploit their greater thermal mass. This contrasts very clearly with the results obtained when there was no thermal storage.

With 50% thermal storage, condenser yields increased, particularly at higher power inputs, with clay soil yields reaching up to 76.2 kWh/m (an increase of about 38.5%) and silt soil yields, up to 79 kWh/m (an increase of about 27.4%) compared to maximum yields of 55 kWh/m and 62 kWh/m, respectively, when there was no thermal storage. Ground area yields also saw substantial gains, especially in silt soil, where yields rose from a maximum of 122 kWh/m² w without thermal storage to 204 kWh/m² with 50% thermal storage, an increase of about 67.2%.

Interestingly, the impact of pile spacing is much less relevant with heat storage than without it (see Table 24). Yet, it is not surprising, since the thermal inertia of the geothermal system is enhanced with thermal storage, and heat transfer is more uniform.

4.4.4 Performance of GEPs with 100% thermal storage

Results of the benchmark simulations with 100% thermal storage (solar thermal storage according to profile in Section 3.4.4) are reported in Table 26. The demand covered with higher evaporator power decreases linearly: for s = 6 m and L = 30 m, 100 W/m covers 85% of the demand, while 200 W/m covers only 70% (derivative value: -0.15). In the case of 50% thermal storage, the rate of decrease was twice as much (derivative value: -0.3). Ignoring thermal storage results in a steeper, parabolic decrease, as seen in Table 24.

Table 26. Summary of the study results in table format, 100 W/m – 200 W/m, thermal storage 100% (Publication 5).

Thermal storage 100%		Silt						Clay					
		step 3m		step 4.5m		step 6m		step 3m		step 4.5m		step 6m	
		15m	30m	15m	30m	15m	30m	15m	30m	15m	30m	15m	30m
100 W/m	power, W/m	90	89	89	87	89	86	85	84	81	79	80	77
	condenser yield, kWh/m a	99	98	97	95	97	95	93	92	89	86	87	84
	ground area yield, kWh/m^{2}a	155	306	62	121	45	88	146	288	56	110	41	78
	required thermal storage, kWh/m a	80	81	72	77	67	73	81	82	74	77	70	74
	demand covered by the heat pump^2	89%	88%	88%	86%	88%	85%	84%	83%	80%	78%	79%	76%
150 W/m	power, W/m	125	124	121	119	120	116	118	118	109	108	106	103
	condenser yield, kWh/m a	137	136	133	130	132	127	129	129	119	118	116	113
	ground area yield, kWh/m^{2}a	215	426	84	165	61	119	202	405	76	150	54	106
	required thermal storage, kWh/m a	122	124	115	119	110	116	124	124	116	120	112	116
	demand covered by the heat pump^2	83%	82%	80%	78%	79%	77%	77%	78%	72%	71%	70%	68%
200 W/m	power, W/m	156	157	148	147	145	142	147	150	134	135	128	128
	condenser yield, kWh/m a	170	172	162	161	159	156	160	164	146	148	140	140
	ground area yield, kWh/m^{2}a	267	538	103	204	74	145	252	515	93	188	65	130
	required thermal storage, kWh/m a	165	167	156	162	153	158	165	167	160	162	155	160
	demand covered by the heat pump^2	77%	78%	73%	73%	72%	70%	73%	73%	66%	66%	63%	63%

[1]thermal storage ratio of 100%

[2]amount of heat demand met by the heat pump in initial simulation (20 W/m, 40 W/m, 60 W/m etc), ideal case is 98.9%, rest is met by top-up

-natural thermal storage from heat loss exceeds storage ratio %

Implementing 100% thermal storage in the benchmark simulation substantially enhances performance across all key metrics. Condenser yields in clay soil rise from 21-55 kWh/m in the case without thermal storage to 84-164 kWh/m with 100% thermal storage, representing an increase of about 198%-282%. In silt soil, there is an increase from 21-62 kWh/m to 95-172 kWh/m, representing an increase of about 177%-352%.

Ground area yields show significant improvements with thermal storage. In clay soil, yields increased from 83 kWh/m² to 515 kWh/m², and in silt soil, from 122 kWh/m² to 538 kWh/m², representing increases of approximately 520% and 341%, respectively.

These findings underscore the substantial positive impact of 100% thermal storage on energy pile performance, as it leads to higher yields and better demand coverage, especially in silt soil.

4.4.5 Top-up heating sizing results

The results of the top-up heating sizing simulations are shown in Table 27. The percentage values represent the ratio of top-up heating to total building design heat load. For example, in the case of a 100 kW design heat load at an outdoor air temperature of -26 °C, when pile length is 30 m, piles are buried in clay with 3 m spacing, and sizing is according to the "60 W/m without storage" case, the appropriate top-up heating should be 85% of 100 kW, which is 85 kW.

Table 27. Sizing the electrical top-up heating results (Publication 5).

Case description	clay				silt			
	step 3m		step 6m		step 3m		step 6m	
	15m	30m	15m	30m	15m	30m	15m	30m
60 W/m without storage	82%	85%	83%	84%	79%	81%	75%	79%
60 W/m with 50% storage	82%	83%	84%	85%	75%	80%	75%	79%
80 W/m with 50% storage	81%	82%[1]	83%	85%[1]	79%	81%	79%	81%
200 W/m with 100% storage	85%	85%	88%	89%	82%	82%	85%	87%

[1]thermal storage was 100%

It should be noted that the values in Table 27 were calculated for cases where the heat pump and thermal storage source were sized according to the results reported in Table 24, Table 25, and Table 26. In the "60 W/m with 50% storage" case, with 15 m-long piles buried in clay with 3 m spacing, the heat pump evaporator was sized at 60 W/m with 20 kWh/m covered by solar thermal storage, and top-up heating size was determined to be 82% of the total design heat load.

4.4.6 Impact of the borehole outer diameter on performance

According to the results of 20 benchmark simulations of a double U-pipe with a pile outer diameter of 170 mm and 125 mm, the pile with the 125 mm outer diameter is approximately 2% less efficient in clay and 1% less efficient in silt than the pile with the 170 mm outer diameter. These findings confirm earlier reports in [10,11], indicating that pile diameter is not critical for heat transfer efficiency.

4.4.7 GEP brine outlet temperature results

Results related to brine outlet temperature in the 20th year of GEP plant operation with different evaporator sizing powers and thermal storage capacities are shown in Figure 51, Figure 52, and Figure 53.

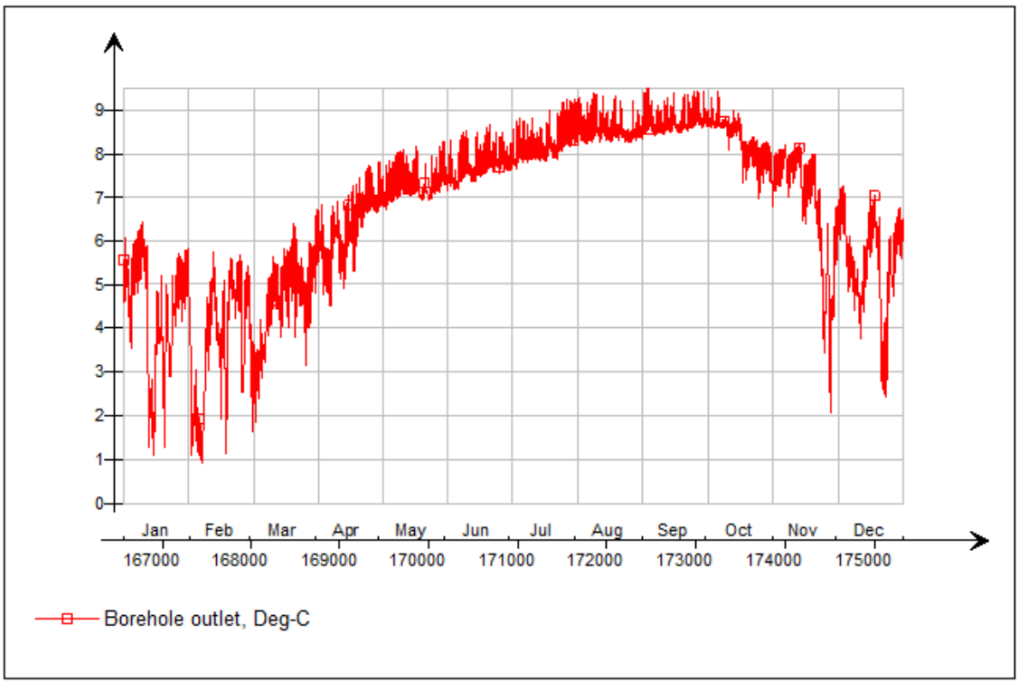

Figure 51. Borehole outlet temperature case: 40 W/m, step 3m, length 30m, storage 50%, silt (Publication 5).

Peak GEP brine outlet temperatures are critical when selecting the heat pump product due to the need to consider operational range.

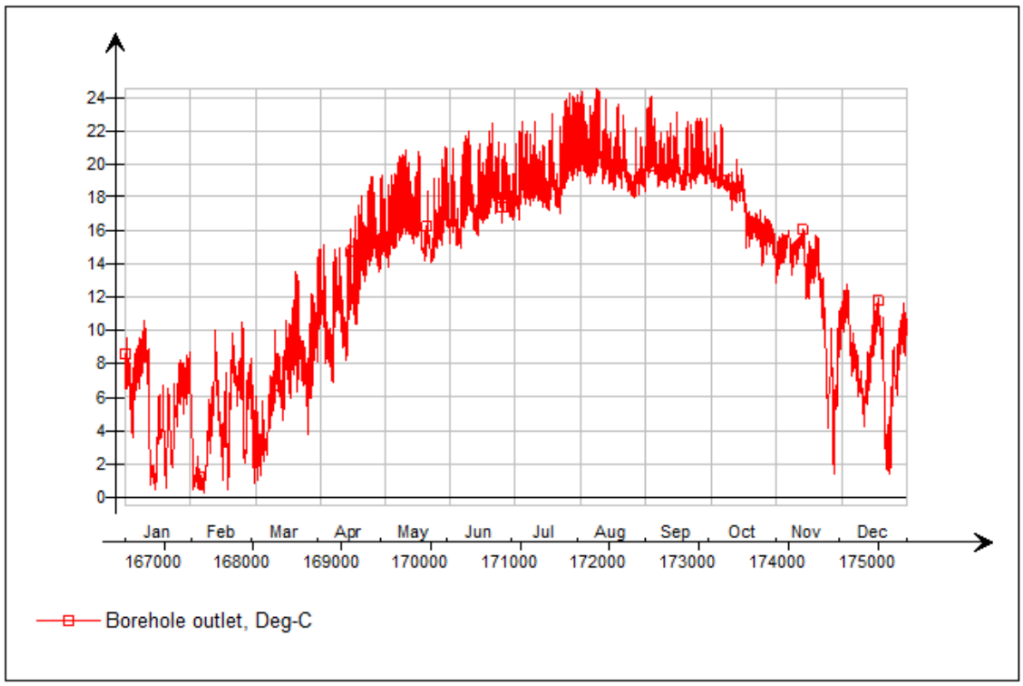

Figure 52. Borehole outlet temperature case: 80 W/m, step 3m, length 30m, storage 100%, clay (Publication 5).

Doubling the evaporator sizing power from 40 W/m (see Figure 51) to 80 W/m (see Figure 52) with 50% thermal storage led to a rise in peak borehole outlet temperature from about 9 °C to 24 °C. With the increase in evaporator power, the required thermal storage amount also increased, resulting in higher peak brine outlet temperatures.

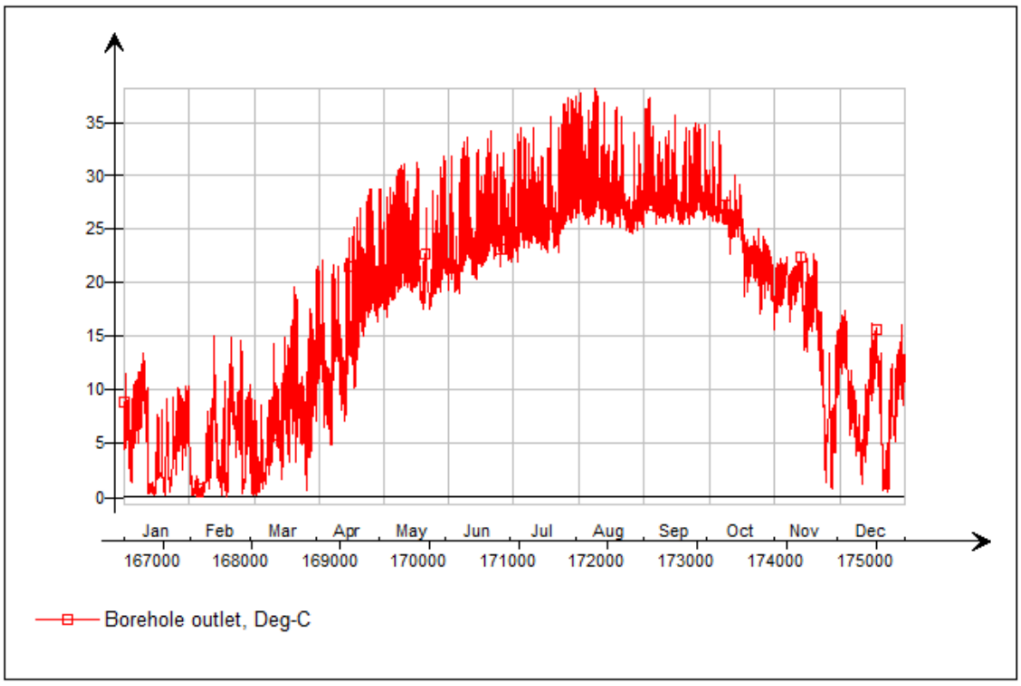

Figure 53. Borehole outlet temperature case: 200 W/m, step 3m, length 30m, storage 100%, silt (Publication 5).

The critical role of thermal storage was clearly demonstrated in Figure 51, Figure 52, and Figure 53, as doubling thermal storage capacity results in a borehole outlet temperature that is nearly three times higher.

4.5 GEP sizing method for use in the early stages of design

The results of the GEP parametric study in the previous section are used here to demonstrate a method for the preliminary sizing of a geothermal plant, in the form of a sizing guide addressing a specific example based on the building design heat load Q and annual energy need E (without DHW). However, it is important to consider the following:

(1) This preliminary sizing guide is suitable for commercial hall-type buildings designed for the climate and load profile described in Section 3.4.2.
(2) After the preliminary sizing is conducted according to this sizing guide, it is important to conduct a detailed simulation with the obtained energy pile system parameters before their implementing them in the actual design.
(3) Figure 54 to Figure 58 were generated using the results of the GEP parametric study in Table 24 to Table 26 for ease of reference.

1. Determining building design heat load and annual heating energy need

In this sizing example, a commercial hall-type building with the following initial parameters is considered:

- Building design heat load (DAT = -26 °C): $Q = 360\ kW$
- Building's annual energy need: $E = 168\ MWh$

2. Sizing the heat pump evaporator

First, the heat pump condenser Q_{cond} needs to be sized. According to the building load profile in Figure 29, a condenser power sized to 50% of the building design heat load can cover up to 98.9% of the annual heating demand. The remaining 1.1% should be covered with top-up heating, and thus a heat pump with 50% less output power can be installed. The heat pump condenser is then sized accordingly as 180 kW and the evaporator as:

$$Q_{evap} = \frac{Q_{cond} \times (COP-1)}{COP} = 140\ kW \quad (9)$$

The annual average $COP = 4.5$ in the equation above is equal to the value in the benchmark simulation in Section 3.4.

3. Estimation of the total pile field length and condenser yield

Assuming that the soil type is clay and the energy piles are 30 meters long, the simulated GEP performance corresponding to these conditions (without thermal storage) is plotted in Figure 36 (which was generated using the results shown in Table 8).

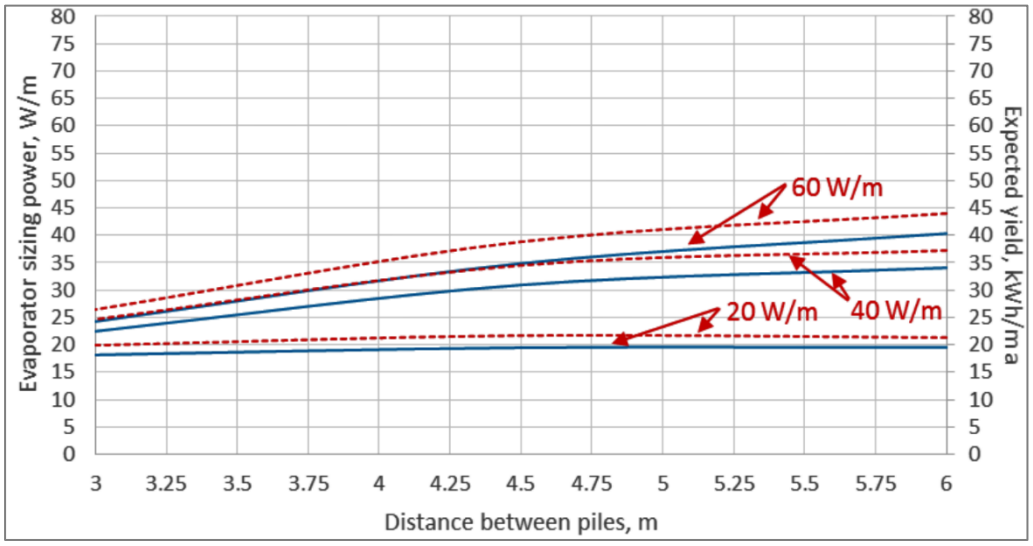

Figure 54. Evaporator power (solid) and condenser yield (dashed) results for 30 m-long energy piles in clay without thermal storage (Publication 5).

Simulated performance data can be collected for three different initial evaporator power sizing values: 20 W/m, 40 W/m, and 60 W/m. The total energy pile length L is only a function of system sizing and geometry. The specific condenser yield per unit length E/L [kWh/m] is then simulated, with a total expected condenser yield remaining constant at $E = E/L \times L$ [kWh].

In this example, sizing the energy piles according to 60 W/m of evaporator power for a total power of $Q_{evap} = 140\ kW$ would result in the following energy pile length:

$$L = \frac{Qevap}{W/m} = \frac{140\ kW * 1000\ \frac{W}{kW}}{60\ W/m} \approx 2333\ m \quad (10)$$

Based on the energy pile length, the total expected condenser yield can now be calculated. The results for an evaporator power sizing of 60 W/m and piles with spacings of 3 m, 4.5 m, and 6 m are given in Table 28.

Table 28. Simulated condenser and total yield for an evaporator power sizing of 60 W/m (Publication 5).

Pile spacing	Specific condenser yield	Total condenser yield
3 m	27 kWh/m	63 MWh
4.5 m	39 kWh/m	91 MWh
6 m	44 kWh/m	103 MWh

With an evaporator power sizing of 60 W/m, maximal energy yield of sized energy piles without thermal storage is 103 MWh when pile spacing of 6 m. However, in this example, the building's annual energy need is $E = 168\ MWh$. Since the demand (168 MWh) is larger than what is produced by the energy piles (103 MWh), one should either install more piles or consider thermal storage.

If more piles are installed, the required length of energy piles with a spacing of 6 m is calculated by dividing the annual energy need E by the specific condenser yield:

$$L = \frac{16800\ kWh}{44\ kWh/m} \approx\ 3818\ m \tag{11}$$

The total number of sized energy piles is $n = 3818\ m \div 30\ m \approx 127$ with 6 m spacing. The heat pump condenser power should be 180 kW, and the evaporator power, 140 kW. Thermal storage is not needed.

4. Evaluating the impact of thermal storage on energy pile length

Instead of adding more piles, thermal storage will now be included, and this should reduce the required total pile length. The simulated performance of energy piles with different thermal storage ratios, in terms of condenser yield per meter (kWh/m), can be determined by referring to either Figure 55 or Figure 56 (generated from GEP parametric study results in Table 25 and Table 26).

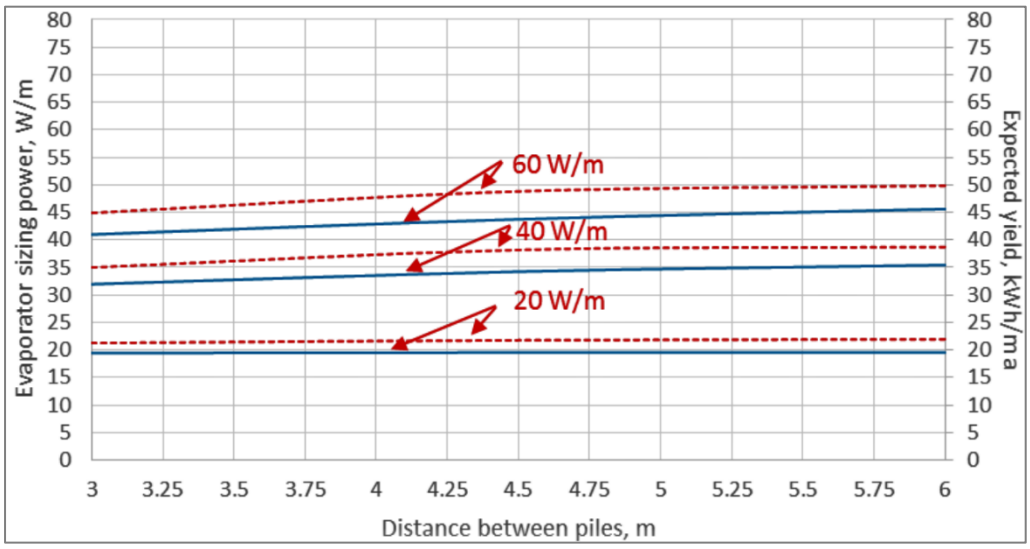

Figure 55. Evaporator power (solid) and condenser yield (dashed) of 30 m-long energy piles in clay, with 50% thermal storage (Publication 5).

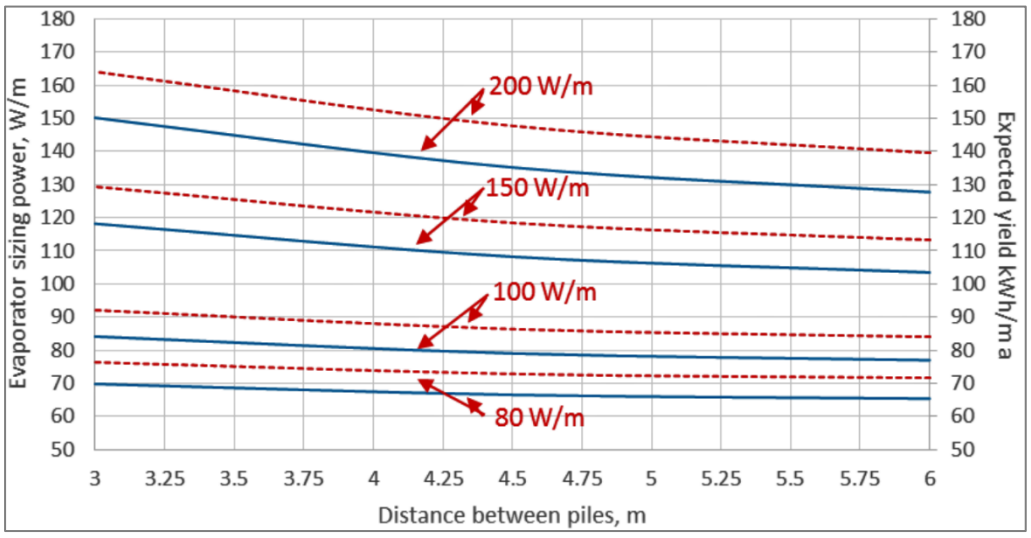

Figure 56. Evaporator power (solid) and condenser yield (dashed) of 30 m-long energy piles in clay, with 100% thermal storage (Publication 5).

By looking at the plots, one can indeed immediately quantify the expected condenser yield (kWh/m) based on the chosen initial evaporator sizing power (W/m) and energy pile field design, for a given amount of thermal storage.

In this specific example, 50% thermal storage is considered. By examining Figure 55, a maximal condenser yield of 50 kWh/m is obtained for an evaporator sizing power of 60 W/m and with a pile spacing of 6 m. This result should now be combined with the thermal storage capacity for this specific case. This can be retrieved from Figure 57 (generated from GEP parametric study results in Table 25).

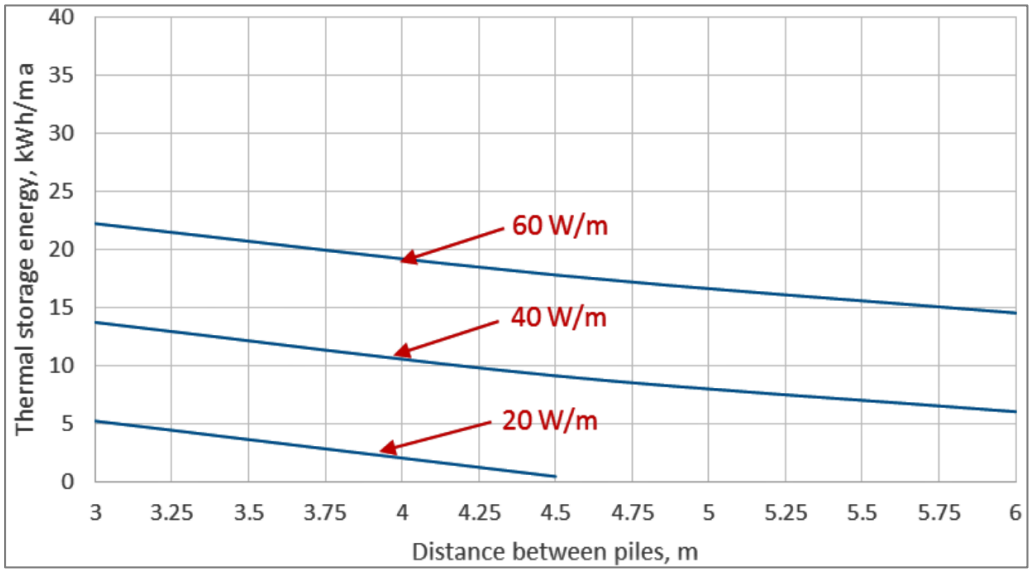

Figure 57. Thermal storage required to achieve 50% for 30 m-long energy piles in clay (Publication 5).

To produce 50 kWh/m of condenser yield, the required amount of thermal storage is 15 kWh/m with an evaporator power of 60 W/m and 6 m spacing. Recalling the above results and assuming 50% thermal storage and 6 m pile spacing, the total condenser yield is:

$$E_{6ts} = 2333\ m \times 50\ kWh/m \approx 117\ MWh \quad (12)$$

The required thermal storage capacity:

$$ET_{6ts} = 2333\ m \times 15\ kWh/m \approx 35\ MWh \quad (13)$$

Since the resulting condenser yield is 117 MWh < 168 MWh, either the pile length or thermal storage capacity needs to be increased. To increase the amount of thermal storage from 50% to 100%, Figure 58 should be examined.

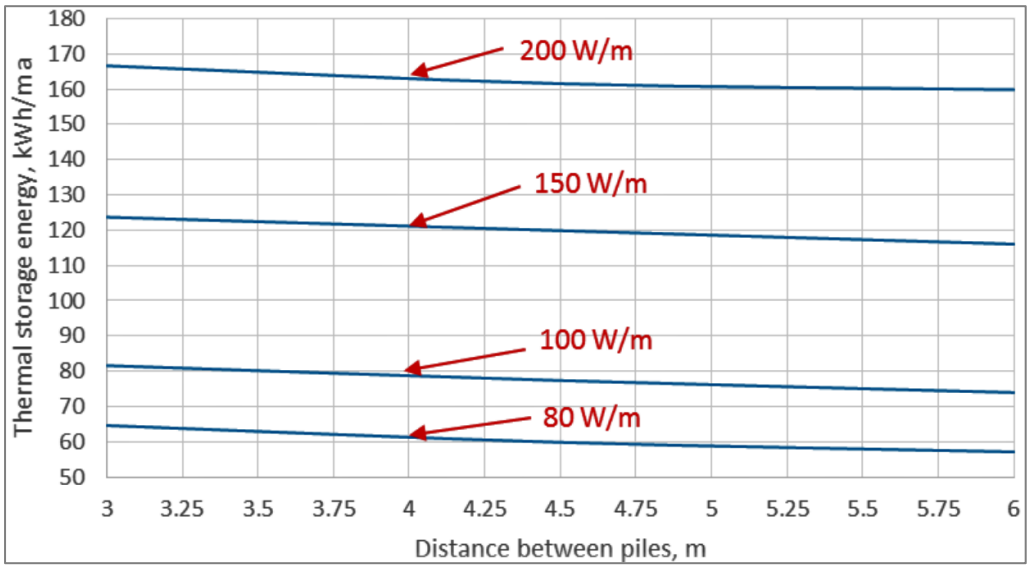

Figure 58. Thermal storage required to achieve 100% for 30 m-long energy piles in clay (Publication 5).

According to the plot, for 100 W/m with 6 m pile spacing, 72 kWh/m of TS is required to achieve a specific condenser yield of 83 kWh/m.

Using this with Figure 56, the following energy pile length is obtained:

$$L_{6ts2} = \frac{168000\ kWh}{83\ kWh/m} \approx 2024\ m \quad (14)$$

The thermal storage capacity is accordingly:

$$QE_{6ts2} = 2024m \times 72\ kWh/m \approx 146MWh \quad (15)$$

The maximal heat pump evaporator power is now:

$$Q_{condmax6ts2} = 2024m \times 100\ W/m \approx 202.4\ kW \quad (16)$$

It should also be kept in mind that the maximal heat pump evaporator power (202 kW) should be equal to or higher than the initial value (140 kW). Otherwise, the heat pump will not be sized to 50%, will not be able to cover most of the building's heat demand, and will require more frequent top-up heating corrections. If more thermal storage energy is available, the pile length can be decreased. For 150 W/m with 6 m spacing, the required TS is about 116 kWh/m, resulting in a condenser yield of 112 kWh/m. The energy pile length required to produce 168 MWh is then computed as:

$$L_{6ts3} = \frac{168000\ kWh}{112\ kWh/m} = 1500\ m \quad (17)$$

The required thermal storage capacity is accordingly:

$$QE_{6ts3} = 1500m \times 116\ kWh/m \approx 174\ MWh \quad (18)$$

The maximal heat pump evaporator power is now:

$$Q_{condmax6ts3} = 1500m \times 150\ W/m \approx 225\ kW \quad (19)$$

To recapitulate the above calculations, the following energy pile system configurations were determined for the three distinct cases (L is length, s is spacing):

- No thermal storage: L = 3813 m for s = 6 m, 127 piles
- 146 MWh thermal storage: L = 2024 m for s = 6 m, 67 piles
- 174 MWh thermal storage: L = 1500 m for s = 6 m, 50 piles

5. Sizing top-up heating

The top-up heating sizing is done using Table 27. The top-up sizing in clay, when L = 30 m and s = 6 m, is as follows:

- 84% x 360 kW = 302 kW for 60 W/m, no thermal storage
- 85% x 360 kW = 306 kW for 100 W/m with thermal storage
- 87% x 360 kW = 313 kW for 150 W/m with thermal storage

5.1. Applied to 16 random building configurations

The sizing procedure in this guide was applied to a total of 16 commercial hall-type buildings using different soils and energy pile lengths, without thermal storage. The results are reported in Table 29.

Table 29. Results of 16 random cases without thermal storage. (Publication 5).

Case	Design heat load	Annual heat demand	clay 30 m	silt 30 m	clay 15 m	silt 15 m	clay 30 m	silt 30 m	clay 15 m	silt 15 m
nr	**kW**	**kWh/a**	**required energy piles length, m**				**maximal evaporator power, %**			
1	360	168	3817	2947	3054	2709	164%	126%	131%	116%
2	360	236	5364	**4667***	**4667***	**4667***	115%	**100%***	**100%***	**100%***
3	360	341	7747	5981	6198	5498	166%	128%	133%	118%
4	360	341	7747	5980	6198	5498	166%	128%	133%	118%
5	270	239	5430	4192	4344	3854	155%	120%	124%	110%
6	261	225	5103	3939	4082	3621	151%	116%	121%	107%
7	257	218	4946	3818	3957	3510	148%	115%	119%	105%
8	272	229	5196	4011	4157	3687	147%	114%	118%	105%
9	271	223	5074	3917	4059	3601	144%	111%	116%	103%
10	255	214	4858	3750	3886	3448	147%	113%	118%	104%
11	241	189	4296	3316	3437	**3124***	138%	106%	110%	**100%***
12	270	239	5430	4191	4344	3853	155%	120%	124%	110%
13	195	151	3439	2655	2751	2528*	136%	105%	109%	**100%***
14	195	150	3399	2624	2720	2528*	134%	104%	108%	**100%***
15	250	204	4632	3576	3706	3288	143%	110%	114%	101%
16	148	43	**1919***	**1919***	**1919***	**1919***	**100%***	**100%***	**100%***	**100%***

*cases where initial evaporator power sizing (e.g., design load*0.5: 60 W/m) produced enough condenser yield

Sizing according to the GEP preliminary sizing guide provided both the heat pump design load and the required annual condenser yield (building heat demand) in only 10 out of 64 cases without thermal storage. Additionally, only 6 cases showed that the sizing almost reached the maximal possible condenser yield at the required evaporator size. In the remaining 48 cases, the energy pile length needed to be increased.

5. Conclusions

The research presented in this thesis has significantly advanced the theoretical understanding and practical implementation of geothermal energy piles (GEPs) coupled with ground source heat pumps (GSHPs) for building heating and cooling. Given the identified research gap, this novel study focused on the development and validation of a modelling method for GEPs with thermal storage, providing a detailed whole-building simulation model, and creating a tabulated early-stage GEP sizing guide.

The main aim of this research consisted of both theoretical and practical components. The theoretical part was achieved by identifying the research gap through a systematic literature review and justifying it through a comparison between BHE and the proposed GEP modelling method.

The practical part of the main aim was fulfilled by validating the proposed GEP modelling method, demonstrating its usefulness and accuracy through a case study involving the design and operational data analysis of a commercial hall-type building in Finland. Additionally, a GEP parametric study was conducted, and a tabulated GEP sizing method for use in the early stages of design was introduced to building engineers, as an aid when GEP technology is being considered as a viable renewable energy alternative. This all helped answer the main research questions and resulted in five research outcomes and publications.

More specifically, the main concepts, approaches, and methods for GEP modelling, design, and sizing were thoroughly reviewed and analyzed. Energy piles, often confused with boreholes due to their similar applications, differ significantly in geometry and boundary conditions. Energy piles are generally shorter, wider, and located beneath building floors, leading to unique performance characteristics. Properly sized heat pump systems with energy piles can achieve high SCOP values (>4.5), and their use with thermal storage may significantly reduce the number of energy piles required (>50%), underlining the importance of accurate design and sizing.

A detailed whole-building simulation approach was developed, to demonstrate its suitability for use in the design and prediction of long-term performance of both GEPs and BHE fields. The key differences between BHEs and GEPs were highlighted, most importantly, the fact that GEPs benefit from natural thermal storage effects due to heat loss through building floor structure, resulting in more stable long-term performance. According to numerical simulations, the long-term performance of a BHE field decreases by 30% after the first year of operation, in contrast to that of GEPs, due to differences in ground surface boundary conditions.

The proposed GEP modelling method was validated by comparing boundary conditions and their impact on heat transfer and predictions of energy performance. A 3D transient heat transfer model using COMSOL Multiphysics was validated against experimental data, showing excellent agreement despite uncertainties in soil properties. A 2D multi-pile reduction assessed different upper boundary conditions—either a floor at 20°C or a combination of floor and soil at 6°C. Results indicated that yearly energy balances were unaffected by specific boundary conditions due to small temperature variations in the active heat extraction zone. This allows simplified modelling using variable ground surface temperatures, eliminating the need for complex multiregional boundary conditions. 3D models in COMSOL and IDA ICE consisting of 20 energy piles embedded in soil beneath a uniform multilayer floor showed that the temperature predictions made by both tools were nearly identical, with an average difference of only 0.05°C. A yearly simulation conducted to evaluate the heating need of a commercial hall-type building with a geothermal plant showed that using the energy pile outlet temperature as an estimate for the ground surface temperature in IDA-ICE resulted in a 54% overestimation of heat flux in the floor slab and a 5% increase in heating demand. In contrast, using the actual ground surface temperature produced results nearly identical to those of COMSOL, with only a 0.03% overestimate in heat flux and a 0.2% increase in heating need.

To demonstrate the usefulness and accuracy of the proposed GEP modelling method, it was applied to the design and energy performance modelling of a Finnish nearly zero-energy building (NZEB) with a geothermal heat pump plant. The building was subjected to data monitoring and measurements were taken. An as-built calibration model was then created in IDA ICE, and the operational measurement data was used to analyze energy use, assess the impact of free cooling on the indoor climate, and evaluate the energy performance of the geothermal heat pump plant. According to the results, the main goal of designing and constructing a commercial hall-type building that complies with Finland's NZEB requirements had been successfully achieved, with a measured Energy Performance Value (EPV) of 91 kWh/m²a, which is 33% lower than the NZEB target value of 135 kWh/m²a. Analysis of the geothermal heat pump plant's performance and modelling revealed significant discrepancies, revealing a low Seasonal Coefficient of Performance (SCOP) of 1.56, compared to the initial design expectation of 2.95. The data indicated that electrical top-up heating was predominantly used instead of the heat pump, which, despite having favor-

able operating conditions, was likely not functioning as expected due to improperly configured automation systems. Modelling results suggest that aligning the automation system with the initial design intent could reduce the EPV by 29% and increase the SCOP to up to 3.45. Additionally, adjusting the secondary side supply temperature of the Air Handling Units (AHUs) according to the heating curve could further improve the heat pump's Coefficient of Performance (COP).

The building model calibration procedure demonstrated that a strong alignment between measured and simulated results can be achieved using the IDA ICE simulation environment, which can handle large input datasets and supports detailed modelling. Despite challenges such as the inability to differentiate lighting, equipment, and heavy machinery in the monitoring of electricity usage, issues with monitoring cargo gate opening times, and missing data on AHU airflow and fan electricity usage, the work successfully produced a well-calibrated monthly model. This model made use of most available hourly data and achieved very good agreement with measured results. An important outcome of this study is the recognition of the critical need for a comprehensive building monitoring and logging system, especially in the case of buildings with unconventional heating and cooling plant designs. This underscores the fact that effective monitoring and logging are essential to ensuring that a plant operates as intended and performs efficiently, and this in turn points to the need for a well-designed system that aligns with building model calibration requirements.

To support engineers in the early stages of design of GEP systems, a new tabulated GEP sizing method was developed based on a parametric study using a benchmark simulation. The study examined various factors, including heat pump evaporator sizing power, pile separation and installation depth, soil types, and the implementation of thermal storage in a commercial hall-type building. Simulations conducted over a 20-year period, including stress tests under very cold conditions, revealed that the expected yield was not proportional to the evaporator extraction power [W/m], but rather favors smaller specific power values. Additionally, it was confirmed that performance is dramatically improved by the addition of thermal storage. In the sizing example, the incorporation of thermal storage reduced the required number of piles from 127 to 50, resulting in substantial construction cost savings. As a novel and general outcome, the results can be presented as explicit extraction powers [W/m] and yields [kWh/m] per pile length for each initial extraction sizing power and energy pile field configuration selected by the user. These results were used to create a sizing guide for the specific example presented in this thesis. The estimation tool and sizing guide developed provide engineers with practical assistance, enabling a more accurate and efficient preliminary design of commercial hall-type buildings in cold climates. The method demonstrated in this thesis can be extended to any climate region and building type, making it a versatile tool for diverse applications.

Future Research

In future research, the investigation of the following key areas is essential:

- **The Modelling of Water Advection and Phase Change:** Future models should incorporate water advection and phase change effects to improve accuracy and allow simulations with different phase change materials.

- **Extension to Other Buildings and Climates:** Extending the proposed tabulated early-stage GEP sizing method to other types of buildings and climate conditions will broaden its applicability and versatility.

- **Development of Adaptive Control Strategies:** Creating adaptive control strategies for thermal storage utilization will help optimize and balance GEP plant heat extraction and rejection on an annual basis.

- **Study of Free Cooling Potential:** Investigating the "free cooling" potential of GEP plants and developing corresponding design guidelines will enhance their efficiency and scope of application.

- **Life-Cycle and Economic Feasibility Analysis:** Conducting life-cycle analyses and economic feasibility studies of GEP plants with comparisons to district heating and cooling networks will provide insights into their long-term viability and cost-effectiveness.

References

[1] Rousselot M, Pinto Da Rocha, F. Energy efficiency trends in buildings in the EU. *ODYSSEE-MURE.* 2021

[2] Buildings Factsheet. *European Commission.* 2021

[3] GREEN PAPER A 2030 framework for climate and energy policies. *European Commission.* 2013

[4] Directive 2010/31/EU of the European Parliament and of the Council of 19 May 2010 on the energy performance of buildings (recast). *Official Journal of the European Union*. 2021

[5] Lund J. W, Toth A. N. Direct utilization of geothermal energy 2020 worldwide review. *Geothermics.* 2021;90(0):101915

[6] Fossa M. The temperature penalty approach to the design of borehole heat exchangers for heat pump applications', *Energy and Buildings.* 2011;43(6):1473-1479

[7] Brandl H. Energy foundations and other thermo-active ground structures. *Geotechnique*. 2006;56(2):81-122

[8] Fadejev J, Kurnitski J. Geothermal energy piles and boreholes design with heat pump in a whole building simulation software. *Energy Build*. 2015;106(0):23-4

[9] Hamada Y, Saitoh H, Nakamura M, Kubota H, Ochifuji K. Field performance of an energy pile system for space heating. *Energy Build*. 2007;39(5):517-524

[10] Pahud D, Hubbucj M. Measured thermal performances of the energy pile system of the dock midfield at Zürich airport. In: *Proceedings European geothermal congress*. 2007. May 31-June 01 unterhatching, Germany; 2007.

[11] Hellstrom G. Ground heat storage: thermal analysis of duct storage systems. Sweden: Department of Mathematical Physics, *University of Lund.* 1991.

[12] Reda F. Long term performance of different SAGSHP solutions for residential energy supply in Finland. *Appl Energy.* 2015;144(0):31-50.

[13] Allaerts K, Coomans M, Salenbien R. Hybrid ground-source heat pump systemwith active air source regeneration. *Energy Convers Manag.* 2015;90(0): 230-7

[14] Morrone B, Coppola G, Raucci V. Energy and economic savings using geothermal heat pumps in different climates. *Energy Convers Manag.* 2014;88(0):189-98

[15] Fadejev J, Simson R, Kurnitski J, Kesti J, Mononen T, Lautso P. Geothermal heat pump plant performance in a nearly zero-energy building. Proceedings of Sustainable Built Environment Tallinn and Helsinki Conference SBE16. *Energy Proced.* 2016;96:489-502

[16] Zhang C, Guo Z, Liu Y, Cong X, Peng D. A review on thermal response test of ground-coupled heat pump systems. *Renew Sustain Energy.* Rev 2014;40(0):851-67

[17] Gao J, Zhang X, Liu J, Li KS, Yang J. Thermal performance and ground temperature of vertical pile-foundation heat exchangers: a case study. *Appl Therm Eng.* 2008;28(17-18):p.2295-2304

[18] Jalaluddin AM, Tsubaki K, Inoue S, Yoshida K. Experimental study of several types of ground heat exchanger using a steel pile foundation. *Renew Energy*. 2011;36(2):p.764-771

[19] Zarrella A, De Carli M, Galgaro A. Thermal performance of two types of energy foundation pile: helical pipe and triple U-tube. *Appl Therm Eng*. 2013;61(2):301-10

[20] Park S, Lee D, Choi H-J, Jung K, Choi H. Relative constructability and thermal performance of cast-in-place concrete energy pile: coil-type GHEX (ground heat exchanger). *Energy.* 2014:1-11 (Article in press)

[21] Carslaw HS, Jaeger JC. Heat conduction in solids. *Oxford: Claremore Press.*1947

[22] Ingersoll LR, Zobel OJ, Ingersoll AC. Heat conduction with engineering, geological, and other applications. *New York: McGraw-Hill.* 1954

[23] Zeng HY, Diao NR, Fang ZH. A finite line-source model for boreholes in geothermal heat exchangers. *Heat Transf Asian.* 2002;31(7):558-67

[24] Man Y, Yang H, Diaoa N, Liua J, Fanga Z. A new model and analytical solutions for borehole and pile ground heat exchangers. *Int J Heat Mass Transf* . 2010;53(13e14):2593-601

[25] Lei TK. Development of a computational model for a ground-coupled heatexchanger. *ASHRAE Trans.* 1993;99(1):149-59

[26] He S, Rees S, Shao L. Improvement of a two-dimensional borehole heat exchanger model. In: Proceedings of conference: IESD PhD conference: energy and sustainable development, institute of energy and sustainable development, queens building. Leicester, *UK: De Montfort University.* 2001

[27] Muraya NK. Numerical modeling of the transient thermal interference of vertical U-tube heat exchangers. Ph. D. theis. *Texas: Texas A&M University.* 1994

[28] Eskilson P. Thermal analysis of heat extraction boreholes. Ph.D. Thesis. *Sweden: University of Lund.* 1987

[29] Yavuzturk C, Spitler JD, Rees SJ. A Transient two-dimensional finite volume model for the simulation of vertical U-tube ground heat exchangers. *ASHRAE Trans.* 1999;105(A):465-74

[30] Chuangchid P, Krarti M. Foundation heat loss from heated concrete slab-on-grade floors. *Build Environ.* 2001;36(0):637-55

[31] Javed S, Claesson J. New analytical and numerical solutions for the short-term analysis of vertical ground heat exchangers. *ASHRAE Trans.* 2011;117(1): 3-12

[32] Zhang W, Yang H, Lu L, Cui P, Fang Z. The research on ring-coil heat transfer models of pile foundation ground heat exchangers in the case of groundwater seepage. *Energy Build.* 2014;71(0):115-28

[33] Zhang W, Yang H, Lu L, Fang Z. The analysis on solid cylindrical heat source model of foundation pile ground heat exchangers with groundwater flow. *Energy.* 2013;55(0):417-25

[34] Wang D, Lu L, Zhang W, Cui P. Numerical and analytical analysis of ground-water influence on the pile geothermal heat exchanger with cast-in spiral coils. *Appl Energy.* 2015;160(0):705-14

[35] Hu P, Zha J, Lei F, Zhu N, Wu T. A composite cylindrical model and its application in analysis of thermal response and performance for energy pile. *Energy Build.* 2014;84(0):324-32

[36] Ingersoll LR, Plass HJ. Theory of the ground pipe heat source for the heat pump, Heating. *Pip Cond.* 1948;20:119-22

[37] Diao N, Li Q, Fang Z. Improvement on modelling of heat transfer in vertical ground heat exchangers. *HVAC&R.* Res 2004;10:459-70

[38] Bandos TV, Campos-Celador A, Lopez-Gonzalez LM, Sala-Lizarraga JM. Finite cylinder-source model for energy pile heat exchangers: effects of thermal storage and vertical temperature variations. *Energy.* 2014;78(0):639-48

[39] Loveridge F, Powrie W. G-Functions for multiple interacting pile heat exchangers. *Energy.* 2014;64(0):747-57

[40] Loveridge F, Powrie W. 2D thermal resistance of pile heat exchangers. *Geothermics.* 2014;50(0):122-35

[41] Eslami-Nejad P, Bernier M. Freezing of geothermal borehole surroundings: a numerical and experimental assessment with applications. *Appl Energy.* 2012;98:333-45

[42] Eslami-Nejad P, Bernier M. Heat transfer in double U-tube boreholes with two independent circuits. *J Heat Transf.* 2011;133(8)

[43] Bonacina C, Comini G, Fasano A, Primicerio M. Numerical solution of phase change problems. *Int J Heat Mass Transf.* 1973;16(10):1825-32

[44] Rottmayer SP, Beckman WA, Mitchell JW. Simulation of a single vertical U-tube ground heat exchanger in an infinite medium. *ASHRAE Trans.* 1997;103(2):651-9

[45] Yavuzturk C. Modeling of vertical ground loop heat exchangers for ground source heat pump systems. Ph. D. thesis. *Oklahoma: Oklahoma State University.* 1999

[46] Lee CK, Lam HN. A simplified model of energy pile for ground-source heat pump systems. *Energy.* 2013;55(0):838-45

[47] Ghasemi-Fare O, Basu P. A practical heat transfer model for geothermal piles. *Energy Build.* 2013;66(0):470-9

[48] He S, Rees S, Shao L. Simulation of a domestic ground source heat pump system using a transient numerical borehole heat exchanger model. In: *Proceedings of conference: building simulation 2009, eleventh international IBPSA conference, Glasgow, scotland.* July 27-30, 2009

[49] Kohl T, Hopkirk RJ. "FRACTure" A simulation code for forced fluid flow and transport in fractured, porous rock. *Geothermics.* 1995;24(3):333-4

[50] Kohl T, Brenni R, Eugester W. System performance of a deep borehole heat exchanger. *Geothermics.* 2002;31:687-708

[51] Signorelli S, Bassetti S, Pahud D, Kohl T. Numerical evaluation of thermal response tests. *Geothermics.* 2007;36(2):141-66

[52] Gashti EHN, Uotinen VM, Kujala K. Numerical modelling of thermal regimes in steel energy pile foundations: a case study. *Energy Build.* 2014;69(0):165-74

[53] Fadejev J, Kurnitski J. Energy pile and heat pump modeling in whole building simulation model. *In: 2nd IBPSA-England conference on building simulation and optimization, London, United Kingdom.* June 2014. p. 23-4

[54] Dupray F, Laloui L, Kazangba A. Numerical analysis of seasonal heat storage in an energy pile foundation. *Comput Geotechnics.* 2014;55(0):67-77

[55] Osterreichischer Wasser- und Abfallwirstschaftsverband. OWAV-RB 207-Thermische Nutzung des Grundwassers und des Untergrunds e Heizen und Kühlen. Austria. 2014

[56] Verein Deutscher Ingegneure. In: VDI 4640 e Blatt 1e4. Thermal use of the underground. Düsseldorf, Germany. 2010

[57] Schweitzer Ingeneur- und Architektenverein. SIA 384/6. Erdwarmesonden, Zürich, Switzerland. 2010

[58] Microgeneration Installation Standard. MIS 3005 Issue 4.0-Requirements for contractors undertaking the supply, design, installation, set to work, commissioning and handover of microgeneration heat pump systems. London, UK. 2013

[59] GSHPA. Thermal pile. Design, installation and material standards. Issue 1.0. *UK: Ground Source Heat Pump Association, National Energy Center.* 2012

[60] Brandl H. Energy piles for heating and cooling of buildings. *In: Proceedings of 7th international conference and exhibition on piling and deep foundations,Vienna.* 1998. p. 341-6

[61] IGSHPA. Ground source heat pump residential and light commercial: design and installation guide. *USA. Oklahoma State University*. 2009

[62] Philippe M, Bernier M, Marchio D. Sizing calculation spreadsheet. Vertical geothermal borefields. *ASHRAE J.* 2010;52(7):20-8

[63] Kavanaugh SP, Rafferty K. Ground-source heat pumps - design of geothermal system for commercial and institutional buildings. Atlanta. *ASHRAE Applications Handbook*. 1997

[64] Kalamees T, Jylha K, Tietavainen H, Jokisalo J, Ilomets S, Hyvonen R, et al. Development of weighting factors for climate variables for selecting the energy reference year according to the EN ISO 15927-4 standard. *Energy Build.* 2012;47:53-60

[65] Sailer E, Taborda DMG, Keirstead J. Assessment of design procedures for vertical borehole heat exchangers. *In: Proceedings of fortieth workshop on geothermal reservoir engineering, Stanford, California.* January 26-28, 2015

[66] Wood CJ, Liu H, Riffat SB. Comparison of a modelled and field tested piled ground heat exchanger system for a residential building and the simulated effect of assisted ground heat recharge. *Int J Low Carbon Technol.* 2010;5(3):137-43

[67] Blocon. Earth energy designer v. 3.2 user's manual. Sweden. 2015.

[68] Spitler JD. GLHEPRO: a design tool for commercial building ground loop heat exchangers. In: Proceedings of the fourth international heat pumps in cold climates conference, Aylmer, Quebec; August 17-18, 2000

[69] IGSHPA. GLHEPro 4.1 for windows User's guide. USA: School of Mechanical and Aerospace Engineering, Oklahoma State University. 2014

[70] Wetter M, Huber A. TRNSYS type 451 e vertical borehole heat exchanger EWS model e model description and implementing into TRNSYS. Zürich/Luzern, Switzerland: Huber Energietechnik AG. 1997

[71] Huber A. Program EWS version 4.7-calculation of borehole heat exchangers software manual. Zürich, Switzerland: Huber Energietechnik AG. 2011

[72] Gaia Geothermal. Ground loop Design™ premier 2014 User's guide, USA. 2014

[73] Pahud D, Fromentin A, Hadorn J-C. The duct ground heat storage model (DST) for TRNSYS used for the simulation of heat exchanger piles, user manual, Lausanne. 1996

[74] Pahud D. Pilesim2 - simulation tool for heating/cooling systems with energy piles or borehole heat exchangers e user manual. Switzerland: *ISAAC-DACD-SUPSI.* 2007

[75] Brandemeuhl M. HVAC2 Toolkit: Algorithms and Subroutines for Secondary HVAC Systems Energy Calculations. Handbook. *ASHRAE*. 1993

[76] Description of the IDA ICE Borehole Model. Internal Report. *Equa*. 2013

[77] Giardina J.J. Evaluation of Ground Coupled Heat Pumps for the State of Wisconsin, USA: *University of Wisconsin*. 1995

[78] Shonder J.A, Beck J.V, Determining effective soil formation thermal properties from field data using a parameter estimation technique, *Oak Ridge: Oak Ridge National Lab.* Nov. 1998

[79] Lautkankare R, Sarola V, Kanerva-Lehto H. Energy piles in underpinning projects—Through holes in load transfer structures. *DFI J. J. Deep Found. Inst.* 2014,(8):3-14

[80] Uotinen V.M, Repo T, Vesamäki H, Energy piles - ground energy system integrated to the steel foundation piles. *Denmark: NGM 2012 Proceedings. Proceedings of the 16th Nordic Geotechnical Meeting, Copenhagen.* 2012,(1-2)*:*837–844

[81] Jõeleht A, Kukkonen I.T. Physical properties of Vendian to Devonian sedimentary rocks in Estonia. *GFF.* 2002,124:65-67

[82] Kukkonen I, Lindberg A, Thermal properties of rocks at the investigation sites : measured and calculated thermal conductivity, specific heat capacity and thermal diffusivity. Finland. 2011

[83] Bauer D, Heidemann W, Diersch H, Transient 3D analysis of borehole heat exchanger modeling. *Geothermics.* 2011,(40):250-260

[84] Al-Khoury R, Kölbel T, Schramedei R. Efficient numerical modeling of borehole heat exchangers. *Computers & Geosciences.* 2010,(36):1301–1315

[85] Fadejev J, Simson R, Kurnitski J, Haghighat F, A review on energy piles design, sizing and modelling . *Energy.* 2017,(122):390–407

[86] Yang H, PCui P, Fang Z. Vertical-borehole ground-coupled heat pumps: A review of models and systems. *Applied Energy.* 2010,(87):16–27

[87] Ympäristöministeriön asetus uuden rakennuksen energiatehokkuudesta. Finland: *FINLEX*. 2017

Publication 1

Fadejev J, Simson R, Kurnitski J, Haghighat F. A review on energy piles design, sizing and modelling. *Energy*, Vol. 122 pp. 390-407. 2017.

Energy 122 (2017) 390–407

Contents lists available at ScienceDirect

Energy

journal homepage: www.elsevier.com/locate/energy

Review

A review on energy piles design, sizing and modelling

Jevgeni Fadejev [a, b, *], Raimo Simson [a], Jarek Kurnitski [a, b], Fariborz Haghighat [c]

[a] Tallinn University of Technology, Ehitajate tee 5, 19086, Tallinn, Estonia
[b] Aalto University, School of Engineering, Rakentajanaukio 4 A, FI-02150, Espoo, Finland
[c] Concordia University, Department of Building, Civil and Environmental Engineering, H3G 1M8c, Montreal, Canada

ARTICLE INFO

Article history:
Received 26 August 2016
Received in revised form
18 January 2017
Accepted 19 January 2017
Available online 24 January 2017

Keywords:
Energy piles
Sizing
Modelling
Fundamental scheme
Thermal storage

ABSTRACT

Boreholes and energy piles coupled with ground source heat pump plants utilize renewable geothermal energy for buildings heating and cooling purposes and need proper design and sizing in order to end up with high plant efficiency. This paper conducted a review of available scientific literature, design standards and guidelines on energy piles performance within the framework of the *IEA-ECES Annex 31*. Main aspects covered were typical plant solutions, configurations of energy piles and their thermal response test performance, available analytical and numerical models with their main features and application in commercial software and design manuals. Four typical fundamental schemes of geothermal plant with energy piles were found, both suitable for cold and hot climate applications. Properly sized heat pump systems with energy piles were characterized with high overall system SCOP values higher than 4.5, while some case studies reported two times smaller SCOP values that illustrates the effect of proper design and sizing of such systems. The lack of specific heat extraction values which could be determined based on the climate and energy pile application show the need to develop general procedures for early stage energy pile sizing that would allow quick estimates of the heat extraction/rejection potential and system performance with reasonable accuracy for conceptual design. Most of available software is borehole oriented and will fit for energy piles sizing if software supports variable ground surface temperature boundary conditions, which, however is not implemented in most of software packages. Expected software features to be implemented are water advection and multiregional surface boundary heat transfer.

Contents

* Corresponding author. Tallinn University of Technology, Ehitajate tee 5, 19086, Tallinn, Estonia.
E-mail address: jevgeni.fadejev@ttu.ee (J. Fadejev).

http://dx.doi.org/10.1016/j.energy.2017.01.097
0360-5442/

1. Introduction

Recently adopted European Parliament directive 2010/31/EU [1] on energy performance of buildings highly promotes application of energy from renewable sources. Renewable energy becomes more accessible and its significance grows in the design of more energy efficient buildings. One widely utilized renewable energy source is geothermal energy, which can be efficiently utilized with ground-source heat pump (GSHP) coupled with ground heat exchanger (GHE). Recently published review on worldwide application of geothermal energy [2] revealed, that installed worldwide GSHPs capacity has grown 2.15 times in the period of 2005–2010 at a compound annual rate of 16.6% and there is an evidence of GSHP application in 78 countries around the globe.

Around 30 years ago, building pile foundations were first introduced as GHE in Austria [3] and further defined as energy piles. Nowadays, worldwide energy piles popularity is constantly growing and in Austria there are more than 100 000 of units installed [4]. Energy piles are known to be cost effective, as they combine two important properties in one solution – structural loadbearing and GHE i.e. thermal. Energy piles are being important research topic due to the complexity of their thermal behaviour.

As the layout of energy piles is generally defined by the foundation plan, thermal interferences between closely located adjacent piles appear. During the ground heat extraction process, the temperature of soil surrounding energy piles decreases with respect to the ground, pile and circulating fluid thermal capacitance and vice versa during the heat rejection process. Unbalanced operation of energy piles, where more heat is being extracted than rejected, in some cases may lead to a significant decrease in long-term energy performance. Therefore, to maintain stable operation of energy piles in a long-term perspective, consideration of seasonal thermal storage may become feasible. Additional thermal interference appear between energy piles ground surface boundary and building floor structure [5]. In cold climate zones, building floor heat loss may heat up the ground over the years and produce natural thermal storage effect, which may enhance thermal performance of energy piles significantly. Considering above-mentioned factors with varying variables like thermal properties of ground, grout, pipe, fluid, temperature boundary conditions, different possible energy pile configurations, distance between piles and their length, design and optimal sizing of energy piles and/or GSHP, the system with energy piles requires complex dynamic numerical modelling.

The goal of this paper is to report energy piles applications and their potential as a renewable energy solution. In this review different fundamental schemes of heat pump plants with energy piles, and various energy pile configuration types and their performance are studied. The study presents and discusses available modelling and software solutions and undergoes sizing and design techniques. As energy piles operation principle is similar to boreholes [5] with known differences in boundary conditions, possible implementation of knowledge obtained in borehole research for energy piles is also discussed. Available scientific literature and design guideline materials related to energy piles topic covered in this paper may further be classified into four major categories presented in Table 1.

In Section 2, relevant studies describing typical fundamental schemes of heat pump plants with energy piles are discussed. Additionally to fundamental schemes, plant performance examples found in scientific literature are also presented. Due to the limited availability of literature regarding energy piles, in some cases performance of borehole field plants is presented as an alternative to energy piles. Section 3 summarized studies regarding the performance of different energy piles configurations assessed with application of thermal response test (TRT). Summaries of literature review in categories of energy piles modelling and sizing are presented in Sections 4 And 5, respectively.

2. Fundamental schemes of plants with energy piles

Fundamental schemes of geothermal plants presented in this section support various types of ground heat exchangers including energy piles and boreholes. Fig. 1 presents one of most common application of energy piles in buildings, where most of the time indoor climate conditions are ensured with heating.

When secondary side demands heat, heat pump starts its operation and heats up the heat carrier in buffer tank. Whenever temperature in the tank drops below the set point value and operating heat pump is unable to further ensure the desired set point, built-in electrical heating coil or some other top-up heating starts its operation and heats up the volume of the tank to desired temperature value.

When secondary side demands cool, fluid circulating in energy piles loop is directed to the “free cooling” heat exchanger, where coupled secondary side circulating fluid is being cooled. Optional cooling circuit is connected through three-way valves in the heat pump loop, see Fig. 1. Three-way valves function is to reverse the flow in the heat pump loop, which results in reverse operation of the heat pump. Therefore, such plant can alternately heat or cool the volume of the buffer tank. Cooling circuit may be considered in buildings, where “free cooling” is unable to fulfil most of the cooling demand. Though, it should be noted, that such plant solution could not cool and heat a building simultaneously.

Two-storey residential building [6] located in Hokkaido, Japan operated according to the plant solution presented on Fig. 1. Measurements of a single heating period with duration of ca 5 month (December 2000–April 2000) revealed, that total of 26 energy piles 9 m deep managed to produce ca 18.3 MWh of heat i.e. 78 kWh per meter of pile length on the heat pump condenser side. Minimal outdoor air temperature during the heating period was ca −17 °C. Average heat pump coefficient of performance (COP) during operation was 3.9. Energy piles heating system seasonal coefficient of performance (SCOP), where ground loop circulation pumps electricity and system control is taken into an account was 3.2.

Plant scheme described on Fig. 2 can be applied in buildings, where both simultaneous heating and cooling demand are needed. Compared to previously presented plant scheme, there is an additional individual cooling machine and cold buffer tank considered in the design.

A good example of a building, where energy piles are used also for cooling is a terminal E of the Zürich airport [7]. Terminal was built in 2003 and it uses 306 concrete energy piles as a GHE in plant design to ensure heating and cooling. Heat pump with capacity of 630 kW covers 85% of the heating demand, where peak power loads are met with top-up district heating. Sizing and designing of the plant was performed with help of PILESIM software, which utilizes finite difference method based duct ground heat storage model (DST) [8]. Cooling demand of the building is mostly covered by energy piles ”free cooling“, where cooling secondary side is coupled with energy piles loop. Whenever “free cooling“ is not sufficient to maintain supply coolant temperature of 14 °C, heat pump starts its operation and cools down energy piles (evaporator) loop and heat pump excess heat is directed to the dry coolers located on the roof. Energy piles are 26.8 m deep with outer diameter ranging from 900 mm to 1500 mm, where each pile is equipped with 5 U-pipes fixed in the concrete reinforcement. Measurements of annual operation revealed, that heat pump managed to produce 2210 MWh, which is ca 73% of overall heat demand, where the remaining 27% were covered with top-up

Table 1
List of studies conducted on topics related to energy piles design in chronological order.

Nr.	Reference	Fundamental schemes	Energy pile configurations	Modelling	Sizing and design
1	S.P. Kavanaugh and K. Rafferty [57]				✓[a]
2	H. Brandl [4,55]				✓
3	B. Sanner [61]	✓[a]			
4	D. Pahud, M. Hubbuch [7]	✓			
5	Y. Hamada et al. [6]	✓	✓		
6	J. Gao et al. [62]		✓		
7	H. Yand et al. [63]			✓[a]	✓[a]
8	T. Man et al. [19]			✓	
9	P. Hu et al. [24]			✓	
10	A. M. Jalaluddin et al. [64]		✓		
12	GSHPA [54]				✓
13	M. Li, A. C.L. Lai [65]			✓	
14	IGSHPA [66]				✓[a]
15	A. Zarrella et al. [34]			✓	
16	W. Zhang et al. [22]			✓	
17	C. K. Lee and H.N. Lam [38]			✓	
18	O. Ghasemi-Fare and P. Basu [39]			✓	
19	S. Park et al. [67]		✓		
20	K. Allaerts et al. [10]	✓[a]			
21	E. Hassani Nezhad Gashti et al. [47]			✓	
22	F. Dupray et al. [49]			✓	
23	F. Loveridge and W. Powrie [29]			✓	
24	T.V. Bandos et al. [28]			✓	
25	J. Fadejev and J. Kurnitski [5,48]	✓		✓	✓
26	F. Loveridge and W. Powrie [30]			✓	
27	W. Zhang et al. [22]			✓	
28	M. Li, A. C.K. Lai [68]			✓[a]	
29	E. Sailer et al. [60]				✓[a]
30	D. Wang et al. [23]			✓	
31	A. Girard et al. [69]	✓[a]			
32	A. Hesaraki et al. [70]	✓[a]			✓
33	M. Aydin, A. Sisman [71]			✓[a]	

[a] studies on boreholes topic.

district heating. Free cooling managed to cover 620 MWh of cooling demand, which is ca 53% of overall annual cooling need. Pile annual extracted heat at the condenser side of the heat pump was ca 270 kWh per meter of pile length and annual rejected heat was 74 kWh per meter of pile length. Average heat pump COP was 4.5 and SCOP was 3.9. From system design perspective, heat pump evaporator capacity per meter of pile length was ca 59.7 W/m. Compared to the district heating system with active cooling, designed plant with energy piles revealed to be more energy efficient and the payback period of 8 years was expected.

As the unbalanced heat extraction/rejection in energy piles may lead to a significant loss in long-term operation performance, thermal storage may be applied to maintain stable long-term operation of GHE. Plant solution presented on Fig. 3 is mostly suitable for buildings located in cold climate zones with low average annual outdoor temperature. The source of thermal storage in such plant may vary – solar storage i.e. solar collector, air source i.e. dry cooler or/and air handling unit exhaust air heat exchanger.

Reda [9] has studied numerically application of solar thermal storage in GSHP plant with borehole field (not energy piles) and its impact on overall system SCOP in a residential building located in cold climate of Finland. Modelling was done in TRNSYS using finite difference method based DST model [8], and the simulation results showed that SCOP of the heat pump plant without thermal storage was 1.6 and heat pump managed to meet 53% of overall heat demand, where rest 47% were met with top-up heating. There were a total of 7 boreholes 50.5 m deep with a single U-pipe and the distance between boreholes was 5 m. When the solar collector with area of 46.8 m^2 was applied as thermal storage source, SCOP of the system increased to 2.5 and the heat pump covered ca 84% of overall heat demand. When solar collector area was doubled, SCOP of the system further increased to 3.0 and the heat pump covered ca 94% of overall heat demand. Average annual extracted heat amount in case of boreholes without thermal storage was ca 93 kWh per borehole meter. In plant with 46.8 m^2 and 93.6 m^2 of the flat plate solar collector average annual extracted heat amount was ca 153 kWh and ca 171 kWh respectively on the heat pump condenser side.

Fig. 4 shows plant solution with both seasonal warm and cold air source storage. During the winter plant operation (heating), heat pump extracts heat from the warm separated energy pile field and dry cooler extracts heat from the cold energy pile field. During the summer plant operation (cooling), heat is being injected to the cold energy pile field, while dry cooler injects heat into the warm energy pile field.

Allaerts et al. [10] modelled the performance of a plant with dual borehole field (not energy piles) and active air source storage numerically of an office building located in Belgium using TRNSYS simulation environment, where borehole field was modelled using finite difference method based DST model [8]. According to the results of study, overall size of borehole field in the above-mentioned plant was 47% smaller compared to the same capacity single borehole field plant without thermal storage.

Up to date in literature, there is quite a small amount of information available regarding measured long-term performance of energy piles. Morrone et al. [11] modelled long-term performance of energy piles numerically in climate of Naples and Milan, Italy with PILESIM2 software for seven-storey building. PILESIM2 software utilizes modified finite difference method based DST model [8]. There were 24 energy piles 25 m deep with outer diameter of 600 mm in simulations, duration of simulations was 20 years and there were 4 U-pipes in each pile. In both climates of Naples and Milan, the same model of seven-storey building considered active cooling in the design of pump. Heating and cooling demands were

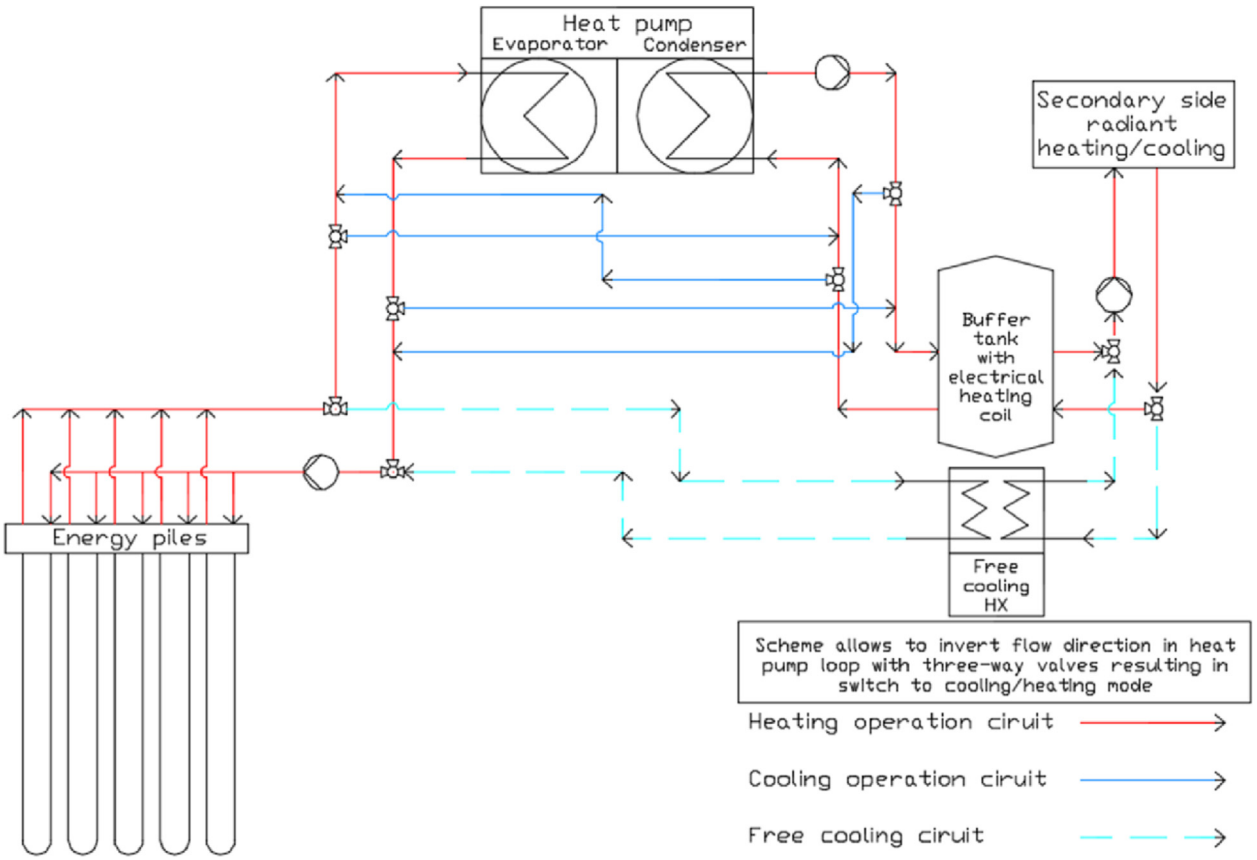

Fig. 1. Hybrid heat pump plant with energy piles and "free cooling" option.

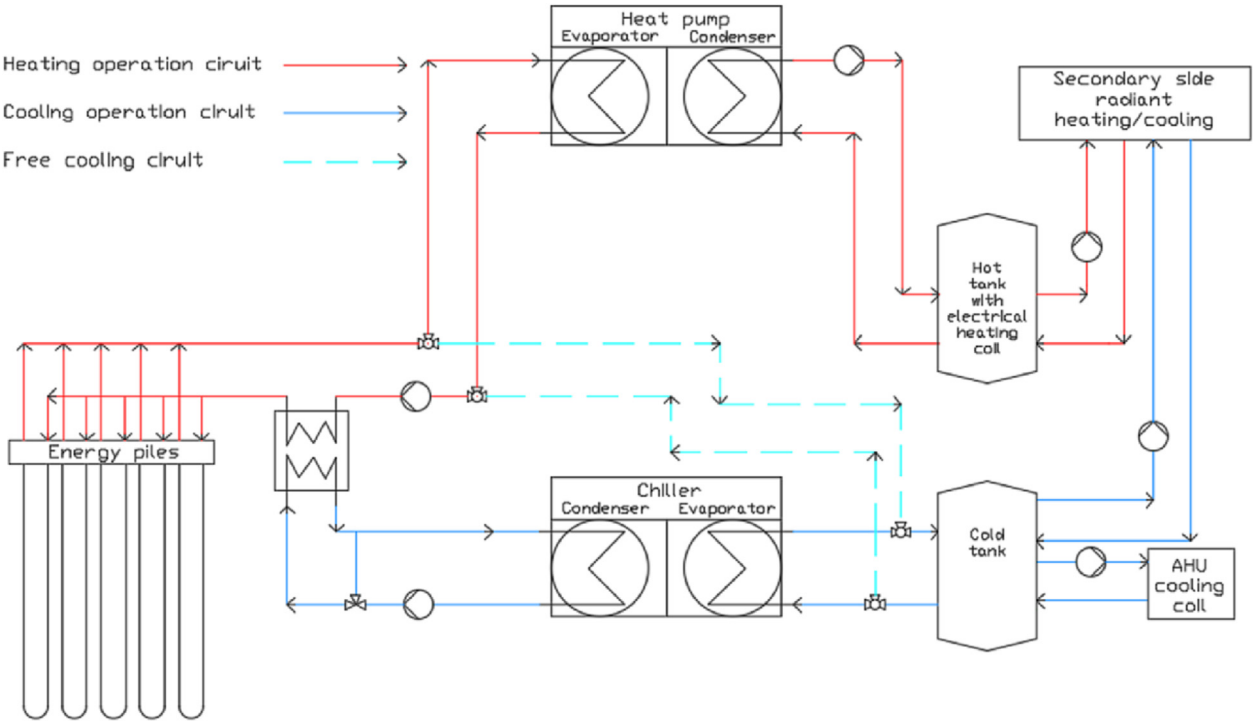

Fig. 2. Heat pump plant with energy piles and active cooling.

meant to be covered with reversed heat pump and plant solution may be considered as one described in Fig. 1. Annual energy use of building in Naples for cooling and heating was 39.5 MWh and 15.5 MWh, respectively. For building in Milan, annual energy use

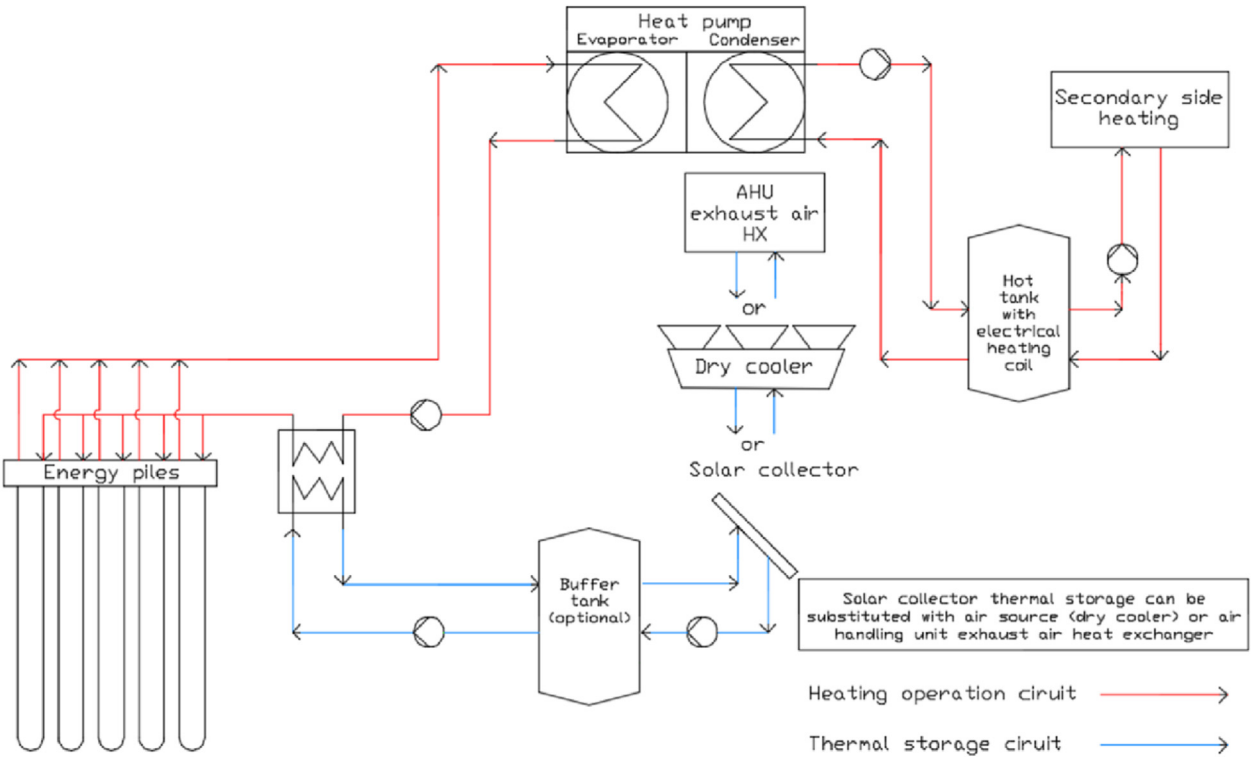

Fig. 3. Heat pump plant with energy piles and solar/air source/AHU exhaust air HX thermal storage.

for cooling was 25.1 MWh and for heating was 52.7 MWh. In climate of Naples case, a 14 kW heat pump managed to cover 98% of annual cooling and 100% of annual heating demand, which is ca 65 kWh per meter of pile length of cooling energy and ca 26 kWh per meter of pile length of heating energy per year. In this case, each meter of energy pile corresponded to ca 18 W/m of the heat pump evaporator capacity. Average SCOP in Naples was 4.6 and seasonal energy efficiency ratio (SEER) was 3.4. For the climate of Milan, a 12 kW heat pump managed to cover 100% of annual cooling and 99% of annual heating demand, which is ca 42 kWh per meter of pile length of cooling energy and ca 87 kWh per meter of pile length of heating energy per year. In this case, each meter of energy pile corresponded to ca 16 W/m of the heat pump evaporator capacity. Average SCOP in Milan was 4.6 and SEER was 3.6. As the thermal operation of energy piles was unbalanced, temperature of soil in Naples increased ca 8 °C, while in Milan only ca 0.5 °C.

Review of actually built geothermal plants with energy piles revealed four typical fundamental plant solutions that were described above and are suitable for both cold and hot climate conditions. Properly sized heat pump systems with energy piles were characterized with high overall system SCOP values higher than 4.5 in one of above described numerical studies [11]. Applied software packages in design of reviewed plants were TRNSYS with finite difference method based DST model, PILESIM with finite difference method based DST model and PILESIM2 with finite difference method based modified DST model. Application of thermal storage produced significant increase of plant performance and may also lead to decrease of overall ground heat exchanger length. Main features of reviewed plant solutions are summarized in Table 2.

Plant scheme nr 1 (Table 2) is mostly suitable for buildings with dominating heating and minor cooling need i.e. heating to cooling ratio up to 1 to 0.1. According to numerical study [81] such plant scheme was capable of meeting only 49% of cooling demand via "free cooling" with seasonal energy efficiency ratio (SEER) of 40. Heating SCOP of such plant was 2.0 due to small amount of energy piles limited by the foundation plan. However, when no electrical top-up heating is taken into an account, heat pump SCOP was 4.62. This plant solution is not capable of producing heat and cool simultaneously and may not be the best option for e.g office buildings. Therefore, in buildings with simultaneous heating and cooling demand, plant scheme nr 2 (Table 2) is the option to be applied. Study [7] revealed that measured heating SCOP of such plant was 3.9, initial investment cost was 5.2 times of annual operation cost and compared to conventional district heating with active cooling system payback period of 8 years is expected (interests of invested capital not taken into an account). Plant scheme nr 3 (Table 2) is capable of producing significantly more heat compared to plant scheme nr 1 (Table 2) due to the application of thermal storage. Application of thermal storage via exhaust air heat exchanger and solar collectors in numerical study [81] enabled to reduce the size of energy piles field by 50%. In previously mentioned case 28.3 MWh of heat were injected to energy piles field with thermal storage and plant was able to extract 12 MWh more heat compared to system without storage i.e. 42% stored heat utilization rate. However, plant scheme nr 3 lacks active cooling option and "free cooling" potential decreases with the increase in thermal storage energy, only 7% of total cooling demand was met by "free cooling" in study [81]. Plant scheme nr 4 (Table 2), compared to plant scheme nr 3 (Table 2), can not only store heat, but also store cool, which results in increased "free cooling" performance.

3. Energy pile configurations

Energy piles configurations can be classified by pile material and by the way a heat exchange loop is installed. Three main pile types by material are used; cast in-situ concrete pile, prestressed high

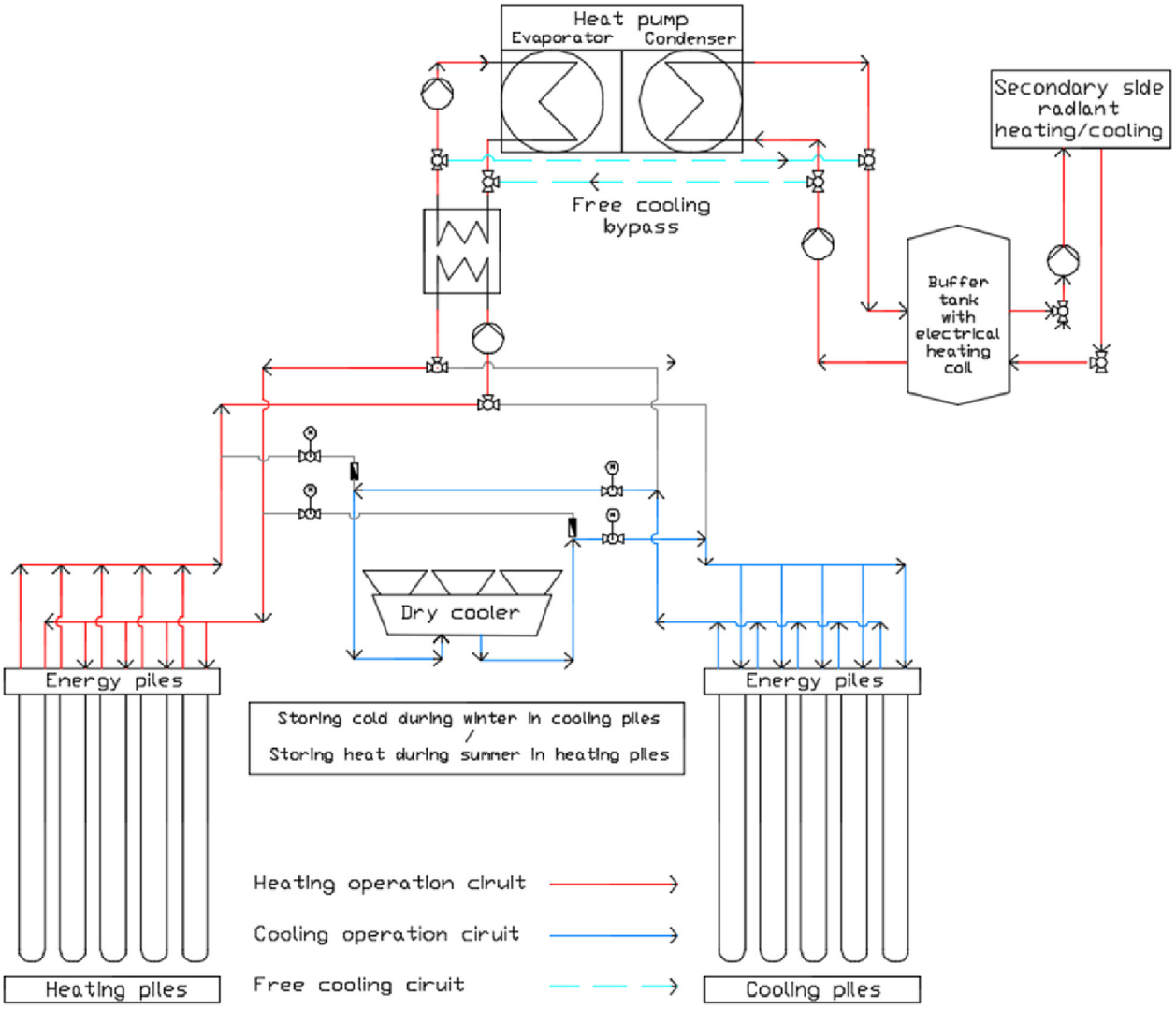

Fig. 4. Heat pump plant with separated energy pile field for cooling and heating with air source thermal storage.

Table 2
Plant fundamental schemes comparison table.

Fundamental scheme nr	1. Hybrid heat pump plant with energy piles (Fig. 1) [81]	2. Energy piles heat pump plant with active cooling (Fig. 2) [7]	3. Energy piles heat pump plant with thermal storage (Fig. 3) [81]	4. Heat pump plant with separated heating/cooling pile fields (Fig. 4) [10]
Heating	✓	✓	✓	✓
Free cooling	✓	✓	✓	✓
Active cooling	✓[a]	✓		
Simultaneous heating and cooling		✓		
Thermal storage			✓	✓
Heating SCOP (HP SCOP)	2.0 (4.62)[c]	3.9 (4.5)[b]	2.0 (4.62)[c]	N/A
Cooling SEER	–	2.7[b]	–	N/A
Free cooling SEER (covered demand)	40 (49%)[c]	61 (78%)[b]	40 (7%)[c]	N/A
Cost category	energy piles €/m heat pump €/kW	energy piles €/m heat pump €/kW chiller €/kW	energy piles €/m, heat pump €/kW solar collectors €/m^2 (or exhaust air heat exchanger €/kW)	energy piles €/m heat pump €/kW dry cooler €/kW

[a] Three-way valves reverse the flow in heat pump loop.
[b] Measured value.
[c] Numerically calculated value.

strength concrete (PHC) and steel pile. Heat exchange loop in the pile can be installed as – single U-tube, double U-tube, multi U-tube, W-tube, also as coil with known pitch and as indirect double-pipe, see Fig. 5.

Amount of U-loops in large diameter energy piles may commonly exceed two. While spiral or helix type exchanger is

popular in research papers, it is relatively uncommon in practice. In order to determine the actual site thermal properties of soil – thermal conductivity and diffusivity, an on-site thermal response test (TRT) [12] can be performed that allows to determine energy pile thermal resistance too. Additionally, TRT can be performed to assess thermal performance i.e. W/m capacity of different pile configurations, but the model applied in TRT results analysis should be capable of capturing short-term behaviour of energy piles accounting for thermal capacities of pile interior components or either the test should be carried out for such period, that is enough to overcome thermal capacity effects of energy pile. During the W/m capacity test, a heat source, which assures constant inlet temperature is connected to an energy pile. Inlet fluid with constant temperature e.g. of 35 °C is being fed at constant flow rate, which is monitored along with the energy pile outlet temperature. However, to determine soil thermal properties, constant heat flux is maintained in energy pile ground loop. TRT test is generally carried out for about 72 h, which can be described as a cooling operation of energy pile acting as a condenser side heat exchanger. Prior the test, undisturbed ground temperature is measured and can be further used in some analytical model along with other measured parameters to determine the 72-h average heat extraction/rejection rates. Results of TRTs can be used to compare different pile configurations thermal performance. As a result of the literature review on topic of energy piles thermal performance Table 3 has been prepared summarizing most of the aforementioned energy piles configurations TRT results.

The following equation is commonly used to process measured data of boreholes TRT (not energy piles) derived from infinite line source model [13] to determine soil thermal properties:

$$T_f(t) = \frac{q}{4\pi t}\cdot\left(\ln\left(\frac{4at}{r^2}\right) - \gamma\right) + q\cdot R_b + T_0 \quad (1)$$

where T_f is the fluid outlet temperature (°C), T_0 is the far field or initial soil temperature (°C), q is the heat flux along borehole length (W/m), t is the time (s), R_b is the pile thermal resistance (W/mK), γ is the Euler constant, a is the soil diffusivity (m^2/s) and r the is borehole radius (m).

Review of different energy pile configurations TRT performance revealed that short term specific heat extraction/rejection rate is highly dependent on the amount of pipe surface area grouted into the pile structure. Highest heat rejection rates have been obtained with coil-type heat exchangers. However, high heat extraction/rejection potential may not be optimal solution in a long run, as the amount of potential ground extracted energy depends also on ground initial temperature and ground source system application (heating/cooling). For example, in cold climate regions with soil temperature of ca 5 °C, application of dense coil-type heat exchanger for heating (heat extraction) may not be feasible, because e.g. double U-tube may yield same amount of ground heat due to ground temperature eventually falling below 0 °C stopping the heat pump operation. Therefore, systems with less length of heat exchange pipe in some cases may be considered more feasible.

4. Energy pile modelling

Extensive research has been done on the borehole modelling, but energy piles modelling is much less studied. At first glance, one might assume that boreholes operate in very similar conditions compared to energy piles. However, significant differences appear in operational conditions of these two types of heat exchangers. Energy piles are generally shorter and radially thicker due to their load bearing function compared to boreholes. Length of the boreholes usually starts from 50 m extending up to 300 m, while their diameter is usually smaller due to the lack of the need to carry building load compared to energy piles. As the diameter of the borehole is so small compared to its length, boreholes are usually modelled as a line sources and borehole structure i.e. grout, pipe

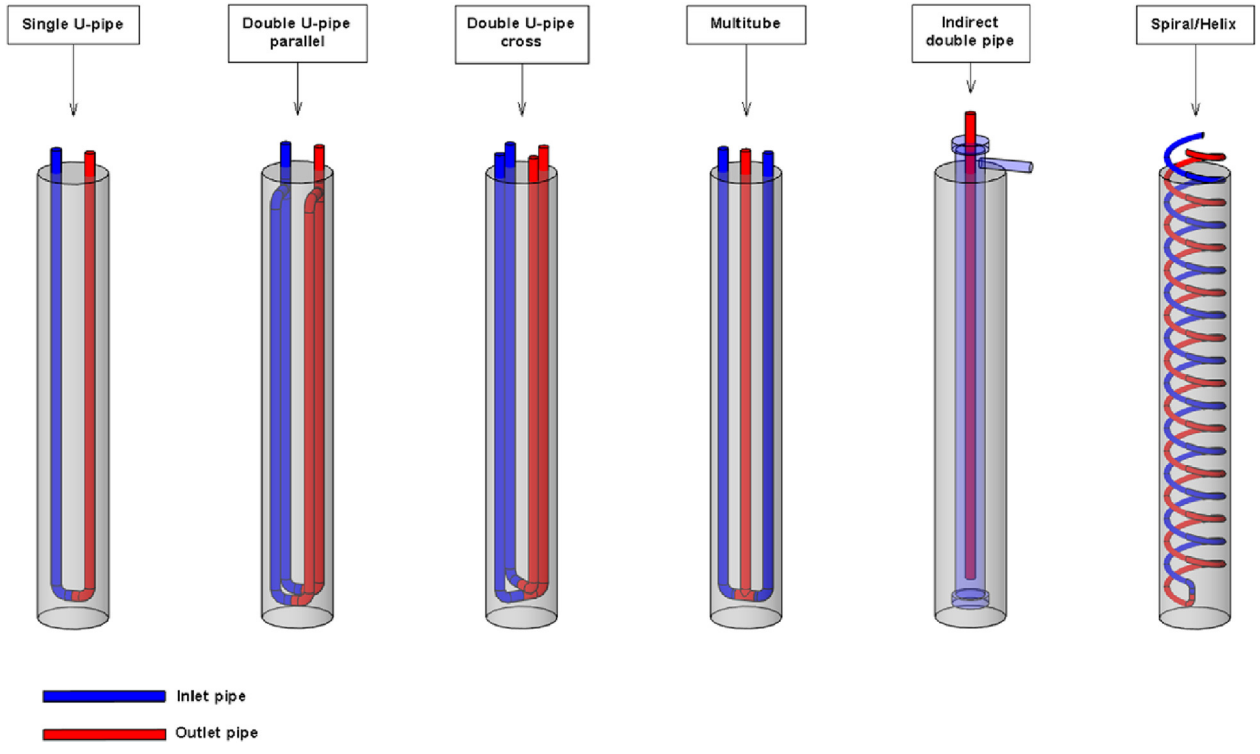

Fig. 5. Energy pile configurations.

Table 3
Energy pile configurations thermal response test performance.

Reference	Pile material	Pile configurations	Soil thermal properties	Test type	TRT Performance
Y.Hamada et al. [6]	PHC	single U-pipe double U-pipe indirect double-pipe $o_d = 302$ mm	–	constant inlet temp	single U = 54 W/m double U = 55 W/m double-pipe = 69 W/m
J.Gao et al. [62]	cast in-situ concrete	W-pipe single U-pipe double U-pipe triple U-pipe $o_d = 600$ mm	$\lambda = 1.3$ W/(mK)	constant inlet temp	W-pipe = 83 W/m single U-pipe = 58 W/m double U-pipe[a] = 89 W/m triple U-pipe[a] = 108 W/m
Jalaluddin et al. [64]	Steel	single U-pipe double-tube multi-tube $o_d = 139.8$ mm	$\lambda = 1.1 \ldots 2.1$ W/(mK)	constant inlet temp	single U-pipe = 30 W/m double-tube = 50 W/m multi-tube = 35 W/m
A. Zarrella et al. [34]	cast in-situ concrete	coil-type pitch 75 mm coil-type pitch 150 mm coil-type pitch 350 mm triple U-pipe $o_d = 500$ mm	$\lambda_{trt} = 1.8$ W/(mK) $cp_{trt} = 2.4$ MJ/(m^{3}K)	constant inlet temp (simulated TRT)	75 mm = 123 W/m 150 mm = 120 W/m 350 mm = 113 W/m triple U-pipe = 107 W/m
S.Park et al. [67]	cast in-situ concrete	coil-type pitch 200 mm coil-type pitch 500 mm $o_d = 1350$ mm	$\lambda_{trt} = 3.3$ W/(mK) $\alpha_{trt} = 4.45 \times 10^{-6}$ m^2/s	constant inlet temp (intermittent)	200 mm = 285 W/m 500 mm = 248 W/m

[a] Flow in double and triple U-pipe was twice and trice higher respectively compared to single U-pipe and W-pipe.

legs, fluid thermal capacitances are neglected. However, energy pile thermal capacitance of grout material impacts short-term thermal behaviour of pile significantly and should be accounted for. Again, due to the length aspect of the boreholes, ground surface boundary is usually modelled as adiabatic, because only minor depth near ground surface is penetrated by the ambient surface temperature fluctuations. On the other hand, energy piles length can be only couple of meters, thus surface boundary should be modelled due to significant impact on heat extraction/rejection of energy piles. Therefore, application of borehole models in the study of energy piles performance should only be done with consideration of facts mentioned above.

Literature review of borehole models presented in this section may become helpful in finding suitable borehole model solutions for energy piles simulation. Published models can be divided into two groups – analytical and numerical. Analytical models have many simplifying assumptions and are mostly feasible for TRT results evaluation to determine soil properties and pile thermal resistance. It is also worth to note, that TRT test with energy pile should be carried out much longer compared to borehole in order to overcome energy pile thermal capacitance. Some of analytical models can be used for transient simulations. On the other hand, numerical models are capable of achieving very high detail of modelling – accountancy for phase change in soil due to freezing, modelling of pile internal components, variable boundary temperature conditions, thermal capacitance of pile inner materials etc. Also, one advantage of numerical simulation is the possibility to quantify the difference between 2D, 3D and quasi 3D models. However, the cost for a detailed modelling is a high computation time and modelling complexity, which are barely applicable for every day engineering design needs.

Results of the literature review on available energy pile models are depicted in Table 4, where models published by scientific community and their most important features are summarized and presented in chronological order.

Reviewed models features and main principles are presented in Fig. 6. Generally, the heat transfer is modelled in two regions – soil and pile. In analytical models, soil and pile (if present) regions are treated as homogenous medium. However, most of numerical models are capable of accounting for multi-layered structure of ground. Some numerical and analytical models are capable of accounting for water advection in soil region. This review found only one numerical model, where phase change of water vapour in porous soil medium due to freezing is modelled.

Temperature development in analytical models is generally modelled as a line source, where thermal capacitance of pile inner components is neglected. Some analytical models account for pile inner pipe layout with the input of pile thermal resistance R_b. Also, thermal capacitance of pile in some analytical models is taken into account (Table 4). Such models are capable of short-time step simulation, producing accurate results for the simulation time step of less than an hour.

Different configurations of piles can be modelled – single U-tube, double U-tube, multi U-tube and coil-type. Generally, detailed pile interior components are modelled numerically. Such models account for geometry of pipe legs and thermal interactions between them, fluid upward/downward flow i.e. heat transfer in axial direction and also for thermal capacitance of fluid and grout.

Regarding potential applications of models described in Table 4, main applications, suitability for practical design problems and limitations of modelling methods are summarized in Table 5.

Multiple piles and thermal interaction between them can be modelled both numerically and analytically. The influence of all piles to the ground temperature is generally summed up by superposition. However, in numerical models, where the geometry of the pile field is modelled, thermal interactions between piles are solved as heat balance equations numerically.

Boundary conditions in analytical models such as ground surface temperature, far field temperature (initial ground temperature) are constant. However, in some of numerical models variable ground surface temperature, which is important for energy piles modelling, can be accounted for. Also, most of analytical models in their original form may only simulate constant heat flux along pile depth compared to varying heat flux handled by numerical models.

One of the goals of this literature review was to find a model that is capable of simulating thermal performance of energy piles field with a high level of detail, where ground surface boundary condition accounts for building floor slab geometry and soil region geometry surrounding the building (Fig. 6) i.e. heat transfer through floor slab to soil beneath is modelled in building region and heat transfer between soil and outdoor air (and solar radiation) is modelled in surrounding soil region. Unfortunately, any such model was not found. Chuangchid and Krarti [14] modelled the impact of heated floor slab heat loss on soil temperatures for building without energy piles. As reported by the results of simulated case with uninsulated heated slab in winter, temperature at ca 2 m

Table 4
Models comparison table.

Reference	Model	Solution			Domain			Pile type			Features										
		Analytical	Numerical	Response factor	1D	2D	3D	Single U-tube	Double U-tube	Coil-type	Surface boundary variable temperature	Adjacent pile interactions	Interactions between pipe legs	Water advection	Phase change in soil	Pile thermal capacitance	Fluid thermal capacitance	Short time-step	Multilayered ground	Pile incline	Finite pile length
H.S. Carslaw, J.C. Jaeger [13]	ILSM[c]	✓			✓																
L.R. Ingersoll et al. [15]	CSM[c]	✓			✓																
P. Eskilson [16]	FDM/g-funct		✓	✓	✓	✓		✓	✓			✓		✓							✓
G. Hellstrom [8]	FDM DST		✓			✓		✓	✓[b]		✓	✓	✓				✓	✓	✓		✓
T.K. Lei [35]	FDM		✓			✓		✓					✓				✓	✓			✓
N.K. Muraya [43]	FEM		✓			✓		✓			✓	✓	✓	✓		✓	✓	✓	✓		✓
T. Kohl, R. J. Hopkirk [44]	FEM		✓				✓		✓		✓	✓	✓	✓		✓	✓	✓	✓		✓
S.P. Rottmayer et al. [36]	FDM		✓				✓	✓					✓				✓	✓			✓
C. Yavuzturk et al. [17,37,40]	FDM/FVM/g-funct		✓	✓		✓		✓				✓	✓			✓	✓	✓			✓
H. Y.Zeng et al. [18]	FLSM	✓				✓		✓				✓									✓
S. He et al. [41,42]	FVM		✓			✓	✓	✓			✓		✓			✓	✓	✓	✓		✓
Y. Man et al. [19]	ISCSM/FSCSM[c]	✓			✓	✓						✓				✓[e]		✓			✓
S. Javed, J. Claesson [20]	Short-term response	✓	✓			✓		✓								✓	✓	✓			✓
P. Eslami-Nejad, M. Bernier [31,32]	2U2ICM[d]	✓	✓[a]		✓[a]	✓			✓				✓		✓		✓				✓
C.K. Lee, H.N. Lam [38]	FDM		✓				✓	✓	✓[b]				✓			✓	✓	✓	✓		✓
O. Ghasemi-Fare, P. Basu [39]	FDM		✓				✓	✓			✓					✓	✓	✓	✓		✓
A. Zarrella et al. [34]	CARM		✓			✓	✓	✓	✓	✓	✓	✓	✓			✓	✓	✓			✓
P. Hu et al. [24]	CCSM	✓			✓			✓	✓[b]			✓				✓		✓			
E.H.N. Gashti et al. [47]	FEM (Comsol)		✓				✓		✓		✓		✓	✓		✓	✓	✓	✓		✓
W. Zhang et al. [21,22]	Solid CSM	✓			✓					✓		✓		✓		✓[e]		✓			✓
T.V. Bandos et al. [28]	FCSM[c]	✓				✓						✓				✓[e]		✓			✓

F. Dupray et al. [49]	FEM (Lagamine)[c]	✓	✓				✓	✓		✓			✓	✓		✓
J. Fadejev, J. Kurnitski [5]	Equa borehole FDM	✓		✓	✓	✓[b]	✓	✓	✓		✓	✓	✓		✓	✓

[a] Ground model with phase change.
[b] Supports multiple U-tube configurations.
[c] Pile interior was not modelled.
[d] Double U-tube with two independent circuits.
[e] Pile is modelled as cylinder filled with soil material.

depth under the building (centre of the building) was ca 10 K and at ca 4 m depth was ca 5 K higher than undisturbed soil temperature. Therefore, in hypothetical case with short pile foundation accountancy for floor slab heat loss in the design phase of geothermal heat exchanger may lead to increase of geothermal plant performance and reduction of overall energy pile field length. However, intensity of heat loss within the slab region varies due to floor slab edge being exposed to ambient conditions, while floor slab surface to indoor conditions. According to results of previously mentioned case modelled by Chuangchid and Krarti [14], soil temperature in building section view starts to drastically decrease at ca 2 m from the edge of the floor slab reaching lowest values at the edge of the floor slab. Hence, in hypothetical case of energy piles design, piles located closer than 2 m from the edge of the slab would operate in totally different temperature conditions compared to piles located closer to the centre of the building. Despite the fact, that abovementioned issues can be modelled in numerical finite element 2 D or 3 D software such as COMSOL, more conventional transient solution that is suitable for engineering field is still to be developed. More detailed description on analytical and numerical models is presented in the following Sections 4.1 And 4.2 respectively.

4.1. Analytical models

According to the history of GHE modelling, most common one dimensional (1-D) analytical solution for the vertical borehole GHE, which applies Kelvin's line source theory [13], is known as an infinite line source model. Grouted borehole with piping is assumed as a line heat source of an infinite length located in an infinite homogeneous medium i.e. ground, where physical dimensions of a borehole are neglected and initial uniform temperature of ground is given. Line source model is capable of calculating temperature response at a given distance perpendicular to the axis of line heat source at given time based on the input of heat output per length of line source and ground thermal conductivity and diffusivity.

Alternative 1-D analytical solution, where size of the borehole is taken into an account is a cylindrical source model [13,15], which is capable of estimating temperature response at the borehole wall. Cylindrical source model requires same input of parameters as the line source model with addition of borehole outer diameter. Both models are mainly used to describe the heat transfer outside borehole. Ground surface boundary conditions and heat capacity of the borehole materials are neglected in these models. After the temperature at borehole wall is calculated, further temperature development inside of the borehole can be solved e.g. via thermal resistances.

Eskilson [16] derived an analytical model that accounted for a finite length of the borehole. It should be noted, that heat capacity of borehole itself was neglected. The boundary and initial conditions in Eskilson's model were assumed constant and the ground was homogenous. Eskilson introduced a dimensionless temperature response at the borehole wall, which is known as g-function and is described as:

$$t_b - t_0 = -\frac{q}{2\pi k} g\left(\tau \Big/ \left(\frac{H^2}{9a}\right),\ r_b/H\right) \tag{2}$$

where g is the dimensionless temperature response, t_b is the temperature at borehole wall (°C), t_0 is the far field temperature (°C) (initial ground temperature), q is the heat flux along borehole length (W/m), H is the borehole length (m), a is the soil diffusivity (m^2/s), and r_b is the borehole radius (m).

Eskilson also introduced the superposition technique to account

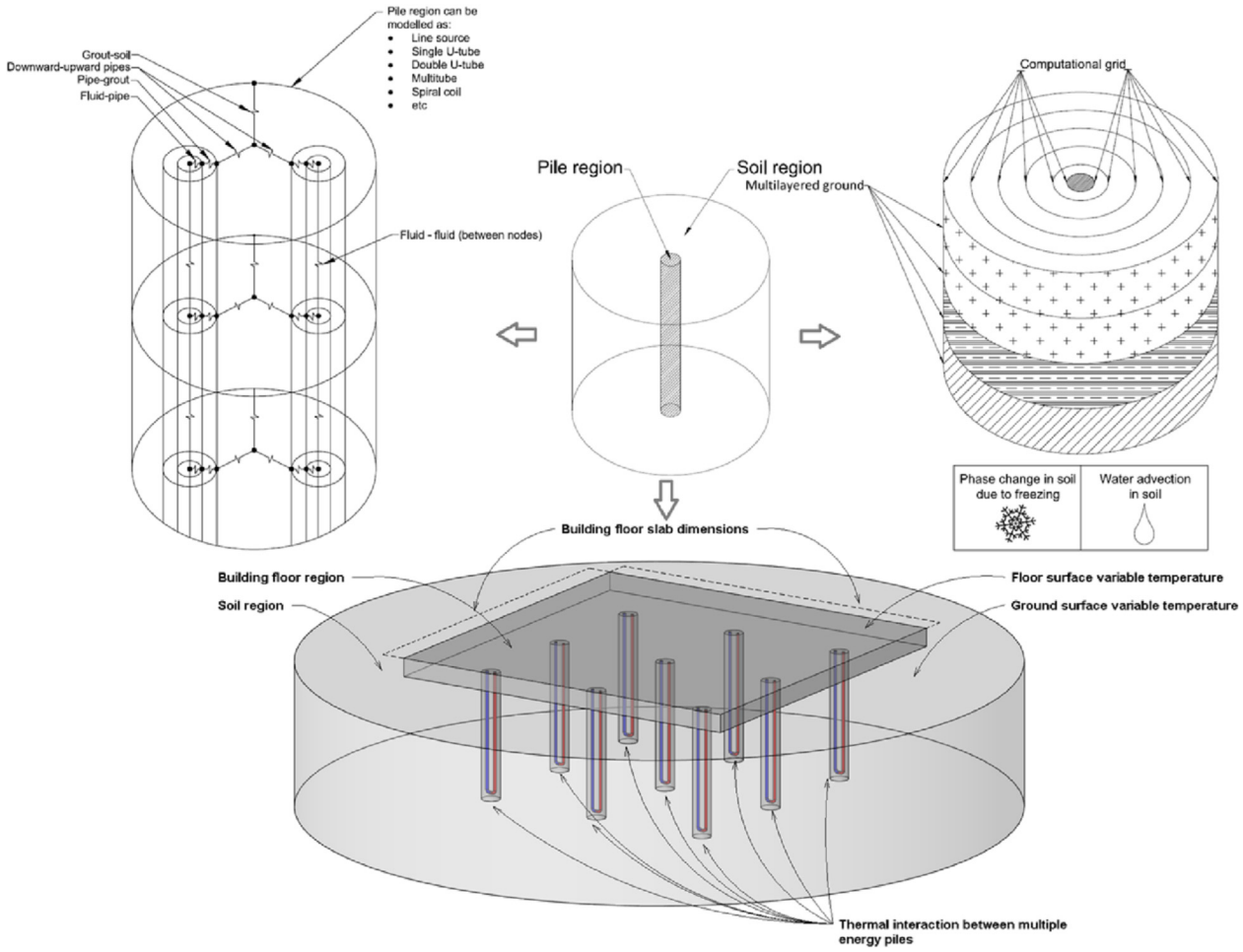

Fig. 6. Energy piles modelling variables and boundary conditions.

Table 5
Borehole models applications and limitations in energy piles analysis.

Modelling method	Applications	Limitations
Analytical infinite heat source models (e.g. Refs. [13,15])	TRT results processing (suitable for longer measuring periods due to lack of thermal capacitance)	Temperature rise tends to infinity due to infinite length, single pile analysis in original form (without superposition), constant heat flux, adiabatic ground surface boundary,
Analytical finite heat source models (e.g. Refs. [18,19])	TRT results processing	Single pile analysis in original form (without superposition), constant heat flux, adiabatic ground surface boundary
Numerical finite difference models (e.g. Refs. [8,35])	Dynamic annual simulation of boreholes/energy piles with custom plant and whole building modelling capability	Long computational time, limitations in boundary conditions depending on the model (non-homogenous ground, no water advection etc), simulation environment modelling knowledge requirements
Numerical finite element/volume models (e.g. Refs. [41,43])	Detailed heat/moisture transfer analysis of any modelled geometry with soil freezing and fluid dynamics capabilities	Extremely long computational time, high modelling and boundary conditions knowledge requirements, non-practical for engineering purposes
Response factor models (e.g. Refs. [16,40])	Annual simulation of boreholes based on the input of building load data (small time-step can be applied, but accuracy loss may appear at very small time-steps)	Only accurate for boreholes simulation due to adiabatic ground surface boundary, limited to precalculated borefield configurations, no coupling with whole building simulation, no detailed thermal storage modelling capabilities

for thermal interactions between multiple boreholes. Using numerical finite difference model, Eskilson calculated g-functions for many different energy piles field configurations. Values of g-functions obtained by Eskilson can be further used to simulate performance of borehole fields analytically using Equation (2). However, results of such modelling are accurate only for time greater than $\frac{5r_b^2}{a}$ due to the neglected heat capacity of the borehole in time, when g-functions were precalculated. Therefore, this model is classified as a long-time step model.

Short-time step model for transient simulation was introduced

by Yavuztzuk and Spitler [17]. Their model was capable of producing accurate results with the time step length of less than an hour. Similar g-function logic is applied in Yavuztzuk and Spitler analytical model and they used two-dimensional finite volume model to calculate g-functions values.

Zeng et al. [18] developed a finite line source analytical solution based on the Eskilson's model, which was further compared to numerical solution with very good agreement. Solution advantage is fast computational times. Compared to Kelvin line source model, where temperature rise during long simulation period tends to infinity, finite line source model temperature tends to initial ground temperature. Initial ground temperature is constant during calculation period.

Man et al. [19] developed infinite and finite "solid" cylindrical source models of pile heat exchanger based on the existing "hollow" cylindrical source model [15]. Thermal capacitance of pile in new analytical solution is modelled by filling "hollow" interior of pile with homogenous material, which its thermal properties are identical to the homogenous ground. Therefore, the inside geometry of pile is not modelled and for accurate analysis thermal properties of grout should be equivalent to soil ones. Model was developed as one- and two-dimensional and validated against the numerical model. The model's prediction was accurate for short time steps compared to results of numerical model. As in most analytical models, the ground surface boundary temperature is constant over the period of simulation.

Javed and Claesson [20] developed analytical short-term response borehole model, which accounts for thermal capacitances of borehole grout and circulating fluid, suitable for calculating average borehole fluid temperature for time-step less than an hour. Pipe legs of a single U-tube are modelled as a single equivalent-diameter pipe, which fluid temperature equals to the average of supply and return pipe leg temperatures. Heat transfer is modelled as radial and solved with help of Laplace transforms. Javed and Claesson validated their analytical model against actual measurement data and against their own developed numerical solution resulting in achievement of a good agreement.

Diao et al. [21] adopted an equation of conduction-advection heat transfer in porous medium for an infinite line source model to account for ground water advection. Assumption is that the groundwater flows in x-direction at a given velocity over the infinite homogenous porous medium. They studied also water advection in a field of boreholes revealing that groundwater flow helps to reach heat transfer steady state much faster than the case without water advection. They have also summarized thermal and hydraulic properties of various rocks and soils for a quick estimation of possible water advection impact on the thermal performance of energy piles.

Zhang et al. [22] modified Man's [19] solid cylindrical source infinite and finite models to account for a groundwater advection. The assumptions made in the development of the model are the same as the ones made by Diao et al. [21] infinite line source water advection model. Study revealed, that groundwater advection can drastically improve heat exchange performance of energy piles up to 5 or higher compared to the case without groundwater seepage. Wang et al. [23] assessed the performance of Zhang et al. [22] model in finite element modelling environment ANSYS CFX and developed an improved analytical model to be more accurate at ground water velocities larger than $1e^{-5}$ m/s.

Hu et al. [24] developed a composite cylindrical model on the basis of composite line source model [25] and cylindrical source model [26]. The composite cylindrical model was further successfully validated against a 3-D numerical model and measured TRT data showing a very good agreement. The advantage of the proposed analytical model is its capability of short-time step simulation, where heat capacitance of the pile is considered. Assumptions made in the development of the model are homogenous ground and neglected heat transfer in the pile axial direction. Layout of pipes in the borehole/energy pile are described with the input of borehole thermal resistance R_b, which can be calculated using equations that were proposed for single U-tube [27] and for double and triple U-tube [8]. The proposed composite cylindrical model was applied in TRT to determine the soil heat conductivity and volumetric heat capacity, results were compared to same data obtained using line-source model. Composite cylindrical model showed good agreement even at very early stage of TRT and the obtained soil thermal conductivity and volumetric heat capacity were both ca 20% smaller than the line-source model results.

Bandos et al. [28] presented a finite cylinder-source analytical model, which was modified to an equation form of single integral compared to its original instead of double ones [19]. Result of such modification is decrease in computational time.

Loveridge and Powrie [29] developed additional g-functions for Eskilson's [16] analytical response factor model for the pile aspect ratios <1000 in order to have analytical solution covering typical geometry of the energy piles. The impact of piles connection on the thermal performance – parallel or serial was studied. They presented g-function graphs with upper and lower bond U-pipes location and a method to calculate almost any energy piles field g-function. They showed the importance of accounting for adjacent piles thermal interactions, as in one calculated case where 9 piles were located very close to each other: their performance was only 16% of individual pile isolated from the group. They verified Eskilson's hypothesis, that thermal interaction between piles appear when distance between adjacent piles is at least equal to the length of pile in group. In case of pile foundations, they also proposed, that activating all the piles in foundation may not be feasible and it might be more efficient not to activate some piles that are located too close to each other. Loveridge and Powrie [30] investigated the heat transfer within the pile region using a 2-D numerical model in COMSOL. They proposed an empirical equation, which can be used to calculate the borehole resistance for pile configurations with varying number of pipes and conductivity ratio.

A ground model capturing phase change effects using effective heat capacity method was developed by Eslami-nejad and Bernier [31]. They have coupled it with developed analytical borehole model [32]. Only fluid heat capacitance was considered in the borehole model and two U-loops were modelled. Thermal interactions between U-pipe legs were considered. Borehole model accounted for fluid axial temperature variation along with the borehole depth. Borehole wall temperature was assumed to be constant along the depth. Heat transfer within the borehole (borehole wall – fluid) was modelled in borehole model, while the heat transfer in soil region in ground model. Eslami-nejad and Bernier further validated the ground model based on small-scale experimental measurements and found a good agreement of model performance with the experimental results. Phase change is modelled according to Bonacina et al. [33] and is described with three phases – liquid, solid and transition phase. In Eslami-nejad and Bernier ground model it is assumed, that due to water freezing density of water remains constant and natural convection and moisture transfer in saturated soil regions were neglected. However, it is worth to note that in order to avoid frost heave, the ground loop outlet temperature is often limited not to drop below 0 °C in order to prevent freezing of soil, and therefore a common design margins reduce the need for ground model with phase change for energy piles applications.

4.2. Numerical models

Numerical energy piles/boreholes models can be grouped into three different categories based on the modelling method – finite difference, finite volume and finite element method. However, literature review revealed also a quasi-numerical model, which neither belongs to any of modelling methods mentioned above. Zarella et al. [34] developed a model called capacity resistance model (CaRM) designed for borehole design and performance analysis. Two versions of model exists – one that not accounts for pile inner components thermal capacitances and other that accounts for thermal capacitances of grout and fluid. In latter models axial heat transfer in grout, ground surface thermal convection, short- and long-wave solar radiation are modelled. Model may theoretically be applied for energy piles design and performance assessment by neglecting the input of solar radiation initial data and substituting outdoor air temperature data by variable temperature above the structure of pile foundation. Model accounts for geometries of single, double, triple U-tube and coaxial pipes. Model is capable of considering multiple piles thermal interaction and calculation of variable outlet temperature. Validation against HEAT2 finite difference model showed very good agreement, as well as validation against measured field data. Authors have also showed the importance of accounting for thermal capacitances of pile inner components by comparing the outlet temperatures of pile with and without thermal capacitances, resulting in ca 0.6 … 2 °C fluid temperature difference.

4.2.1. Finite difference

Eskilson [16] developed a two-dimensional finite difference model, where boundary conditions were constant and the pile thermal and fluid thermal capacitance were neglected. The model was then used to calculate g-functions for his analytical solution described in Section 4.1.

Hellstrom [8] developed a model for simulation of multiple boreholes designed for seasonal thermal storage operation. So called duct storage model (DST) utilizes finite difference method to solve the temperature distribution in ground. DST model is available as a TRNSYS library component; it is capable of short-time step transient simulation and supports variable surface boundary conditions.

Lei [35] proposed a finite difference 2-D numerical model to simulate a borehole heat exchange with ground in radial-axial coordinates. Borehole cross section is divided into two regions – inner and outer. In outer region heat transfer between ground and fluid is modelled, while in inner region heat transfer between U-pipe adjacent legs is modelled. Model accounted only for axial heat transfer of fluid, while heat transfers in ground, grout and pipe were neglected.

Rottmayer et al. [36] introduced a quasi-three-dimensional finite difference method to model the heat transfer processes within the borehole region. Axial heat transfer was modelled in fluid, while grout axial heat transfer was neglected. Pipe wall and grout heat capacitance were neglected. To account for heat transfer in a radial dimension, borehole section is divided into a cylindrical grid of nodes and further solved using finite difference method. In Rottmayer's model U-pipe cross section is not circular, but trapezoidal due to the calculation grid specifics. Cylindrical grid is generated so that the area of trapezoidal section equals to actual U-pipe section area. As the thermal resistance in trapezoidal and circular domains differs, Rottmayer introduced an empirically obtained geometric factor to model circular thermal resistance in part of cylindrical grid.

Yavuzturk and Spitler [37] introduced a two-dimensional finite difference transient borehole model, where grout, U-pipe and circulating fluid heat capacitance were taken into an account. Cylindrical grid in Yavuzturk and Spitler model is generated similarly to Rottmayer et al. model, while grid for circular pipe section is generated as an equivalent U-pipe area “pie sector”. Model's major advantage is capability to model short-term response e.g. in whole-year simulation coupled with ground-source heat pump model.

Lee and Lam [38] developed a three-dimensional finite difference model for a single energy pile. Presented model has two different soil material regions – one is soil surrounding the energy pile in radial direction and other is bedrock layer beneath the energy pile, where pile tip rests on. Additionally to soil and bedrock, pile grout and fluid are modelled and heat capacitances of these elements are considered in heat balance equations. Pipe wall heat capacitance is neglected. Model can account for multiple U-pipes and different pipe connection configurations. However, modelled pipes can only have equal distance from the piles centre, but distance between pipes can be different. Each pipe has same exact fluid flow rate, and ground surface and boundary temperatures are assumed to be constant. The model was first validated against analytical finite line source model over a period of 10 years, where pipe legs in analytical model were represented as superpositioned heat sources. Model showed very good agreement with analytical solution and the maximum result difference was only 0.11 °C. Further, developed model was used to calculate the steady-state thermal resistance of one pile configuration and result was validated with Hellstrom's [8] steady-state approach producing a difference of only 3.6%. A number of studies using validated model revealed that bedrock layer thermal conductivity underneath the pile has very low impact on the pile heat rejection/extraction performance due to very small heat conduction below the pile. However, change in thermal conductivity of soil surrounding the pile in the radial direction impacts the performance drastically. Study revealed, that 4 U-pipes connection had minor impact on the pile performance resulting in temperature difference of only 0.02 °C when parallel pipe legs connection is compared to serial. However, decrease in distance between U-pipe legs showed significant reduction of pile heat extraction/rejection performance.

Ghasemi-Fare and Basu [39] presented an annular cylinder heat source model that utilizes explicit finite difference method to calculate the evolution of temperature within radial and axial pile/soil regions, which models single geothermal pile. A symmetry condition is applied at centre of the pile and only one leg of U-pipe is modelled. Therefore, thermal interactions between adjacent U-pipe legs are neglected. Also, heat transfer through pipe wall is not modelled as the pipe wall thickness is assumed to be negligible. Heat capacitances of fluid, grout and soil are considered; model performs accurately at short-time step. Heat transfer within fluid is modelled only in axial direction. Ground water flow is neglected. Authors stated, that the model has showed good agreement during field test; but duration of validation period was only 3 h and resulted circulation tube vicinity temperature was ca 1 °C smaller than the reference temperature. Model is capable of accounting for non-homogenous pipe/soil material conditions. In utilized finite difference scheme initial boundary condition, such as ground surface (top boundary), bottom boundary and far-field (radial boundary) temperatures are given as node temperature values. Therefore, it can be concluded that variable surface temperature can be applied in the model, which is very important for modelling energy pile and floor structure thermal interface. A sensitivity analysis of this model revealed that the energy output of modelled pile depends mostly on the temperature difference between inlet fluid temperature and soil temperature, soil thermal conductivity and size of circulation tube/pipe.

Equa IDA-ICE borehole model [5] applies finite difference method to calculate a number of temperature fields that are

combined by superposition to generate the three-dimensional field. Model supports input of temperature gradient and borehole inclination. In multiple borehole configurations, first each single borehole thermal behaviour is calculated. Then the influence of all boreholes to the ground temperature is summed up by superposition. Model is capable of performing short time-step calculation and accounting for thermal interferences between adjacent boreholes and thermal capacitance of ground, borehole fluid and filling material, while pipe material thermal mass is neglected. Model accounts for heat transfer between U-pipe, upward and downward flowing liquid, grout, ground, ground surface and ambient air. Ground surface boundary condition can vary in time. Model supports only U-pipe configuration of GHE, where specific number of U-pipes in a borehole can be specified by the user. The length of each pile is assumed to be equal, ground homogeneous and ground water movement is not taken into an account.

4.2.2. Finite volume

Yavuzturk and Spitler [40] developed a two-dimensional finite volume model. Their model generates computational grid automatically based on the geometry of borehole and its internal components. As already mentioned in Section 4.1, this model was used to calculate g-function values for Yavuzturk and Spitler analytical solution.

He et al. [41] modelled borehole heat exchanger using finite volume method in two and three-dimensional domain. Two-dimensional model represented a 1 m deep cell in a three-dimensional model. Mentioned models were developed in environment called general elliptical multi-block solver in two/three dimension [42] (GEMS2D/3D). Compared to the grid solved in finite difference models, boundary fitted grid in GEMS2D is capable of solving complex geometry without additional simplifications. The advantages of a three dimensional model include fluid transport along the pipe loop and the dynamics of the fluid can be represented. Fluid, borehole and ground temperature variation along the borehole depth can be modelled. Different layers of rock and soil can be explicitly represented. Climate dependent boundary conditions at the surface can be applied. Heat transfer below the borehole can be explicitly considered. Initial vertical ground temperature gradients can be applied. However, major disadvantage of this very detailed model is computational time.

4.2.3. Finite element

Muraya [43] introduced a two-dimensional finite element model of borehole heat exchanger, which was used to simulate transient heat and mass transfer in soil surrounding boreholes coupled with ground source heat pump. Model is capable of accounting for water advection heat transfer. He also studied the impact of grout material and moisture content in soil on the pile thermal performance.

Three-dimensional finite element model was developed by Kohl et al. [44,45]. Borehole heat exchanger was modelled in environment called FRACTure. According to Signorelli et al. [46], this model is capable of accounting for hydraulic, thermal and elastic processes in transient conditions.

Finite element models are known for their long computational periods. Though, due to specifics of grid scheme, such models are capable of accounting for non-homogenous ground and backfill, uneven thermal loading of different U-pipe legs and complex geometry configurations of fluid circulation piping.

Gashti et al. [47] modelled five various single energy pile cases numerically in COMSOL software, which utilizes finite element method. Model was further validated against 28 days of measured experimental data and showed acceptable agreement. It was also possible to model ground water advection, but no essential ground water flow in measured area was presented. The goal of conducted study was to assess thermal regimes generated by pile application in heating/cooling mode conditions for mechanical behaviour investigation, where pile operates in cooling mode as a heat sink of solar collector. The idea behind the application of solar collector in GSHP system with energy pile is to maintain energy balance between heat extraction/rejection in cold climate of Finland, as most of the time heat is being extracted from the ground for heating purposes, which results in decrease of system performance over the years of operation [48]. Study showed, that some minor temperature differences of up to 1.5 °C appeared in heating operation of energy pile. However, in cooling mode high temperature differences up to 15 °C appeared in first meter of pile shaft and ca 11 °C in the bottom end of the pile below the U-curve spot, which denotes the need of further mechanical behaviour investigation. As results calculated with most finite element analysis software are generally presented in form of graphical visualisation, such modelling method is good for detailed study of single elements on smaller time scale due to high modelling effort and long simulation times involved.

Dupray et al. [49] modelled a field of energy piles in contact with floor slab using finite element software Lagamine. They simplified three-dimensional problem to a form of two dimensional, where thermo-hydro-mechanical behaviour of energy piles was modelled and pile interior components were neglected. Initial ground and floor surface temperature boundary conditions were constant. Clayey soil was fully saturated with no water flux present. However, change in water pressure in soil pores was modelled. A mechanical load of 3 MPa was applied to each modelled pile, which equals to an average building mechanical system. They further conducted a parametric study by applying different heat extraction/rejection scenarios with a simulation period of five years to study the impact of high temperature thermal storage on energy piles thermal and mechanical performance. Study revealed that with an injection rate of 245 W/m and extraction rate of 225 W/m initial ground temperature rise was ca 13 °C and efficiency loss per additional °C in average storage temperature was only 1.4%. It was also found, that it is important to account for a pile group compared to a single pile when studying thermo-mechanical behaviour. From mechanical perspective, application of high temperature thermal storage may impact piles bearing function and thermal stresses should be accounted for in pile design as both heating and cooling trigger measurable changes in soil conditions.

5. Energy pile sizing and design

Major available literature, design and installation guidelines, sizing manuals are related to boreholes and not for energy piles. Design and installation guidelines often refer to some standard or sizing manual or recommend applying detailed numerical calculation in form of specific software to size the GSHP system. Standards cover the simplified graphical/table data and manuals utilize more complex analytical sizing procedures. Most of simplified methods have very strict limitations, resulting in suitability for small scale systems mainly to ensure heating with design load of up to 45 kW. Such methods are used in Austrian [50], German [51], Swiss [52] and UK [53] standards. As an example of standards limitations, German VDI 4640 [51] states, that accurate sizing can be done only for individual borehole length ranged in 40–100 m, UK standard MCS MIS 3005 [53] requires the minimal spacing between adjacent boreholes to be at least 6 m. Sizing is done for a fixed number of heat pump operation hours (e.g. in VDI 4640 for 1800 or 2400 h/y) based on the established heat extraction rates that vary with soil/rock type and its thermal conductivity. Therefore, sizing data of standards is bound to local climate conditions

and in most cases may only be applicable in the country of origin.

GSHPA [54] energy pile design and installation guide proposes to follow MCS MIS 3005 to size energy pile systems with capacity of up to 45 kW or hire a GSHP designer, who utilizes the specific software. Also Brandl [4,55] emphasizes the need to perform calculations using the sizing software to assess the performance of energy piles. IGSHPA [58] borehole design and installation guide proposes to follow ASHRAE [56,57] sizing manual when designing borehole heat exchangers. Borehole analytical sizing procedures are based on cylindrical source model (CSM) and are described in manuals IGSHPA [58] and ASHRAE [56,57]. They can be used to size complex larger borehole systems in a preliminary design phase, but further detailed simulation using sizing software is again recommended.

Important aspect barely mentioned in standards and manuals is heat pump sizing ratio. MCS MIS 3005 proposes to size the heat pump to 100% of the design heat load. However, in some countries e.g. Finland or Estonia it is common to size the heat pump to 50–60% of the peak heat demand and auxiliary heating covers the rest of the peak load. This minimizes the investment cost of the heat pump, as a heat pump sized for 60% of the design heat load is still capable to cover more than 90% of building annual heating need during the test reference year (TRY) [59].

Because of aforementioned limitations, application of available borehole related standards and manuals for energy piles sizing is barely possible due to the differences in piles and boreholes geometry and boundary conditions. However, in future research, ASHRAE analytical sizing procedure might be used as a template for preparation of a new sizing procedure specifically for energy piles. More detailed description and comparison of standards and manuals along with the equations is presented in Ref. [60].

Sailer et al. [60] has compared aforementioned sizing techniques for a hypothetical (ca 70 m^2) UK dwelling, which resulted in difference over 40% of sized borehole length depending on the standard/manual applied. As the simplified methods of above listed standards had very limited input data to describe the system, Sailer preferred ASHRAE analytical sizing procedure, which is capable of accounting for more detailed geometry of the boreholes, bore-field layout, material thermal properties and multiple U-pipe configurations. ASHRAE analytical sizing procedure with exactly the same initial data as according to MCS MIS 3005 has yielded almost the same calculated borehole length of 173 m compared to latter standard's 168 m.

Most of available commercial software is designed specifically for borehole sizing. Table 6 summarizes most relevant commercial software, some of which might be possibly considered as a tool for energy piles sizing and design.

Commercial software presented in Table 6 can be grouped into two main categories based on the model applied – analytical or numerical. Software packages that utilize analytical models are EED, GLHEPro and GLD. Numerical models are applied in software Program EWS, IDA-ICE with borehole model extension, TRNSYS with DST model extension, TRNSYS with EWS model extension and PILESIM2.

Commercial software packages EED, GLHEPro and GLD utilize analytical response factor models, that support the least amount of features presented in Table 6. As already mentioned in modelling section, response factor i.e. g-function is used to describe temperature response of specific borefield configuration and is generally determined numerically. Precalculated g-functions of different borefield configurations are stored in software databases. Therefore, for buildings with pile foundation where piles are located according to foundation plan in chaotic order, EED and GLHEPro software database may lack g-function describing such pile field configuration. However, response factor based software GLD has an option to calculate and utilize g-function according to user specified piles location in two-dimensional Cartesian coordinate system. Exact pile location according to foundation plan in numerical model based software may only be defined in IDA-ICE and Program EWS.

Software that has no coupling capability with whole building simulation software requires the user to input building heating/cooling demand data in hourly or monthly time-step resolution, depending on the software capabilities. All of aforementioned response factor software packages are capable of handling building heating/cooling demand data only with monthly time-step resolution, while peak loads are defined separately as a number of hours per selected month. However, all of presented numerical model based software packages in Table 6 are capable of performing at time-step of an hour or less. The only response factor based software that can be coupled with whole building simulation via export of g-function to HVACSIM + software package is GLHEPro. Whole building simulation can be performed in IDA-ICE and TRNSYS. Therefore, numerical component models for IDA-ICE and IDA borehole and for TRNSYS - EWS and DST can be coupled with whole building simulation model as well.

User defined or calculated by whole building simulation heating/cooling demand data is converted to heat pump load data within the software. Depending on the software package, heat pump performance is either described as a fixed SCOP value or by applying the dynamic heat pump model. Applied heat pump model may either be a simple curve fitting model or a performance map based model with physical heat exchanger models. Heat pump in most software packages operates as an ideal capacity controlled heat pump within part load range of 0 … 100% which reasonably corresponds to actual inverter controlled heat pumps going down to a part load operation of about 20%. Aside from part load operation, many large heating/cooling plants are designed to operate on full load only. i.e with on/off control. The length of each heat pump operation cycle mainly depends on fluid volume in the system and actual heat demand. Therefore, performance of capacity controlled heat pump operation may drastically differ when compared to ON/OFF heat pump operation. Numerical models of IDA-ICE and TRNSYS software packages are capable for on/off operation.

As the energy piles amount and layout is bound to the foundation plan, thermal interferences between adjacent piles appear. To increase the yields and stabilize the long-term performance of GSHP plant, thermal storage is generally applied. In order for the software to account for different thermal storage sources or their combinations, software has to have an option to use component models and be capable of custom plants modelling. Numerical model based IDA-ICE and TRNSYS software packages support custom plant modelling and there are component models for different thermal storage sources available on the market. The rest of software packages listed in the Table 6 may only account for thermal storage in more simplified manner, by manipulating heat extraction/rejection load data e.g. assuming that storage will produce specific amount of energy during each month and adding this amount of energy to input heating/cooling demand data.

Wood et al. [72] compared measured mean fluid temperatures of energy pile field against computationally obtained temperatures in response factor software EED for a heating season. Measured mean fluid temperature resulted to be constantly ca 2 °C higher than predicted by EED, which g-functions does not account for pile thermal capacitance. For climate regions with low mean annual soil temperature e.g. 5 °C aforementioned underestimation of mean fluid temperature would result in ca 40% loss in actual system heat extraction potential. Therefore, application of response factor based borehole sizing software for energy piles appears to be least favorable when compared to numerical model based software presented in this section.

Table 6
Sizing and design software.

Product	Model	Variable floor surface temperature boundary	Coupling with whole building simulation	Loads input		Thermal storage				Heat pump		Piles location by (X,Y)
				Hourly	Monthly	Solar	Cooling tower	Exhaust air	Simplified[f]	Fixed SCOP	Dynamic	
EED [72,73]	g-funct				✓[c]				✓	✓		
GLHEPro [79,80]	g-funct		✓[e]		✓[c]				✓		✓[d]	
TRNSYS DST [8]	DST	✓	✓	✓		✓	✓	✓			✓	
TRNSYS EWS[g] [74]	FDM	✓	✓	✓		✓	✓	✓			✓	
Program EWS [75]	FDM	✓		✓					✓	✓		✓
GLD [76]	CSM + g-funct				✓[c]				✓		✓	✓
PILESIM2 [77,78]	modified DST	✓[a]		✓					✓		✓	
IDA borehole [5]	FDM	✓	✓	✓[b]		✓	✓	✓			✓	✓

[a] Building floor domain is separated from outdoor ground surface domain by the input of different variable temperatures.
[b] Calculation step can be less than an hour.
[c] Peak load value and duration during each month can be defined.
[d] Curve fitting is applied to describe the heat pump performance.
[e] g-function export to HVACSIM+.
[f] Simplified accountancy for thermal storage in form of additional heat extraction/rejection load data.
[g] Single pile only.

Fadejev and Kurnitski [5] have modelled a commercial hall-type building's geothermal plant coupled with boreholes and with energy piles in software package IDA-ICE with IDA borehole model extension. Difference between borehole and energy pile cases appeared in ground surface boundary conditions. Borehole field was exposed to ambient air, while energy piles soil surface was interconnected with floor slab, initial soil temperature in both cases was 8 °C. Pile and borehole fields had equivalent parameters – diameter of 115 mm, depth 15 m, distance in between 4.5 m and total amount of 196 units. Energy pile case was modelled with assumption, that whole ground surface domain was assumed as floor, so no actual building floor geometry was accounted for. Validity of such assumption is justified by the results of study conducted by Chuangchid and Krarti [14], where according to results of simulated winter case with uninsulated slab, soil temperature in building section view starts to drastically decrease at ca 2 m from the edge of the floor slab reaching lowest values at the edge of the floor slab. Therefore, energy piles modelling approach of Fadejev and Kurnitski [5] is appropriate for piles located further than 2 m away from the edge of the floor slab, as the initial temperature conditions of such piles are roughly same as in the centre of the slab. According to study results, changes in soil temperature affected the intensity of floor heat loss and simulation results revealed that geothermal plant with energy piles performed ca 23% more efficient compared to plant with boreholes. In energy piles case, soil temperature higher than initial 8 °C soil temperature appeared down to depth of ca 12 m during winter below soil surface (floor slab) boundary. However, in boreholes case at the same time soil temperature close to soil surface boundary was lower than initial 8 °C soil temperature due to the exposure to cold winter outdoor air. Such significant impact on soil surface temperature and plant performance emphasizes the importance of accounting heat transfer through floor structure when sizing GSHP systems with energy piles. This is possible if software supports at least variable surface temperature. All of discussed numerical model based software in this paper supports aforementioned feature. On the other hand, response factor based software appears to be least favorable for energy piles sizing, as numerically determined g-functions have been obtained with adiabatic ground surface boundary condition and the lack of variable floor surface temperature neglects the heat transfer through floor structure.

Software PILESIM 2 has two variable surface temperatures as the building floor domain is separated from ground surface domain that is exposed to ambient air. However, with reference to software manual [78], exact geometry of building floor cannot be defined. Building floor geometry in PILESIM2 depends on the input of piles amount and distance between them. Piles in PILESIM2 are located in circular storage volume and their exact location cannot be defined. As stated in software manual [78], PILESIM2 is not suitable for simulation of single pile or piles located in line, while is suitable for systems with relatively large amount of energy piles located in field shape of circle or square. It is worth to note, that previous version of PILESIM was applied in the design of Zürich Airport E-terminal geothermal plant and based on the measurements of actually built energy piles system [7] existing version of PILESIM2 was developed, where main changes were influencing geocooling module of the software.

Main differences between analytical and numerical model based software appear in computational time, modelling accuracy, ability to define exact location of piles and dynamic heating/cooling plant modelling capabilities. Response factor based software may instantly plot the results of 25-year period simulation, while numerical software may take days to perform a similar simulation in case of very large pile fields [48]. However, most of numerical model based software tend to be more precise and capable of accounting for sub-hourly time-step, exact piles location and can be coupled with whole building simulation software, that allows the user to model more complex dynamic heating/cooling plants. It is worth to note, that software with custom plant modelling capabilities such as IDA-ICE and TRNSYS has noticeably longer learning curve compared to the rest of software packages discussed in this section.

6. Conclusions

Review of available scientific literature revealed that energy piles are frequently misinterpreted as boreholes. Extensive research on boreholes, available models and software tools explain why energy piles have often being modelled and sized as boreholes. However, due to significant differences between energy piles and boreholes in geometry - energy piles are generally shorter and wider - and ground surface boundary conditions - energy piles are located beneath the building floor slab, their performance (based on the results of numerical studies) may remarkably vary and proposed to be taken into account in modelling.

Review of actually built geothermal plants with energy piles revealed four typical fundamental plant solutions that are

presented and described in this paper. They represent plant solutions suitable for both cold and hot climates. Properly sized heat pump systems with energy piles were characterized with high overall system SCOP values higher than 4.5, while in some case studies SCOP values were two times smaller that illustrates the effect of proper design and sizing.

Different pile configurations and their TRT test performance are summarized in the pile configuration section of this paper. TRT tests results show that short term specific heat extraction/rejection rate is highly dependent on the amount of pipe surface area grouted into the pile structure, however the long term performance is more limited by the soil heat capacity. The lack of specific heat extraction values which could be determined based on the climate and energy pile application and the fact that design guidelines, sizing manuals and standards are available mostly for boreholes, show the need to develop general procedures for early stage energy pile sizing that would allow quick estimates of required pile lengths and system performance with reasonable accuracy for conceptual design. The only energy piles related UK design guideline proposes either to use boreholes sizing manual or to hire a GHX designer, who utilizes sizing software. Most of boreholes sizing manuals are bound to country specific climate conditions, mostly suitable for sizing of small systems up to 45 kW and not suitable for energy piles sizing. ASHRAE analytical boreholes sizing procedure was found suitable for sizing fields of multiple boreholes in different climate conditions. This method can be suggested to be used as a starting point for future energy piles design guidelines development.

From the energy piles modelling perspective, most of available models are analytical, designed for borehole analysis and their main purpose is to process the results of TRT test in order to obtain thermal properties of soil. However, energy pile TRT generally requires a longer measurement period compared to borehole in order to overcome pile thermal capacitance. Transient hourly time-step simulation for energy performance analysis of energy piles can be performed with numerical models applied in dedicated simulation environments which are complicated to be used for everyday engineering purposes. The important feature not yet implemented in reviewed models is the ability to model heat transfer in two regions of energy piles surface boundary – in the floor of the building and soil.

Range of commercial software for energy piles sizing is very limited, however, there are many software packages available for boreholes sizing. Review of borehole sizing software features revealed that response factor based software packages are least favorable for energy piles sizing, as their g-functions database was generated with adiabatic ground surface boundary. When using boreholes sizing software for energy piles sizing, numerical model based software packages with variable ground surface temperature are to be considered. Most flexible software packages can be coupled with whole building simulation and can be used for customized detailed plant modelling. Based on this review such dynamic numerical simulation environments are IDA-ICE and TRNSYS. However, these software packages have a long learning curve and only experienced users are expected to utilize most advanced software features like custom plant modelling. There exists more user friendly software specifically designed for energy piles sizing such as Pilesim2. However, it is limited from the perspective of detailed thermal storage modelling and for exact pile location definition. Features that are suggested to be implemented in software packages in future development are soil water advection and the ability to simulate the ground floor heat loss.

Acknowledgment

This review was conducted within *IEA-ECES Annex 31*: Energy Storage with Energy Efficient Buildings and Districts: Optimization and Automation. The research was supported by the Estonian Centre of Excellence in Zero Energy and Resource Efficient Smart Buildings and Districts, ZEBE, funded by the European Regional Development Fund grant TK146, and by the Estonian Research Council, with Institutional research funding grant IUT1–15.

References

[1] Directive 2010/31/EU of the European parliament and of the Council of 19 May 2010 on the energy performance of buildings. Official Journal of the European Union; 2010.
[2] Lund JW, Freeston DH, Boyd TL. Direct utilization of geothermal energy 2010 worldwide review. Geothermics 2011;40(3):159–80.
[3] Brandl H. Energy foundations and other thermo-active ground structures. Geotechnique 2006;56(2):81–122.
[4] Brandl H. Thermo-active ground-source structures for heating and cooling. Proced. Eng 2013;57(0):9–18.
[5] Fadejev J, Kurnitski J. Geothermal energy piles and boreholes design with heat pump in a whole building simulation software. Energy Build 2015;106(0):23–4.
[6] Hamada Y, Saitoh H, Nakamura M, Kubota H, Ochifuji K. Field performance of an energy pile system for space heating. Energy Build 2007;39(5):p.517–524.
[7] Pahud D, Hubbucj M. Measured thermal performances of the energy pile system of the dock midfield at Zürich airport. In: Proceedings European geothermal congress 2007. May 31-June 01 unterhatching, Germany; 2007.
[8] Hellstrom G. Ground heat storage: thermal analysis of duct storage systems. Sweden: Department of Mathematical Physics, University of Lund; 1991.
[9] Reda F. Long term performance of different SAGSHP solutions for residential energy supply in Finland. Appl Energy 2015;144(0):31–50.
[10] Allaerts K, Coomans M, Salenbien R. Hybrid ground-source heat pump system with active air source regeneration. Energy Convers Manag 2015;90(0):230–7.
[11] Morrone B, Coppola G, Raucci V. Energy and economic savings using geothermal heat pumps in different climates. Energy Convers Manag 2014;88(0):189–98.
[12] Zhang C, Guo Z, Liu Y, Cong X, Peng D. A review on thermal response test of ground-coupled heat pump systems. Renew Sustain Energy Rev 2014;40(0):851–67.
[13] Carslaw HS, Jaeger JC. Heat conduction in solids. Oxford: Claremore Press; 1947.
[14] Chuangchid P, Krarti M. Foundation heat loss from heated concrete slab-on-grade floors. Build Environ 2001;36(0):637–55.
[15] Ingersoll LR, Zobel OJ, Ingersoll AC. Heat conduction with engineering, geological, and other applications. New York: McGraw-Hill; 1954.
[16] Eskilson P. Thermal analysis of heat extraction boreholes. Ph.D. Thesis. Sweden: University of Lund; 1987.
[17] Yavuzturk C, Spitler JD. A short time step response factor model for vertical ground Loop heat exchangers. ASHRAE Trans 1999;105(2):475–85.
[18] Zeng HY, Diao NR, Fang ZH. A finite line-source model for boreholes in geothermal heat exchangers. Heat Transf Asian Res 2002;31(7):558–67.
[19] Man Y, Yang H, Diaoa N, Liua J, Fanga Z. A new model and analytical solutions for borehole and pile ground heat exchangers. Int J Heat Mass Transf 2010;53(13–14):2593–601.
[20] Javed S, Claesson J. New analytical and numerical solutions for the short-term analysis of vertical ground heat exchangers. ASHRAE Trans 2011;117(1):3–12.
[21] Zhang W, Yang H, Lu L, Cui P, Fang Z. The research on ring-coil heat transfer models of pile foundation ground heat exchangers in the case of groundwater seepage. Energy Build 2014;71(0):115–28.
[22] Zhang W, Yang H, Lu L, Fang Z. The analysis on solid cylindrical heat source model of foundation pile ground heat exchangers with groundwater flow. Energy 2013;55(0):417–25.
[23] Wang D, Lu L, Zhang W, Cui P. Numerical and analytical analysis of groundwater influence on the pile geothermal heat exchanger with cast-in spiral coils. Appl Energy 2015;160(0):705–14.
[24] Hu P, Zha J, Lei F, Zhu N, Wu T. A composite cylindrical model and its application in analysis of thermal response and performance for energy pile. Energy Build 2014;84(0):324–32.
[25] Bixel HC, van Pollen HK. Pressure drawdown and buildup in the pressure of radial discontinuities. SPF J 1967;7:301–9.
[26] Ingersoll LR, Plass HJ. Theory of the ground pipe heat source for the heat pump, Heating. Pip Cond 1948;20:119–22.
[27] Diao N, Li Q, Fang Z. Improvement on modelling of heat transfer in vertical ground heat exchangers. HVAC&R Res 2004;10:459–70.
[28] Bandos TV, Campos-Celador A, Lopez-Gonzalez LM, Sala-Lizarraga JM. Finite cylinder-source model for energy pile heat exchangers: effects of thermal storage and vertical temperature variations. Energy 2014;78(0):639–48.
[29] Loveridge F, Powrie W. G-Functions for multiple interacting pile heat exchangers. Energy 2014;64(0):747–57.
[30] Loveridge F, Powrie W. 2D thermal resistance of pile heat exchangers. Geothermics 2014;50(0):122–35.

[31] Eslami-Nejad P, Bernier M. Freezing of geothermal borehole surroundings: a numerical and experimental assessment with applications. Appl Energy 2012;98:333–45.
[32] Eslami-Nejad P, Bernier M. Heat transfer in double U-tube boreholes with two independent circuits. J Heat Transf 2011;133(8).
[33] Bonacina C, Comini G, Fasano A, Primicerio M. Numerical solution of phase change problems. Int J Heat Mass Transf 1973;16(10):1825–32.
[34] Zarrella A, De Carli M, Galgaro A. Thermal performance of two types of energy foundation pile: helical pipe and triple U-tube. Appl Therm Eng 2013;61(2):301–10.
[35] Lei TK. Development of a computational model for a ground-coupled heat exchanger. ASHRAE Trans 1993;99(1):149–59.
[36] Rottmayer SP, Beckman WA, Mitchell JW. Simulation of a single vertical U-tube ground heat exchanger in an infinite medium. ASHRAE Trans 1997;103(2):651–9.
[37] Yavuzturk C. Modeling of vertical ground loop heat exchangers for ground source heat pump systems. Ph. D. thesis. Oklahoma: Oklahoma State University; 1999.
[38] Lee CK, Lam HN. A simplified model of energy pile for ground-source heat pump systems. Energy 2013;55(0):838–45.
[39] Ghasemi-Fare O, Basu P. A practical heat transfer model for geothermal piles. Energy Build 2013;66(0):470–9.
[40] Yavuzturk C, Spitler JD, Rees SJ. A Transient two-dimensional finite volume model for the simulation of vertical U-tube ground heat exchangers. ASHRAE Trans 1999;105(A):465–74.
[41] He S, Rees S, Shao L. Improvement of a two-dimensional borehole heat exchanger model. In: Proceedings of conference: IESD PhD conference: energy and sustainable development, institute of energy and sustainable development, queens building. Leicester, UK: De Montfort University; 21st May 2010.
[42] He S, Rees S, Shao L. Simulation of a domestic ground source heat pump system using a transient numerical borehole heat exchanger model. In: Proceedings of conference: building simulation 2009, eleventh international IBPSA conference, Glasgow, scotland; July 27-30, 2009.
[43] Muraya NK. Numerical modeling of the transient thermal interference of vertical U-tube heat exchangers. Ph. D. theis. Texas: Texas A&M University; 1994.
[44] Kohl T, Hopkirk RJ. "FRACTure" A simulation code for forced fluid flow and transport in fractured, porous rock. Geothermics 1995;24(3):333–44.
[45] Kohl T, Brenni R, Eugester W. System performance of a deep borehole heat exchanger. Geothermics 2002;31:687–708.
[46] Signorelli S, Bassetti S, Pahud D, Kohl T. Numerical evaluation of thermal response tests. Geothermics 2007;36(2):141–66.
[47] Gashti EHN, Uotinen VM, Kujala K. Numerical modelling of thermal regimes in steel energy pile foundations: a case study. Energy Build 2014;69(0):165–74.
[48] Fadejev J, Kurnitski J. Energy pile and heat pump modeling in whole building simulation model. In: 2nd IBPSA-England conference on building simulation and optimization, London, United Kingdom; June 2014. p. 23–4.
[49] Dupray F, Laloui L, Kazangba A. Numerical analysis of seasonal heat storage in an energy pile foundation. Comput Geotechnics 2014;55(0):67–77.
[50] Österreichischer Wasser- und Abfallwirstschaftsverband. ÖWAV-RB 207-Thermische Nutzung des Grundwassers und des Untergrunds – Heizen und Kühlen. Austria. 2014.
[51] Verein Deutscher Ingegneure. In: VDI 4640 – Blatt 1–4. Thermal use of the underground. Düsseldorf, Germany; 2010.
[52] Schweitzer Ingeneur- und Architektenverein. SIA 384/6. Erdwärmesonden, Zürich, Switzerland. 2010.
[53] Microgeneration Installation Standard. MIS 3005 Issue 4.0-Requirements for contractors undertaking the supply, design, installation, set to work, commissioning and handover of microgeneration heat pump systems. London, UK. 2013.
[54] GSHPA. Thermal pile. Design, installation and material standards. Issue 1.0. UK: Ground Source Heat Pump Association, National Energy Center; 2012.
[55] Brandl H. Energy piles for heating and cooling of buildings. In: Proceedings of 7th international conference and exhibition on piling and deep foundations, Vienna; 1998. p. 341–6.
[56] Philippe M, Bernier M, Marchio D. Sizing calculation spreadsheet. Vertical geothermal borefields. ASHRAE J 2010;52(7):20–8.
[57] Kavanaugh SP, Rafferty K. Ground-source heat pumps—design of geothermal system for commercial and institutional buildings. Atlanta: ASHRAE Applications Handbook; 1997.
[58] IGSHPA. Ground source heat pump residential and light commercial: design and installation guide. USA: Oklahoma State University; 2009.
[59] Kalamees T, Jylhä K, Tietäväinen H, Jokisalo J, Ilomets S, Hyvönen R, et al. Development of weighting factors for climate variables for selecting the energy reference year according to the EN ISO 15927-4 standard. Energy Build 2012;47:p.53–60.
[60] Sailer E, Taborda DMG, Keirstead J. Assessment of design procedures for vertical borehole heat exchangers. In: Proceedings of fortieth workshop on geothermal reservoir engineering, Stanford, California; January 26-28, 2015.
[61] Sanner B. Shallow geothermal energy. In: Proceedings of the internetional summer school of direct application of geothermal energy. Geothermische Verinigung GtV, Germany; 2001.
[62] Gao J, Zhang X, Liu J, Li KS, Yang J. Thermal performance and ground temperature of vertical pile-foundation heat exchangers: a case study. Appl Therm Eng 2008;28(17–18):p.2295–2304.
[63] Yang H, Cui P, Fang Z. Vertical-borehole ground-coupled heat pumps: a review of models and systems. Appl Energy 2010;87(1):p.16–27.
[64] Jalaluddin AM, Tsubaki K, Inoue S, Yoshida K. Experimental study of several types of ground heat exchanger using a steel pile foundation. Renew Energy 2011;36(2):p.764–771.
[65] Li M, Lai ACL. Heat-source solutions to heat conduction in anisotropic media with application to pile and borehole ground heat exchangers. Appl Energy 2012;96(0):p.451–458.
[66] IGSHPA. Closed-loop/geothermal heat pump systems: design and installation standards. 2013 edition. International Ground Source Heat Pump Association, Oklahoma State University; 2013.
[67] Park S, Lee D, Choi H-J, Jung K, Choi H. Relative constructability and thermal performance of cast-in-place concrete energy pile: coil-type GHEX (ground heat exchanger). Energy 2014:1–11 (Article in press).
[68] Li M, Lai ACK. Review of analytical models for heat transfer by vertical ground heat exchangers (GHEs): a perspective of time and space scales. Appl Energy 2015;151(0):178–91.
[69] Girard A, Gago EJ, Muneer T, Gaceres G. Higher ground source heat pump COP in a residential building through the use of solar thermal collectors. Renew Energy 2015;80(0):26–39.
[70] Hesaraki A, Holmberg S, Haghighat F. Seasonal thermal energy storage with heat pumps and low temperatures in building projects – a comparative review. Renew Sustain Energy Rev 2015;43(0):1199–213.
[71] Aydin M, Sisman A. Experimental and computational investigation of multi U-tube boreholes. Appl Energy 2015;145(0):p.163–171.
[72] Wood CJ, Liu H, Riffat SB. Comparison of a modelled and field tested piled ground heat exchanger system for a residential building and the simulated effect of assisted ground heat recharge. Int J Low Carbon Technol 2010;5(3):137–43.
[73] Blocon. Earth energy designer v. 3.2 user's manual. Sweden. 2015.
[74] Wetter M, Huber A. TRNSYS type 451 – vertical borehole heat exchanger – EWS model – model description and implementing into TRNSYS. Zürich/Luzern, Switzerland: Huber Energietechnik AG; 1997.
[75] Huber A. Program EWS version 4.7-calculation of borehole heat exchangers – software manual. Zürich, Switzerland: Huber Energietechnik AG; 2011.
[76] Gaia Geothermal. Ground loop Design™ premier 2014 User's guide, USA. 2014.
[77] Pahud D, Fromentin A, Hadorn J-C. The duct ground heat storage model (DST) for TRNSYS used for the simulation of heat exchanger piles, user manual, Lausanne. 1996.
[78] Pahud D. Pilesim2 – simulation tool for heating/cooling systems with energy piles or borehole heat exchangers – user manual. Switzerland: ISAAC-DACD-SUPSI; 2007.
[79] Spitler JD. GLHEPRO: a design tool for commercial building ground loop heat exchangers. In: Proceedings of the fourth international heat pumps in cold climates conference, Aylmer, Quebec; August 17-18, 2000.
[80] IGSHPA. GLHEPro 4.1 for windows User's guide. USA: School of Mechanical and Aerospace Engineering, Oklahoma State University; 2014.
[81] Fadejev J, Simson R, Kurnitski J, Kesti J, Mononen T, Lautso P. Geothermal heat pump plant performance in a nearly zero-energy building. Proceedings of Sustainable Built Environment Tallinn and Helsinki Conference SBE16. Energy Proced 2016;96:489–502.

Publication 2

Fadejev J, Kurnitski J. Geothermal energy piles and boreholes design with heat pump in a whole building simulation software. *Energy and Buildings*, Vol. 106 pp. 23-34. 2015.

Energy and Buildings 106 (2015) 23–34

Contents lists available at ScienceDirect

Energy and Buildings

journal homepage: www.elsevier.com/locate/enbuild

Geothermal energy piles and boreholes design with heat pump in a whole building simulation software

Jevgeni Fadejev[a,b,*], Jarek Kurnitski[a,b]

[a] Tallinn University of Technology, Ehitajate tee 5, 19086 Tallinn, Estonia
[b] Aalto University, School of Engineering, Rakentajanaukio 4 A, FI-02150 Espoo, Finland

ARTICLE INFO

Article history:
Received 14 January 2015
Received in revised form 2 June 2015
Accepted 3 June 2015
Available online 6 June 2015

Keywords:
Energy piles
Borehole heat exchanger
Seasonal thermal storage
IDA-ICE
Heat pump modelling

ABSTRACT

With growing demand in improving building's energy efficiency, utilization of energy from renewable sources, such as ground energy, becomes more common. This paper focuses on the detailed modelling issues in a whole building simulation environment providing an approach for a design of a heat pump plant with boreholes or energy piles, that was developed for a case of one storey commercial hall building. Modelling was performed in whole building simulation software IDA-ICE, where most of the modelled components were defined as manufacturer specific products. Recently developed three dimensional borehole model was validated with the use of actual borehole measurement data. Heat pump model calibration parameters equations, which are needed to setup model according to manufacturer specific performance map product data, were derived and applied. According to results of conducted 20-years long-term simulations, consideration of seasonal thermal storage can become feasible. Validation of borehole model showed that the model can simulate very accurate dynamic performance and is highly suitable for coupling with dynamic plant models. Different ground surfaces boundary conditions of geothermal energy piles and field of boreholes resulted in 23% more efficient performance of energy piles in the case of the same field configuration.

1. Introduction

Geothermal energy, as a renewable energy source, can be efficiently utilized with an application of ground-source heat pump (GHSP) coupled with ground heat exchanger (GHE). GHSPs are widely used all over the world [1] to meet buildings with high energy performance heating and cooling demand. GHEs are generally classified according to their installation position – horizontal or vertical. One common vertical GHE solution is a borehole heat exchanger (BHE), which can be installed as a single borehole or in a group – BHE field [2]. Another vertical GHE solution is geothermal pile foundation [3], which is frequently referred to as geothermal energy piles (GEP). GEPs have two main functions – building load bearing to ground and ground heat exchanger. Because of these multiple features, GEPs can be highly cost-effective.

Thermal performance of GEPs differs from the common BHE field performance due to different ground surface boundary conditions. Generally, BHE field is located next to the building, where ground surface of BHE field is exposed to outdoor air and solar radiation. In case of GEPs, ground surface of pile foundation is interconnected with building's floor structure and solar radiation incident is limited by the building. Floor structure above the GEPs is exposed to indoor air, which temperature exceeds undisturbed ground temperature during the year in most climate zones. In GEPs case, heat conduction through the floor structure heats up the ground over the year and produces natural thermal storage effect, which BHE field lacks. Amount of GEPs in the design is usually limited by the foundation plan. When piles are located close to each other, thermal interference between adjacent piles appear. Therefore, assessment of GEPs or BHE field thermal performance and design includes quite many complex aspects typically modelled numerically.

The most recent European standard describing the design of heat pump heating systems EN 15450:2007 [4] lacks design guidelines for GHSPs coupled with GEPs or BHE field. The design and thermal performance assessment of BHE field is commonly performed in commercial software such as EED [5], GLHEPRO [6], Energy Plus [7] and TRNSYS [8].

In GLHEPRO, Energy plus and EED software, heat exchange between boreholes and ground is modelled with Eskilson's g-function [9]. Building operation is described with the input of

* Corresponding author at: Tallinn University of Technology, Ehitajate tee 5, 19086 Tallinn, Estonia. Tel.: +372 55 517 784.
E-mail address: jevgeni.fadejev@ttu.ee (J. Fadejev).

http://dx.doi.org/10.1016/j.enbuild.2015.06.014
0378-7788/

Nomenclature

Pr	Prandtl number
μ	dynamic viscosity (Pa s)
C_p	specific heat [W/(m K)]
ρ	density (kg/m^3)
m	mass flow (kg/s)
V	volume (m^3)
K	heat transfer coefficient (W/K)
κ	thermal conductivity [W/(m K)]
k_g	grout thermal conductivity [W/(m K)]
R_b	borehole resistance [(m K)/W]
d_b	borehole diameter (m)
d_p	pipe diameter (m)
n	number of U-pipes
T	temperature (°C)
$\Delta Tlog$	logarithmic mean temperature difference (°C)
Q	thermal power (W)
P	electric power (W)
COP	coefficient of performance
EER	energy efficiency ratio
out	index for outlet
in	index for inlet
$cond$	index for condenser
$evap$	index for evaporator
dim	index for parameter value at rating conditions
f	index for full load
e	exponent
NTU	number of transfer units
t	time

average monthly load data. *G*-function value depends on the depth of boreholes in ground and the distance between them. *G*-function is used to describe specific borehole configuration performance over time and calculate the temperature at borehole wall. According to [10], determination of *g*-function is a time consuming process. Therefore, *g*-functions are pre-calculated for a limited amount of borehole field configurations and stored in software databases. This allows the software to instantly calculate and plot the results of the long-term simulation, where simulated period may exceed 20 years. Though, software user is limited to predetermined borehole field configurations. Also, the results are only available as an average monthly data. As it is not possible to define ground surface boundary conditions, calculation of GEPs case in such software can become problematic. A detailed simulation of a single borehole in TRNSYS is possible with EWS model [20], which can perform at short time-step and accounts for thermal capacitance of fluid and borehole filling materials. EWS model utilizes finite difference method – Crank–Nicolson method. BHE field in TRNSYS can be simulated using a DST component model [11]. DST model is capable of annual hourly simulation and has also ground surface temperature input variable, which makes it possible to simulate the GEPs case. Depending on the software, the applied heat pump model [12] is either a simple quasi steady state performance map model or more complex parameter estimation based model [13].

The aim of this study was to model and assess the performance of the detailed heating/cooling plant with heat pump and GEPs/BHE field in the whole-building IDA-ICE simulation environment. The modelled plant considers application of recently developed three-dimensional model for an arbitrary combination of boreholes, correlation parameter based heat pump model with physical heat exchangers models and standard IDA-ICE model library components. This approach is suitable for detailed design, i.e. sizing of plant and BHE/GHE components with known limitations. Detailed plant was implemented in the whole-year energy performance simulation of a one storey commercial hall-type building.

To ensure the results accuracy, we validated IDA-ICE borehole model extension using experimental borehole measurements data. We studied IDA-ICE heat pump mathematical model and derived straightforward equations for calibration parameters, which are needed to setup heat pump model according to actual heat pump performance map product data. To simulate GEPs case, we modelled the impact of heat losses through floor structure on ground temperature and assessed its impact on the energy performance relative to BHE field. We studied the impact of borehole thermal resistance and long-term application of GEPs/BHE field on absorbed ground heat allowing to assess the importance of seasonal thermal storage [14].

2. Methods

The modelling in IDA-ICE was performed in advanced level interface, where user can manually edit connections between model components, edit and log model specific parameters, observe models code. An early stage building optimization (ESBO) plant, which is a part of a standard IDA model library, was utilized to generate the plant model. Abovementioned plant was modified to meet specific simulated case design intent. Total of two plant modifications were modelled – plant for building with GEPs (Fig. 1) and plant for building with BHE field (Fig. 1).

2.1. Building model description

Modelled plant modifications were coupled with a commercial hall-type one storey building (Fig. 2) located in Helsinki, Finland.

Ambient boundary conditions, regarding local weather data were described in recently updated Helsinki test reference year climate file [15] that was applied in the simulation. In cold climate conditions, buildings indoor climate requirements are generally ensured with heating. The heating and cooling energy use ratio in particular building is 1 to 0.056. Building's heating and cooling demand is met with radiant heating/cooling panels. Abovementioned room units were modelled with standard IDA ICE component library model, where manufacturer specific performance are described with the input of power law coefficient and exponent values. Detailed overview of general parameters describing the building model is presented in Table 1.

2.2. Heat pump model description

The design intent was to size the heat pump at ca 40% of building's design heat load at design ambient air temperature of −26 °C. The rest of the peak load was meant to be covered with electric top-up heating. Model of the brine-to-brine heat pump from the standard IDA ICE component library was applied in the study. The parameter estimation based heat pump model consists of a heat exchanger model [16] and compressor performance descriptive correlation model. The heat exchanger model, which is based on the NTU-method, describes heat pump condenser and evaporator. Abovementioned heat pump model is capable of performing at either full or part load. Plant design intent in this study considers application of "ON/OFF" heat pump. Therefore, part load operation of the heat pump model is not discussed in this paper. In the following, mathematical model of IDA ICE heat pump operation at full load is presented.

Heat pump condenser side produced heat at full load is described with the following equation:

$$Q_{cond_f} = P_f + Q_{evap_f} \quad (1)$$

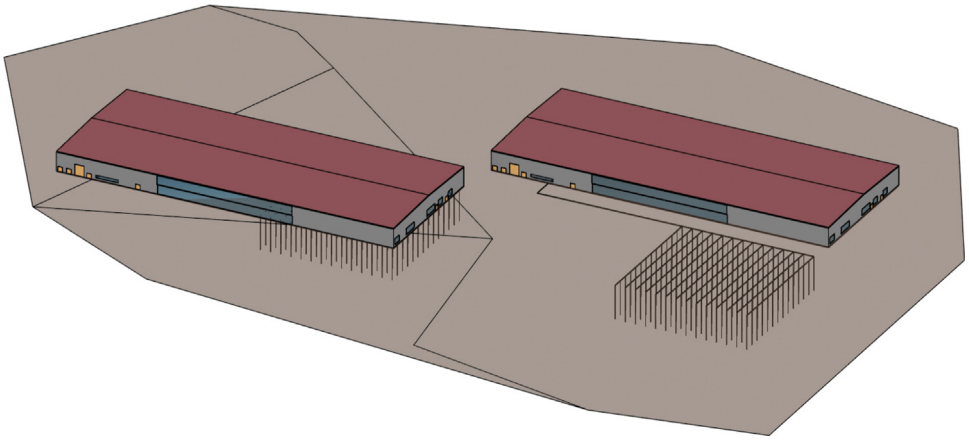

Fig. 1. Building with GEPs (left) and BHE field (right).

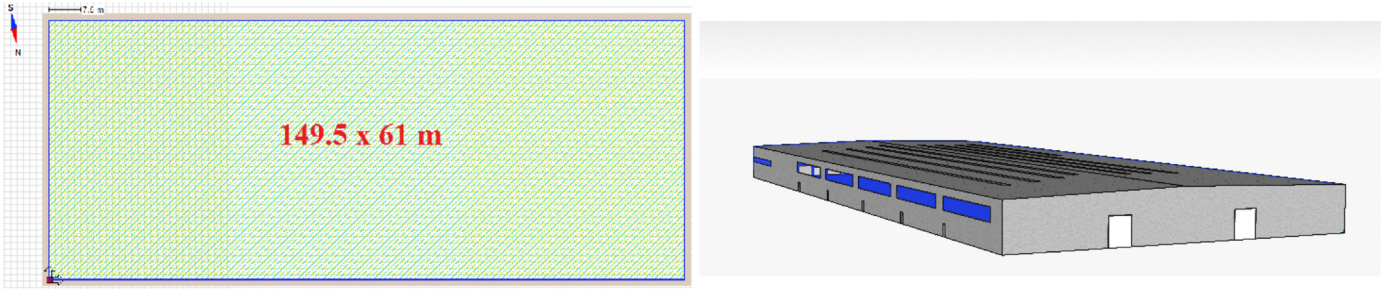

Fig. 2. Building model plan view and 3D view in IDA-ICE.

where P_f is compressor consumed electricity and Q_{evap_f} is evaporator absorbed heat at full load. Compressor electric power at a specific moment of time is described with following equation:

$$P_f = \frac{e^{F*T_{cond}+E*T_{evap}}}{e^{F*T_{conddim}+E*T_{evapdim}}} * P_{dim} \quad (2)$$

where values of condensing temperature T_{cond} and evaporation temperature T_{evap} are calculated by NTU heat exchanger model. Constant parameters with index *dim* describe heat pump model performance at rating conditions. Outside of the rating conditions range, heat pump model utilizes constant calibration parameters

Table 1
Building model parameters overview.

Descriptive parameter	Value
Location	Finland
Net floor area, m^2	9119.5
External walls area, U = 0.16 W/(m^2 K), m^2	2552
Roof area, U = 0.15 W/(m^2 K), m^2	9123
External floor area, U = 0.09 W/(m^2 K), m^2	9120
Windows area, SHGC = 0.51, U = 0.97 W/(m^2 K), m^2	726
External doors, U = 0.97 W/(m^2 K), m^2	89
Heating set point, °C	18
Cooling set point, °C	25
Occupancy/lighting schedule	8:00–21:00
AHU operation schedule	7:00–22:00
Occupants, 1.2 met, 0.8 clo, no	213
Lights load, kW	72.9
AHU air flow, m^3/s	10.1
AHU heat recovery, %	80
Air tightness, ACH	0.3 @50 Pa
Supply air temperature, °C	18
Radiant heating/cooling panels, b = 1.2 m, m	750
Heat load design temperature, °C	−26
Design heat load, kW	463
Heat pump capacity, kW	172

B, *C*, *E* and *F* to calculate heat pump model variables. Evaporator absorbed heat at a specific moment of time is calculated with the following equation:

$$Q_{evap_f} = \frac{e^{C*T_{cond}+B*T_{evap}}}{e^{C*T_{condim}+B*T_{evapdim}}} * P_{dim} * EER_{dim} \quad (3)$$

where P_{dim} is compressor power at rating conditions. Energy efficiency ratio at rating conditions is calculated with the following equation:

$$EER_{dim} = COP_{dim} - 1 \quad (4)$$

where COP_{dim} is heat pump coefficient of performance at rating conditions. Condensing temperature at rating conditions is calculated with the following equation:

$$T_{conddim} = \frac{T_{condin} - (T_{condout} * e^{(T_{condout}-T_{condin})/(\Delta T \log conddim)})}{1 - ee^{(T_{condout}-T_{condin})/(\Delta T \log conddim)}} \quad (5)$$

where T_{condin} is condenser inlet temperature, $T_{condout}$ is outlet temperature and $\Delta Tlogconddim$ is condenser logarithmic temperature difference at rating conditions. Evaporation temperature at rating conditions is calculated with the following equation:

$$T_{evapdim} = \frac{T_{evapin} - (T_{evapout} * e^{(T_{evapin}-T_{evapout})/(\Delta T \log evapdim)})}{1 - e^{(T_{evapin}-T_{evapout})/(\Delta T \log evapdim)}} \quad (6)$$

where T_{evapin} is evaporator inlet temperature, $T_{evapout}$ is outlet temperature and $\Delta Tlogevapdim$ is logarithmic temperature difference at rating conditions. Generally, logarithmic temperature difference for evaporator will differ from condenser value.

To setup the heat pump model to perform as a manufacturer specific product, user is required to specify total of 12 parameters, Table 2.

Eight parameters describing the performance of the heat pump at rating conditions can be collected from the heat pump

Table 2
Heat pump model parameters overview.

Descriptive parameter	Value
Nominal capacity at rating, kW	171.2
Coefficient of performance at rating, *COP*	4.65
Evaporator LMTD at rating, $\Delta Tlogevapdim$, °C	3
Condenser LMTD at rating, $\Delta Tlogconddim$, °C	5
Evaporator inlet temperature at rating, T_{evapin}, °C	0
Evaporator outlet temperature at rating, $T_{evapout}$, °C	−3
Condenser inlet temperature at rating, T_{condin}, °C	30
Condenser outlet temperature at rating, $T_{condout}$, °C	35
Calibration parameter *B*, %	3.21
Calibration parameter *C*, %	−1.6
Calibration parameter *E*, %	0.72
Calibration parameter *F*, %	1.97

performance map, Fig. 3. Four calibration parameters *B*, *C*, *E* and *F* should be calculated by the user.

Equations for calculating heat pump model calibration parameters were derived from IDA-ICE heat pump model open-source code and calculation example is presented in Section 3.2.

2.3. Borehole model description

Boreholes in GEPs and BHE field plant modifications were modelled with IDA-ICE borehole model extension [19]. Total of 196 boreholes (Fig. 4) were modelled in both studied cases. Borehole model applies finite difference method [17] to calculate a number of temperature fields that combined by superposition generate the three-dimensional field. The following temperature fields are computed for each borehole [19]:

- One-dimensional heat transfer in U-pipe for upward and downward flowing liquid;
- One-dimensional heat transfer between grout, liquid and ground;
- Two-dimensional heat transfer in cylindrical coordinates around borehole and between grout and liquid.

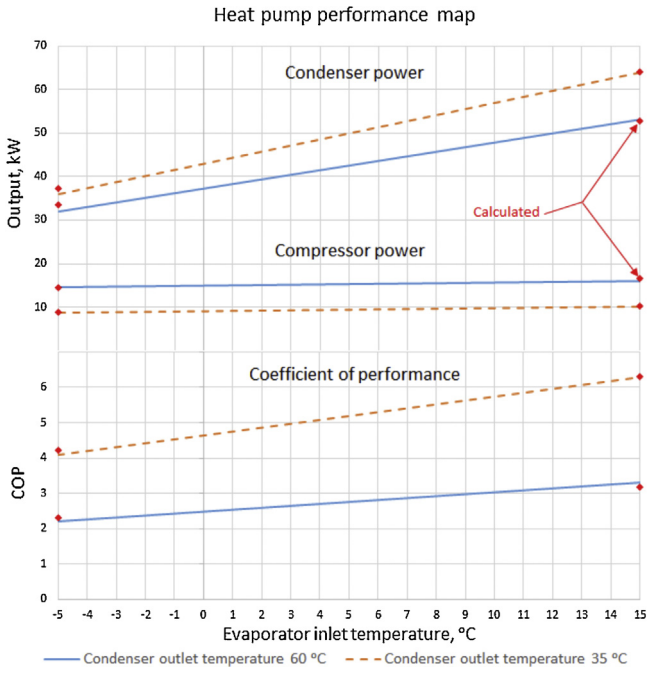

Fig. 3. Heat pump performance map. Solid and dashed lines are manufacturer specification and IDA-ICE heat pump model output is shown with markers for selected points.

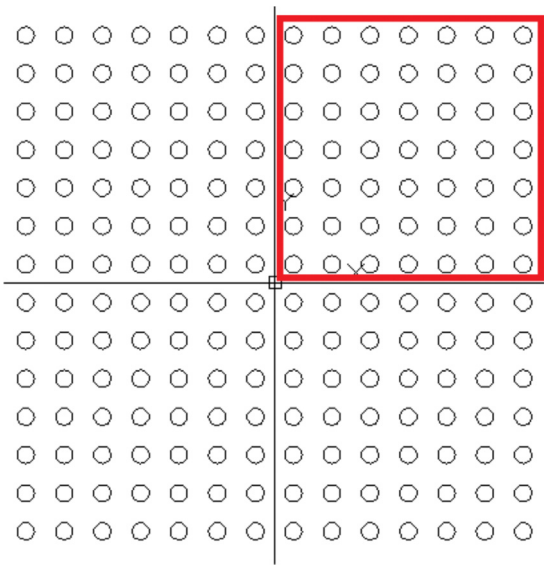

Fig. 4. GEPs/BHE field layout, dimensions are 58.5 × 58.5 m and the distance between piles 4.5 m.

Additionally, an undisturbed ground temperature field is computed with one-dimensional heat equation applying heat transfer coefficient towards ambient temperature at ground surface. Model supports input of temperature gradient and borehole inclination. The actual ground temperature at the boreholes wall is computed using superposition. In multiple borehole configurations, first each single borehole thermal behaviour is calculated. Then the influence of all boreholes to the ground temperature is summed up by superposition [19].

Model is capable of performing at short time-step and accounts for thermal interferences between adjacent boreholes and thermal capacitance of ground, borehole fluid and filling material, while pipe material thermal mass is neglected. Model accounts for heat transfer between U-pipe, upward and downward flowing liquid, grout, ground, ground surface and ambient air. Ground surface boundary condition can vary in time. Model supports only U-pipe configuration of GHE, where specific number of U-pipes in a borehole can be specified by the user. The length of each pile is assumed to be equal, ground homogeneous and ground water movement is not taken into an account.

Energy balance of fluid in IDA-ICE borehole model [19] is expressed with a set of following equations:

$$\rho_{Liq} c_{p,Liq} V_{Liq} \cdot \frac{dTd_{i,j}}{dt} = m_i \cdot c_{p,Liq} \cdot (Td_{i,j-1} - Td_{i,j}) + K_{LiqGrout,i} \cdot (T_{Groutd,i,j} - Td_{i,j}) + K_{LiqEarth,i} \cdot (T_{real,i,j} - Td_{i,j}) \quad (7)$$

$$\rho_{Liq} c_{p,Liq} V_{Liq} \cdot \frac{dTu_{i,j}}{dt} = m_i \cdot c_{p,Liq} \cdot (Tu_{i,j+1} - Tu_{i,j}) + K_{LiqGrout,i} \cdot (T_{Groutu,i,j} - Tu_{i,j}) + K_{LiqEarth,i} \cdot (T_{real,i,j} - Tu_{i,j}) \quad (8)$$

where $Td_{i,j}$ and $Tu_{i,j}$ is temperature of the down and up flowing fluid respectively in node *j* of borehole *i*, $T_{Groudt,i,j}$ and $T_{Groutu,i,j}$ is grout temperature around down and up flow pipe(s) respectively at layer *j* of borehole *i*, $T_{real,i,j}$ is temperature at the borehole wall for borehole *i* in node *j*, $K_{LiqGrout,i}$ is the heat transfer coefficient

Table 3
Borehole model parameters overview.

Descriptive parameter	Value
Borehole amount, pcs	196
Borehole depth, m	15
Borehole diameter, mm	115
Distance between boreholes, m	4.5
Pipes outside walls distance, mm	52.4
U-pipe outer diameter, mm	25
U-pipe inner diameter, mm	20.4
Ground heat conductivity, W/(m K)	1.1
Ground volumetric heat capacity, kJ/(m^3 K)	2019
Ground average annual temperature, °C	8
Borehole grouting heat conductivity, W/(m K)	1.8
Grout volumetric heat capacity, kJ/(m^3 K)	2160
Pipe material heat conductivity, W/(m K)	0.3895
Pipe volumetric heat capacity, kJ/(m^3 K)	1542
Brine ethanol concentration, %	25
Brine freezing temperature, °C	−15
Brine heat conductivity, W/(m K)	0.43
Brine volumetric heat capacity, kJ/(m^3 K)	4023
Brine density, kg/m^3	969
Brine viscosity, Pa s	0.006
Borehole thermal resistance, (m K)/W	0.1
Heat transfer coefficient at ground surface, W/(m^2 K)	0.15
Prandtl number	58

between fluid and filling material and $K_{LiqEarth,i}$ is the heat transfer coefficient between fluid and ground in borehole i.

Energy balance for the borehole filling material in IDA-ICE borehole model [19] is expressed with a set of following equations:

$$Mc_{p,Grout2} \cdot \frac{dT_{Grout,i,j}}{dt} = K_{GroutGrout} \cdot (T_{Groutd,i,j} + T_{Groutu,i,j} - 2T_{Grout,i,j}) + K_{GroutEarth} \cdot (T_{Real,i,j} - T_{Grout,i,j}) \quad (9)$$

$$Mc_{p,Grout1} \cdot \frac{dT_{Groutd,i,j}}{dt} = K_{GroutGrout} \cdot (T_{Grout,i,j} - T_{Groutd,i,j}) + K_{LiqGrout,i} \cdot (Td_{i,j} - T_{Groutd,i,j}) + K_{RingEarth} \cdot (T_{Real,i,j} - T_{groutd,i,j}) \quad (10)$$

$$Mc_{p,Grout1} \cdot \frac{dT_{Groutu,i,j}}{dt} = K_{GroutGrout} \cdot (T_{Grout,i,j} - T_{Groutu,i,j}) + K_{LiqGrout,i} \cdot (Td_{i,j} - T_{Groutu,i,j}) + K_{RingEarth} \cdot (T_{Real,i,j} - T_{groutu,i,j}) \quad (11)$$

where $Mc_{p,Groudt1}$ and $Mc_{p,Groudt2}$ is absolute heat capacity of inner and outer grout respectively, $T_{Groudt,i,j}$ and $T_{Groutu,i,j}$ is the grout temperature around down and up flow pipe(s) respectively at node j in borehole i, $T_{Groudt,i,j}$ and $T_{Real,i,j}$ is temperature of outer grout and temperature at the borehole wall for borehole i in node j respectively, $K_{GroutGrout}$ is heat conductivity coefficient between grout ring and outer grout, $K_{RingEarth}$ is heat conductivity coefficient between grout ring and ground and $K_{GroutEarth}$ is heat conductivity between grout and ground. More detailed description of IDA ICE borehole model can be found in [19].

Model considers the input of parameters (Table 3), which describe thermal and physical properties of ground, pipe, grout and brine.

In order to decrease the duration of the simulation with high amount of boreholes, model provides an option to mirror (Fig. 5) part of the calculated domain results. In this particular study, mirror option 2 (Fig. 5) was applied. Therefore, coordinates of only 49 of 196 boreholes were actually defined in the borehole model.

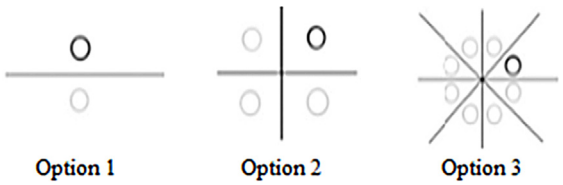

Fig. 5. Borehole field mirror.

In BHE field plant modification, ground surface is exposed to the ambient air. Therefore, we linked borehole model ground surface temperature variable to outside air variable. Heat transfer rate between ground surface and ambient air is described with the ground surface heat transfer coefficient.

Specifics of GEPs plant modification consider that the ground surface above the energy piles is interconnected with floor slab. Because the modelled building is located in the cold climate of Finland, average annual ground temperature is ca 8 °C, while indoor air temperature set point during heating season is 18 °C. Big temperature difference between ground and floor slab surface temperature produces a natural heat loss from floor to ground, which results in ground temperature increase. In building with GEPs, GSHP extracts heat from the ground during the heating season until the temperature of evaporator entering fluid drops below 0 °C. Increase of ground temperature due to the floor heat loss to ground enables the heat pump to operate for longer periods and energy piles are capable of extracting more heat. Building with GEPs will have higher annual floor heat loss compared to building without GEPs, because GSHP cools the ground during the heating season and the resulting average ground temperature will be much lower compared to building without GEPs average ground temperature. Considering the statements above, a significant difference in BHE field and GEPs plant performance exists. Therefore, it is very important to model such connection between floor slab and borehole model in GEPs plant modification. Considering the fact, that IDA ICE borehole model was primarily designed for simulation of borehole field and not GEPs, some known modelling limitations presented further cannot be neglected. In order to model the GEPs plant modification, we linked 58.5 × 58.5 m zone slab model surface temperature variable to borehole model ground surface temperature variable. The slab structure is defined in both slab and borehole model. In slab model, floor structure is defined as material layers with thermal properties. While in borehole model, an insulated slab is defined as a ground surface heat transfer coefficient, which value is equivalent to slab thermal transmittance.

In IDA ICE, zone slab finite difference model calculates the heat flux based on the difference between two temperatures – floor surface temperature and ground surface temperature. By default, ground surface temperature is calculated by IDA ICE ground model, which has no connection to borehole model. Therefore, a connection between borehole model and slab model is needed. Though, borehole model is not capable of calculating ground surface temperature, as this parameter is an input variable. Therefore, borehole outlet temperature parameter was linked to zone slab model's ground surface temperature variable. By doing actions described above, we have modelled the impact of heat conduction through floor structure on the ground temperature and vice versa. Fig. 6 describes the links between borehole and zone floor structure model in plant modification with GEPs.

It should be noted, that limitation of GEPs plant modification is a rough estimation of heat conduction intensity through floor structure. That is because borehole outlet fluid temperature is applied as the ground surface temperature. Another known limitation is

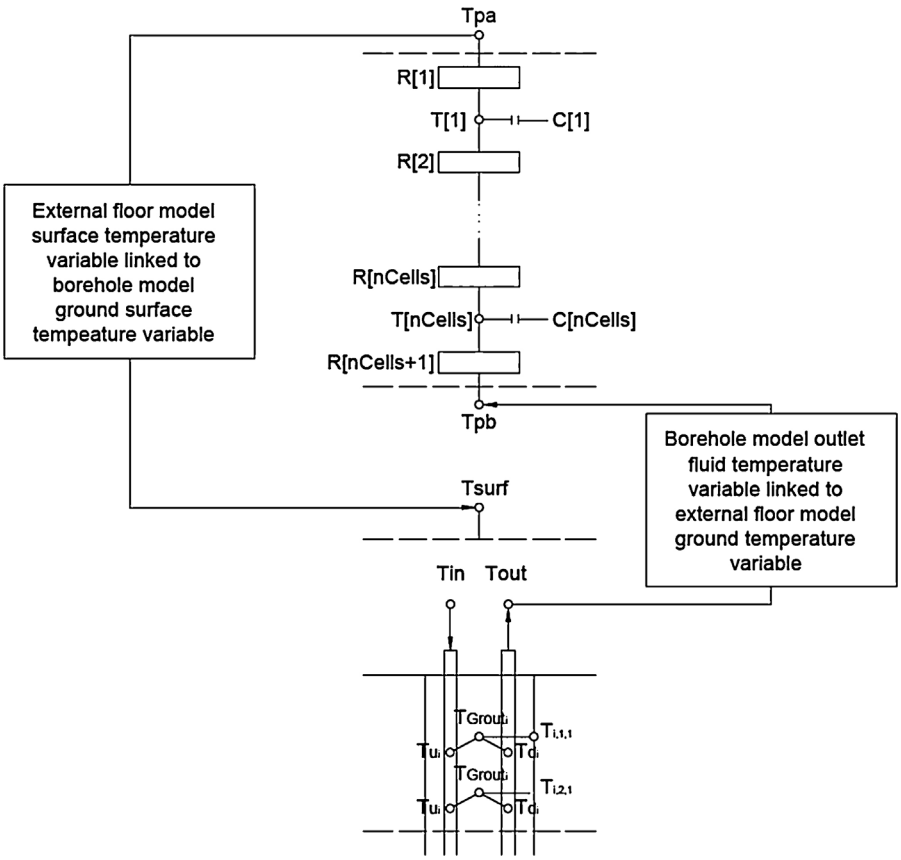

Fig. 6. Scheme of links between borehole and external floor model.

that floor surface temperature is constant over the whole domain of energy piles. In reality, the temperature at slab edges in contact with soil is different compared to the temperature in the centre of the floor. Therefore, when simulating a case where energy piles field is located close to the perimeter of building, the model will overestimate natural thermal storage effect caused by the heat conduction through floor structure. To minimize this effect, energy piles should not only be located close to the centre of the floor, but also their length should be relatively small compared to slab width. However, impact of this effect on GEPs plant performance is not studied in this paper.

Table 3 presents more detailed description of borehole model input parameters and values applied in this study.

There are two additional parameters in the borehole model, which values should be calculated by the user. One is the borehole thermal resistance. In this study, it was calculated with following equation [18]:

$$R_b = \frac{1}{2\pi k_g} \ln\left(\frac{d_b}{d_p\sqrt{n}}\right) \quad (12)$$

Another parameter is Prandtl number, which value can be calculated using following equation:

$$Pr = \frac{C_p \mu}{\kappa} \quad (13)$$

To assess the impact of borehole resistance on borehole energy performance, two cases with different borehole resistance were simulated and presented in Section 3.3.

2.4. Borehole model validation

Borehole model was validated based on the field measurement data obtained at energy pile test station in Hämeenlinna, Finland. The following measurements were taken at energy piles station and logged with 10-min interval:

- Borehole entering brine temperature;
- Borehole leaving brine temperature;
- Brine flow rate in borehole.

Additionally to abovementioned data, ambient air temperature was measured near the station and logged with an hour interval. As the measured borehole was not a part of the building foundation and ground surface was exposed to outdoor air, results of validation can only be referred to the modelled BHE field case. Validation results can be also related to the modelled GEPs case, when known model limitations described in Section 2.3 are considered. The measured borehole consisted of double U-pipe concrete-grouted into steel casing with an overall length of 20.6 m. Borehole model calculates the outlet temperature of brine based on the input of variable inlet flow and temperature. Model can also be linked with variable ambient air temperature to account for heat exchange between ground surface and surrounding air. In order to validate the borehole model, a simple validation environment (Fig. 7) was modelled, where measured data was used as an input for the variables described above. Validation procedure consisted of two phases – parameter identification phase and validation phase.

Overall measured data (Fig. 8) of 5000 h included both heat extraction (heating) and rejection (cooling) periods of borehole operation. It should be noted, that some of the data contained errors, as the measuring sensors were not able to register

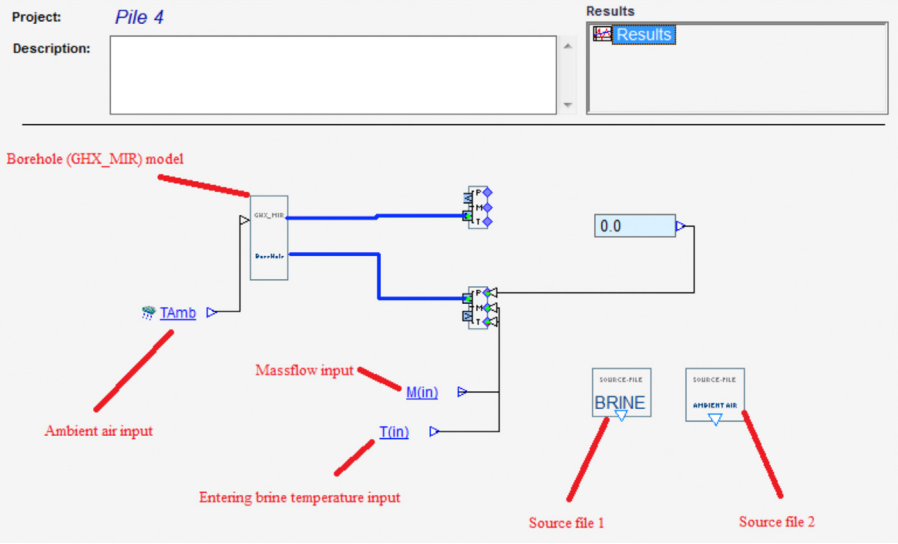

Fig. 7. Validation model.

temperatures below 0 °C. Therefore, error free periods were selected for the validation procedure. Parameter identification phase considered application of heat rejection measured data. During the validation phase heat extraction data was applied as an input.

Physical and thermal properties describing ground and borehole (Table 4) at measured site were defined as constants in the borehole model. Ground heat conductivity was determined in situ by thermal resistance test and overall borehole resistance was calculated according to Eq. (12). Groundwater levels at site appeared below the active length of measured borehole. There was only one unknown constant value to define in the borehole model – annual mean ground temperature. It was determined during the parameter identification phase. Based on the results of validation phase, extracted heat amount was calculated and compared to measured data in Section 3.1.

2.5. Plant description and operation principles

The modelled detailed plant (Fig. 9) heating equipment consists of the brine-to-brine heat pump coupled with GEPs or BHE field. The condenser side of the heat pump is connected to the stratification tank (hot). An additional electric boiler, the top-up heating, is connected to the same tank, to meet building peak heating loads. The heat pump is modelled to meet the performance maps of manufacturer specific product. Plant cooling equipment consists of the stratification tank (cold) connected to the ground heat exchange loop via heat exchanger to provide free cooling effect that operates only when needed. No additional cooling equipment such as chiller was considered. The operational principles of the plant were intended to fulfil several conditions. Secondary side supply water temperature, i.e. the heating curve (left upper corner of Fig. 9) was controlled according to outdoor air temperature.

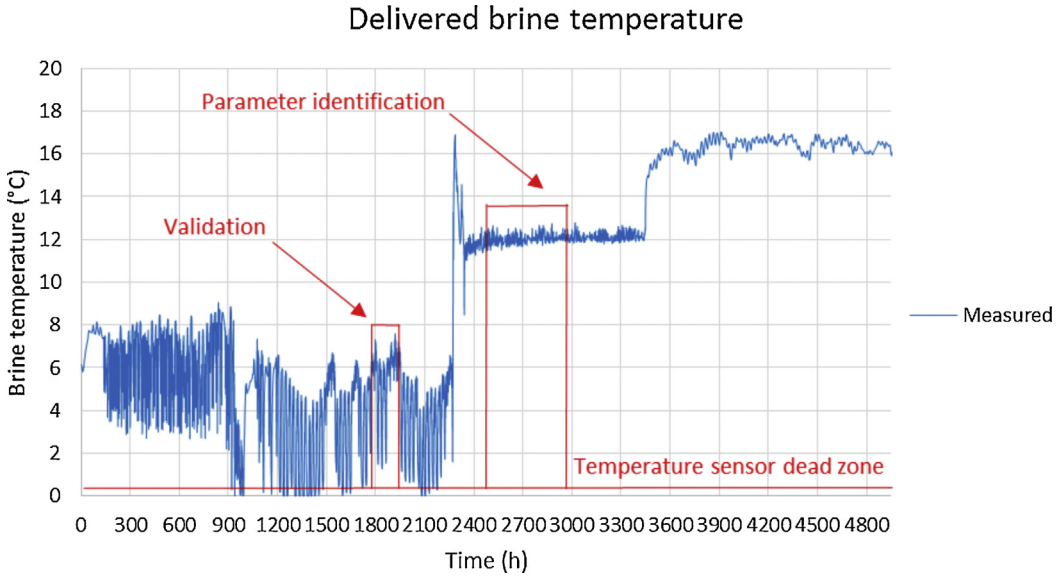

Fig. 8. Measured borehole data.

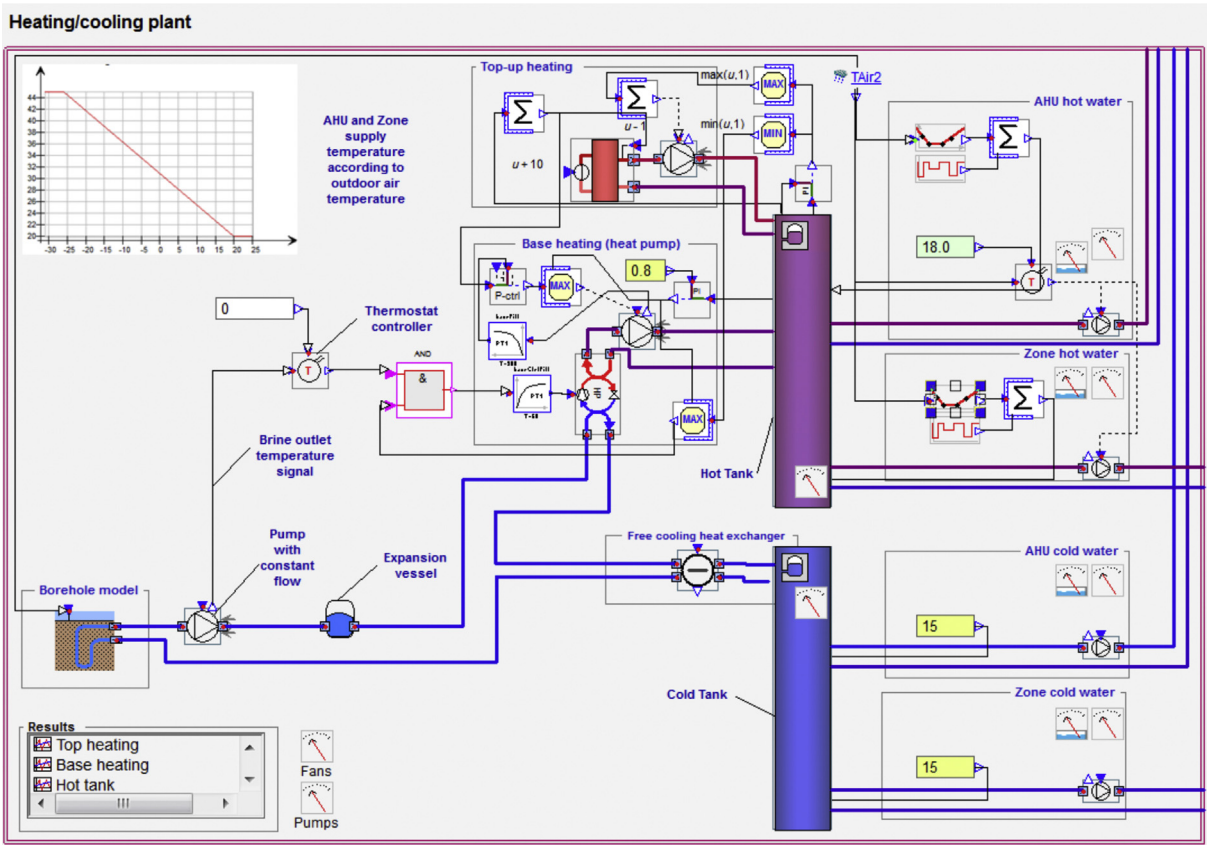

Fig. 9. Detailed heating/cooling plant modelled in IDA-ICE.

Table 4
Validation borehole model settings.

Descriptive parameter	Value
Borehole depth, m	20.6
Borehole diameter, mm	170
U-pipe outer diameter, mm	25
U-pipe inner diameter, mm	20.4
U-pipe amount, pcs	2
Ground heat conductivity, W/(m K)	1.8
Ground volumetric heat capacity, kJ/(K m^3)	1488
Borehole grouting heat conductivity, W/(m K)	1.8
Grout volumetric heat capacity, kJ/(K m^3)	2160
Pipe material heat conductivity, W/(m K)	0.3895
Pipe volumetric heat capacity, kJ/(K m^3)	1542
Brine ethanol concentration, %	28
Brine heat conductivity, W/(m K)	0.43
Brine volumetric heat capacity, kJ/(K m^3)	3533
Brine viscosity, Pa s	0.006
Borehole thermal resistance, (m K)/W	0.1
Ground average annual temperature, °C	8.5

In order to avoid ice formation in the underground layers, a thermostat model was applied to switch off the heat pump, when temperature of the brine supplied from the borehole drops below 0 °C. As the high capacity ground-source heat pumps usually lack compressor inverter, a logical on–off controller model was applied to allow heat pump on–off (no part load) operation.

The operation of the plant with described control logic is presented in Fig. 10. Heat pump starts to operate at full load whenever the temperature in the hot tank drops below the set point according to the heating curve. Whenever the temperature in hot tank reaches the desired set point or borehole outlet temperature drops below 0 °C, heat pump stops its operation.

Due to the thermostat dead band of 1 K, delivered brine temperature has dropped below the desired set point. In order to avoid numerical difficulties and errors, that prevent the simulation from running, a signal smoother of control signal was applied. Due to long integration time in signal smoother, the heat pump was still operating, when thermostat controller signal was “off”. As a result delivered brine temperature has dropped (Fig. 10) sometimes below the dead band of thermostat.

3. Results

3.1. Borehole model validation results

Parameter identification simulations were conducted with measured data obtained within 14.06.2012–11.07.2012 period. Measured rejected heat amount within that period was 120.6 kWh. After several adjustments, the model with mean annual ambient temperature parameter value of 8.5 °C produced 120.7 kWh result. Fig. 11 compares outlet brine temperature obtained during parameter identification simulation to measured data.

In parameter identification simulation, 650 h of measured data was applied and mass flow rate fluctuated within 0.09–0.14 kg/s range.

Data obtained in the parameter identification phase was used to run the validation period of 20.05.2012–28.05.2012. The calculated extracted ground heat amount for the measured data was 387.2 kWh. As a result of simulation, extracted ground heat amount in the borehole model was 387.1 kWh. Fig. 12 compares outlet brine temperature obtained during validation simulation to measured data. In validation phase simulation, 192 h of measured data was applied and mass flow rate fluctuated within 0.15–0.19 kg/s range.

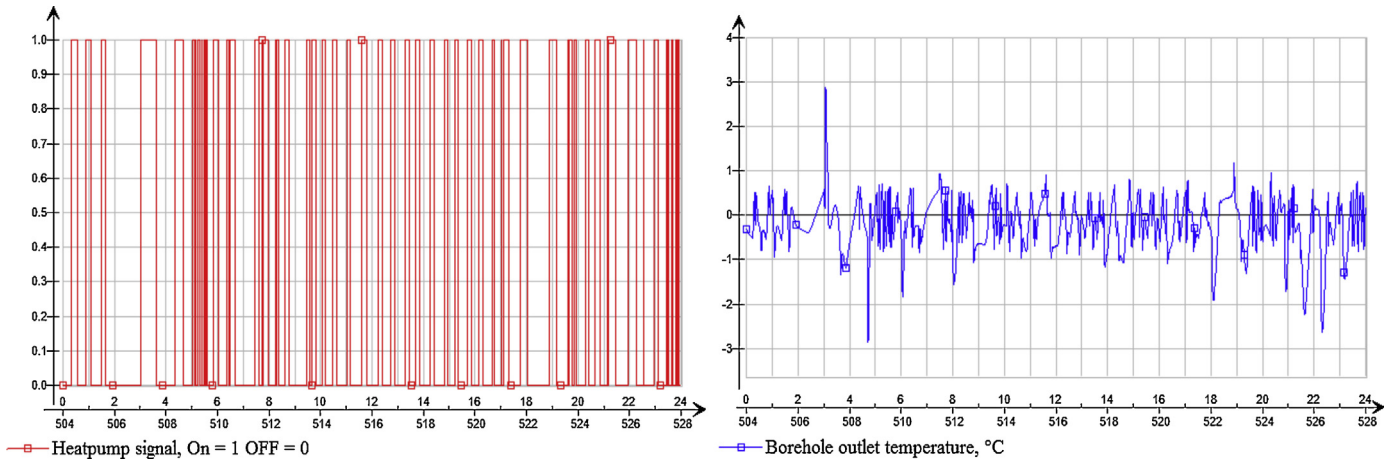

Fig. 10. Heat pump operation.

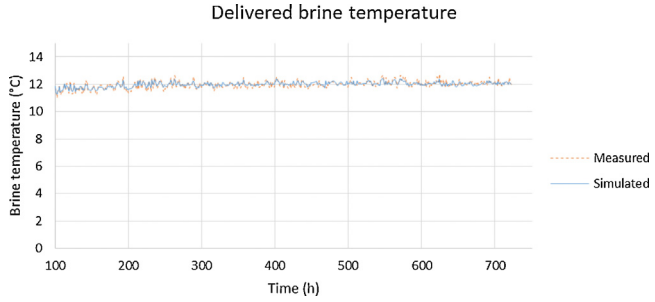

Fig. 11. Parameter identification phase results.

3.2. Heat pump model calibration parameters equations

Calibration parameter B value for manufacturer specific heat pump can be calculated using Eq. (3) at conditions, when condensing temperature T_{cond} value equals to condensing temperature at rating conditions T_{condim} value. Eq. (3) would take the following form:

$$Q_{evap_f} = \frac{e^{C*T_{conddim}+B*T_{evap}}}{e^{C*T_{conddim}+B*T_{evapdim}}} * P_{dim} * EER_{dim} \quad (14)$$

By further developing Eq. (14), calibration parameter B equation can be derived:

$$B = \frac{\ln\left(\frac{Q_{evap_f}}{P_{dim}*EER_{dim}}\right)}{T_{evap} - T_{evapdim}} \quad (15)$$

Calibration parameter E value for manufacturer specific heat pump can be calculated using Eq. (2) at conditions, when condensing temperature T_{cond} value equals to condensing temperature at rating conditions T_{condim} value. Then Eq. (2) would take the following form:

$$P_f = \frac{e^{F*T_{conddim}+E*T_{evap}}}{e^{F*T_{conddim}+E*T_{evapdim}}} * P_{dim} \quad (16)$$

By further developing Eq. (16), calibration parameter E equation can be derived:

$$E = \frac{\ln\left(\frac{P_f}{P_{dim}}\right)}{T_{evap} - T_{evapdim}} \quad (17)$$

Furthermore, an example of calibration parameter B and E values calculation is presented based on the heat pump performance map data from Fig. 3. Initial data for calibration parameter B and E values calculation is following:

- Evaporator rating conditions are $T_{evapin} = 0^\circ$ C, $T_{evapout} = -3^\circ$ C, $\Delta T \log evapdim = 3^\circ$ C;
- Condenser rating conditions are $T_{condin} = 30^\circ$ C, $T_{condout} = 35^\circ$ C, $\Delta Tlogconddim = 5^\circ$ C;
- Evaporation temperature at rating conditions $T_{evapdim} = -4.74593^\circ$ C (Eq. (6));
- Compressor power at rating conditions $P_{dim} = 9.12$ kW (Fig. 3);
- Energy efficiency ratio at rating conditions $EER_{dim} = 3.65$ (Fig. 3 and Eq. (4));
- Evaporation temperature at $T_{evapin} = 15^\circ$ C conditions $T_{evap} = 10.25^\circ$ C (Eq. (6));
- Evaporator power $T_{evapin} = 15^\circ$ C and $T_{condout} = 35^\circ$ C conditions $Q_{evap_f} = 53.84$ kW (Fig. 3);
- Compressor power at $T_{evapin} = 15^\circ$ C and $T_{condout} = 35^\circ$ C conditions $P_f = 10.16$ (Fig. 3).

Calibration parameter B value according to initial data above can be calculated with Eq. (15):

$$B = \frac{\ln\left(\frac{53.84}{9.124*3.65}\right)}{10.25 - (-4.74593)} = \frac{0.480405}{14.99593} = 0.032036 = 3.21\%$$

Calibration parameter E value according to initial data above can be calculated with Eq. (17):

$$E = \frac{\ln\left(\frac{10.16}{9.124}\right)}{10.25 - (-4.74593)} = \frac{0.107422}{14.99593} = 0.007172 = 0.72\%$$

Calibration parameter C value for manufacturer specific heat pump can be calculated using Eq. (3) at conditions, when evaporation temperature T_{evap} value equals to evaporation temperature

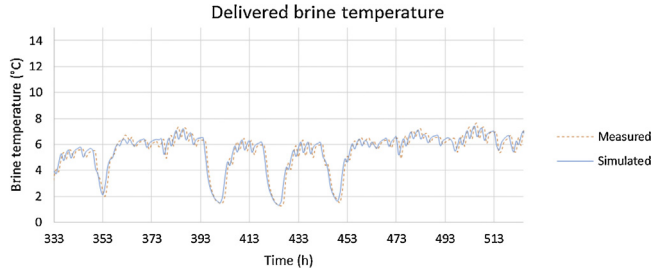

Fig. 12. Validation phase results.

at rating conditions $T_{evapdim}$ value. Then Eq. (3) would take the following form:

$$Q_{evap_f} = \frac{e^{C*T_{cond}+B*T_{evapdim}}}{e^{C*T_{conddim}+B*T_{evapdim}}} * P_{dim} * EER_{dim} \quad (18)$$

By further developing Eq. (18), calibration parameter C equation can be derived:

$$C = \frac{\ln\left(\frac{Q_{evap_f}}{P_{dim}*EER_{dim}}\right)}{T_{cond} - T_{conddim}} \quad (19)$$

Calibration parameter F value for manufacturer specific heat pump can be calculated using Eq. (2) at conditions, when evaporation temperature T_{evap} value equals to evaporation temperature at rating conditions $T_{evapdim}$ value. Then Eq. (2) would take the following form:

$$P_f = \frac{e^{F*T_{cond}+E*T_{evapdim}}}{e^{F*T_{conddim}+E*T_{evapdim}}} * P_{dim} \quad (20)$$

By further developing Eq. (20), calibration parameter F equation can be derived:

$$F = \frac{\ln\left(\frac{P_f}{P_{dim}}\right)}{T_{evap} - T_{evapdim}} \quad (21)$$

Furthermore, an example of calibration parameter C and F values calculation is presented based on the heat pump performance map data from Fig. 3. Initial data for calibration parameter C and F values calculation is following:

- Condenser rating conditions are $T_{condin} = 30^\circ$ C, $T_{condout} = 35^\circ$ C, $\Delta Tlogconddim = 5^\circ$ C;
- Evaporator rating conditions are $T_{evapin} = 0^\circ$ C, $T_{evapout} = -3^\circ$ C, $\Delta T\log evapdim = 3^\circ$ C;
- Condensing temperature at rating conditions $T_{conddim} = 37.90988^\circ$ C (Eq. (5));
- Compressor power at rating conditions $P_{dim} = 9.12$ kW (Fig. 3);
- Energy efficiency ratio at rating conditions $EER_{dim} = 3.65$ (Fig. 3 and Eq. (4));
- Condensing temperature at $T_{condout} = 60^\circ$ C conditions $T_{cond} = 62.9^\circ$ C (Eq. (5));
- Evaporator power $T_{evapin} = 0^\circ$ C and $T_{condout} = 60^\circ$ C conditions $Q_{evap_f} = 22.33$ kW (Fig. 3);
- Compressor power at $T_{evapin} = 0^\circ$ C and $T_{condout} = 60^\circ$ C conditions $P_f = 14.92$ (Fig. 3).

Calibration parameter C value according to initial data above can be calculated with Eq. (19):

$$C = \frac{\ln\left(\frac{22.33}{9.124*3.65}\right)}{62.9 - 37.90988} = \frac{-0.3997}{24.99} = -0.01599 = -1.6\%$$

Calibration parameter F value according to initial data above can be calculated with Eq. (21):

$$F = \frac{\ln\left(\frac{14.92}{9.124}\right)}{62.9 - 37.90988} = \frac{0.491794}{24.99} = 0.01968 = 1.97\%$$

By using derived calibration parameters and Eqs. (1)–(6), the performance map of the heat pump was recalculated to in order to demonstrate the IDA-ICE heat pump model accuracy. Calculated results are shown in Fig. 3 with markers for selected points.

3.3. Simulation results

Simulation results of modelled detailed heating/cooling plant with BHE field and GEPs in commercial hall-type building are presented in Table 5. Presented average annual results are obtained from simulations with duration period of 20 years.

Table 5
Simulation results of plant modifications with BHE field and GEPs.

	BHE field	GEPs
Evaporator absorbed heat, MWh/a	66.4	112.2
Compressor electricity, MWh/a	15.3	27.2
Condenser rejected heat, MWh/a	81.7	139.4
Top-up heating energy, MWh/a	106.4	64.6
Circulation pumps, MWh/a	8.2	8.2
Thermal storage heat through floor structure, MWh/a	0.0	32.2
Heat pump seasonal coefficient of performance	5.3	5.1
Heating system seasonal coefficient of performance	1.4	2.0
Heat pump operation duration, h	477	804
Borehole specific heat extraction rate, W/m	47.3	47.5
Borehole average annual yield at condenser, kWh/(m a)	28	47
Specific electricity use for building heating, kWh/(m^2 a)	14.2	11.0
Average annual ground temperature, °C	2.9	6.7

In case of plant modification with BHE field, absorbed evaporator heat i.e. extracted ground heat was ca 40% smaller than in GEPs case. Average annual ground temperature due to operation of plant resulted in 2.9 °C for BHE field case and 6.7 °C for GEPs case respectively. Annual heat demand (sum of top-up and condenser heat) in GEPs case resulted in 204 MWh/a versus BHE field case 188.1 MWh/a. Difference in heat demand is explained by the increased heat losses through the floor structure in GEPs case. Annual electricity demand for building heating purposes in GEPs case was 100 MWh/a and in BHE field case was 129.9 MWh/a. Therefore, plant modification with GEPs performed ca 23% more efficiently compared to similar plant with BHE field.

An overall heating system seasonal coefficient of performance (SCOP), that considers top-up heating and circulation pumps energy use, has ranged from 1.4 to 2.0 depending on the plant modification. Low overall system SCOP can be explained by a small number of installed boreholes, which operation is sufficient for the heat pump to cover only ca 44% and ca 68% of overall heat demand in BHE field and GEPs case respectively, while rest of the heat is supplied by top-up heating. Based on the simulation results, calculated specific heat extraction rate was ca 47 W/m, where heat pump in BHE field case operated for 477 h and in GEPs case for 804 h. Average annual energy yield at condenser side was 28 kWh/(m a) in BHE field case and 47 kWh/(m a) in GEPs case respectively.

Fig. 13 describes the long-term performance of plant modifications with GEPs and BHE field.

Long-term performance of BHE field was reducing over the years, where compared to first year of operation performance dropped by ca 30%. In plant modification with GEPs, plant performed more stable due to the heat conductance through floor structure i.e. natural thermal storage effect. In GEPs case, extracted

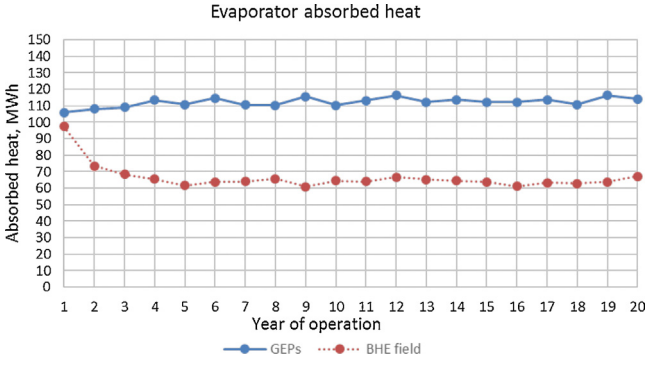

Fig. 13. Long-term simulation results.

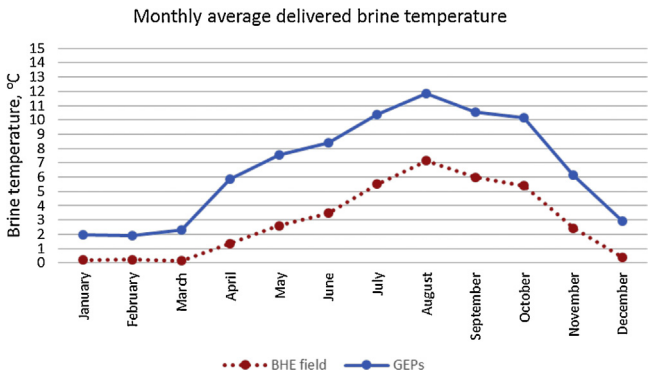

Fig. 14. Delivered brine temperature.

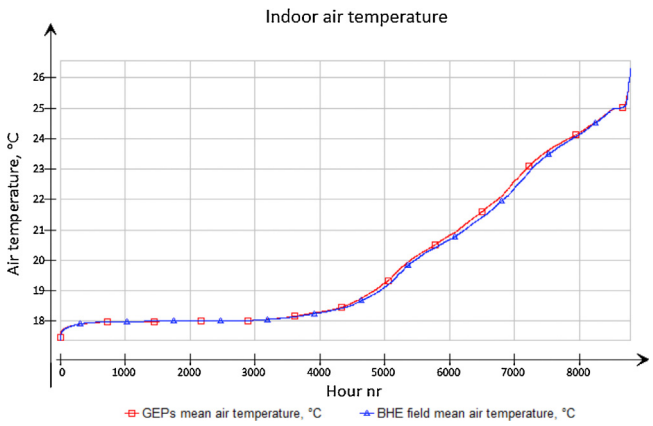

Fig. 15. Indoor air temperature cumulative graph.

ground heat at last year of operation was ca 7% higher compared to first year of operation.

Monthly average delivered brine temperatures are presented in Fig. 14. During the heat pump winter operation delivered brine temperature from BHE field stayed above 0 °C due to plant control logics. In GEPs case, delivered brine temperature within December–March period was ca 2–3 °C higher compared to BHE field case.

Delivered brine temperature peaked at +15 °C during the summer in BHE field case and +17 °C in GEPs case. Due to radiant cooling ceiling panels limited cooling capacity, indoor air temperature in both BHE field and GEPs case could not be maintained below the set point of +25 °C (Fig. 15) during very limited time. Most of the time indoor air temperature in both simulated cases stayed within the set point range. Indoor air temperature in GEPs case was almost identical to the result of BHE field case simulation.

Impact of borehole thermal resistance on extracted ground energy amount is described in Fig. 16, where results of two simulated cases are presented.

In first case, thermal resistance of boreholes was almost twice smaller (Rb = 0.1), though the reduction of absorbed annual ground heat amount in second case (Rb = 0.19) was negligible.

Visualized temperature field of GEPs operation in summer and winter is presented in Fig. 17. Minimum registered temperature in winter around energy piles was ca +7 °C, while borehole outlet temperature at that moment was ca 0 °C.

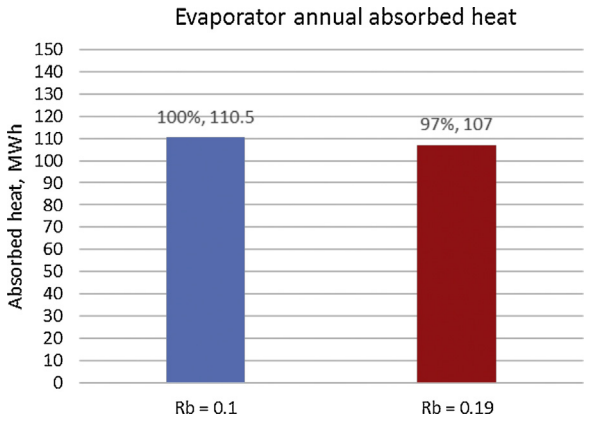

Fig. 16. Impact of borehole thermal resistance on evaporator absorbed heat.

In summer, when borehole outlet temperature was +26 °C, highest registered ground temperature at pile tip was ca +10 °C. Initial ground temperature in simulation was +8 °C and it should be noted, that temperature close to ground surface is higher than initial ground temperature. Temperature gradient close to ground surface is caused by the floor structure heat losses.

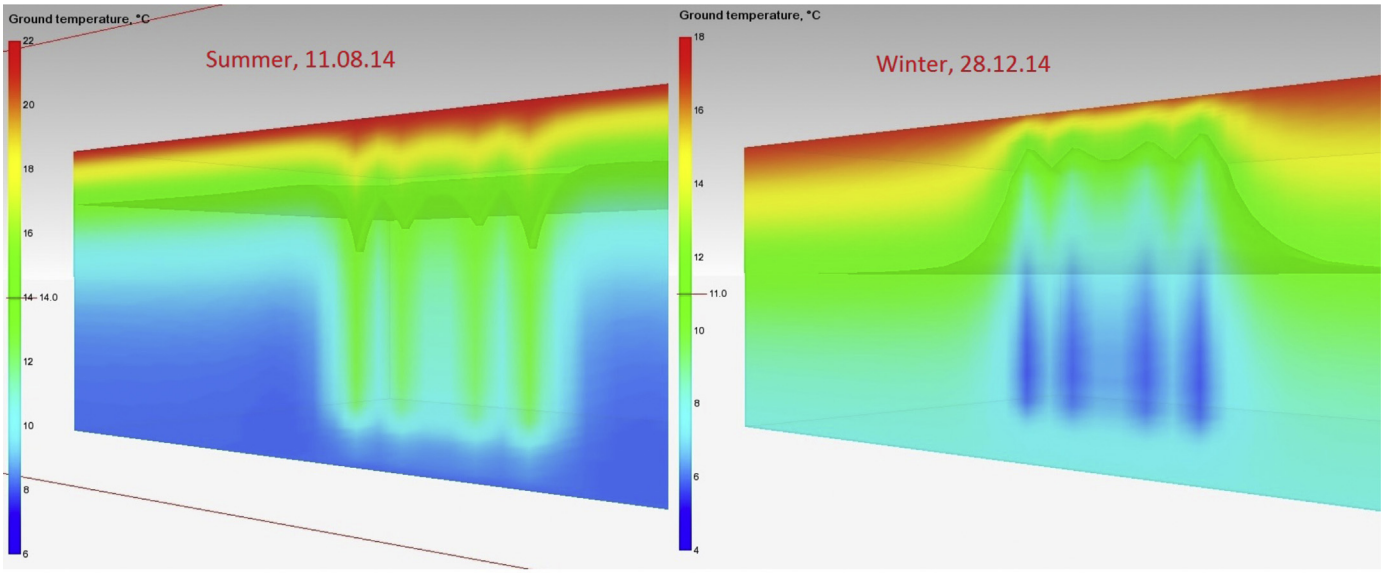

Fig. 17. GEPs case temperature field. Borehole outlet temperature in summer was 26 °C and in winter 0 °C.

4. Conclusions

A whole building simulation approach developed in a case of one storey hall building revealed to be suitable for detailed design of BHE field, GEPs with significant limitations listed in Section 2.3, heat pump and other plant components allowing to appropriate sizing and predict long term performance and dynamics with hourly resolution. It should be noted, that the performance of borehole model extension were validated only as BHE field, but not as GEPs. Therefore, this study will be continued with GEPs case validation and GEPs parametric study.

Results of three-dimensional borehole model validation as BHE field for IDA-ICE using actual measured data showed, that borehole model can perform very accurately as long as appropriate input data is available. While a borehole extension of IDA-ICE was suitable for detailed design purposes as it is, the heat pump model provided a bottleneck because of four calibration parameters needed. To solve this problem we derived straightforward equations for calibration parameters identification from product data allowing to setup heat pump model according to manufacturer specific performance map with minimal effort.

Results of conducted simulations revealed that geothermal energy piles and field of borehole heat exchangers can produce high heat pump SCOP results of up to 5.3 in a cold climate of Finland in studied commercial hall-type building, when a low temperature heating curve was considered in the design. Rather low SCOP of total heating system of 2.0 could be improved by increasing the amount of boreholes and heat pump capacity.

A significant difference in performance of BHE field and GEPs was shown, which was explained by the difference ground surface boundary conditions. Long-term simulation results showed a reduction in BHE field heat extraction performance over the years of operation because the amount of heat extracted from borehole field was much higher than loaded during cooling season. This reveals that there is a need for a thermal storage for instance with solar collector in commercial hall-type buildings with BHE field.

On the other hand, plant modification with GEPs performed more stable due to the appropriate amount of natural thermal storage produced by the heat losses through the floor structure. Though, the borehole extension of IDA-ICE has a limitation not allowing to assess the impact of heat losses at slab perimeter which may become important in the case of smaller buildings.

From the perspective of cooling, both plant modifications managed to meet building cooling demand via free cooling within most of the time of building operation without the need of additional cooling equipment. Despite the fact, that IDA-ICE allows the user to perform very detailed simulations almost with unlimited freedom to construct specific plant solutions, it may become also very complicated and will need specific training course for non-experienced users and designers to be capable for this type of simulations conducted in this paper.

Acknowledgments

The research was supported by the Estonian Research Council, with Institutional Research Funding grant IUT1-15, and with a grant of the European Union, through the European Social Fund, Mobilitas grant no MTT74.

References

[1] J.W. Lund, D.H. Freeston, T.L. Boyd, Direct utilization of geothermal energy 2010 worldwide review, Geothermics 40 (3) (2011) 159–180.
[2] M. Fossa, The temperature penalty approach to the design of borehole heat exchangers for heat pump applications, Energy Build. 43 (2011) 1473–1479.
[3] H. Brandl, Energy foundations and other thermo ground structures, Geotechnique 56 (2006) 81–122.
[4] EN 15450:2007, Heating Systems in Buildings – Design of Heat Pump Heating Systems, CEN, 2007.
[5] C.J. Wood, H. Liu, S.B. Riffat, Comparison of a modeled and field tested piled ground heat exchanger system for a residential building and the simulated effect of assisted ground heat recharge, Int. J. Low Carbon Technol. 5 (3) (2010) 137–143.
[6] J.D. Spitler, GLHEPRO: a design tool for commercial building ground loop heat exchangers, in: Proceedings of the Fourth International Heat Pumps in Cold Climates Conference, Aylmer, Quebec, August 17–18, 2000.
[7] C. Yavuzturk, J. Spitler, A short time step response factor model or vertical ground loop heat exchangers, ASHRAE Trans. 105 (2) (1999) 475–485.
[8] S. Javed, P. Fahlén, J. Claesson, Vertical ground heat exchangers: a review of heat flow models, in: Proceedings of the 11th international conference on thermal energy storage, Stockholm, June 14–17, 2009.
[9] P. Eskilson, Thermal Analysis of Heat Extraction Boreholes (Doctoral thesis), University of Lund, Lund, Sweden, 1987.
[10] S.L. Do, J.S. Haberl, A review of ground coupled heat pump models used in whole-building computer simulation programs, in: Proceedings of the 17th Symposium for Improving Building Systems in Hot and Humid Climates, Austin, TX, August 24–25, 2010.
[11] D. Pahud, A. Fromentin, J.-C. Hadorn, The Duct Ground Heat Storage Model (DST) for TRNSYS used for the Simulation of Heat Exchanger Piles, User Manual, 1996, Lausanne.
[12] Y. Michel, E. Bertramb, R. Dottc, T. Afjeic, F. Ochsd, J.-C. Hadorne, Review of component models for the simulation of combined solar and heat pump heating systems, Energy Procedia 30 (2012) 611–622.
[13] H. Jin, J.D. Spitler, A parameter estimation based model of water-to-water heat pumps for use in energy calculation programs, ASHRAE Trans. 108 (2002) 3–17.
[14] X. Wang, M. Zheng, W. Zhang, S. Zhang, T. Yang, Experimental study of a solar-assisted ground-coupled heat pump system with solar seasonal thermal storage in severe cold areas, Energy Build. 42 (2010) 2104–2110.
[15] T. Kalamees, K. Jylhä, H. Tietäväinen, J. Jokisalo, S. Ilomets, R. Hyvönen, S. Saku, Development of weighting factors for climate variables for selecting the energy reference year according to the EN ISO 15927-4 standard, Energy Build. 47 (2012) 53–60.
[16] M. Brandemeuhl, HVAC 2 Toolkit: Algorithms and Subroutines for Secondary HVAC Systems Energy Calculations, Handbook, ASHRAE, 1993.
[17] J.J. Giardina, Evaluation of Ground Coupled Heat Pumps for the State of Wisconsin (Thesis), University of Wisconsin, USA, 1995.
[18] J.A. Shonder, J.V. Beck, Determining effective soil formation thermal properties from field data using a parameter estimation technique, ASHRAE Trans. 105 (1) (1999) 458–466.
[19] Description of the IDA ICE Borehole Model. Internal Report, Equa, 2013.
[20] M. Wetter, A. Huber, TRNSYS Type 451 – Vertical Borehole Heat Exchanger – EWS Model – Model description and implementing into TRNSYS, Huber Energietechnik AG, Zürich/Luzern, Switzerland, 1997.

Publication 3

Ferrantelli A, Fadejev J, Kurnitski J. Energy Pile Field Simulation in Large Buildings: Validation of Surface Boundary Assumptions. *Energies*, Vol. 12 Iss. 5 Art.No. 770 pp. 1-20. 2019.

energies

MDPI

Article

Energy Pile Field Simulation in Large Buildings: Validation of Surface Boundary Assumptions

Andrea Ferrantelli [1,*], Jevgeni Fadejev [1,2] and Jarek Kurnitski [1,2]

[1] Department of Civil Engineering and Architecture, Tallinn University of Technology, Ehitajate tee 5, 19086 Tallinn, Estonia; jevgeni.fadejev@taltech.ee (J.F.); jarek.kurnitski@taltech.ee (J.K.)
[2] Department of Civil Engineering, Aalto University, P.O. Box 12100, 00076 Aalto, Finland
* Correspondence: andrea.ferrantelli@taltech.ee

Received: 21 January 2019; Accepted: 20 February 2019; Published: 26 February 2019

Abstract: As the energy efficiency demands for future buildings become increasingly stringent, preliminary assessments of energy consumption are mandatory. These are possible only through numerical simulations, whose reliability crucially depends on boundary conditions. We therefore investigate their role in numerical estimates for the usage of geothermal energy, performing annual simulations of transient heat transfer for a building employing a geothermal heat pump plant and energy piles. Starting from actual measurements, we solve the heat equations in 2D and 3D using COMSOL Multiphysics and IDA-ICE, discovering a negligible impact of the multiregional ground surface boundary conditions. Moreover, we verify that the thermal mass of the soil medium induces a small vertical temperature gradient on the piles surface. We also find a roughly constant temperature on each horizontal cross-section, with nearly identical average values when either integrated over the full plane or evaluated at one single point. Calculating the yearly heating need for an entire building, we then show that the chosen upper boundary condition affects the energy balance dramatically. Using directly the pipes' outlet temperature induces a 54% overestimation of the heat flux, while the exact ground surface temperature above the piles reduces the error to 0.03%.

Keywords: energy piles; validation; floor slab heat loss; energy; computer simulations

1. Introduction

According to the European Parliament directive 2010/31/EU [1], each and every new construction should be nearly zero-energy buildings (nZEB) by the end of 2020. Such a requirement clearly demands an extensive use of renewable sources.

A recent review [2] on the utilization of geothermal energy [3,4] revealed that, by 2015, 49 countries invested over 20 billion USD in geothermal plants, which resulted in energy savings of ca 52.5 million tonnes of equivalent oil. This prevented respectively 46 and 148 million tonnes of carbon and CO_2 from being released into the atmosphere every year. Furthermore, the installed ground-source heat pump capacity grew 1.51 times from 2010 to 2015.

Ground-source heat pumps utilize ground heat exchangers (GHE) [5–7] to exploit geothermal energy. In buildings with pile foundations, installation of heat exchange piping into such piles enables them to perform as a GHE; the resulting systems are known as geothermal energy piles [8,9]. Their immediate advantage is that installation of heat exchange piping into a foundation pile is much cheaper than drilling a new borehole, therefore energy piles tend to be a very cost effective GHE solution.

Heat exchange processes occurring in boreholes are object of continuous studies from many different sides; a more refined design can reduce installation costs and improve heat transfer and heat pump efficiency (see for instance the reviews [10,11] and references quoted therein). Specifically,

the physical processes involved can be addressed at various levels: from heat transfer into the soil to heat transport within the heat exchanger and the absorber pipes, investigating the role of design geometry, quantifying thermal interactions in multiple borehole fields etc. [11–13]. Classical analytical models include line-source [14] and cylindrical-source [15] solutions, which tend however to make too strong approximations, such as infinitely extended line sources and a constant heat flux inside an infinite and homogeneous medium. These could be extended in several ways though [13,16,17], from analytical *g-functions* [18] to superposition of thermal response functions (the so-called Hellström approach) [19,20]. Unfortunately, unavoidable approximations (such as constant wall temperatures) still limit the predictive power of these models [11,13].

Numerical computations can instead relax many assumptions that are generally needed to solve analytical models [21,22]. The geometry in particular can be more complex, accounting for finite lengths, thermal interaction of the heat exchangers, multilayer soil [23] and inclusion of the ground water flow [24,25]. A large number of different software types is being used in these investigations. Finite difference methods (FDM) used by TRNSYS [18,26] and IDA-ICE [27–30] are widely adopted, due to their ability to account for variable ground surface temperatures [31,32]. In some recent approaches, these can even be combined with probabilistic analysis [33].

The Finite Element Method (FEM) [34–36] is extensively used as well, for instance with ABAQUS [37–39] or COMSOL Multiphysics [40–43]. Several sensitivity studies assess design issues such as the role of heat exchanger configurations with a given energy pile, or the spacing and configuration of an energy pile group [44] and its vertical displacement [45]. FEM modelling is also used for developing analytical GHE heat transfer models [12,46], and Computational Fluid Dynamics (CFD) allows e.g., comparison of different types of ground heat exchangers [47]. Finally, thermomechanical effects that are induced on the heat exchanger constitute an emergent and promising field of investigation [48,49]. Experimental research is very active as well, on each and every level, providing empirical support and validation to both analytical and numerical models [11,50].

Despite a number of encouraging results, even in the numerical modelling of GHE a number of issues still need to be addressed [11,13,51]. In this paper we are mostly concerned with the assessment of variable ground surface temperatures. In the case of energy piles, this is generally described as the surface temperature of the building floor slab, which is assumed to coincide with the indoor air temperature. The soil region surrounding the building floor slab is exposed to outdoor air temperature, which unfortunately cannot be modelled in TRNSYS nor IDA-ICE due to lack of implementation [13,28]. Hypothetically, heat transfer in the soil region surrounding the building should affect the soil temperature development underneath, altering the heat transfer between the energy piles and, ultimately, their thermal yield. However, according to the present literature, the transient soil temperature profile still needs to be quantified.

Clearly, since the floor heat loss and temperature profile right under the concrete slab (or floor) are crucial for the correct implementation of energy pile analyses, one should pay particular attention to the upper boundary condition. One first objective of this study was indeed to quantify how the soil temperature and the energy piles thermal yield are affected by heat transfer processes in the soil region surrounding the building. This was accomplished numerically with COMSOL Multiphysics [34], which as remarked above, uses a finite element method (FEM).

We believe that reducing the gap between simulations and reality is essential: as it was proven in [52], energy consumption estimates from building simulations can differ by 30% when compared to measured values. Accordingly, to provide a phenomenological foundation for our analysis, we validate this specific FEM numerical model against measured data. These were taken from an undisturbed reference energy pile of an office building called Innova 2, located in Jyväskylä, Finland. Such validation is then used in simulations of heat transfer for a multi-pile system under a building, to investigate how the heat transfer processes depend on different temperature boundary conditions (b.c.) at the surface (multiregional or floor slab). We find that assuming a simple floor slab gives virtually no different

result than a more complex multiregional b.c. proposed in [13], which can be safely disregarded in practical studies.

Another known bottleneck of energy piles modelling in IDA-ICE, prior to the November 2017 release, is the lack of calculated ground surface temperature as disturbed by the operation of an energy piles plant [28]. Such temperature constitutes the boundary condition in the floor slab model of a zone located directly above the energy piles. Since operation of the heat pump in heating mode cools the soil, heat losses in the floor slab increase the building heating need. To account for this phenomenon, a rough estimate of the disturbed ground surface temperature was applied in [28] (in this paper we will refer to this earlier method as "IDA-ICE outlet"). However, up to now the accuracy of such rough estimation was still unknown.

In this work we attempt to fill this gap by means of analogous calculations performed with a new version of IDA-ICE and with COMSOL. We define a borehole model for 20 energy piles, and compare the effect of two distinct upper boundary conditions: (i) energy piles outlet temperature—"IDA-ICE outlet", and (ii) ground surface temperature—"IDA-ICE slab". We find that the heat flux through the floor and the yearly energy demand computed according to (i) are overestimated by 54% and 5% respectively, in comparison with (ii), which is adopted both in COMSOL and in the updated version of IDA-ICE. Furthermore, when using the ground surface temperature as in case (ii), differences in the thermal yield between the two software are found to be quantitatively negligible.

The present paper is organized as follows: In Section 2 we define a 3D COMSOL model for a single energy pile, and validate it against measured data. In Section 3 a 2D reduction of the previous model performs ground surface boundary analysis for multiple energy piles. In Section 4 we validate an IDA-ICE energy piles model against a 3D COMSOL computation extended to multiple piles, and finally in Section 5 we compare the effect of different boundary conditions on a calculation of yearly energy demand. Our findings are then exposed in the Section 6.

2. Validation of a COMSOL Model for a Single Pile against Measured Data

In this section we discuss the validation of an FEM-based numerical simulation, performed with the software COMSOL Multiphysics. This preliminary was necessary as we use the same setup in the energy pile heat transfer analysis discussed in the rest of the paper, Sections 3–5.

2.1. Method

The first building with pile foundation used as GHE in Finland is an office building called Innova 2, built in summer 2012 in Jyväskylä. The geothermal heat pump plant is equipped with energy meters and two piles of foundation, with temperature sensors placed along the depth, Figures 1 and 2 (see [9] for a thorough description of the piles' construction, in combination with heat exchangers and heat pumps).

Additionally, a reference energy pile located near the building measures the undisturbed soil temperature with 11 sensors installed along its depth as well, as in Table 1. In our COMSOL simulation, we modelled precisely this isolated energy pile, together with its surrounding soil layers. The temperatures calculated in the model were logged from the location of each sensor of the reference pile. Depth, density ρ and thermal conductivity λ of each layer were measured on site [53].

As illustrated in Figure 3, the reference pile was modelled per measurements as a 22 m-long concrete cylinder, with λ = 1.8 W/mK, ρ = 2400 kg/m^3 and c_p = 900 kJ/kgK, and diameter 170 mm. It was embedded in a 10 m $\times$ 10 m, 26.7 m deep multilayer block with material properties listed in Table 2.

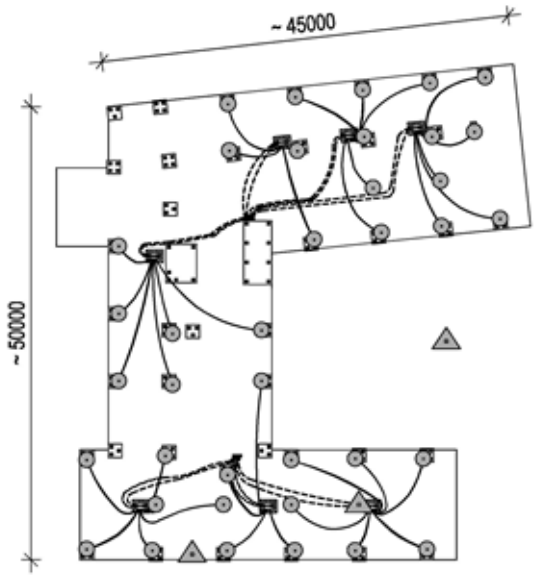

Figure 1. Energy piles (circles) and monitoring layout (undisturbed T monitored at the isolated triangle) [53].

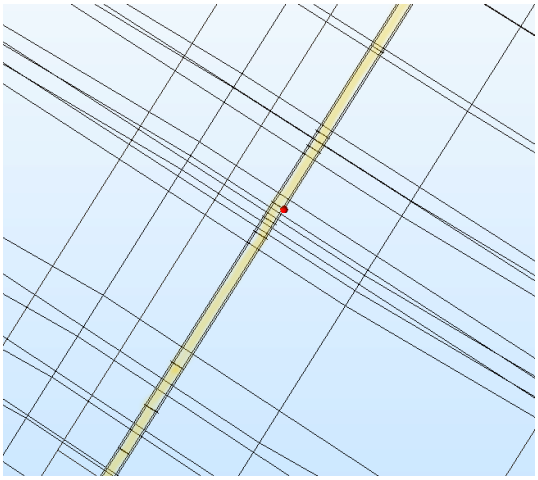

Figure 2. Sketch of sensor placement in soil, on the surface of each pile.

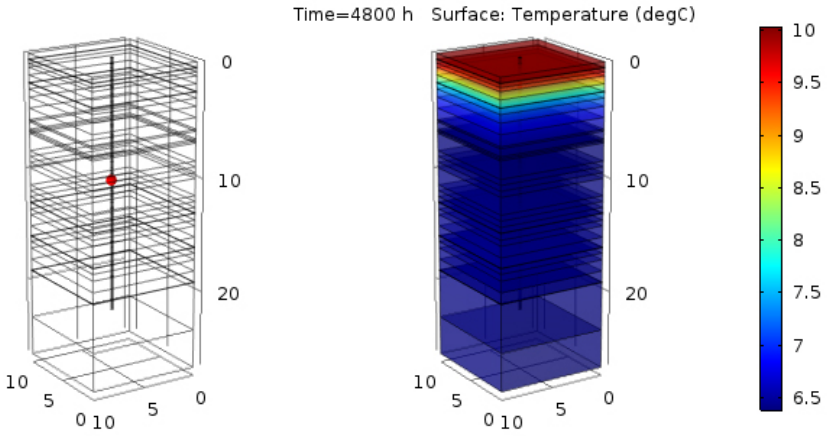

Figure 3. COMSOL simulation for the Innova office building reference pile. (**Left**) the pile geometry (sensor T31 in red). (**Right**) the result after t = 4800 h.

Table 1. Temperature sensors location for the reference energy pile [53].

Temperature Sensor	Depth, m
Ground surface	0
Pile top	−0.5
T28	−0.5
T29	−2.5
T30	−4.5
T31	−6.5
T32	−8.5
T33	−10.5
T34	−12.5
T35	−14.5
T36	−16.5

Table 2. Soil layer properties for the single pile simulation [53].

Layer nr	Depth, m	ρ, t/m^3	c_p, kJ/kgK	λ, W/mK
1	3.73	1.4	1.8	0.87
2	5.67	1.72	1.82	1.24
3	5.84	1.66	1.78	1.08
4	6.5	1.80	1.71	1.25
5	6.67	1.83	1.72	1.39
6	6.84	1.91	1.57	1.42
7	12.9	2.03	1.40	1.89
8	12.91	2.01	1.39	1.81
9	15.90	2.06	2.32	1.92
10	15.91	2.05	2.33	1.91
11	19	1.99	2.39	1.53
12	19.01	1.95	2.41	1.5
13	23.3	2.28	2.10	2.52
14	26.7	2.21	2.16	2.44

The specific heat c_p was obtained instead by combining dry specific heat values from [54,55] with the measured humidity content of each soil layer, again obtained from [53], assuming a value 4.2 kJ/kgK for the water specific heat (we will comment on the effect of this uncertainty on the results in the next section).

The version of COMSOL used was 5.3a, with the module Heat Transfer in Solids: the FEM method solves the time-dependent heat conduction equation in three dimensions with no heat source, namely

$$\rho C_p \frac{\partial T}{\partial t} - \nabla \cdot k \nabla T = 0, \tag{1}$$

where $\mathbf{q} = -k\nabla T$ is the heat flux through each layer of the medium. According to the large simulation scale, the mesh was defined as follows (a few tests performed with finer meshes showed a negligible impact of the resolution on the temperature profiles): maximum and minimum element sizes respectively 2.67 m and 0.481 m, maximum element grow rate 1.5, curvature factor 0.6 and resolution of narrow regions 0.5.

The actual pile temperatures were measured with sensors placed in soil on the edge of the structure, Figure 2, at depths listed in Table 1. The temperatures of each soil layer at $t = 0$ were defined as initial conditions in COMSOL according to the measured data. The upper boundary condition, namely the temperature at the ground level, consisted of measured data of a sensor located on top of the pile for the period 7 March 2014–2 October 2014 (i.e., for 4800 h). The transient study was performed with a constant time step Δt = 1 h.

Even though the above setup is rather simple and the physical phenomenon investigated is straightforward, involving a relatively small amount of degrees of freedom, reproducing the

measurements accurately was not trivial. This is due to the inherent inhomogeneity of the soil layers, whose composition and thermophysical properties might well be approximated by Table 2 *globally*, but on a smaller scale this lack of accuracy becomes relevant.

For instance, the computed specific heat for Layer 1 was 2.5 kJ/kgK, however this value returned erroneous initial temperatures for the layer's sensors T28 and T29 (see Table 1). In the simulation we therefore fine-tuned the specific heat to 1.8 kJ/kgK, which gives correct initial T for T28 (0.5 m curves in Figure 4). This c_p value is also consistent with Layer 2 right below, as one would more naturally expect. We will comment more on this in the Results, Section 2.2.

The initial temperature of each pile section was the same of the surrounding soil layer, while the measured surface T was interpolated as in Figure 4 and used as boundary condition. The main difficulty in validating the simulation consisted of matching the initial conditions also for the other sensors, not only for T28. This occurs since several layers (for which the software demands uniform initial conditions) contain sensors with different initial temperatures.

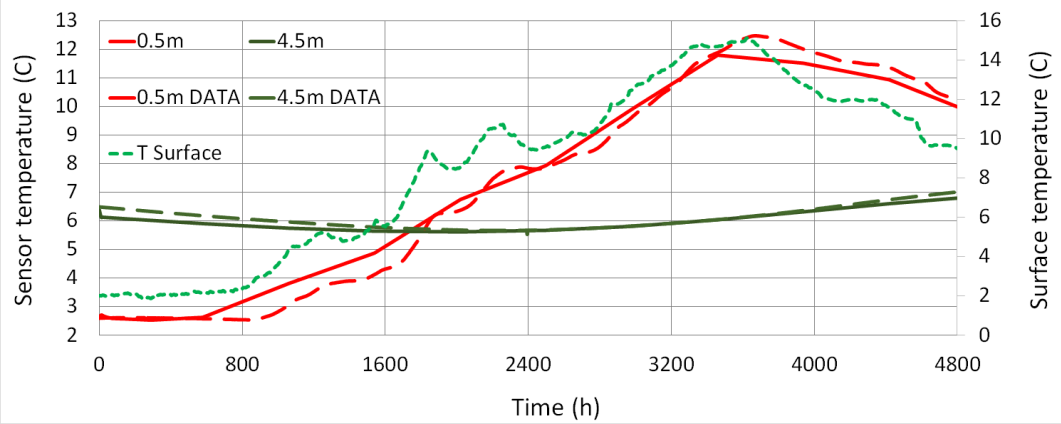

Figure 4. Measured (dashed) vs. COMSOL simulated (solid) temperatures for a single pile, sensors at 0.5 m and 4.5 m. Surface temperature in small dashes.

To increase accuracy, we accordingly refined the soil stratification around the pile. As illustrated in Figure 3, the original 14 layers were split when necessary into a total of 36 layers, to allow for a finer initial temperature profile. This means that 36 different initial temperatures were set in the model, still keeping the thermophysical properties in Table 2 unaltered. Avoiding sharp differences at the interface of contiguous layers, we were indeed aiming to a more physical initial temperature profile in the soil.

2.2. Results

The plot presented in Figure 4 compares the temperature profile for the sensors at 0.5 m, 2.5 m and 4.5 m as computed by COMSOL with the data measurements. We find a very good agreement for all sensors. In Figure 5 the temperature profiles at 4.5 m (with error well below 5% for almost all time steps), at 10.5 m and at 16.5 m show a remarkable agreement, considering that the specific heat was unknown and had to be computed. The difference data-simulation is very minimal, never larger than 0.2 °C∼3%, and is clearly a reflection of the uncertainty in the thermal mass.

These results thus seem to be convincing; more accurate soil properties around the sensors would provide with an even more precise validation. In any case, we can conclude that our COMSOL setup is reliable enough for our purpose, and constitutes a solid foundation for the set of simulations described in the next sections.

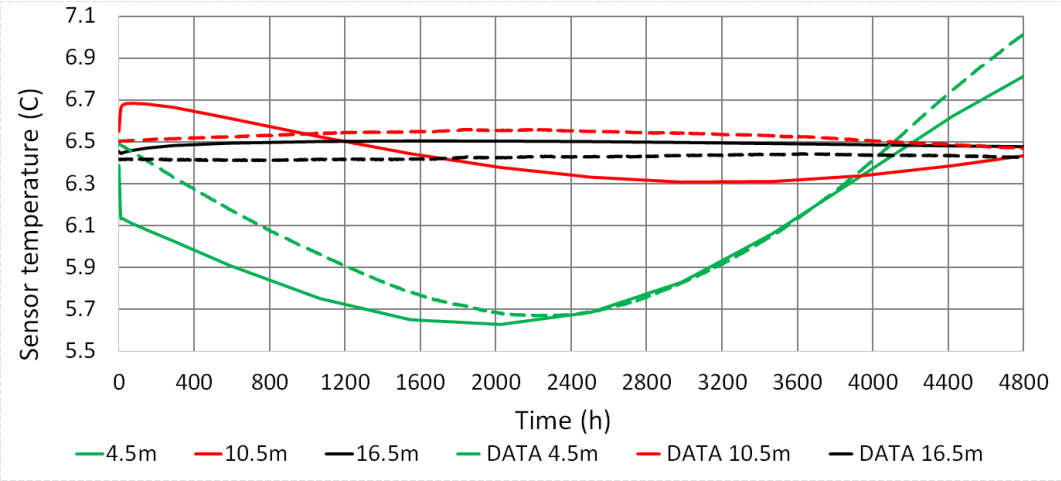

Figure 5. Data (dashed) vs. COMSOL T (solid) for sensors at 4.5 m, 10.5 m and 16.5 m depth.

3. Ground Surface Boundary Analysis in COMSOL

After validating the simulation setup, we are now going to use an analogous COMSOL model to study a 2D heat transfer analysis in energy piles with two different boundary conditions at the surface: case (a) single uniform indoor floor, and case (b) outdoor soil/indoor floor slab. The goal of this second case study was assessing the importance of the multiregional boundary condition proposed in [13].

3.1. Method

The calculation at hand consists of a 2D dimensional reduction of the 3D model addressed in Section 2, extended to a multiple piles layout. The 2D COMSOL model in Figures 6 and 7 studies the heat transfer processes occurring between five 15 m-long energy piles, placed under the building, and the surrounding homogeneous soil.

We modelled a 20 m-large floor slab, consisting of two layers: a lower 20 cm-thick EPS layer with k = 0.034 W/mK, ρ = 20 kg/m^3 and c_p = 750 kJ/kgK, and an upper 10 cm-thick concrete slab with k = 1.8 W/mK, ρ = 2400 kg/m^3 and c_p = 880 kJ/kgK. Each pile was implemented as a 15 m-long concrete grout with diameter 115 mm, surrounding a U-pipe of external diameter 25 mm (their modelling is discussed more into detail in the next Section 3.1). The piles spacing was 4.5 m and they were buried into a soil medium with k = 1.1 W/mK, ρ = 1800 kg/m^3 and c_p = 1800 kJ/kgK.

The two cases investigated correspond to two different upper boundary conditions: (a) floor only, set at 20 °C, namely the average annual indoor air temperature of a commercial hall-type building; (b) floor + soil, where the soil extends for 5 m further from each floor edge (see Figure 8). The soil surface was set at T = 5.67 °C, which corresponds to the average annual outdoor air temperature in Southern Finland.

The initial T values were the following: soil layer and grout 5.67 °C, U-pipes 0 °C, upper concrete floor layer 20 °C. The U-pipes were always kept at constant T = 0 °C (corresponds to constant heat pump operation), the floor at 20 °C for both (a) and (b) and the soil surface for case (b) at 5.67 °C. A 2D heat conduction module was used, defined by an equation analogous to (1) that naturally takes into account the mutual thermal interaction of adjacent piles. The mesh was normally sized, tetrahedral and physics-controlled, finer at the soil/pile interface and coarser near the boundaries (Figures 6 and 7), with minimum element size 9 mm and maximum 2 m. The simulation was carried out for 2400 h, with time interval Δt = 1 h.

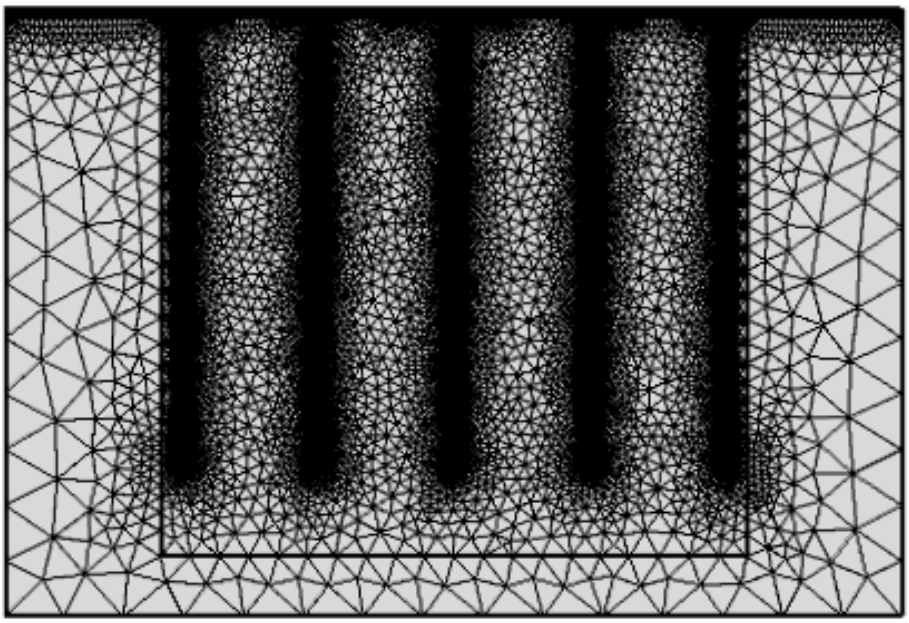

Figure 6. COMSOL mesh for case (a), only floor.

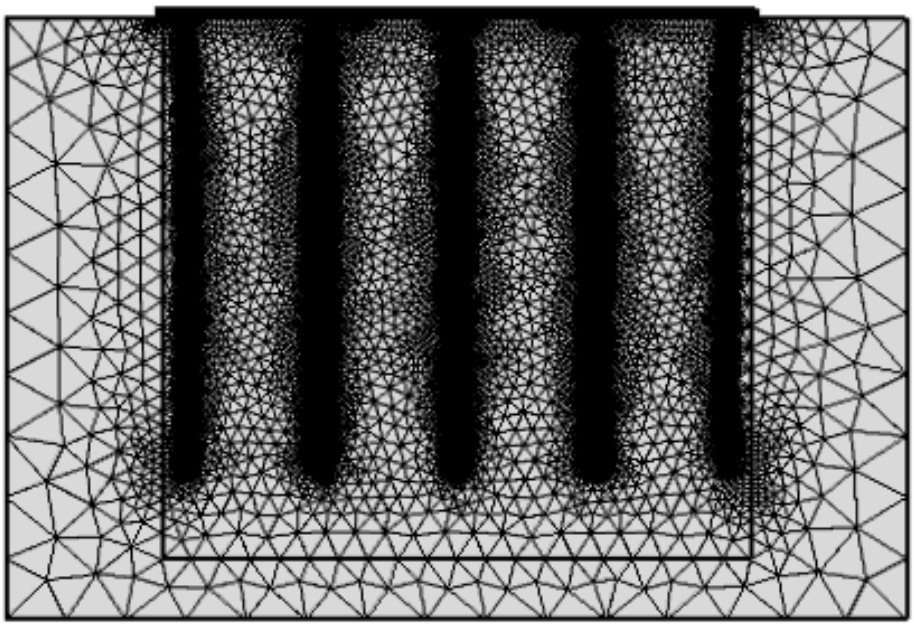

Figure 7. COMSOL mesh for case (b), floor and soil.

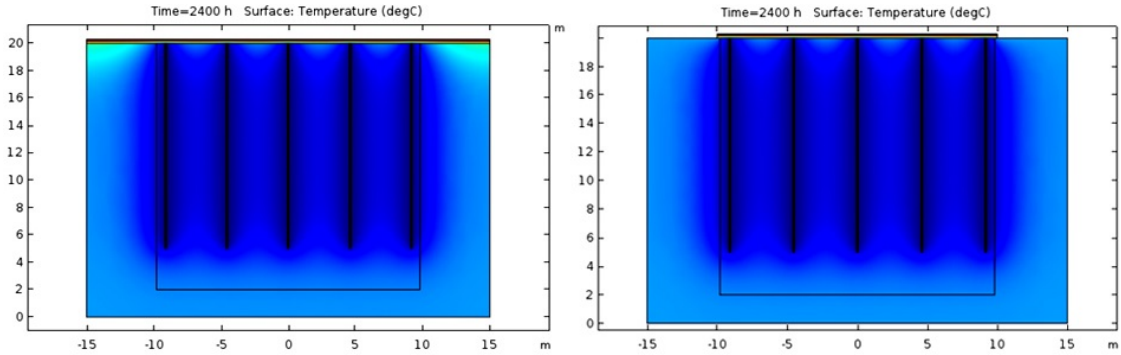

Figure 8. 2D COMSOL result after 2400 hrs for (**left**) (a) only floor and (**right**) (b) floor + soil as upper boundary.

Brine Flow Modelling

In standard constructions, the U-pipes inside the energy piles are usually made of high-density polyethylene (HDPE), with a brine fluid (mostly a water/ethanol mixture) flowing inside [53].

Since the simulations here performed are characterized by large geometry and time scales (Δt = 1 h and t_{tot} = 2400 h), it is legitimate to be concerned with the computational problems related to the inclusion of a fluid dynamics module. For the same reasons though, simulating the fluid flow in the pipes should not be necessary, since high-resolution microphysical processes (inducing fluctuations, turbulences and local irregularities in the brine flow and temperature) should not be relevant.

This reasoning seems to find support in the literature: several examples (see e.g., [56,57]) can be found illustrating how models of transient fluid transport inside the tubes would be justified only for much smaller time scales. In particular, Ref. [56] shows that a steady-state, a transient and a semi transient model converge already after ∼3 h.

There are different ways to simplify the implementation of fluid flow, in order to reduce the computational time; for example, in [25,43] the convective heat transfer associated with the fluid flow was simulated by an equivalent solid with the same thermophysical properties of the actual circulation fluid. In order to quantify the error induced by neglecting the fluid flow, we therefore considered the system in Figure 6 only with heat conduction, and modelled the U pipes as made of concrete at constant temperature 0 °C. The surrounding grout was at 5.67 °C at $t = 0$, and then subject to heat transfer for 2400 h. On the other hand, we created another simulation based on the exact same setup, but this time with U-pipes made of water that was flowing at 0 °C, with inlet velocity $V_{in} = 0.45$ m/s and ignoring the pipe thickness.

The result is plotted in Figure 9, where we compare the average temperature in the soil area surrounding the piles, which is active for heat extraction and is highlighted in Figure 8. One can see that the difference is negligible, confirming our assumption at the beginning of this section that we can safely ignore the fluid flow. We accordingly model the U-pipes as made of concrete with constant T, both in the 2D computations and in the full 3D simulations performed in Sections 4 and 5. Let us remark however that the above discussion pertains only COMSOL; IDA-ICE, on the other hand, considers the fluid turbulence already by default when computing the convection heat transfer coefficient h.

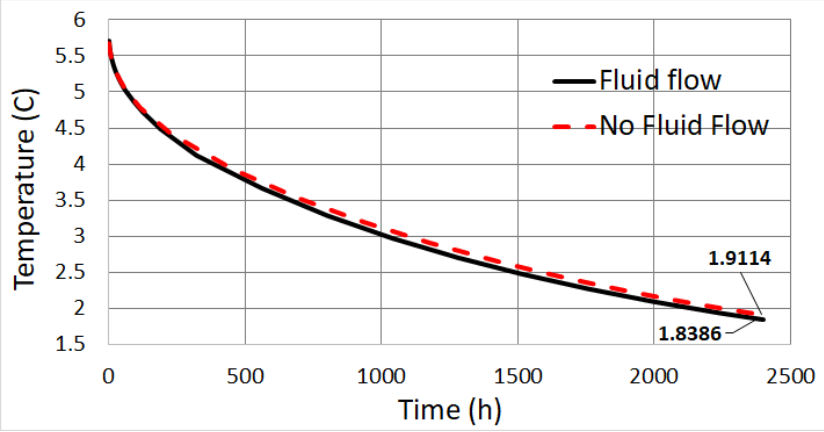

Figure 9. Average temperature in the highlighted area of Figure 8 with fluid flow modelling (solid) compared with no fluid modelling (dashed).

3.2. Results

In this section we compare and discuss the thermal profiles calculated by COMSOL in the two cases corresponding to two different boundary conditions at surface. To quantify differences in the soil region that is active for heat extraction, we computed the average temperature for the rectangular region highlighted in Figure 8 for both (a) and (b). This extends for 1.5 m from the most external piles

on both sides, and for 1m from the piles bottom. Thermal insulation effects at the boundaries (at 0 m, −5 m and 15 m in the plot), which are embedded in COMSOL, should not alter the result as they are washed out by the large amount of soil between boundaries and the region's edges.

The result is plotted in Figure 10. It is rather evident that, even after so many hours of heat pump operation at full load, no appreciable difference can be discerned, only ∼0.015 °C at the most. We thus conclude that when interested in average temperatures and energy balance, we can freely choose either boundary conditions without compromising our results.

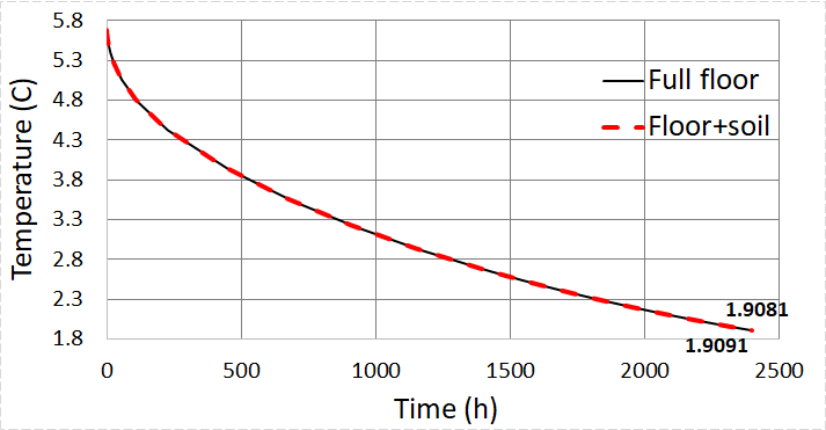

Figure 10. Average temperature in the highlighted slab portion, (a) floor (dashed) vs. (b) floor + soil (solid). T [°C] values for the last point in bold.

4. IDA-ICE Borehole Model Validation against COMSOL

In this third study we consider a 3D IDA-ICE finite difference borehole model, together with the COMSOL FEM counterpart. The latter is a direct 3D extension of the 2D model discussed in Section 3. Here we compute the outlet temperatures at different depths on the edge of 20 energy piles, which are buried in soil under a multilayer floor. Results from the IDA-ICE model are compared with those obtained from COMSOL, in order to estimate the accuracy of the IDA-ICE calculation.

4.1. Method

A 3D FEM COMSOL extension of the 2D model discussed in Section 3 is here performed, with 20 identical energy piles that are 15 m-long and with 4.5 m spacing; the same geometry is implemented both in COMSOL (Figure 11) and in IDA-ICE, with a 3D finite element (COMSOL) or finite difference (IDA-ICE) borehole model that accounts for the mutual thermal interaction of adjacent piles.

The piles were buried in a 25 m × 25 m × 20 m soil medium (layout listed in Table 3), with the same multilayer floor (concrete slab over an EPS layer) addressed in Section 3 as the upper boundary condition. In IDA-ICE this is set by default because, as remarked earlier, the option to define multiple ground surface boundary regions is not available. Temperature loggers were set on the centre pile #10, on the centre-edge pile #12 and on the edge pile #20, to quantify the impact of surrounding piles on the temperature fields. Temperatures were logged at 1.5 m, 3 m, 6 m and 12 m depth, with loggers located on the pile edge in contact with soil.

In the COMSOL simulation piles, floor and soil were modelled exactly as in Section 3.1, with the same material properties. The concrete floor was kept at 20 °C at all times, and the U-pipes were kept at steady T = 0 °C (corresponding to a constant heat pump operation). In order to decrease the simulation time, no fluid flow was modelled, as explained in Section 3.1; in IDA-ICE instead, the fluid at constant T = 0 °C entered the energy piles at a very high flow rate. Simulations in COMSOL and IDA-ICE ran for 2400 h, with time interval Δt = 1 h.

Table 3. Spatial arrangement (view from above) of the energy piles for both IDA-ICE and COMSOL.

17	18	19	20
13	14	15	16
9	10	11	12
5	6	7	8
1	2	3	4

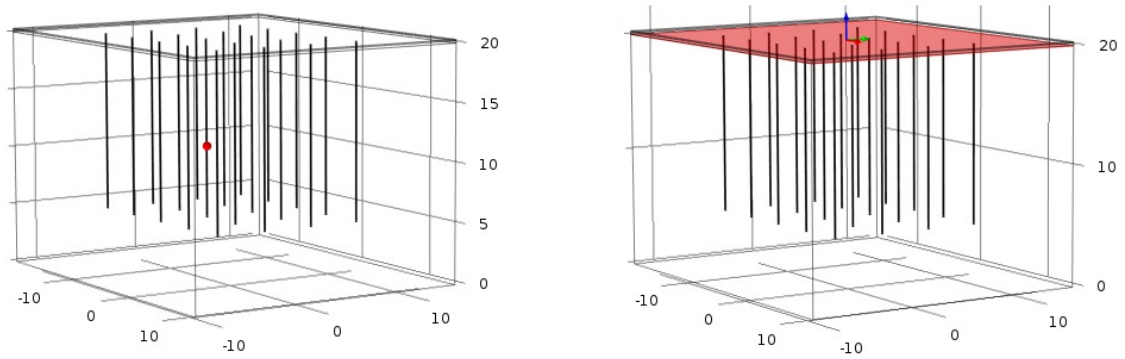

Figure 11. Floor slab with 20 energy piles in COMSOL. Data point at 9 m shown as a red dot.

4.2. Results

Looking at Figures 12–14, one can clearly see that, as expected, only the central pile #10 is slightly colder than the other two. We do not really see a major impact of the specific placement. Furthermore, predictions of COMSOL and IDA-ICE are extremely close, on the average of the order 0.05 °C. Regardless of the software used, the temperature difference is overall very small, accounting for the soil medium and piles temperature homogeneity. Even a very large depth difference shows little discrepancy, e.g., 1.5 m and 12 m give $\Delta T < 0.4$ °C. Specifically, notice how for every pile, the 12 m curves overlap exactly with those at 6 m. Surface effects are indeed strongly hindered by the large thermal mass of the soil medium. Figure 15 also illustrates that, for different boundary conditions at the surface (full floor vs. floor + soil), COMSOL shows a similar $\Delta T \sim 0.4$ °C. This effect is compensated by averaging over the large area that is active for heat extraction, as we discussed in Section 3.

Surface effects should however be relevant for small depths. We thus consider a point in between the central piles, at 0.5 m under the floor, and compare its temperature profile to that of another point right above, very close to the floor, at 3 cm depth. As illustrated in Figure 16, after about 200 h (i.e., after the FEM simulation is stabilised) there is a constant $\Delta T \sim 0.8$ °C. This means that, differently from what we have seen above for points sitting deeper underground, when approaching the surface T differences are relevant and cannot be ignored.

More importantly though, Figure 16 also shows that the integrated average temperature on a plane located at 3 cm under the floor, pictured in Figure 11, always coincides with T as computed at a central point at the same depth. This is a natural consequence of the simulation's geometrical and physical symmetry, showing that for a similar setup one can use averages instead of point values. This result might be valuable for practitioners and on-site applications.

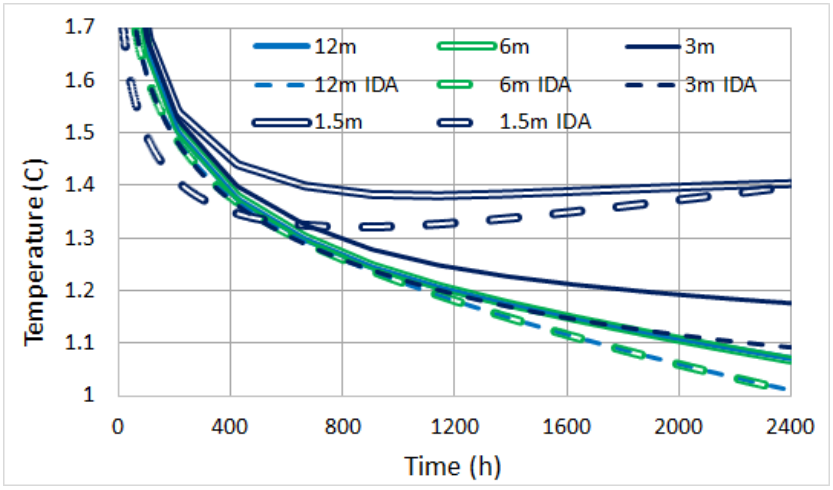

Figure 12. Pile #10.

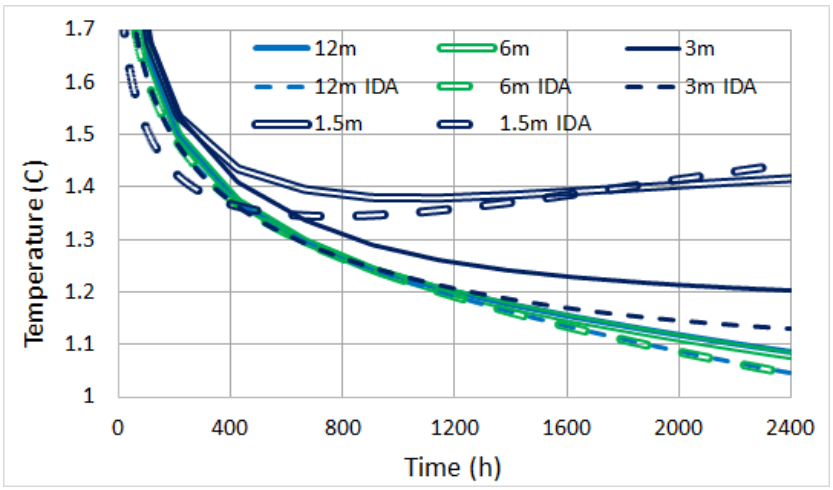

Figure 13. Pile #12.

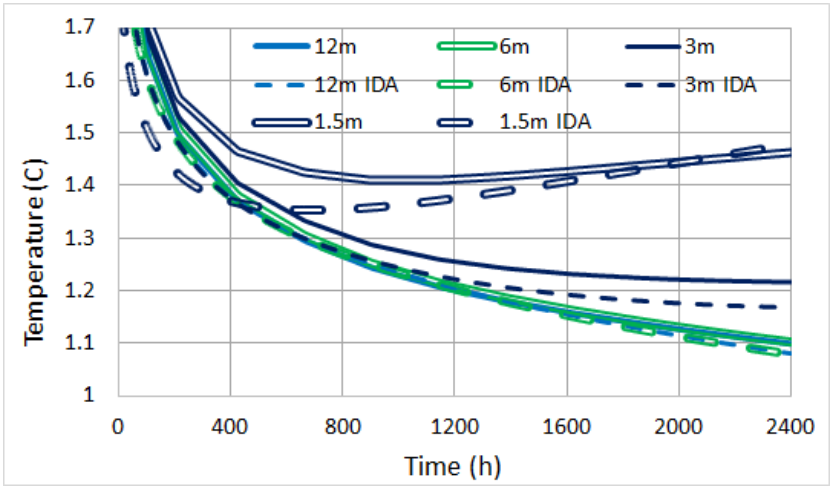

Figure 14. Pile #20.

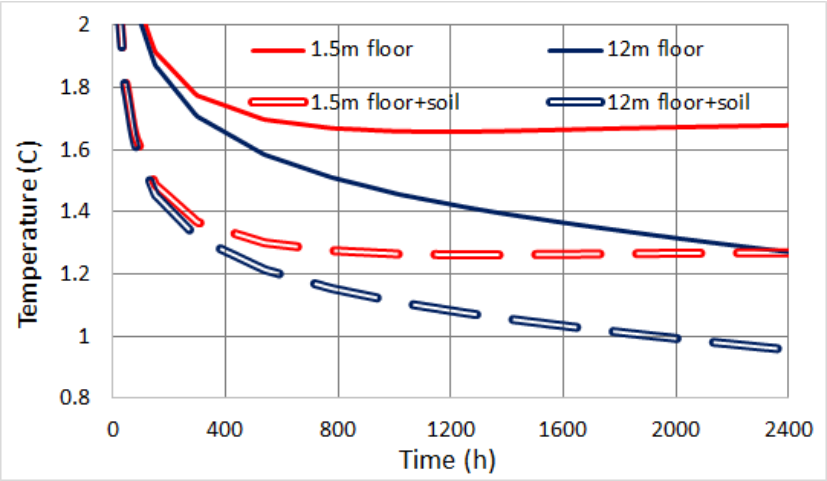

Figure 15. COMSOL comparison of different boundary conditions.

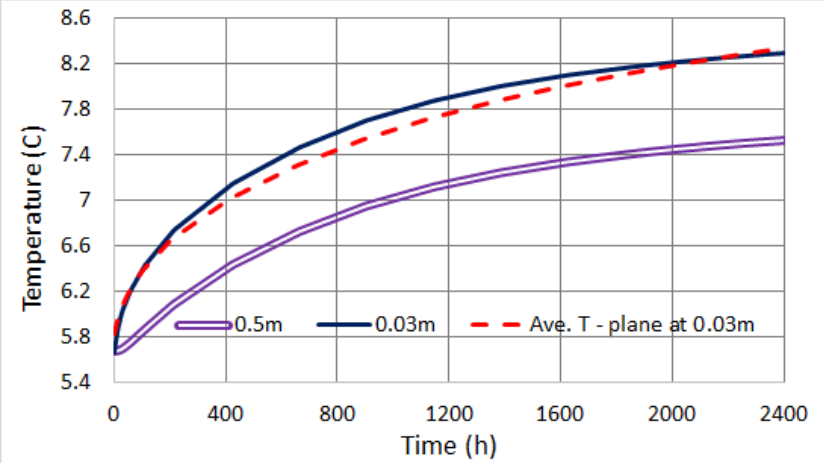

Figure 16. Temperature at mid points and on a plane parallel to the floor.

5. Impact of Boundary Conditions on Energy Efficiency Calculations

In this final case, we apply to a 3D COMSOL FEM model the data obtained in [28] by modelling the energy piles with IDA-ICE, in order to calculate the temperature underneath the floor slab (also called "ground surface temperature"). The result is then compared to the rough estimation made in [28] (the "outlet" solution here), and to an analogous IDA-ICE calculation using a new software version updated in November 2017 (the "slab" solution here). We find that the new implementation "slab" shows a remarkable improvement over the "outlet" method in terms of energy consumption assessment.

5.1. Method

Geothermal energy piles with heat pump in a whole building were modelled in IDA-ICE following the design proposed in [28] and addressing the same commercial hall-type building (Figure 17). The total number of energy piles was 192, the initial soil temperature 5.67 °C and the piles were 15 m-long. The soil properties were k = 1.1 W/mK, ρ = 1800 kg/m^3 and c_p = 1800 kJ/kgK.

In the present study, we performed an annual IDA-ICE simulation according to this design. We obtained inlet and outlet energy piles temperatures with hourly resolution, which we used to calculate the average energy piles fluid temperature. These were then implemented in COMSOL as boundary conditions, to avoid including a fluid dynamics module for the reasons explained in Section 3.1. Our COMSOL simulation accordingly involves only heat conduction, but uses the IDA-ICE values to increase the precision.

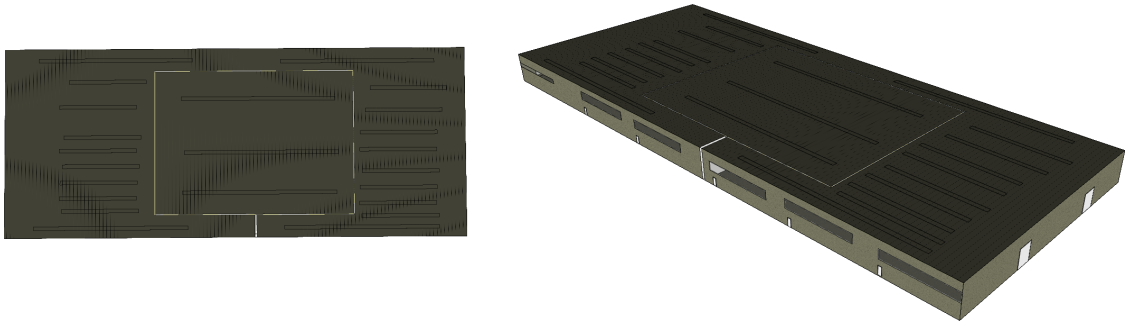

Figure 17. Building model with a separated zone (centre) above energy piles modelled in IDA-ICE.

To compute the yearly energy demand for this building, the model was divided into two zones—one with energy piles and one without. The building floor slab above the energy piles accounts for ca. 33% of the total floor slab area. In the original "outlet" approach presented in [28], a variable temperature underneath this surface is roughly estimated as the energy piles outlet temperature, with connection scheme presented in Figure 18. This was necessary since before November 2017 it was not possible for IDA-ICE to calculate the exact ground surface temperature above the piles, which we accomplish instead with the new solution called "slab".

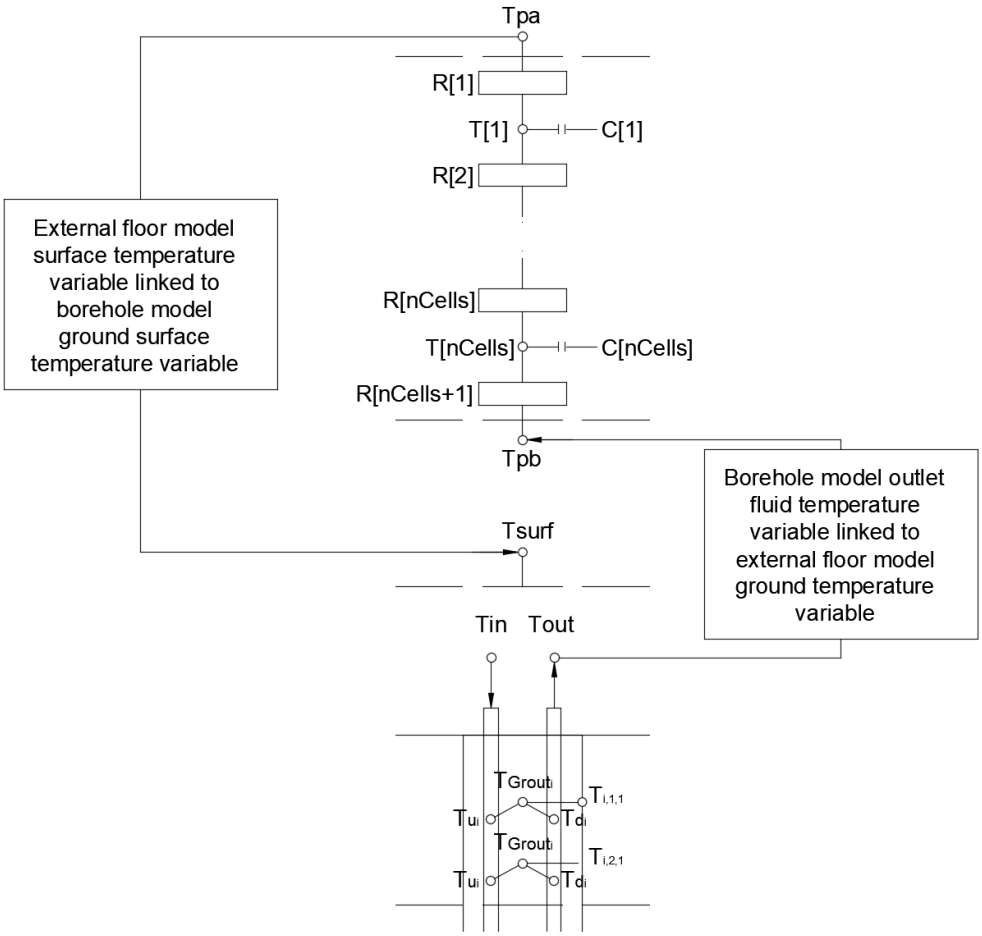

Figure 18. Connection scheme for "slab" (**left**) and "outlet" (**right**) IDA-ICE borehole models.

The annual simulation with hourly resolution performed in COMSOL returned the average ground surface temperature T_s beneath the floor slab, then compared against the same T_s calculated by

the new "slab" borehole model. Finally, we quantify the discrepancy between COMSOL and the two IDA-ICE models "outlet" and "slab" when computing the yearly energy need for the above building.

5.2. Results

Figure 19 compares the COMSOL-calculated ground surface temperature against the two temperatures estimated in IDA-ICE. In the previous IDA-ICE "outlet" approach [28], the results were obtained with an outdated version of the software, where the borehole model uses the energy piles outlet temperature as a rough estimate for the ground surface temperature.

The newer IDA-ICE "slab" estimates use instead the latest version of borehole model, which is now capable of estimating the ground surface temperature. One can observe a significant difference of 5.8 °C between the new and old version over the simulated annual period. Remarkably, the new result of IDA-ICE borehole model differs by only 0.6 °C from COMSOL.

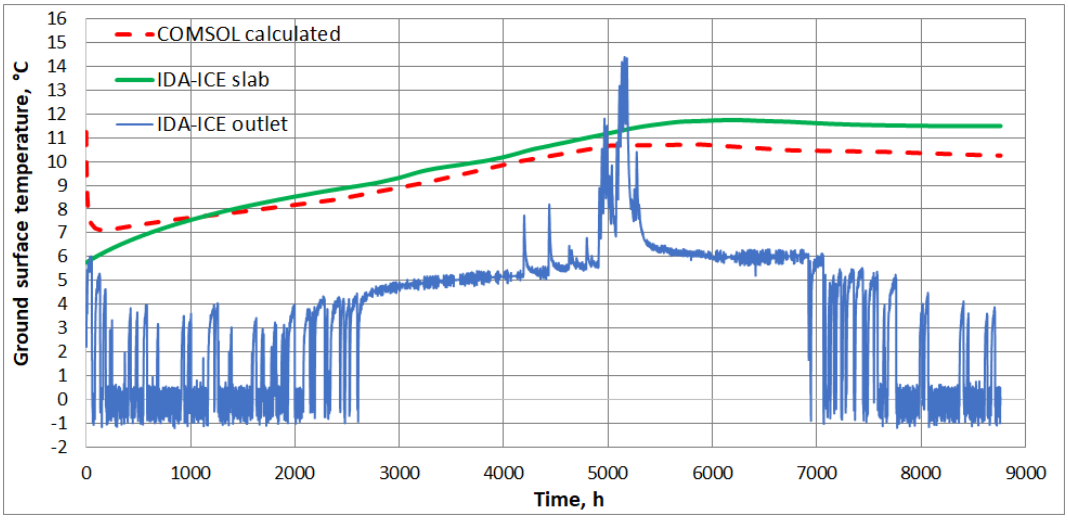

Figure 19. Estimated IDA-ICE ground surface temperature vs. calculated in COMSOL.

Table 4 shows how improper modelling of the ground surface temperature affects the floor slab heat flux over the energy piles, and accordingly the overall annual heat demand of the building. From the perspective of annual heat flux difference, simply applying the outlet temperature of energy piles as ground surface boundary condition in "outlet" produces a difference in ca. 54%, which induces nearly a 5% overestimation of building annual heating need. In contrast, the new version of borehole model "slab" performs in a very good agreement with COMSOL, within an acceptable heat flux and heating need difference of 0.03% and 0.2% respectively.

Table 4. Validation results for the IDA-ICE estimated ground surface temperature.

Case	Floor Slab Heat Flux, kWh/a	Heating Need, kWh/a	Heat Flux, % Difference	Heating Need, % Difference
COMSOL	24066	142900	-	-
IDA-ICE slab	24073	142580	0.03%	0.2%
IDA-ICE outlet	37127	150196	54%	5%

The new IDA-ICE implementation of a borehole model is therefore free from previous heating consumption overestimations, providing a reliable tool for investigations of building heating needs.

6. Conclusions

In this paper we have investigated into detail geothermal plants modelling, by comparing different boundary conditions and their impact on numerical studies of heat transfer and energy performance.

First we considered the finite element method (FEM) software COMSOL Multiphysics, and validated a 3D model of transient heat transfer against experimental data. We found an excellent agreement, despite uncertainties in the measurements and estimated soil properties.

Next we simulated transient heat transfer in a multi-pile 2D reduction of the previous simulation, and addressed the effect of different upper boundary conditions, namely either (i) a unique floor multilayer at 20 °C or (ii) a floor at 20 °C and soil at ∼6 °C. We found that for practical purposes, the average temperatures and energy balance for a yearly calculation are unaffected by the specific boundary condition. This holds by virtue of extremely small temperature differences in the active heat extraction region: modelling of energy piles can thus be performed using borehole models with variable ground surface temperature, which can be set as the indoor air temperature above the energy piles area. The implementation of multiregional surface boundary conditions proposed in [13] can be accordingly neglected in future studies.

As a side result, we discussed the role of fluid flow modelling inside the pipes. We confirm earlier findings that for the length and time scales of interest, one can safely ignore the fluid flow and model the U-pipes as made of concrete with constant T, both in 2D and 3D simulations.

A third computation was then performed with both COMSOL and IDA-ICE, addressing transient heat transfer for 2400 h. The simulations consisted of a 3D model with 20 energy piles embedded in a soil medium, under a uniform multilayer floor, revealing that temperature predictions of COMSOL and IDA-ICE are extremely close, on the average of the order 0.05 °C. In particular, the piles temperatures are not affected by the specific placement, as they are approximately constant for a given depth. The large thermal mass of piles and medium also provides a very small vertical gradient, e.g., the difference between 1.5 m and 12 m depth gives only $\Delta T < 0.4$ °C. Moreover, for every pile the 12 m curves overlap exactly with those at 6 m.

Figure 15 illustrates a comparable $\Delta T \sim 0.4$ °C also for different boundary conditions at the surface (full floor vs. floor + soil) in COMSOL. This effect is compensated by averaging over the large area that is active for heat extraction, as we discussed in Section 3. However, close to the surface the different boundary conditions (full floor vs. floor + soil) do give a different temperature. Interestingly, we also found that the integrated average T on a horizontal plane at height h is nearly identical to the one at a point laying on it. This result could be useful for practical calculations of energy balance over the same time scale.

Finally, we performed a yearly simulation to assess the heating need of a commercial building employing a geothermal plant. Assuming the COMSOL FEM calculation validated in Section 1 as our benchmark, two IDA-ICE FDM simulations illustrated the impact of different upper boundary conditions on the final energy consumption estimate. We found that in IDA-ICE, adopting the energy piles outlet temperature as a rough estimate for the ground surface temperature overestimates the heat flux in the floor slab by 54% and the heating need by 5%. On the other hand, using the ground surface temperature produced a consistent result with COMSOL, overestimating the heat flux and heating need by only 0.03% and 0.2% respectively.

One might now wonder about the long-term effects of the heat discharge. This has been studied into details in [28] for a heat pump plant with energy piles serving a one storey commercial hall building. Long-term simulations encompassing 20 years of usage showed a consistent reduction in performance of the energy piles regarding heat extraction. It was found indeed that, over the years, the heat extracted from the energy piles exceeds the amount which is loaded during the cooling season. Evidently, this implies a need for thermal storage, at least for the case of commercial hall-type buildings.

In conclusion, this paper provides a through comparison of software widely used in simulations of heating systems adopting borehole and energy piles. In particular, focusing on the role of upper boundary conditions, we showed that multiregional b.c. are fairly equivalent to a single surface with uniform temperature. Moreover, we proved that using the pipes outlet temperature induces a severe overestimation of the heat flux through the heated floor and of the energy demand for the whole building.

All these results are relevant especially for practical purposes, in the development of geothermal energy methods in compliance with international Standards and towards sustainability. In this perspective, they set the foundation for a number of necessary developments and improvements: for instance, longer term simulations (such as 10–20 years) could investigate the effect of a reverse operation mode in summer, for decharging the ground to limit the thermal drift observed in [28]. Other possibilities could be the extension of our methodology to other types of climates, and the assessment of thermomechanical effects on the piles' structure.

Author Contributions: Conceptualization, A.F., J.F. and J.K.; methodology, A.F. and J.F.; software, A.F. and J.F.; validation, A.F.; investigation, A.F. and J.F.; writing—original draft preparation, A.F. and J.F.; writing—review and editing, A.F.; supervision, J.K.; funding acquisition, J.K.

Funding: The research was supported by the Estonian Research Council with Institutional research funding grant IUT1-15. The authors are also grateful to the Estonian Centre of Excellence in Zero Energy and Resource Efficient Smart Buildings and Districts, ZEBE, grant 2014-2020.4.01.15-0016 funded by the European Regional Development Fund.

Conflicts of Interest: The authors declare no conflict of interest.

Abbreviations

The following abbreviations have been used in this manuscript:

GHE	Ground Heat Exchangers
FEM	Finite Element Method
FDM	Finite Difference Method
b.c.	Boundary Conditions

Nomenclature

ρ	Density [kg/m^3]
c_p	Specific heat at constant pressure [kJ/(kgK)]
T	Temperature [°C]
λ	Thermal conductivity [W/(mK)]
Δt	Time step [h]

References

1. European Parliament. Directive 2010/31/EU of the European Parliament and of the Council of 19 May 2010 on the energy performance of buildings. *Off. J. Eur. Union* **2010**, *53*, 13–35.
2. Lund, J.W.; Boyd, T.L. Direct utilization of geothermal energy 2015 worldwide review. *Geothermics* **2016**, *60*, 66–93. [CrossRef]
3. Agemar, T.; Weber, J.; Moeck, I.S. Assessment and Public Reporting of Geothermal Resources in Germany: Review and Outlook. *Energies* **2018**, *11*, 332. [CrossRef]
4. Park, K.S.; Kim, S. Utilising Unused Energy Resources for Sustainable Heating and Cooling System in Buildings: A Case Study of Geothermal Energy and Water Sources in a University. *Energies* **2018**, *11*, 1836. [CrossRef]
5. Aydin, M.; Sisman, A. Experimental and computational investigation of multi U-tube boreholes. *Appl. Energy* **2015**, *145*, 163–171. [CrossRef]
6. Bose, J.E.; Smith, M.; Spitler, J. Advances in ground source heat pump systems-an international overview. In Proceedings of the 7th IEA Heat Pump Conference, Beijing, China, 19–22 May 2002; Volume 324, pp. 313–324.
7. Spitler, J. Editorial: Ground-Source Heat Pump System Research—Past, Present, and Future. *HVAC R Res.* **2005**, *11*, 165–167. [CrossRef]
8. Brandl, H. Energy foundations and other thermo-active ground structures. *Geotechnique* **2006**, *56*, 81–122. [CrossRef]
9. Lautkankare, R.; Sarola, V.; Kanerva-Lehto, H. Energy piles in underpinning projects—Through holes in load transfer structures. *DFI J. J. Deep Found. Inst.* **2014**, *8*, 3–14. [CrossRef]

10. Faizal, M.; Bouazza, A.; Singh, R.M. Heat transfer enhancement of geothermal energy piles. *Renew. Sustain. Energy Rev.* **2016**, *57*, 16–33. [CrossRef]
11. Bourne-Webb, P.; Burlon, S.; Javed, S.; Kuerten, S.; Loveridge, F. Analysis and design methods for energy geostructures. *Renew. Sustain. Energy Rev.* **2016**, *65*, 402–419. [CrossRef]
12. Li, M.; Lai, A.C. Review of analytical models for heat transfer by vertical ground heat exchangers (GHEs): A perspective of time and space scales. *Appl. Energy* **2015**, *151*, 178–191. [CrossRef]
13. Fadejev, J.; Simson, R.; Kurnitski, J.; Haghighat, F. A review on energy piles design, sizing and modelling. *Energy* **2017**, *122*, 390–407. [CrossRef]
14. Ingersoll, L.R.; Zobel, O.J.; Ingersoll, A.C. Heat conduction with engineering, geological and other applications. *Q. J. R. Meteorol. Soc.* **1955**, *81*, 647–648. [CrossRef]
15. Goldenberg, H. A problem in radial heat flow. *Br. J. Appl. Phys.* **1951**, *2*, 233. [CrossRef]
16. Hu, P.; Zha, J.; Lei, F.; Zhu, N.; Wu, T. A composite cylindrical model and its application in analysis of thermal response and performance for energy pile. *Energy Build.* **2014**, *84*, 324–332. [CrossRef]
17. Abdelaziz, S.L.; Ozudogru, T.Y. Selection of the design temperature change for energy piles. *Appl. Therm. Eng.* **2016**, *107*, 1036–1045. [CrossRef]
18. Hellström, G. Ground Heat Storage: Thermal Analyses of Duct Storage Systems. Ph.D. Thesis, School of Mathematical Physics, Lund University, Lund, Sweden, 1991.
19. Claesson, J.; Hellström, G. Analytical studies of the influence of regional groundwater flow on the performance of borehole heat exchangers. In Proceedings of the 8th International Conference on Thermal Energy Storage, Terrastock 2000, Stuttgart, Germany, 28 August–1 September 2000; pp. 195–200.
20. Bozis, D.; Papakostas, K.; Kyriakis, N. On the evaluation of design parameters effects on the heat transfer efficiency of energy piles. *Energy Build.* **2011**, *43*, 1020–1029. [CrossRef]
21. Rosa, M.D.; Ruiz-Calvo, F.; Corberán, J.M.; Montagud, C.; Tagliafico, L.A. Borehole modelling: A comparison between a steady-state model and a novel dynamic model in a real ON/OFF GSHP operation. *J. Phys. Conf. Ser.* **2014**, *547*, 012008. [CrossRef]
22. Kwong Lee, C.; Nam Lam, H. Thermal Response Test Analysis for an Energy Pile in Ground-Source Heat Pump Systems. In *Progress in Sustainable Energy Technologies: Generating Renewable Energy*; Dincer, I., Midilli, A., Kucuk, H., Eds.; Springer: Cham, Switzerland, 2014; pp. 605–615.
23. Li, Z.; Zheng, M. Development of a numerical model for the simulation of vertical U-tube ground heat exchangers. *Appl. Therm. Eng.* **2009**, *29*, 920–924. [CrossRef]
24. Nam, Y.; Ooka, R.; Hwang, S. Development of a numerical model to predict heat exchange rates for a ground-source heat pump system. *Energy Build.* **2008**, *40*, 2133–2140. [CrossRef]
25. Lazzari, S.; Priarone, A.; Zanchini, E. Long-term performance of BHE (borehole heat exchanger) fields with negligible groundwater movement. *Energy* **2010**, *35*, 4966–4974. [CrossRef]
26. Diersch, H.J.; Bauer, D.; Heidemann, W.; Rühaak, W.; Schätzl, P. Finite element modeling of borehole heat exchanger systems: Part 2. Numerical simulation. *Comput. Geosci.* **2011**, *37*, 1136–1147. [CrossRef]
27. Salvalai, G. Implementation and validation of simplified heat pump model in IDA-ICE energy simulation environment. *Energy Build.* **2012**, *49*, 132–141. [CrossRef]
28. Fadejev, J.; Kurnitski, J. Geothermal energy piles and boreholes design with heat pump in a whole building simulation software. *Energy Build.* **2015**, *106*, 23–34. [CrossRef]
29. Østergaard, D.; Svendsen, S. Space heating with ultra-low-temperature district heating—A case study of four single-family houses from the 1980s. *Energy Procedia* **2017**, *116*, 226–235. [CrossRef]
30. Schweiger, G.; Heimrath, R.; Falay, B.; O'Donovan, K.; Nageler, P.; Pertschy, R.; Engel, G.; Streicher, W.; Leusbrock, I. District energy systems: Modelling paradigms and general-purpose tools. *Energy* **2018**, *164*, 1326–1340. [CrossRef]
31. Lee, C.; Lam, H. A simplified model of energy pile for ground-source heat pump systems. *Energy* **2013**, *55*, 838–845. [CrossRef]
32. Mehrizi, A.A.; Porkhial, S.; Bezyan, B.; Lotfizadeh, H. Energy pile foundation simulation for different configurations of ground source heat exchanger. *Int. Commun. Heat Mass Transf.* **2016**, *70*, 105–114. [CrossRef]
33. Xiao, J.; Luo, Z.; Martin, J.R.; Gong, W.; Wang, L. Probabilistic geotechnical analysis of energy piles in granular soils. *Eng. Geol.* **2016**, *209*, 119–127. [CrossRef]

34. Pryor, R.W. *Multiphysics Modeling Using COMSOL: A First Principles Approach*, 1st ed.; Jones and Bartlett Publishers, Inc.: Burlington, MA, USA, 2009.
35. Dupray, F.; Laloui, L.; Kazangba, A. Numerical analysis of seasonal heat storage in an energy pile foundation. *Comput. Geotech.* **2014**, *55*, 67–77. [CrossRef]
36. Diersch, H.J.; Bauer, D.; Heidemann, W.; Rühaak, W.; Schätzl, P. Finite element modeling of borehole heat exchanger systems: Part 1. Fundamentals. *Comput. Geosci.* **2011**, *37*, 1122–1135. [CrossRef]
37. Park, H.; Lee, S.R.; Yoon, S.; Choi, J.C. Evaluation of thermal response and performance of PHC energy pile: Field experiments and numerical simulation. *Appl. Energy* **2013**, *103*, 12–24. [CrossRef]
38. Cecinato, F.; Loveridge, F.A. Influences on the thermal efficiency of energy piles. *Energy* **2015**, *82*, 1021–1033. [CrossRef]
39. Ng, C.; Ma, Q.; Gunawan, A. Horizontal stress change of energy piles subjected to thermal cycles in sand. *Comput. Geotech.* **2016**, *78*, 54–61. [CrossRef]
40. Go, G.H.; Lee, S.R.; Yoon, S.; byul Kang, H. Design of spiral coil PHC energy pile considering effective borehole thermal resistance and groundwater advection effects. *Appl. Energy* **2014**, *125*, 165–178. [CrossRef]
41. Loveridge, F.; Powrie, W. 2D thermal resistance of pile heat exchangers. *Geothermics* **2014**, *50*, 122–135. [CrossRef]
42. Alberdi-Pagola, M.; Poulsen, S.E.; Jensen, R.L.; Madsen, S. Thermal design method for multiple precast energy piles. *Geothermics* **2019**, *78*, 201–210. [CrossRef]
43. Batini, N.; Loria, A.F.R.; Conti, P.; Testi, D.; Grassi, W.; Laloui, L. Energy and geotechnical behaviour of energy piles for different design solutions. *Appl. Therm. Eng.* **2015**, *86*, 199–213. [CrossRef]
44. Caulk, R.; Ghazanfari, E.; McCartney, J.S. Parameterization of a calibrated geothermal energy pile model. *Geomech. Energy Environ.* **2016**, *5*, 1–15. [CrossRef]
45. Loria, A.F.R.; Vadrot, A.; Laloui, L. Analysis of the vertical displacement of energy pile groups. *Geomech. Energy Environ.* **2018**, *16*, 1–14. [CrossRef]
46. Li, M.; Lai, A.C. Heat-source solutions to heat conduction in anisotropic media with application to pile and borehole ground heat exchangers. *Appl. Energy* **2012**, *96*, 451–458. [CrossRef]
47. Park, S.; Lee, D.; Lee, S.; Chauchois, A.; Choi, H. Experimental and numerical analysis on thermal performance of large-diameter cast-in-place energy pile constructed in soft ground. *Energy* **2017**, *118*, 297–311. [CrossRef]
48. McCartney, J.S.; Murphy, K.D. Investigation of potential dragdown/uplift effects on energy piles. *Geomech. Energy Environ.* **2017**, *10*, 21–28. [CrossRef]
49. Sung, C.; Park, S.; Lee, S.; Oh, K.; Choi, H. Thermo-mechanical behavior of cast-in-place energy piles. *Energy* **2018**, *161*, 920–938. [CrossRef]
50. Singh, R.; Bouazza, A.; Wang, B. Near-field ground thermal response to heating of a geothermal energy pile: Observations from a field test. *Soils Found.* **2015**, *55*, 1412–1426. [CrossRef]
51. Suryatriyastuti, M.; Mroueh, H.; Burlon, S. Understanding the temperature-induced mechanical behaviour of energy pile foundations. *Renew. Sustain. Energy Rev.* **2012**, *16*, 3344–3354. [CrossRef]
52. Eguaras-Martínez, M.; Vidaurre-Arbizu, M.; Martín-Gómez, C. Simulation and evaluation of Building Information Modeling in a real pilot site. *Appl. Energy* **2014**, *114*, 475–484. [CrossRef]
53. Uotinen, V.M.; Repo, T.; Vesamäki, H. Energy piles—Ground energy system integrated to the steel foundation piles. In Proceedings of the 16th Nordic Geotechnical Meeting (NGM 2012), Copenhagen, Denmark, 9–12 May 2012; pp. 837–844.
54. Jõeleht, A.; Kukkonen, I.T. Physical properties of Vendian to Devonian sedimentary rocks in Estonia. *GFF* **2002**, *124*, 65–72. [CrossRef]
55. Kukkonen, I.; Lindberg, A. *Thermal Properties of Rocks at the Investigation Sites: Measured and Calculated Thermal Conductivity, Specific Heat Capacity and Thermal Diffusivity*; Working Report; Ilmo Kukkonen Antero Lindberg: Helsinki, Finland, 1998.

56. Bauer, D.; Heidemann, W.; Diersch, H.J. Transient 3D analysis of borehole heat exchanger modeling. *Geothermics* **2011**, *40*, 250–260. [CrossRef]
57. Al-Khoury, R.; Kölbel, T.; Schramedei, R. Efficient numerical modeling of borehole heat exchangers. *Comput. Geosci.* **2010**, *36*, 1301–1315. [CrossRef]

Publication 4

Fadejev J, Simson R, Kesti J, Kurnitski J. Measured and simulated energy performance of OLK NZEB with heat pump and energy piles in Hämeenlinna. *E3S Web of Conferences, NSB 2020 Tallinn -12th Nordic Symposium on Building Physics*, Vol. 172 Art.No. 16012 pp. 1-11. 2020.

Measured and simulated energy performance of OLK NZEB with heat pump and energy piles in Hämeenlinna

Jevgeni Fadejev[1, 2*], *Raimo* Simson[1], *Jyrki* Kesti[3], and *Jarek* Kurnitski[1, 2]

[1]Tallinn University of Technology, Ehitajate tee 5, Tallinn 19086, Estonia
[2]Aalto University, School of Engineering, Rakentajanaukio 4 A, Espoo FI-02150, Finland
[3]Ruukki Construction Oy, Panuntie 11, Helsinki 00620, Finland

Abstract. In this work, measured energy use of the building space heating, ventilation supply air heating, appliances and lighting is compared against simulated energy use modelled in IDA ICE. As built energy need and detailed measured input data is applied in building model calibration procedure. Calibrated building model energy performance is studied in both measured and test reference year climate conditions. Previously modelled as built plant automation and implemented control logics are compared against measured. Geothermal plant in this study consists of heat pump, solar collectors, boreholes and energy piles. Heat pump SCOP estimated by post processing according to heat pump manufacturer's performance map is compared against measured SCOP on the monthly basis. Opinion on actual plant operation is given and energy performance improvement potential is quantified. Important parameters for successful building model calibration are presented. Building compliance with Finland NZEB requirements are assessed. The results show good match with measured energy use after the model calibration.

1 Introduction

According to European Parliament directive 2010/31/EU [1] all new buildings built from January 2021 are to comply with nearly zero-energy buildings (NZEB) national requirements. NZEB requirements for public buildings are already in force. Meeting NZEB requirements considers application of renewable energy sources such as geothermal and solar in the design. Geothermal energy utilization is mainly performed with a ground source heat pump (GSHP) and according to a review on worldwide application of geothermal energy [2] total installed worldwide GSHPs capacity has grown 2.15 times in the period of 2005 to 2010 and 45% from 2010 to 2015, application of GSHP is registered in 82 countries around the globe.

Annual GSHP SCOP values up to 4.5 and overall geothermal plant SCOP values up to 3.9 (including control and distribution losses) were obtained based on measured performance of actual GSHP installations [3-4]. In most cases, operation of a heat pump is accompanied by the unbalanced geothermal energy extraction/injection that leads to a significant loss in long-term operation performance [5]. To maintain stable long-term operation of GSHP plant and improve geothermal energy yield along with seasonal coefficient of performance (SCOP), a source of thermal storage to be considered in the plant design. Reda [6] studied the benefits of solar thermal storage numerically in a GSHP plant with a borehole field type ground heat exchanger (GHE), where application of solar thermal storage helped in improvement of GSHP plant SCOP from 1.6 to 3.0. Allaerts et al. [7] has modelled the performance of a GSHP plant with dual borehole field and active air source storage in TRNSYS, where cooling tower i.e. dry cooler was applied as a thermal storage source. According to results of such thermal storage application, overall size of borehole field was reduced by 47% compared to the same capacity single borehole field plant without thermal storage.

GSHP plant performance is depended on the type of GHE considered in the plant design. Typical closed loop GHEs are classified by the position of installation - horizontal and vertical. Horizontal GHE is generally cheaper to install compared to vertical GHE, however requires more land area for the installation. In buildings with limited land area, vertical GHE in form of a borehole reaching up to 400 meters in depth might be a solution instead of horizontal GHE installation. Though, drilling very deep boreholes might be not only very expensive, but also drilling depth might be limited by the government regulations in the region of interest. In this case, field of multiple shorter boreholes (not exceeding the drilling depth limit) spaced at known distance to each other might be considered as a GHE alternative.

In buildings with pile foundations, installation of heat exchange piping into foundations piles enables the foundation piles to perform as a ground heat exchanger similarly to previously described field of boreholes. Geothermal pile foundations are known also as geothermal energy piles [8]. As the installation of heat exchange piping into foundation pile compared to the

* Corresponding author: jevgeni.fadejev@taltech.ee

drilling of a new borehole is much cheaper, energy piles tend to be a very cost effective GHE solution. As the layout of energy piles is generally defined by the foundation plan, thermal interferences between closely located adjacent piles appear. Thermal interferences may also appear in field of boreholes, depending on the spacing between them. Sizing and assessment of borehole field or energy piles performance is generally carried out with help of numerical modelling regarding which more detailed aspects are described in previously conducted study by Fadejev and Kurnitski [9].

From the perspective of thermal storage application, not all types of GHEs would benefit from a thermal storage due to varying thermal losses intensity, GHE storage capacity and peak heat extraction/rejection rates. To consolidate previous statement, assuming that the same exact amount of heat is stored in a single borehole GHE compared to the same amount of heat stored in a GHE consisting of multiple boreholes and total length of single borehole is equal to the sum of multiple boreholes, field of multiple boreholes would be capable of extracting more heat compared to a single pile due to rejected storage heat of boreholes located in the centre of the field still can be utilized by the boreholes located at the edges of borehole field in the process of storage heat dissipation.

In cold climate regions, where indoor climate conditions are generally ensured with heating, operation of GSHP plant during the heating season cools down the ground surrounding GHE. Installing a "free cooling" heat exchanger between the ground loop and cooling system buffer tank allows to partly cover buildings cooling demand via direct "free cooling".

Considering all abovementioned benefits of GSHP plant, it appears to be very attractive heat source option in NZEB design. Especially in regions, where no heat sources such as district heating with low primary energy conversion factors are available and only electricity energy source is present.

The present study is the continuation of previously conducted research [10] on topic of design and energy performance modelling of geothermal heat pump plant in commercial hall-type building OLK NZEB located in Häämenlinna, Finland. This study covers the analysis of OLK NZEB measured energy use for the period of 01.02.18-01.31.19 along with free cooling impact on indoor climate and geothermal heat pump plant energy performance assessment. Simulated energy use of case 14 from [10] corresponding to energy use of as built initial design case is compared against measured energy use of room unit heat, air handling unit (AHU) heating coil heat, lighting and equipment electricity. As measured outdoor climate conditions and actual building use differ from test reference year (TRY) climate [12] and initial design building use, a building model calibration was conducted in IDA ICE applying detailed hourly based measured data and as built documentation parameters. Building model is being calibrated on the monthly basis and is further applied in TRY climate to assess the impact on building energy performance and quantify the modelling accuracy. Calibrated building model allows further research in terms of coupling it with detailed modelled geothermal plant model and assessment of different parameters impact such as indoor temperature setpoints, AHU setpoints on building energy performance. Measured case conditions are compared against initial design intent and suggestions regarding improving the energy performance are provided. Building model calibration procedure is described in detail and suggestions on required measured parameters by building monitoring/logging system are given to allow successful building model calibration in IDA ICE.

Further results provide an insight on geothermal heat pump plant seasonal coefficients of performance (SCOP) for simulated and measured cases. Energy performance values (EPV) of each case are presented, compliance with Finland NZEB requirements is assessed. Measured heat pump SCOP is compared against one estimated by post processing according to heat pump manufacturer's performance map. Opinion regarding geothermal heat pump plant operation and suggestions on improving its energy performance with quantified expected performance increase are presented.

2 Methods

Measured data for period of 01.02.18-01.31.19 with a hour timestep resolution was obtained from OLK NZEB building monitoring/logging system, processed, then analyzed in Excel. For building model calibration procedure, measured data was converted to input files that comply with IDA ICE simulation environment. The modelling in IDA ICE was performed in advanced level interface, where user can manually edit connections between model components, edit and log model specific parameters, observe models code. A detailed OLK NZEB building model was prepared in IDA ICE based on the as built documentation with accountancy for available measured input data. Building model calibration was performed on the monthly basis with the goal to achieve perfect fit against measured AHU heat and room unit heat, while outdoor climate conditions correspond to measured climate, indoor air temperatures

Fig. 1. (a) Initial design model in IDA ICE. (b) OLK NZEB in Hämeenlinna. (c) Building calibration model in IDA ICE

and AHU setpoints are are defined as hourly based measured data, internal gains are AHU operation schedules are modified due to not being either measured and/or include additional separately cooled equipment electricity use. Simplified heat pump SCOP calculation model based on the actual heat pump performance map and measured evaporator/condenser inlet/outlet temperatures was completed in Excel mainly using second-degree polynomial equations.

2.1 Building model data

Compared to initial design model on Fig. 1 (a), a more detailed room-based model of OLK NZEB depicted on Fig. 1 (c) has been modelled in IDA ICE based on as built documentation for building model calibration procedure. Table 1 presents a detailed overview of general parameters describing the building model.

Table 1. Building descriptive parameters

Descriptive parameter	Value
Location	Finland
Net floor area, m^2	1496.5
External walls area, U = 0.16 W/(m^2 K), m^2	1201
Roof area, U = 0.12 W/(m2 K), m^2	1467
External floor area, U = 0.14 W/(m2 K), m2	1496.5
Windows area, SHGC = 0.33, U = 0.79 W/(m^2 K), m^2	158
External doors, U = 1.0 W/(m^2 K), m^2	67
Initial design heating set point, °C	18
Initial design cooling set point, °C	25
AHUs heat recovery, % (TK01/TK02)	75/78
Measured air tightness, m^3/m^2 h	0.76 @50 Pa
Heating/cooling room units	radiant panels
Heat load design temperature, °C	-26
Design heat load, kW	84
Heat pump capacity, kW	40

Thermal bridges in calibration model were defined according to calculated values obtained during the design process and further presented on Fig. 2.

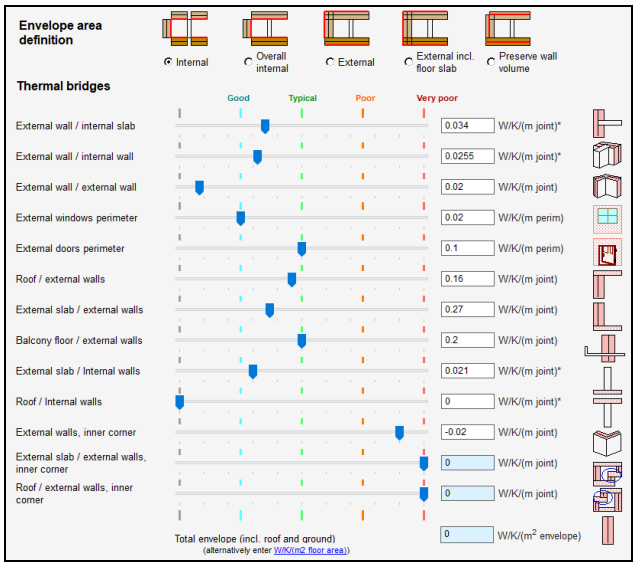

Fig. 2. Thermal bridges values of building calibration model

It is worth to note, that thermal bridges were modelled as internal due to the room-based calibration model.

2.2 Input data and modelling

This section describes the measured input data applied in building model calibration along with individual components modelling methods. Measured data contained missing periods that were filled with interpolated data between them. For this reason, some data spikes might occur on figures presented in the results section of this paper.

Ambient climate conditions were defined in IDA ICE climate file according to measured outdoor air temperature, relative humidity, wind direction, wind velocity, direct and diffusive solar radiation.

2.2.1 Heating system modelling

There are two secondary heating systems in OLK NZEB calibration model – floor heating and radiant ceiling heating panels. Both were modelled as ideal heaters. Floor heating was modelled with design power of 40 W/m2. Radiant heating ceiling panels total design power of ca 40 kW was spread across the building model in locations according to design documentation.

2.2.2 Air handling units modelling

There are two main air handling units installed in OLK NZEB – TK01 and TK02, both equipped with rotary heat exchanger and water heating coils. In actual installation, supply air temperature setpoint is controlled according to exhaust air temperature value. However, this feature was neglected in modelling due to the fact that measured supply air temperatures with a hour timestep resolution were applied (different for each AHU) to achieve match with measured AHU heat value. AHUs technical parameters were obtained from design and commissioning documentation, while initial operational schedules were presented by OLK NZEB staff, they are discussed in results section.

AHU TK01 serviced high hall-type rooms, while TK02 all other rooms. AHU TK02 operated according to design airflow of 0.7 m3/s, while TK01 operated at 1 m3/s (operation at part load of design airflow). Part load was accounted with coefficient of 0.625 to AHU airflow since actual design airflow is 1.6 m3/s. Such modelling approach was applied to properly calculate fans electricity consumption. For this reason, exact fans pressure and efficiency values were setup to obtain design documentation specific fan power (SFP).

2.2.3 Internal gains modelling

Building internal gains consist of following components – occupancy gains, lighting gains, equipment gains and solar gains. Solar gains are calculated in IDA ICE based on climate description and building geometry/envelope properties. Occupancy, lighting and equipment gains were described according to measured and estimated data.

In OLK NZEB, lighting and equipment consumptions were not measured separately. On the

room basis there were four electricity measuring points – Total annual consumption of these zones for the period of 01.02.2018- 31.1.2019 was ca 91.3 MWh/a.

In OLK NZEB, there is heavy machinery installed in one of measuring points. This equipment is also being cooled by separate active cooling system and for this reason cannot be accounted as internal gains in a building heat balance. As the machinery electricity consumption was not measured separately, that internal gains had to be then estimated. Method of estimation was proposed by building constructor, as the installed total lighting power of 8.71 kW was known, it was proposed to sum up the total consumption of that measuring point on an hourly basis and limit maximal consumption value to 8.71 kW, account only for working hours and without weekends. This resulted initial electricity consumption of 71 MWh/a being cut down to ca 23.9 MWh/a due to exclusion of heavy machinery electricity consumption. Measured electricity consumption for other measuring points was left as it is resulting in ca 20.2 MWh/a. Final internal heat gain for lighting and equipment applied in first calibration case was 44.1 MWh/a.

As the measured electricity consumption was available in hour resolution, three control signal input files were created based on measured and estimated data. The data was first sorted into the correct order to match IDA ICE date structure. Measured data starting date in excel was 00:00 01.02.18 which corresponds to hour 744 in IDA input file. Input files were created accounting for previous. IDA ICE model zones were further grouped into three separate categories to allow lighting signal being controlled according to input files data.

Occupancy was modelled according to estimated data presented by OLK NZEB staff. Total of 10 occupants are accounted in the modelling that are spread across the building heated spaces. Two different occupancy profiles were prepared based on that data.

2.2.4 Cargo gates opening modelling

Total of three cargo gates opening phase were measured. However, measured data appeared to be illogical and was neglected in the modelling. Though, in last calibration case presented in results section, some estimated cargo gates opening was applied.

2.2.5 Indoor air temperature setpoints modelling

In OLK NZEB, indoor air temperature along with actual setpoint at point of time in particular room were measured and exported from building monitoring system in one-hour resolution for 11 rooms accordingly. Successful attempts were made to account for either measured indoor air temperature in each room, as well as measured setpoint in each room. However, due to the wide variations in indoor air temperature measured results, it was decided to calculate hourly based building average weighted temperature to use it as a heating system setpoint input in all building calibration model zones. Building weighted average temperature (BWAT) was calculated based on specific heat loss of each room and its measured indoor air temperature.

2.3 Geothermal heat pump plant description

OLK NZEB geothermal heat pump plant fundamental scheme is presented on Fig. 3. Plant design considers option to separate energy piles loop via closing motorized valve (V-3) during the summer thermal storage cycle from the boreholes loop, in order to allow boreholes to provide “free cooling” while at the same time energy piles are being loaded with heat from source of thermal storage. In order to prevent the formation of the ice in the ground and possible frost heave, geothermal loops brine outlet temperature should not drop below 0…-1 °C. Therefore, circulation pumps (V-2 and V-3) in each loop will stop when measured (T2 and T3) brine outlet temperature drops below the set point of 0 °C. Condenser side of the heat pump is connected to a hot buffer tank, in which heat carrier temperature is maintained according to a supply schedule temperature that is dependent on outdoor air temperature value with its maximal value of supply side +50 °C at design outdoor air temperature conditions of -26 °C. Heat pump is capable of operation whenever the temperature in one of the loops is above the set point of 0 °C. On the contrary, heat pump stops its operation when there is no flow in the system (both loops are below the set point).

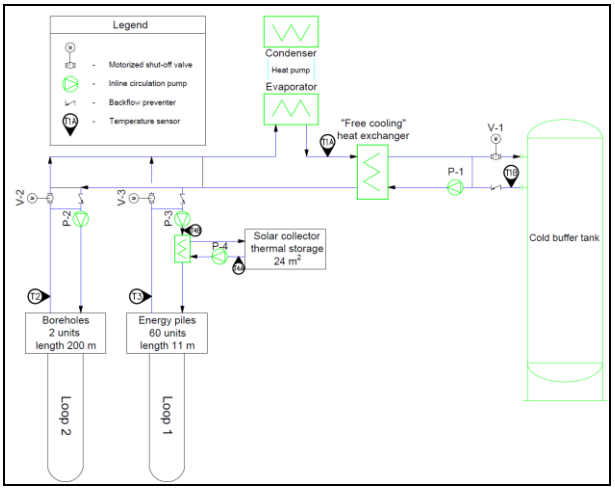

Fig. 3. Geothermal heat pump plant fundamental scheme

With this control logics all the available geothermal energy will be absorbed.

Whenever the cooling cycle starts, there is no heat demand in the system and heat pump will not operate. As the heat pump is inactive, energy piles loop should be separated by e.g. three-way valve from evaporator circuit. In this case only boreholes (heat wells) are active and flow in their circuit goes through “free cooling” heat exchanger.

For each of two loops there is a separate thermal storage. In case of boreholes (heat wells), the required amount of heat is supplied during their free cooling operation.

Solar collector (with/without buffer tank) is applied as a thermal storage source in energy piles loop. Thermal

storage source is connected via heat exchanger to energy piles loop inlet pipe. Whenever the heap pump is inactive, energy piles loop should be separated by e.g. three-way valve and design flow is maintained in energy piles, which are loaded with heat separately from energy wells.

Solar thermal storage is controlled according to a temperature difference (ΔT) set point logics, where two temperatures are measured and desired value of ΔT is maintained. In solar thermal storage loop ΔT = 6K. Measured temperatures in solar thermal storage loops on Fig. 3 are T4A and T4B. Whenever T4A temperature value is higher than 6K of T4B temperature value, pump P-4 starts it operation until the temperature of T4A reaches the desired ΔT = 6K. Control of "Free cooling" loop operates by the logics "when beneficial" i.e. pump P-1 starts it operation whenever temperature T1B is higher than T1A.

3 Results and discussion

Results presented in this section are divided into two subsections – Section 3.1 describes a building model calibration results and Section 3.2 presents energy performance analysis, respectively.

3.1 Building model calibration results

Fig. 4 presents the results of building model calibration of OLK NZEB in IDA-ICE on the monthly basis for a building operation period of 01.02.18-01.31.19. Three out of four cases were simulated, while one out of four corresponds to actual measured data obtained via building monitoring system during the prior mentioned measuring period. Each case consists of three delivered energy components - room units delivered heat, air handling unit (AHU) heating coil delivered heat and lights/equipment delivered electricity i.e. building internal heat gains. In measured case, lighting/equipment energy component (green coloured on Fig.4) additionally contains heavy machinery electricity use since both lights and equipment electricity are measured together on the room basis and no exclusive separation for each consumer source exists. Besides, heavy machinery has a separate cooling system installed and therefore heavy machinery electricity use does not contribute as an internal heat gain in the building heat balance.

Results of Case 1 on Fig. 4 correspond to a simulation with initial settings where AHU operational profiles where defined according to Building Owner (HAMK) proposal and lights/electricity internal gains where modified to meet maximal internal lights load in order to exclude heavy machinery from building heat balance (see Section 2.2). In Case 1, simulated room unit heat resulted in 41.4 MWh/a and AHU heat was 18.9 MWh/a which is ca 35% smaller compared to 63.3 MWh/a of measured room unit heat and ca 19% less than 23.3 MWh/a of measured AHU heat respectively. In terms of month by month analysis, in heating period of Feb – May simulated AHU heat was exceeding measured one, while in heating period of Sept – Jan simulated AHU heat falls behind the measured dramatically. AHU operational profile proposed by HAMK in Case 1 in AHU TK01 was slightly shorter (64 hours per week) than in AHU TK02 (77 hours per week), while each repeated from month to month for the whole simulated period for both AHUs (see Table 2). AHUs modelled supply temperature corresponded to the measured one while modelled heat recovery performance corresponded to design documentation.

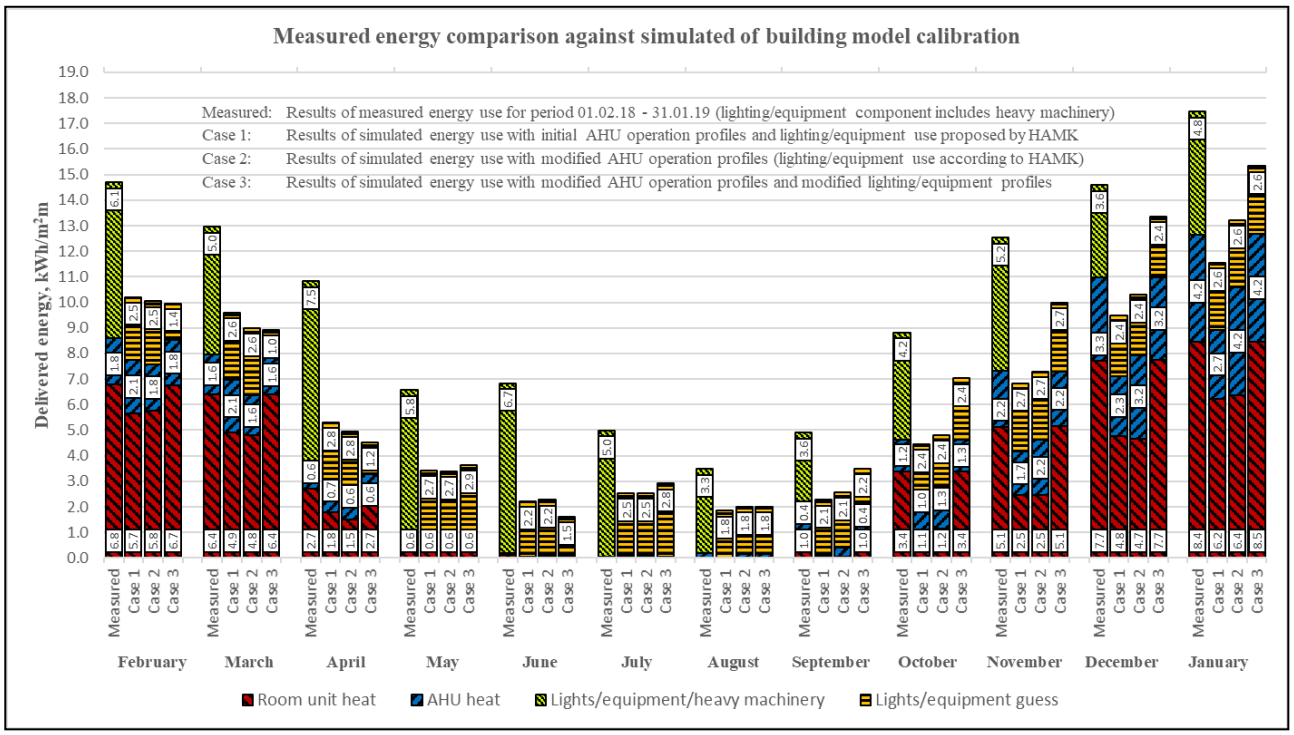

Fig. 4. Building model calibration results

However, as there significant measured and simulated AHU heat difference exists, it can be assumed that Case 1 AHU operational profiles proposed by HAMK do not match measured case scenario. Case 2 was generated specifically based on the assumption above, where initial AHU profiles were modified month by month to meet measured AHU heat on the monthly basis.

Table 2. AHUs working hours results

Month	AHU operational time					
	Case 1		Case 2		Case 3	
	hours/week					
	TK01	TK02	TK01	TK02	TK01	TK02
February	64	77	35	59	40	58
March	64	77	35	38	35	38
April	64	77	30	28	28	25
May	64	77	55	64	54	60
June	64	77	64	93	64	93
July	64	77	63	98	63	101
August	64	77	160	168	116	140
September	64	77	110	94	65	71
October	64	77	64	78	64	66
November	64	77	64	85	64	70
December	64	77	68	89	63	76
January	64	77	105	86	100	83
Average	**64**	**77**	**71**	**82**	**63**	**73**

As a result of calibration Case 2 (see Fig. 4), perfect match in simulated AHU heat of 23.3 MWh/a compared to measured 23.3 MWh was obtained in simulation with AHUs operational hours presented in Table 2. On the other hand, simulated room unit heat resulted in 41.1 MWh/a that produces a difference of -35% compared to the measured room unit heat i.e. practically same result as in Case 1. Assuming that building envelope thermodynamic properties were defined in coherence with building as built design documentation and indoor air temperatures setpoints were defined according to measured data with an hour resolution, significant simulated and measured room unit heat difference can be imposed by either inaccurate overestimated internal heat gains i.e. lights/equipment electricity use and/or additional sources of heat loss. Former can be explained by the lack of separate heavy machinery electricity use monitoring which led to initial guess regarding the lights/equipment internal gain from measured 90.9 MWh/a (heavy machinery included) to 44 MWh/a (heavy machinery excluded) i.e. ca -52% in first two simulated cases. Latter can be explained by the systematic cargo doors opening which behaviour is logged but due to the monitoring system failure could not be included in the modelling of first two cases. Additionally, some exhaust fans exist in laboratory part of the building, but their operation is not separately monitored and was neglected in the modelling. To further meet simulated room unit heat with the measured for completing the building model calibration procedure, either lights/equipment electricity use should be decreased and/or additional sources of heat loss should be implemented in the model. Case 3 was generated based on prior mentioned.

In Case 3 on Fig. 4 for a period of Feb – July lights/equipment electricity input data was scaled on the monthly basis which resulted in simulated room unit heat meeting measured. In same case for a period of Aug – Jan lights/equipment electricity was left unscaled and this input corresponded to Case 1 and Case 2, while cargo gates opening was implemented in the model which daily opening durations presented in Table 3. As a result of such modifications, internal gains for lights/equipment resulted in 37.3 MWh/a compared to 44 MWh/a of initial guess, while cargo doors were opened on average for 15 minutes per day within the year. In Case 3, additional modifications to AHU operational profiles of Case 2 were also conducted (see Table 2), to obtain perfect match in both simulated room unit heat and AHU heat.

Table 3. Cargo gates opening results

Month	Cargo gates opening		
	Case 1	Case 2	Case 3
	min/day		
February	0	0	0
March	0	0	0
April	0	0	0
May	0	0	0
June	0	0	0
July	0	0	0
August	0	0	20
September	0	0	43
October	0	0	32
November	0	0	42
December	0	0	30
January	0	0	12
Average	**0**	**0**	**15**

As mentioned in Section 2.2.5, simulations were performed by applying measured building weighted average temperature (solid red in left Fig. 5) as a heating system setpoint for each zone in the calibration IDA ICE building model. Building weighted average (BWA) temperature was calculated based on each zone specific heat loss and its measured hourly indoor air temperature. Fig. 5 (left) compares measured BWA temperature against initial design indoor temperature from simulations conducted in [10]. During the heating period of Feb – May and Oct - Jan measured BWA temperature was on average ca 1.54 °C higher than initial design indoor temperature. From the perspective of room overheating analysis, measured BWA temperature exceeded cooling setpoint of 25 °C during working hours of 08:00-17:00 for 135 °Ch. However, only rooms serviced by radiant ceiling panels are cooled via the connection to geothermal "free cooling" heat exchanger. Measured indoor air temperature in cooled room Hall 103 is depicted on Fig. 2 in yellow and peaked at +26.3 °C. In cooled room Hall 103 indoor air temperature exceeded cooling setpoint for 22 °Ch during working hours of the measuring period. According to Finnish and Estonian regulations, indoor air temperature should not exceed 100 °Ch during the summer period i.e.

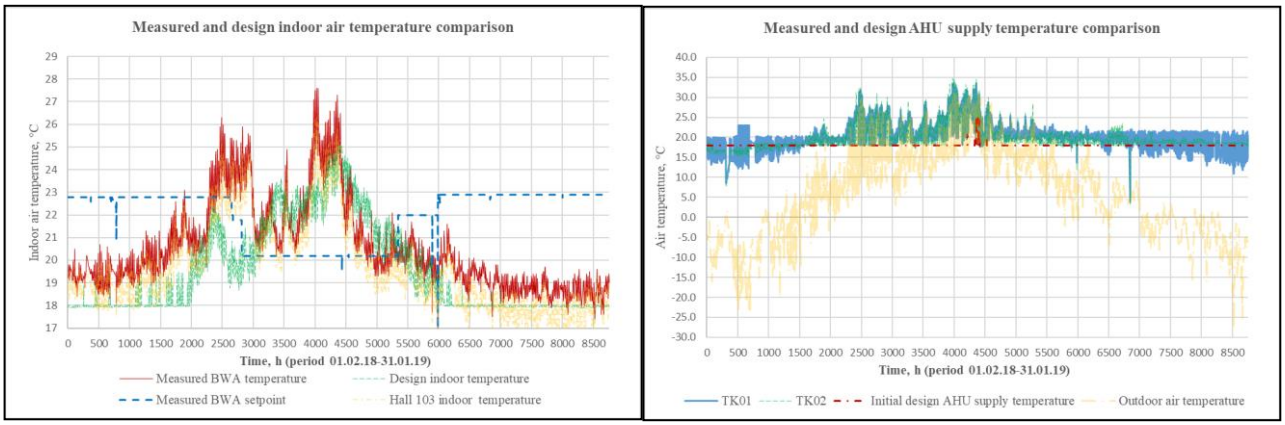

Fig. 5 (left) Measured and design indoor air temperatures. (right) Measured and design AHU temperatures

01.06 – 31.08 in test reference year (TRY) climate. Fig. 5 (right) compares measured AHUs TK01/TK02 supply air temperatures applied in simulations against initial design AHU supply temperature. On average, within the heating period, measured supply air temperature was ca 1 °C higher than initial design AHU supply air temperature in case of both AHUs. As built design lacks "free cooling" connection to AHUs and for this reason measured supply air temperature is much higher during cooling period than initial design supply AHU temperature.

3.2 Energy performance analysis results

Results of measured and simulated OLK NZEB energy performance for a period of 01.02.18 – 31.01.19 are presented in Table 4. Total number of presented cases is four. First one corresponds to a reference initial design case from [10]. Second case describes actual measured energy performance. Third case presents calibrated model energy performance with heat pump operation modelled in Excel according to installed heat pump performance map and measured evaporator/condenser

Table 4. Measured and simulated OLK NZEB annual energy performance results

	Case	Initial design (simulated SCOP)	Measured data (actual SCOP)	Calibrated model (Excel SCOP)	Calibrated model in TRY climate (Excel SCOP)
	Units	Specific annual energy consumption per floor area (kWh/m²a)			
Building	Delivered room unit heat	32.1	42.3	42.3	41.8
Building	Delivered AHU heat	9.5	15.5	15.5	15.5
Building	Delivered DHW heat	4.1	3.6	3.6	3.6
Plant	Top-up heating	2.8	14.9	0.3	0.3
Plant	Heat pump compressor	9.2	20.1	13.0	12.9
Plant	Cooling electricity	0.0	0.0	0.0	0.0
Plant	Fans electricity	9.2	9.5[1]	9.5	9.5
Plant	Pump electricity	2.0	2.0[1]	2.0[1]	2.0[1]
Plant	Lighting and equipment electricity	13.0	24.9	24.9	24.9
Plant	DHW electricity	1.5	4.5	4.5	4.5
	EPV[2]	**45(64)**	**91(129)**	**65(92)**	**65(92)**
	Units	Seasonal coefficient of performance value (SCOP)			
	Heat pump SCOP	**4.68**	**2.88**	**4.46**	**4.46**
	Whole plant heating SCOP	**3.28**	**1.97**	**3.80**	**3.80**
	Whole plant SCOP with DHW	**2.95**	**1.56**	**3.45**	**3.45**

[1]Pumps/fans electricity in measured case are estimated values. Measured data is only available as total AC equipment. Automation and BMS electricity were deducted.
[2]Energy performance value (EPV) is calculated with electricity primary energy factor of 1.2 and 1.7 in parentheses (valid for buildings constructed before 01.01.2018)

inlet/outlet fluid temperatures i.e. inlet to heat pump evaporator from geothermal heat exchanger and outlet from heat pump condenser to hot tanks. Fourth case describes calibrated model energy performance in TRY climate conditions with applied Excel calculated SCOP from the previous case. Energy usage components are depicted as delivered energy values that account for efficiencies and distribution losses of the heating/cooling system's generation and consumption side.

Compared to initial design case, measured heat consumption of hydronic heating system (room unit heat in Table 4) and AHU heating coil turned out to be ca 32% and ca 63% higher than in design case, respectively. On the other hand, domestic hot water (DHW) heat is ca 12% lower than in initial design case. Indoor climate conditions in measured case were less favorable in terms of heat consumption due to 1.54 °C higher average heating system setpoint temperature and 1 °C higher average AHU supply air temperature within the heating period. Initial design AHUs heat recovery temperature efficiency is slightly better i.e. n = 0.8 compared to as built AHUs n = 0.78. From the perspective of internal gains, measured case appliances (lighting and equipment electricity in Table 4) delivered

energy of 24.9 kWh/m^{2}a is ca 17.8 MWh/a i.e. ca 92% higher compared to reference case. Nevertheless, decrease in heat consumption due to higher appliance's internal gains is significantly reduced by the additional heat losses through cargo gate opening and lower overall solar radiation in measured case compared to reference. In reference case opening of cargo gates was not modelled. As mentioned in Section 3.1, cargo gates opening in measured case is a rough estimation due to malfunction of monitoring system and lack of appropriate separation in the logging/monitoring of lights/equipment/cooled heavy machinery electricity consumption which also led to rough estimation of measured appliances electricity. Impact of cargo gates opening on OLK NZEB heating need in calibration case is ca 32%. Impact of climate conditions on the heating need can be quantified by comparing measured case room unit heat of 42.3 kWh/m^{2}a against the calibration case in TRY climate room unit heat of 41.9 kWh/m^{2}a which yields a difference of ca 1.2%. On the other hand, comparison of measured and reference climate data resulted in measured degree days of 3803 °Cd against reference degree days of 3661 °Cd at balance point temperature of +15 °C. Additionally, the sum of measured diffuse and direct solar radiation is ca 2.8% i.e 23.4 MWh/a smaller in measured climate in comparison to TRY climate case within the heating period. There is a good agreement in almost matching fans electricity consumption of measured 9.5 kWh/m^{2}a against reference 9.2 kWh/m^{2}a. However, specific fan power (SFP) in measured case is slightly lower and on average AHUs operation duration was ca 13% higher compared to reference. Measured and simulated delivered room unit and AHUs heat are also presented in form of 24h moving averages on Fig. 7 (left) resulting in good agreement.

Results of seasonal coefficient of performance (SCOP) in Table 4 are divided into three categories – heat pump SCOP only accounts for AHU and room unit heat, whole plant heating SCOP also considers top-up heating and pumps electricity, the last one accounts additionally for domestic hot water (DHW) heat.

Table 5. measured and calculated COP results heating

Month	Measured cond.outlet	Measured evap.inlet	Calculated COP	Measured COP
Feb	46	7	4.82	1.26
Mart	49	5	4.19	2.01
April	48	12	4.68	1.99
May	55	13	3.53	1.52
June	55	15	3.24	0.94
July	55	17	2.90	0.26
August	55	15	3.24	0.78
Sept	55	12	3.80	1.77
Oct	54	9	3.86	2.32
Nov	54	8	4.12	2.73
Dec	50	4	4.21	2.26
Jan	48	3	4.16	2.67
Average	**52**	**10**	**3.90**	**1.71**

According to results, geothermal heat pump plant in measured case underperformed dramatically resulting in overall plant SCOP of 1.56 which compared to simulated initial design whole plant SCOP of 2.95 is ca 47% lower than was expected. Without accountancy for top-up heating, heat pump SCOP in measured case resulted in 2.88 compared to initial design 4.68 underperforming by 38%. Top-up heating electricity value represents the energy consumption at point when ON/OFF heat pump was not able to meet building heat demand (due to evaporator entering temperature reached 0 °C limit) and top-up heating would provide additional energy to keep temperature in hot buffer tank according to desired setpoint. In measured case top-up heating electricity

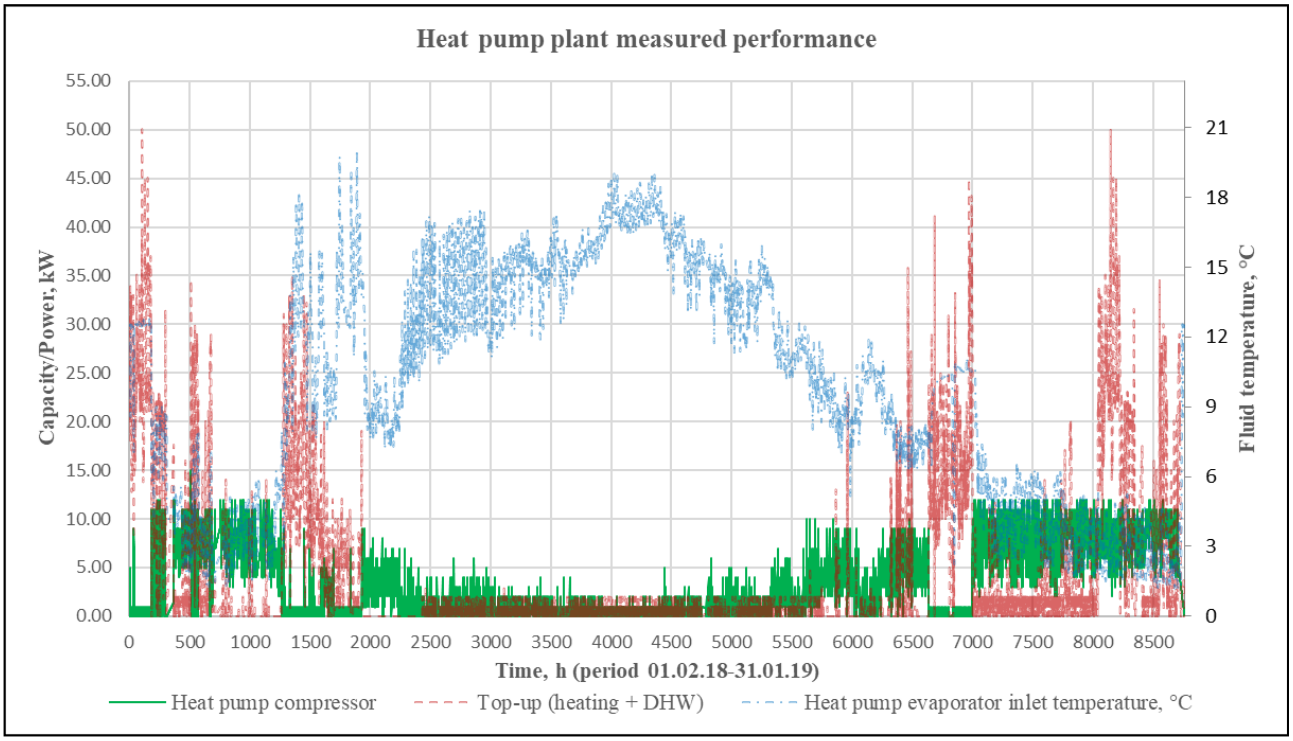

Fig. 6. Measured heat pump plant performance

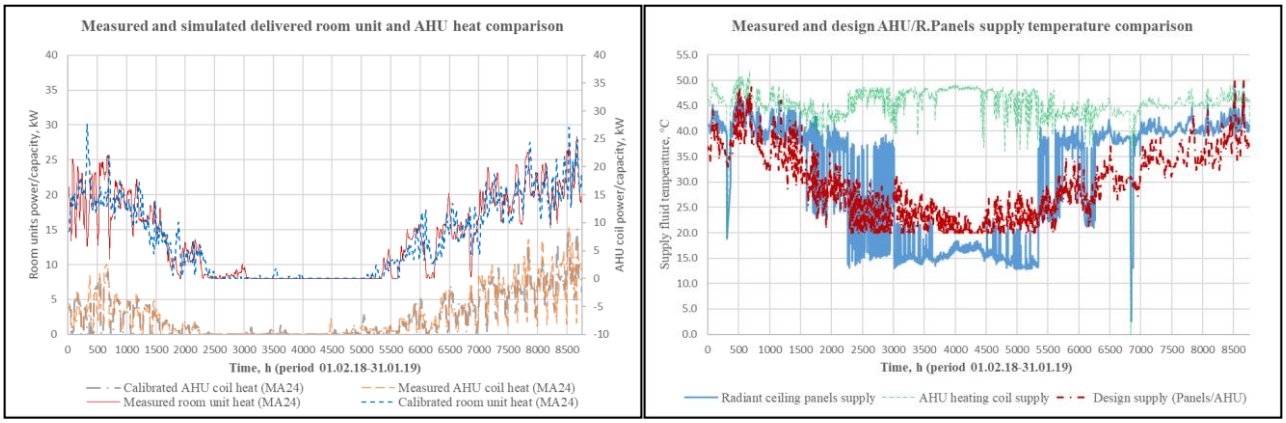

Fig. 7. (left) Measured and calibrated delivered heat. (right) Measured and design plant supply temperatures

consumption of 14.9 kWh/m^{2}a is ca five times higher than in initial design case 2.8 kWh/m^{2}a. Poor measured geothermal plant performance can be also observed on the monthly basis in Table 4, where in July measured average plant COP equals to 0.26. Low measured overall plant SCOP is caused by improper geothermal plant operation due to wrong control algorithms and/or faulty plant automation system, where top-up heating dominates as a heat source instead of heat pump. This can be observed on Fig. 6 where e.g. in the beginning of February (0 – 200 h) evaporator inlet fluid temperature was ca +12.5 °C i.e. supply fluid from energy piles and boreholes loop to heat pump was within the heat pump operation range, yet measured heat pump compressor power ranged in 0…1 kW barely operating, while top-up heating was operating with power of ca 20…55 kW. Same can be also observed in the beginning of April (1400 – 1500 h) and November (6700 – 7000 h). Also, during the cooling period (2500 – 5000 h), when mostly DHW consumption is present and geothermal loop fluid temperatures are within +10…+18 °C range, top-up heating is still operating, while according to initial design it should not. According to measured results, plant clearly operates not in coherence with initial design intent. To quantify the potential of geothermal plant in measured case conditions, heat pump performance was modelled in Excel with second-degree polynomial equations at an hourly time step based on the actual heat pump performance map data and measured evaporator inlet and condenser outlet fluid temperatures. This simplified modelling approach has known limitations and assumptions, where all thermodynamic processes in soil and geothermal heat exchanger (GHX) are neglected i.e. GHX and heat source are assumed to be infinite, heat pump evaporator inlet temperature corresponds to measured one and is not influenced by the operation of modelled heat pump. Hypothetically, results of this case roughly correspond to highest achievable SCOP at measured GHX temperature conditions based on the heat pump performance map data and measured secondary side temperatures. Whole plant SCOP with DHW modelled in Excel based on the measured data resulted in 3.45 i.e. 17% higher compared to simulated initial design case of 2.95 and ca 2.2 times higher compared to actual measured SCOP. It is worth to note, that actual installed heat pump model differs from one simulated in initial design case. However, in initial design case [10] SCOP was obtained as a result of detailed numerical simulation, which is far more accurate than simplified SCOP estimation approach applied in this study. Nevertheless, due to poor measured plant performance it was decided that a simplified SCOP estimation would be enough to quantify the possible best performance of actual as built plant.

Additional discrepancies in measured plant operation compared to initial design case can be observed on Fig. 7 (right), where according to initial design intent both AHU and radiant ceiling panels secondary side supply fluid temperatures were meant to be maintained according to a heating curve presented on Fig. 8.

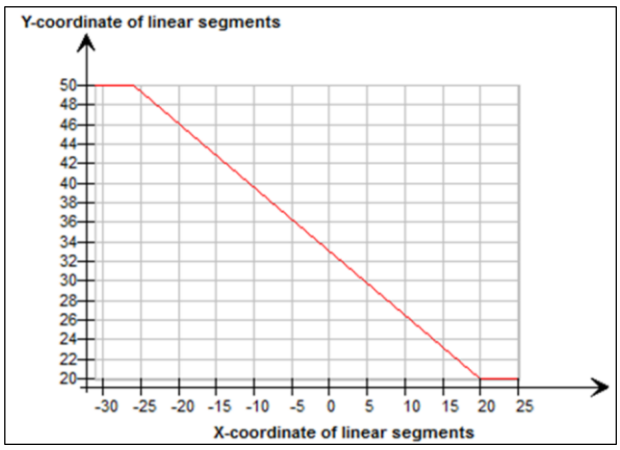

Fig. 8. Secondary side supply temperature schedule

Initial design heating curve at -26 °C outdoor air temperature value requires the supply side temperature to be equal to its maximal value of +50 °C decreasing with outdoor air temperature decline down to +20 °C when outdoor air temperature reaches a value of +20 °C. However, according to Fig. 7, measured AHUs supply fluid temperature is not dependent on the heating curve, while radiant ceiling panels supply temperature shows signs of dependency still being higher than designed. Latter might be explained by radiant ceiling panels not being capable of maintaining the desired setpoint (see Fig. 5 left) temperature, which in turn might result in

plant supply temperature increase. This negatively impacts the heat pump COP decreasing overall plant energy performance. According to heat pump performance modelling in Excel, installed heat pump with rating conditions capacity of ca 40 kW is capable of meeting ca 99.5% of heat demand in measured climate conditions.

Global goal of OLK NZEB design and construction was to reach Finland NZEB target [11] which is 135 kWh/m^{2}a of primary energy consumption in case of commercial hall-type building. Each case energy performance values (EPV) are presented in Table 4. Since 01.01.2018 new NZEB requirements took place in Finland [11], while initial design phase occurred in early 2014. Before year 2018 primary energy factor for electricity was 1.7 and after 1.2 in Finland. For convenience, EPV results presented in parentheses (Table 4) correspond to primary energy factor applied before year 2018. Initial design simulated EPV according to most recent primary energy factors resulted in 45 kWh/m^{2}a exceeding the Finland NZEB target by the factor of 3. On the other hand, measured case EPV resulted in 91 kWh/m^{2}a i.e. two times higher than initial design result. Nevertheless, measured case EPV complies with Finland NZEB commercial hall-type building requirements either with both pre and after year 2018 primary energy factors and carries official status of nearly zero-energy building. However, there is a room for improvement, as EPV in calibrated case with Excel modelled geothermal plant SCOP resulted in 65 kWh/m^{2}a i.e. ca 29% improvement in EPV compared to measured case scenario. As already discussed in this section, operation of plant automation system should be checked and adjusted/tuned for the plant to operate in accordance with initial plant design intent/control logics.

4 Conclusion

According to the results of the present study, main goal of designing and constructing OLK NZEB - a commercial hall-type building that complies with Finland NZEB requirements has been successfully achieved resulting in measured EPV of 91 kWh/m^{2}a i.e. ca 33% lower than the NZEB target value of 135 kWh/m^{2}a.

Analysis of measured geothermal heat pump plant performance and modelling revealed the discrepancies in plant operation that resulted in surprisingly low overall geothermal heat pump plant SCOP of 1.56 compared to initial design expectation of 2.95. Nevertheless, measured data analysis exposed inappropriate plant operation where electrical top-up heating dominated instead of heat pump, while heat pump on the other hand had favorable operating conditions but was not operating due to most likely inappropriately adjusted automation system. As an output of this study, it is suggested for the OLK NZEB building owner to check and readjust/tune the plant automation system to meet initial design intent/control logics. According to modelling results, prior mentioned adjustments could possibly lead to decrease of EPV up to ca 29% and overall plant SCOP increase of up to 3.45 according to simplified Excel based model. Also, in terms of heat pump COP increase, it is suggested to control AHUs secondary side supply temperature according to heating curve.

From the perspective of plant operation during cooling period, installed “free cooling” heat exchanger managed to deliver enough cool via radiant cooling panels system to observed room Hall 103 which resulted in indoor air temperature peak of +26.3 °C, while outdoor air temperature was +32 °C. According to Finnish and Estonian regulations, indoor air temperature should not exceed 100 °Ch during the summer period. In observed room Hall 103 indoor air temperature exceeded cooling setpoint for 22 °Ch, which perfectly meets the overheating regulations.

Building model calibration procedure confirmed that it is possible to reach a good agreement between measured and simulated results in IDA ICE simulation environment, which is capable of processing enormous amount of measured input data via source files and allows to perform high detail modelling. Despite the lack in separation of measured lighting/equipment/heavy machinery electricity, issues with monitoring cargo gates opening times and some missing measured data, non-measured AHUs airflows and fans electricity use, with some effort, assumptions and input data modifications, this study produced a calibrated monthly basis model using most of the available measured hourly based data as an input and achieved a very good agreement. For improvement of building energy performance, it is suggested to lower the indoor air temperature in building by ca 1.5 °C to meet the design intent, as measured weighted average indoor air temperature appeared to be ca 1.54 °C higher. Also, it is suggested to lower AHUs supply air temperature by 1 °C to meet the initial design intent.

This study unveiled the importance of building monitoring/logging system, especially in buildings with non-conventional custom heating/cooling plant design, as in actual operation plant may underperform dramatically. And specifically, for assuring the as designed heating/cooling plant and systems operation, it is extremely important to have an appropriate well-designed building monitoring/logging system in coherence with building model calibration needs. Based on this study, the following list of measured parameters with hourly resolution for whole year period to be included in building monitoring/logging system for conduction of successful detailed building model calibration in IDA ICE:

- Outdoor climate data (outdoor air temperature, relative humidity, wind velocity, wind direction, direct and diffuse solar radiation);
- Indoor air temperatures, setpoints;
- Plant primary and secondary side temperatures (including heat pump evaporator/condenser inlet/outlet, thermal storage components etc);
- Plant energy consumptions by component (heat pump compressor/condenser/evaporator, cooling equipment, top-up heating/cooling/DHW, circulation

pumps, AHU heating/cooling coils, buffer tanks primary secondary side energies, chillers etc);
• Internal gains data by component (lights, equipment, cooled equipment);
• AHUs energy and operation by components (supply/return air flows, fans electricity, supply/return air temperatures, air conditioning components energies/temperatures);
• Cargo gates/big-sized windows opening data.

This study will be continued with the assessment of improved/fixed OLK NZEB geothermal plant energy performance with accordance to suggestions presented in the present study.

This research was supported by Ruukki Construction Oy, Terveellinen digitalo -hanke, EAKR-hank A72991, Estonian Centre of Excellence in Zero Energy and Resource Efficient Smart Buildings and Districts, ZEBE (grant No. 2014-2020.4.01.15-0016) funded by the European Regional Development Fund and by European Commission through the H2020 project Finest Twins (grant No. 856602).

References

1. Directive 2010/31/EU of the European Parliament and of the Council of 19 May 2010 on the energy performance of buildings, *Official Journal of the European Union*, (2010)
2. J.W. Lund, T.L. Boyd, Direct utilization of geothermal energy 2015 worldwide review, *Geothermics*, **60**, p.66-93, (2016)
3. Y. Hamada, H. Saitoh, M. Nakamura, H. Kubota, K. Ochifuji, Field performance of an energy pile system for space heating, *Energy and Buildings* **39(5)**, p.517-524, (2007)
4. D. Pahud, M. Hubbucj, Measured Thermal Performances of the Energy Pile System of the Dock Midfield at Zürich Airport. *Proceedings European Geothermal Congress 2007*, Germany, (2007)
5. J. Fadejev, J. Kurnitski, Energy pile and heat pump modeling in whole building simulation model, *2nd IBPSA-England conference on Building Simulation and Optimization*, United Kingdom, (2014)
6. F. Reda, Long term performance of different SAGSHP solutions for residential energy supply in Finland, *Applied Energy*, **144(0)**, p.31-50, (2015)
7. K. Allaerts, M. Coomans, R. Salenbien, Hybrid ground-source heat pump system with active air source regeneration, *Energy Conversion and Management,* **90(0),** p.230-237, (2015)
8. J. Fadejev, R. Simson, J. Kurnitski, F. Haghighat, A review on energy piles design, sizing and modelling, *Energy*, **122**, p.390-407, (2017)
9. J. Fadejev, J. Kurnitski, Geothermal energy piles and boreholes design with heat pump in a whole building simulation software, *Energy and Buildings,* **106(0),** p.23-24, (2015)
10. J. Fadejev, R. Simson, J. Kurnitski, J. Kesti, T. Mononen, P. Lautso, Geothermal Heat Pump Plant Performance in a Nearly Zero-energy Building, *Energy Procedia,* **Sept 2016**, p.489-502, (2016)
11. Ympäristöministeriön asetus uuden rakennuksen energiatehokkuudesta, (2017)
12. T. Kalamees, K. Jylhä, H. Tietäväinen, J. Jokisalo, S. Ilomets, R. Hyvönen, S. Saku, Development of weighting factors for climate variables for selecting the energy reference year according to the EN ISO 15927-4 standard, *Energy and Buildings*, **47**, p.53-60, (2012)

Publication 5

Ferrantelli A, Fadejev J, Kurnitski J. A tabulated sizing method for the early stage design of geothermal energy piles including thermal storage. *Energy and Buildings*, Vol. 223 Art.No. 110178 pp. 1-16. 2020.

Energy & Buildings 223 (2020) 110178

Contents lists available at ScienceDirect

Energy & Buildings

journal homepage: www.elsevier.com/locate/enb

A tabulated sizing method for the early stage design of geothermal energy piles including thermal storage

Andrea Ferrantelli [a,*], Jevgeni Fadejev [a,b], Jarek Kurnitski [a,b]

[a] Tallinn University of Technology, Department of Civil Engineering and Architecture, 19086 Tallinn, Estonia
[b] Aalto University, Department of Civil Engineering, P.O.Box 12100, 00076 Aalto, Finland

ARTICLE INFO

Article history:
Received 7 April 2020
Revised 13 May 2020
Accepted 21 May 2020
Available online 3 June 2020

Keywords:
Energy piles
Ground source heat pump
Renewable energy
Computer simulations
Parametric studies

ABSTRACT

Geothermal systems are often employed for both the heating and cooling of sustainable constructions. Energy piles (U-shaped heat exchangers inserted into the foundation piles) are widely included in these installations, whose performance is usually estimated by means of complex, time-consuming simulations already at an early design stage.

Here we propose a simple methodology, where a hand calculation tool provides the condenser yield per pile meter, ground area yield and demand covered by the heat pump by specifying only building heat load and geometric characteristics of the energy piles field. Our tool is tested by assuming 20 years of operation in a hall-type commercial building in a cold climate. A validated IDA-ICE parametric study couples the heat pump evaporator operation with heat transfer processes between energy piles and soil. Various system configurations are considered and thermal storage in the soil is included.

We find that the expected yield is not directly proportional to pile separation, while a smaller extraction power is favoured. Thermal storage in the soil is also confirmed to be critical. Besides our specific quantitative results, our practical guideline is qualitatively general and can be extended to any given building type and climate.

1. Introduction

Energy efficient buildings constitute one of the primary concerns of the construction industry. Future structures will be subject to increasingly stringent energy consumption constraints [1], making renewable resources and their usage a prominent field of investigation.

Geothermal energy is one of the most compelling candidates [2,3], due to feasibility of installations and possibility of hiding them underground. The heat stored inside the ground is typically extracted by ground-source heat pumps via ground heat exchangers (GHE) [4], recovering thermal energy that can satisfy even the district heat demand [5]. In this paper we shall discuss a GHE system known as geothermal energy piles [6,7], i.e. heat exchange piping that is installed into the pile foundations. Similar to employing boreholes for geothermal energy extraction [8–10], this method is economically favoured since the GHE can be installed into an already existing foundation pile.

The design of these systems is naturally complex and needs to be performed in several stages. In conceptual design, the feasibility of heat pump and energy pile system can be forecasted with rough estimates of heating and cooling needs, which typically change as the design evolves. At this stage it is important to estimate approximately the energy pile field size and the heat pump capacity, while explicit system configurations can be simulated and sized later on.

As a matter of fact, no simple methods to obtain such preliminary estimates currently exist. Here we attempt to fill this gap by developing a hand calculation method for the early stage design of the *entire* geothermal system, including energy piles as well as heat pumps. The user is only required to input the system parameters (heat pump evaporator sizing, COP, geometry of the energy piles field...), without having to do any computation.

In other words, our tool allows to quickly produce performance estimates at a preliminary design stage. While doing so, it also provides the necessary boundary conditions for thorough computer simulations that are to be performed in later design stages, when accurate building and system configuration data are available.

Our tabulated method is grounded on a comprehensive parametric study of the long-term performance of the entire

* Corresponding author.
E-mail address: andrea.ferrantelli@taltech.ee (A. Ferrantelli).

https://doi.org/10.1016/j.enbuild.2020.110178
0378-7788/

geothermal system, performed with IDA-ICE 4.61 [11], which investigates the coupling of heat transfer processes among the GHE inside the ground with the heat pump above. The numerical simulation was validated in [12] with field measurements of a comparable installation, and it included the effect of floor surface temperature and thermal storage profile.

Specifically, heat transfer processes between energy piles and surrounding soil are naturally complex [7], and have been studied already for many years with different methodologies [13]. The according calculations are naturally involved, due to the geothermal system size, convection inside very long pipes, and uneven thermal properties of soil at different locations and depths [14,15].

Analytical attempts to model this phenomenology date back to some classic works from the 1980s (e.g. [16], see also the review [17]). Whilst a number of successful results does exist in the literature [18–20], it is very hard (if not impossible) to solve the heat transfer equations analytically for the full geothermal system.

Numerical simulations have instead proven to be effective in the energetic assessment of concrete geostructures [14,21], since they can account for the whole system without critical simplifications. A recent FEM model found the number of pipes to be the most influential design parameter [22], while the parametric studies performed in [23] investigated the effect of pile geometry on the overall performance.

A realistic performance assessment of the full geothermal plant should include the coupling to heat exchangers and pumping system as well, see e.g. [14,15,24]. Studies addressing the yearly performance of specific configurations revealed indeed a critical influence of thermal cycles and a performance loss due to the building's unbalanced heating and cooling loads, which hinder the soil to recover by itself [25,26].

The present work follows this line of thought. We performed a full parametric study of the coupled system GHE installation-heat pumps, and used it to develop our tool for preliminary geothermal plant design.

We considered the energy piles' performance for a commercial hall-type building by simulating with IDA-ICE the long-term performance of about 120 different energy piles configurations, Fig. 1.

Our results address two different pile lengths, with evaporator sizing power [W/m] and expected yield per pile unit length [kWh/ma], as well as per ground surface area [kWh/m2a], listed in function of the pile separation. We also calculated the energy demand covered by the heat pump and provided a specific example of our design tool with a geothermal system sizing guide. This paper extends the study discussed in [27], where only piles buried in clay with no energy storage were considered.

The article is organized as follows: the building model is discussed in Section 2.1, and our method is highlighted in Section 2, addressing building modelling, heat pump load profile, floor surface temperature, thermal storage profile and top-up sizing simulation. Our results are discussed in Section 3 and a sizing guide is illustrated in Section 4 with an example. Results for a randomization of 16 cases are shown in Section 4.1, and we finally discuss the full body of our results and draw our conclusions in Sections 5 and 6 respectively.

2. Methods

2.1. Building model and case study parameters

Our case study corresponds to the building geometry and envelope parameters reported in Table 1. The design heating load at −26 °C is plotted in Fig. 2 and amounts to about 465 kW, which is the sum of Air Handling Unit (AHU) heating coil power (290 kW) and heat pump evaporator power (170 kW). The weather data source for location and input parameters for the energy piles field are shown in Table 2; we considered an average annual ground temperature of 5.62 °C.

The operation performance of energy piles and boreholes is usually assessed on a simulation period of 20 years [6,17]. In order

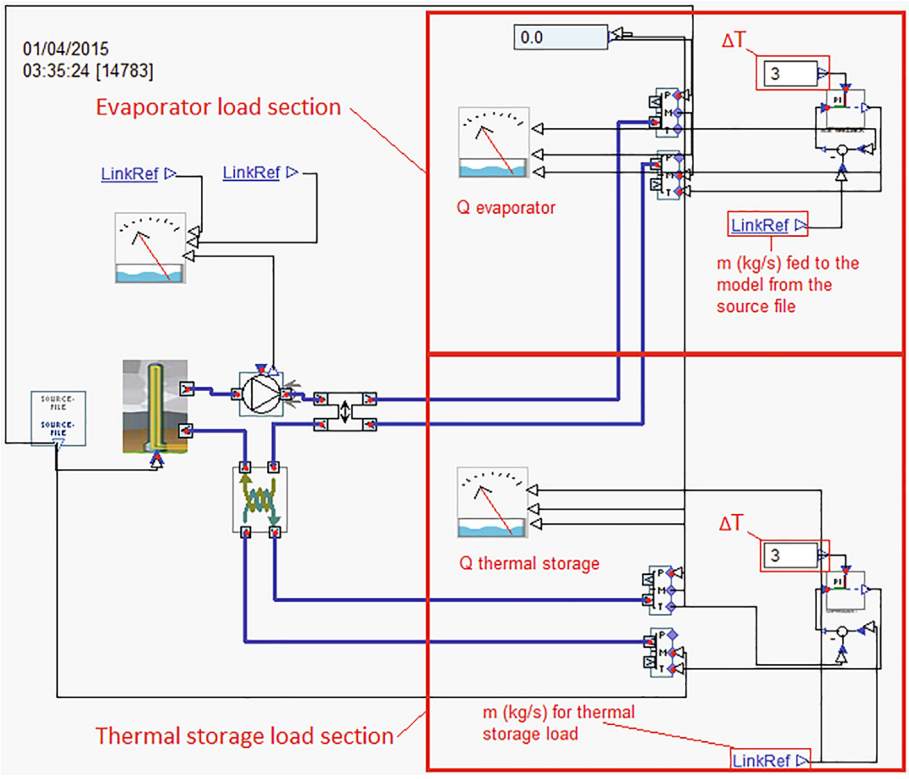

Fig. 1. Simulation model based on the source file.

Table 1
Building model parameters for the reference simulation.

Building and envelope		
Building size	66 × 137.4	m
Roof (310 mm) U	0.12	W/(m^{2}K)
Floor (EPS100) U	0.09	W/(m^{2}K)
Walls (Sandwich 230 mm) U	0.16	W/(m^{2}K)
Windows (SHGC 0.51) U	1.0	W/(m^{2}K)
Air tightness q_{50}	2	m^3/(m^{2}h)
Fresh air flow	1.1	l/(s m^2)
Heat gains and occupancy		
Occupant	2	W/m^2
Lighting	8	W/m^2
Equipment	1	W/m^2
Occupancy period (6d/7d)	8:00–21:00	–
Occupancy rate	1.0	–
AHU heat recovery	80	%

Table 2
Input parameters for the energy piles field.

Field size	30 m × 30 m
Pipe size	DN 20
Pile diameter	170 mm (Double U-pipe), (125 mm special cases)
Depth in the ground	15 m, 30 m
Distance between piles	3 m, 4.5 m, 6 m
Ground heat conductivity	Clay 1.1 W/(mK), Silt 2 W/(mK)
Ground volumetric heat capacity	Clay 3343 kJ/(m^{3}K), Silt 4259 kJ/(m^{3}K)
Fluid type	Ethanol
Thermal storage ratio	0%, 50%, 100%
Heat pump design power (evaporator)	20 W/m, 40 W/m, 60 W/m, 80 W/m, >100 W/m
Heat pump power to heat demand ratio	50%
Climate file	Helsinki-Vantaa 2012

to make all the considered cases comparable, the envelope size was varied according to the heat pump power (always sized at 50% of the total heating demand). Besides, 15 different building models were created to account for various energy piles' total length and specific heat extraction rate [W/m].

A detailed IDA-ICE simulation for a single case may take up to 3 days, therefore we isolated the GHE by replacing heat pump and building with an hourly time-step, which was based on the heat pump evaporator load data, as the piles' input.

E	energy amount [Wh]
$\dot{Q}_{evap}$	evaporator load [W]
$\dot{Q}_{cond}$	building heat load [W]
L	pile length [m]
E/L	specific yield per unit length [kWh/m]
$\dot{m}$	mass flow rate [kg/s]
ΔT	temperature difference [K]
c	specific heat [J/kgK]
T_{outlet}	brine outlet temperature [°C]
T_{inlet}	brine inlet temperature [°C]

In theory, such data depend on each specific heat pump size and annual operational profile. The latter is determined by the building instantaneous energy demand, therefore by running a simulation for the model defined in Table 1 (our "benchmark case"), we generated the annual building load profile in Fig. 3, namely the hourly time-step load data for the heat pump evaporator. These will be used for each simulation, since the upper limit (1.0) in Fig. 3 corresponds to the building design heat load at −26 °C. In other words, each case is generated by using only one input parameter – the design heat load.

The benchmark model is based on an analogous three dimensional borehole field simulation that was introduced and experimentally validated in [12]. The IDA-ICE model was capable of predicting the measured borehole and ground temperatures with excellent accuracy. Ground surfaces also showed to be critical as boundary conditions, and earlier results showing a performance reduction over the years (see e.g.[25,26]) were verified. We will confirm the importance of thermal storage as well in Sections 3.3 and 3.4.

2.2. Heat pump load profile and operation

Fig. 1 illustrates the heat pump modelling. The evaporator load $\dot{Q}_{evap}$ [W] is defined as

$$\dot{Q}_{evap} = \dot{m}c\Delta T, \quad (1)$$

where $\dot{m}$ [kg/s] is the mass flow, c [J/kgK] the brine specific heat capacity and ΔT [K] the temperature difference between borehole outlet and inlet. Our model is operating at partial load within the

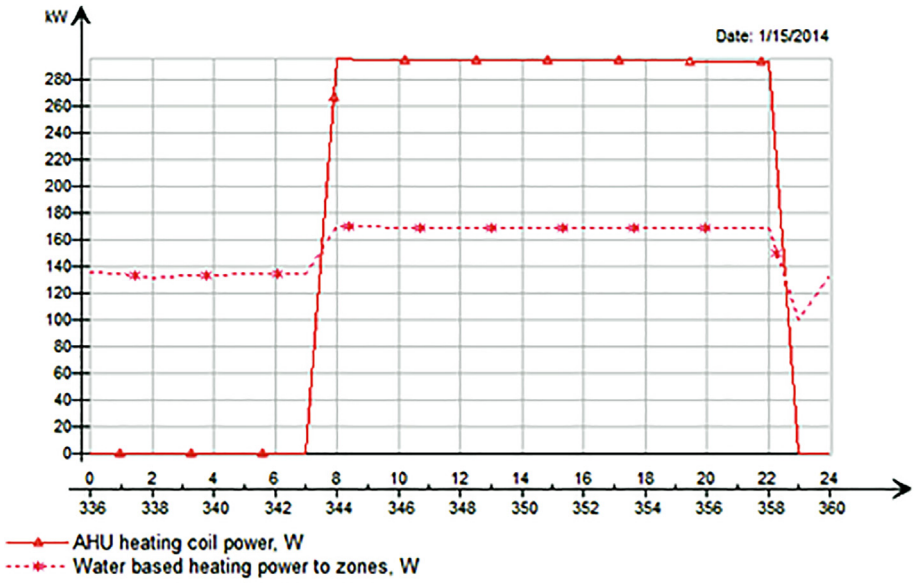

Fig. 2. Building heating load for a design T = −26 °C.

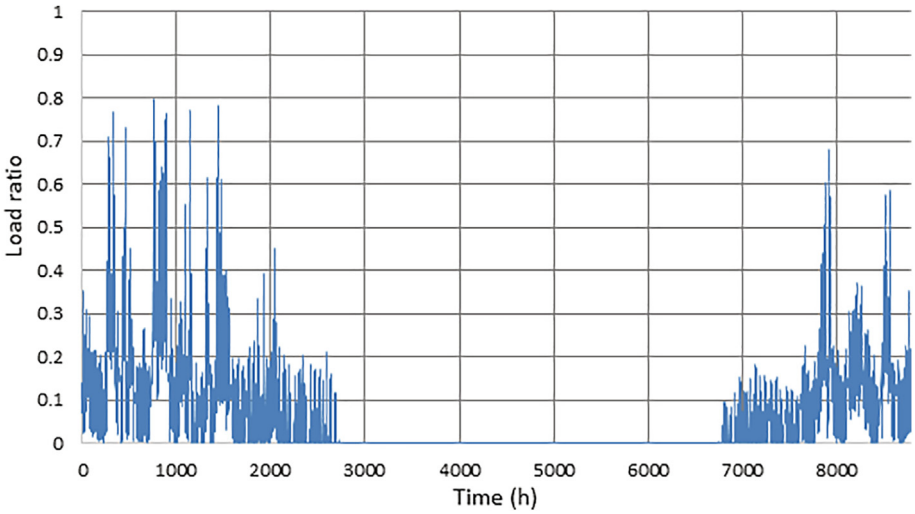

Fig. 3. Building load profile for the benchmark simulation.

range 0–100% (a sort of design limitation, since an actual heat pump will operate at ~30–100%).

Heat pumps can operate with two modalities, i.e. at constant (on/off) load or with partial (inverter) load. In the case of constant load operation, the heat pump is turned ON and will operate at full load under heat demand. Otherwise, the inverter heat pump manages a partial load operation between ca 30% and 100%. Since as discussed we use as input some hourly average (dynamic) data generated from the benchmark profile, our heat pump can operate at partial load. Our results are accordingly applicable only to plants provided with inverter heat pumps.

The heat pump evaporator load data are generated from the building load data, which are based on the annual average COP of the heat pump. The mean annual ground T and the resulting average brine temperature were assumed to remain in the 0 °C to 10 °C range during operation. An annual average heat pump COP of 4.5 was assumed, according to heat pump performance map data (Fig. 5) with a condenser side outlet temperature of 45 °C. This is justified by the long simulation period, which will compensate small fluctuations in the soil temperature together with the according deviations from the average COP value. In Fig. 4, the evaporator load profile is presented in green colour and the heat pump condenser load in yellow, while top-up heating should cover the remaining amount in red.

The evaporator load data thus generated were fed to a simulation model based on a source file shown in Fig. 1. This requires input of annual (8784 h) hourly time-step data of both liquid mass flow [kg/s] of the heat pump evaporator load and eventual thermal storage load. Due to the IDA-ICE specifics, hourly loads cannot be fed directly as units of power [kW], so we developed a specific control to maintain a predefined temperature difference ΔT, with a variable mass flow [kg/s] that is fed from the source file to the model.

The control logic in our model is the following. First, the borehole outlet temperature depends on the inlet temperature, flow and thermal processes that occur in the fluid-borehole-soil system (those are computed by the borehole model). To avoid frost heave, soil temperatures should not drop below 0 °C, while for short periods of time we can tolerate a borehole inlet temperature of −1 °C, which we use as a preset limit. We accordingly simulate a heat pump turning off due to a low evaporator inlet fluid temperature.

As the liquid mass flow data enter the energy piles model input, a feedback controller measures the brine outlet temperature and supplies a new inlet T, which is computed according to a pre-set

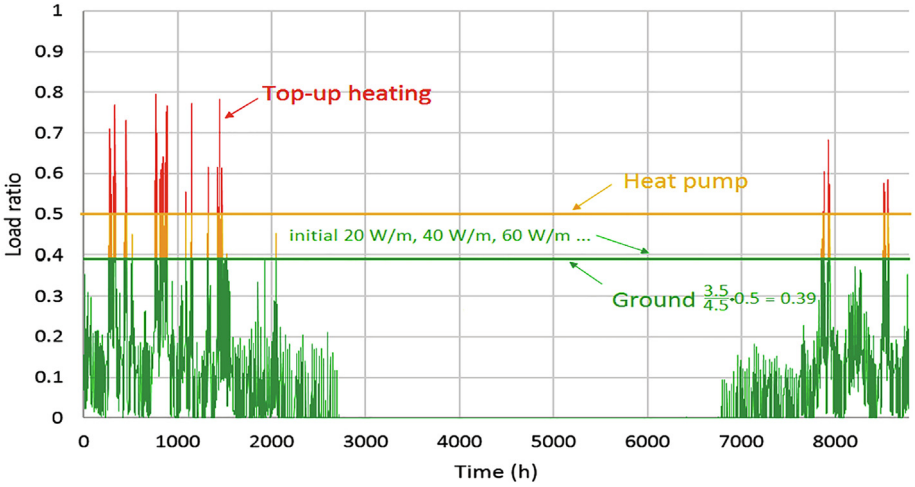

Fig. 4. Annual load profile for the heat pump evaporator.

$\Delta T = T_{outlet} - T_{inlet} = 3$ °C. The source file provides, at intervals $\Delta t = 1$ h, a mass flow $\dot{m}$ corresponding to the building heating demand. Our borehole model then calculates the outlet temperature based on the inlet temperature and brine flow. The model calculates T_{inlet} by using the preset ΔT for most of the time (see the paragraph below for the exceptions). For a given mass flow and inlet temperature, the borehole model can accordingly calculate the new outlet temperature before starting a new cycle. Eq. (1) allows to create source files by using the mass flow [kg/s] as the only parameter, once the building heat load is converted into evaporator load with the formula

$$\dot{Q}_{evap} = \dot{Q}_{cond}(COP - 1)/COP, \quad (2)$$

for the heat pump evaporator sizing.

The $\Delta T = 3$ °C value is in reality "semi-constant", to guarantee avoidance of the frost heave. Let us recall that we demand $T_{inlet} \leqslant$-1 °C, and consider two extremal cases to illustrate this functionality: an extremely large and an extremely small pile field.

- For the very large case, the soil initial temperature is 5 °C. Outdoors are very cold, the heat pump starts working, the source file feeds the brine flow into the model. The last known outlet temperature (which will be 5 °C as in the soil) is then used to calculate the inlet temperature, namely 5 °C – ΔT = 2 °C. Because our borehole field is nearly infinitely long, it might happen that locally $T_{outlet} < 5$ °C, depending on the thermal resistances between fluid, energy pile and soil. If for instance T_{outlet} = 3 °C, which as an average is a substantial drop, T_{inlet} = 0 °C. This way we can account for local drops in soil temperature and still avoid frost heave: the heat pump will be able to operate anytime and cover the whole building heat demand as designed.
- Now the pile field is extremely small, thus very sensitive to thermal inhomogeneities in the soil. The boundary conditions are the same as above. The heat pump starts operating and the building heat demand cools down the soil due to the small heat exchange area of the piles field.
  With T_{outlet} = 2 °C, T_{inlet} = −1 °C, thus hitting the threshold value that blocks the pump. So now the flow still comes from the source file, but the inlet temperature is fixed to −1 °C. The borehole model will therefore calculate the outlet temperature based on these conditions, returning a T_{outlet} that may become smaller than 2 °C. If we assume it to be 1 °C, then ΔT = 1 °C – (-1 °C) = 2 °C < 3 °C. As 2 °C is now smaller than our original preset, the heat pump was not able to account for the whole building heat load, but it managed to cover only 2 °C/ΔT ∼66% of the actual load.

Once the simulation is completed, we compare the calculated value to the initial evaporator load that was used in the source file, making it possible to determine how much top-up energy is needed to fulfil the building heating demand.

2.3. Floor surface temperature

In buildings with energy piles, the floor heat loss to the ground provides a so-called "free thermal storage" effect that can substantially increase the piles' performance. This was easily implemented in IDA-ICE by feeding the floor surface temperature to the GHE model as a ground surface T, see Fig. 6. The floor thermal properties are defined in the energy piles model, Table 1.

The estimation is based on a 20-years averaged ground temperature, which is calculated for every year by estimating the floor heat loss induced by the volumetric heat capacity of the energy piles field ground mass. As the floor heat loss over time will heat up the ground under the building, the heat amount that is lost through ground annually will vary from year to year. After obtaining an average ground temperature for 20 years, the annual floor heat loss amount can be easily calculated analytically by using heat conduction equations. This also implies that the "free storage" energy amount is a function of energy piles length and ground types.

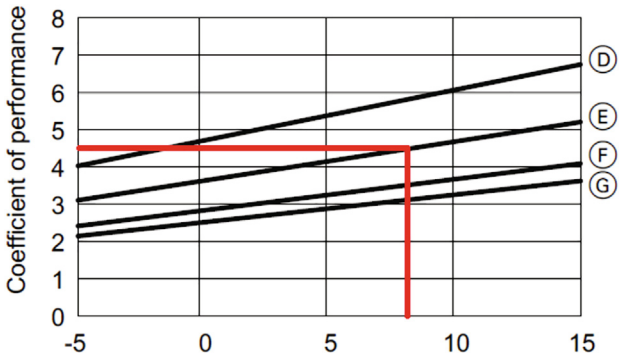

Fig. 5. Heat pump performance graph.

2.4. Thermal storage profile

The hourly load data of solar thermal storage (either 50% or 100%) are logged rather similarly to the heat pump evaporator load data we discussed in Section 2.2. For each case, these are generated from a benchmark solar storage profile (Fig. 7), which was obtained by modelling in IDA-ICE a solar collector with orientation 300° and angle 40°, connected to the energy piles inlet pipe via heat exchanger.

In the cases with thermal storage, the total annual amount of stored energy equals the sum of solar storage and floor heat loss (i.e. the "free storage" energy plotted in Fig. 6). The latter is estimated in MS Excel by assuming a 20-years average for the ground temperature, which is computed for each year from volumetric heat capacity of the soil surrounding the GHE and from floor heat losses. As the floor heat loss will gradually heat up the ground under the building, the annual heat loss through the ground will vary from year to year.

Once a 20-years averaged ground temperature is obtained, the energy provided annually by floor heat loss can be easily calculated using standard heat conduction equations.[1] The thermophysical characteristics of the soil region surrounding the building floor slab are listed in Table 3.

2.5. Top-up sizing simulation

The inverter heat pump was sized at 50% of the building design load, while the remaining peak load was meant to be covered with top-up heating. Due to the unsteady performance of the energy piles, the inverter heat pump can operate at full load only for a limited amount of time, i.e. until the fluid in the evaporator circuit falls below ∼-3 °C, stopping the heat pump.

When this occurs, a top-up heating sized e.g. at 50% might not be capable to fully cover the building heat demand. To determine the optimal size of top-up heating, we therefore developed a sizing scenario in critical conditions. An additional building load profile was developed and converted to the heat pump evaporator load profile. The first three years of operation were computed following

[1] It should be noted that such energy amount from free storage varied according to piles' length and ground types.

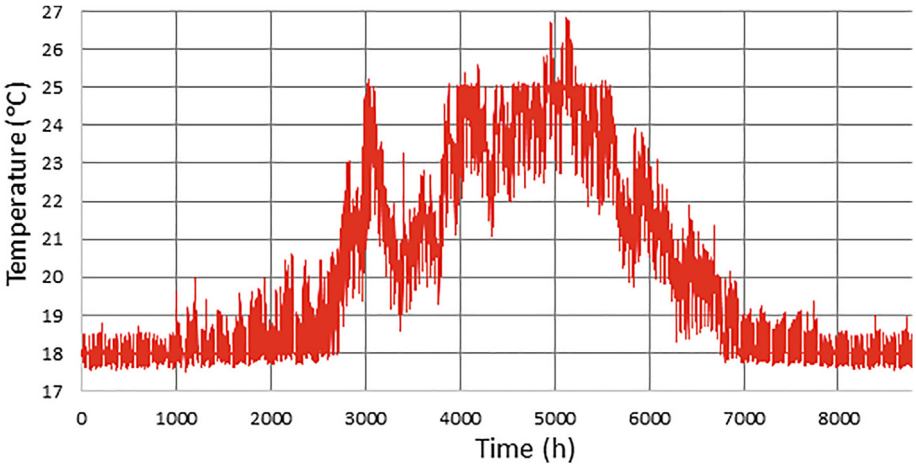

Fig. 6. Annual floor surface temperature profile.

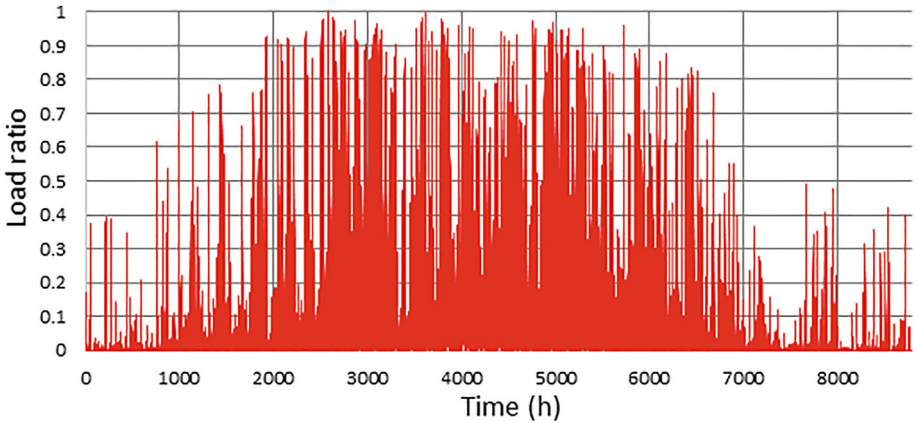

Fig. 7. Annual thermal storage profile.

Table 3
Soil thermal properties.

Material	λ W/mK	Porosity %	Saturation %	Bulk density kg/m^3	Wet density kg/m^3	Volumetric heat capacity kJ/(m^{3}K)	Heat capacity J/(kg K)
Clay	1.1	56	100	1250	1812	3343	1845
Silt	2	31	100	1529	1835	4259	2321

a Test Reference Year (TRY), while for the fourth year we set a temperature between −20 °C and −26 °C for two January weeks. We then logged the heat pump output power at the 14th day of operation in such extreme conditions, and compared the minimal output to the sized value. The sizing of top-up heating for specific cases was then calculated.

3. Energy pile field simulations

In this work we performed simulations concerning energy piles with 3 m (121 piles), 4.5 m (48 piles) or 6 m (36 piles) pile separation, that were buried in either clay or silt. For each case study, the design heat load and annual heating demand were obtained from the benchmark simulation that was described in Section 2.1, by accordingly rescaling the building load profile in Fig. 4.

For easy reference, our results are summarized in Tables 6–10 and divided into eleven categories, comparing different pile lengths and thermal storage amounts as well as addressing the impact of pile outer diameter and brine temperature[2].

As an example, Fig. 8 gives the results for the simulated condenser yield [kWh/m a] (dashed line) and evaporator sizing power [W/m] (solid line) in function of the pile spacing [m] for a heat pump evaporator sized at 215 kW, with the following parameters: 200 W/m, clay, 6 m spacing and 30 m length.

3.1. Top-up heating

The results of top-up heating sizing simulations are illustrated in Table 4. The percentage values represent the top-up heating ratio to the total building design heat load. For example, at −26 °C this holds as 100 kW; for 30 m-long energy piles, buried in clay with 3 m spacing and sized according to the case

[2] The missing entries correspond to cases where the heat pump was oversized.

Table 4
Results for the top-up heating sizing. The entries marked with * consider 100% thermal storage.

Case description	clay				silt			
	step 3 m		step 6 m		step 3 m		step 6 m	
	15 m	30 m	15 m	30 m	15 m	30 m	15 m	30 m
60 W/m, 0% storage	82%	85%	83%	84%	79%	81%	75%	79%
60 W/m, 50% storage	82%	83%	84%	85%	75%	80%	75%	79%
80 W/m, 50% storage	81%	82%*	83%	85%*	79%	81%	79%	81%
200 W/m, 100% storage	85%	85%	88%	89%	82%	82%	85%	87%

Table 5
Simulated condenser and total yield for 60 W/m evaporator sizing.

Pile spacing	Condenser yield	Total yield
6 m	44 kWh/m	103 MWh
4.5 m	39 kWh/m	91 MWh
3 m	27 kWh/m	63 MWh

"60 W/m without storage", the appropriate top-up heating should be 85% of 100 kW, namely 85 kW.

We should remark that the values in Table 4 are calculated for those cases where the heat pump and thermal storage source were sized according to our results as reported in Tables 6–10. For the "60 W/m with 50% storage" case, with 15 m-long piles that are buried in clay with 3 m spacing, sizing the heat pump evaporator to power 49 W/m with 20 kWh/m solar thermal storage determined a top-up heating sized at 82% of the total design heat load.

3.2. Energy piles without thermal storage

The effect of energy piles spacing for different simulated initial design loads of the evaporator is here investigated without thermal storage. The energy piles, either 15 m or 30 m long, are buried in clay or silt and 6 m, 4.5 m and 3 m separations correspond to 36, 48 and 121 piles respectively. The results for silt are reported in Table 6, while those for clay are illustrated in [27].

3.3. Energy piles with thermal storage, 50%

Here we add the effect of thermal storage and consider 50% TS for both 15 m-long and 30 m-long piles. Tables 7 and 8 report the amount of thermal storage that was applied in the simulations to reach 50% of the ideally expected ground heat extracted at the evaporator side, according to the building load profile in Fig. 3.

3.4. Energy piles with thermal storage, 100%

Results for a 100% thermal storage amount are reported in Tables 9 and 10.

3.5. Impact of the outer diameter on performance

Our simulations of a double U-pipe have compared 170 mm and 125 mm pile outer diameters. The results of 20 simulations show that, if compared to a 170 mm pile, a 125 mm pile will be less efficient by ∼2% in clay and ∼1% in silt. This confirms earlier findings reported in [22,28], namely that pile diameter is not important for heat transfer efficiency. Some results for the brine outlet temperature, for the first 20 years as well as only for the last year, are displayed in Figs. 13–18.

4. Sizing guide: an example

Our simulation results are here utilized to highlight a method for the preliminary sizing of a geothermal plant, in the form of a sizing guide addressing a specific example. Using the heat pump evaporator sizing $\dot{Q}_{evap}$ in Eq. (2), with COP = 4.5 as discussed in Section 2.2, the energy piles length is derived as $L = \dot{Q}_{evap}/(W/m)$. Depending on the building design heat load Q and annual energy need E, we shall now estimate the approximate piles length (or number) and their performance. The suggested steps are the following:

1. **Determining building design heat load and annual heating energy need.**
   Consider a commercial hall-type building with design heat load (at design temperature −26 °C) $\dot{Q}$ = 360 kW and annual energy need E ∼183 MWh.
2. **Sizing the heat pump evaporator.**
   First, the heat pump condenser sizing $\dot{Q}_{cond}$ needs to be estimated. According to the building load profile in Fig. 4, a con-

Table 6
Summary of the study results in table format, 20 W/m - 60 W/m, no thermal storage, silt.

			Silt					
			spacing 3 m		spacing 4.5 m		spacing 6 m	
			15 m	30 m	15 m	30 m	15 m	30 m
No thermal storage	20 W/m	power, W/m	20	20	20	20	-	20
		yield, kWh/m	21	21	22	22		21
		ground area yield, kWh/m2a	34	67	14	27		20
		demand covered by the heat pump	97%	97%	97%	97%		97%
	40 W/m	power, W/m	39	32	39	38	39	38
		yield, kWh/m	42	35	43	42	42	42
		ground area yield, kWh/m2a	66	110	27	52	20	39
		demand covered by the heat pump	95%	80%	96%	93%	96%	95%
	60 W/m	power, W/m	51	36	55	48	56	52
		yield, kWh/m	56	39	62	53	62	57
		ground area yield, kWh/m2a	87	122	38	66	29	53
		demand covered by the heat pump	84%	59%	91%	79%	93%	85%

Table 7
Summary of the study results in table format, 20 W/m - 80 W/m, 50% thermal storage, clay. *the natural thermal storage from heat loss exceeds the storage ratio %.

			Clay					
			step 3 m		step 4.5 m		step 6 m	
			15 m	30 m	15 m	30 m	15 m	30 m
Thermal storage 50%	20 W/m	power, W/m	20	19	-	20	-	-
		yield, kWh/m a	21	21		22		
		ground area yield, kWh/m2a	34	67		27		
		required thermal storage, kWh/m a	3.3	5.2		0		
		demand covered by the heat pump	97%	96%		97%		
	40 W/m	power, W/m	37	32	38	34	38	35
		yield, kWh/m a	41	35	42	38	42	39
		ground area yield, kWh/m2a	64	110	26	48	19	36
		required thermal storage, kWh/m a	12	14	6	9	2	6
		demand covered by the heat pump	92%	79%	93%	85%	94%	88%
	60 W/m	power, W/m	49	41	51	44	52	46
		yield, kWh/m a	53	45	57	49	57	50
		ground area yield, kWh/m2a	83	141	35	61	26	47
		required thermal storage, kWh/m a	20	22	15	18	11	15
		demand covered by the heat pump	80%	68%	84%	72%	86%	75%
	80 W/m	power, W/m	58	69.8*	60	66.5*	62	65.3*
		yield, kWh/m a	64	76.2*	67	72.7*	68	71.4*
		ground area yield, kWh/m2a	100	239*	42	92.3*	32	66.7*
		required thermal storage, kWh/m a	30	64.6	23	59.8	19	57.3
		demand covered by the heat pump	72%	86%*	75%	82%*	77%	81%*

Table 8
Summary of the study results in table format, 20 W/m - 80 W/m, 50% thermal storage, silt.

			Silt					
			step 3 m		step 4.5 m		step 6 m	
			15 m	30 m	15 m	30 m	15 m	30 m
Thermal storage 50%	20 W/m	power, W/m	20	20	-	-	-	-
		yield, kWh/m a	21	21				
		ground area yield, kWh/m2a	34	67				
		required thermal storage, kWh/m a	3.3	4.9				
		demand covered by the heat pump	97%	97%				
	40 W/m	power, W/m	39	37	39	38	-	39
		yield, kWh/m a	43	41	43	43		42
		ground area yield, kWh/m2a	67	128	27	53		39
		required thermal storage, kWh/m a	12	13	4	8		5
		demand covered by the heat pump	96%	93%	96%	95%		95%
	60 W/m	power, W/m	56	49	56	53	57	54
		yield, kWh/m a	61	54	63	59	62	59
		ground area yield, kWh/m2a	95	169	39	73	29	55
		required thermal storage, kWh/m a	20	22	13	17	8	14
		demand covered by the heat pump	92%	81%	93%	87%	94%	89%
	80 W/m	power, W/m	68	59	70	64	72	67
		yield, kWh/m a	75	65	79	72	78	73
		ground area yield, kWh/m2a	117	204	49	89	37	68
		required thermal storage, kWh/m a	29	30	22	26	17	22
		demand covered by the heat pump	84%	73%	87%	80%	89%	83%

denser power sized to 50% of the building design heat load can cover up to 98.9% of the annual heating demand. The remaining 1.1% should be covered with top-up heating, therefore a heat pump with 50% less output power can be installed. The heat pump condenser is then sized accordingly as 180 kW and the evaporator as

$$\dot{Q}_{evap} = \frac{\dot{Q}_{cond}(COP - 1)}{COP} = 140\,kW, \tag{3}$$

with an annually averaged COP, see Section 2.2.

3. **Estimation of the total pile field length and condenser yield.** Assume 30 m-long piles, the simulated GHE performance corresponding to steps 1. and 2. above (without thermal storage) is plotted in Fig. 8. We can accordingly collect simulated performance data for three different initial evaporator sizing values: 20 W/m, 40 W/m and 60 W/m. The total energy piles length L is computed as in Section 2.2 and is only a function of system sizing and geometry.
The specific yield per unit length E/L [kWh/m] is then simulated, with a total expected condenser yield holding as $E = E/L \times L$ [kWh]. The results for an evaporator sizing of 20 W/m, 40 W/m and 60 W/m and 3 m, 4.5 m and 6 m pile spacing are given in Table 5.
Accordingly, if the building annual energy need is 168 MWh, for e.g. 60 W/m and 6 m pile spacing the maximal energy yield without thermal storage is 103 MWh. Since the demand (168 MWh) is larger than what is produced by the energy piles (103 MWh), one should either install more piles or consider thermal storage.
To calculate the piles number, we simply divide the annual need by the condenser yield to get L,

Table 9
Summary of the study results in table format, 100 W/m - 200 W/m, 100% thermal storage, clay.

			Clay					
			step 3 m		step 4.5 m		step 6 m	
			15 m	30 m	15 m	30 m	15 m	30 m
Thermal storage 100%	100 W/m	power, W/m	85	84	81	79	80	77
		yield, kWh/m a	93	92	89	86	87	84
		ground area yield, kWh/m2a	146	288	56	110	41	78
		required thermal storage, kWh/m a	81	82	74	77	70	74
		demand covered by the heat pump	84%	83%	80%	78%	79%	76%
	150 W/m	power, W/m	118	118	109	108	106	103
		yield, kWh/m a	129	129	119	118	116	113
		ground area yield, kWh/m2a	202	405	76	150	54	106
		required thermal storage, kWh/m a	124	124	116	120	112	116
		demand covered by the heat pump	77%	78%	72%	71%	70%	68%
	200 W/m	power, W/m	147	150	134	135	128	128
		yield, kWh/m a	160	164	146	148	140	140
		ground area yield, kWh/m2a	252	515	93	188	65	130
		required thermal storage, kWh/m a	165	167	160	162	155	160
		demand covered by the heat pump	73%	73%	66%	66%	63%	63%

Table 10
Summary of the study results in table format, 100 W/m–200 W/m, 100% thermal storage, silt.

			Silt					
			step 3 m		step 4.5 m		step 6 m	
			15 m	30 m	15 m	30 m	15 m	30 m
Thermal storage 100%	100 W/m	power, W/m	90	89	89	87	89	86
		yield, kWh/m a	99	98	97	95	97	95
		ground area yield, kWh/m2a	155	306	62	121	45	88
		required thermal storage, kWh/m a	80	81	72	77	67	73
		demand covered by the heat pump	89%	88%	88%	86%	88%	85%
	150 W/m	power, W/m	125	124	121	119	120	116
		yield, kWh/m a	137	136	133	130	132	127
		ground area yield, kWh/m2a	215	426	84	165	61	119
		required thermal storage, kWh/m a	122	124	115	119	110	116
		demand covered by the heat pump	83%	82%	80%	78%	79%	77%
	200 W/m	power, W/m	156	157	148	147	145	142
		yield, kWh/m a	170	172	162	161	159	156
		ground area yield, kWh/m2a	267	538	103	204	74	145
		required thermal storage, kWh/m a	165	167	156	162	153	158
		demand covered by the heat pump	77%	78%	73%	73%	72%	70%

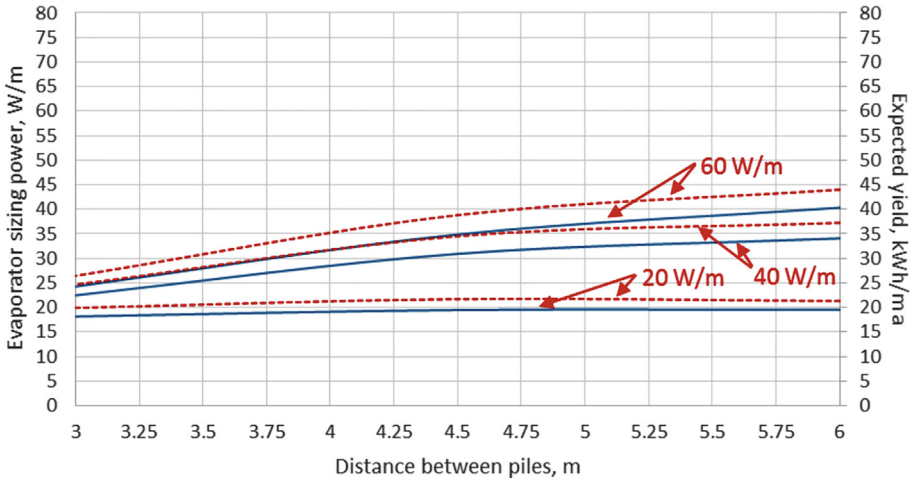

Fig. 8. Evaporator power (solid) and condenser yield (dashed) results for 30 m-long energy piles in clay without thermal storage.

$$L = 168000\,kWh : 44\,kWh/m \sim 3818\,m, \quad (4)$$

giving n = 3818 m/30 m = 127.3 ∼ 127 energy piles with 6 m spacing. The heat pump condenser power should be 180 kW and the evaporator power 140 W; thermal storage is not needed.

4. **Evaluating the thermal storage impact on the energy piles length.**
Instead of adding piles, we now wish to include thermal storage (TS), which should reduce the required total pile length.

The simulated performance of energy piles with different thermal storage ratios, in terms of yield per meter [kWh/m], can be determined by recalling either Figs. 9 or 10. By looking at the plots, one can indeed immediately quantify both the evaporator power [W/m] and expected yield [kWh/m] that are induced by a chosen initial evaporator design load and energy piles field design, for a given thermal storage amount.

For this specific example we consider 50% TS, therefore we examine Fig. 10 and obtain a maximal condenser yield of 50 kWh/m for 60 W/m evaporator power, with 6 m piles spacing.

This result should now be combined with the thermal storage amount for this specific situation, which can be retrieved from Fig. 11. We obtain 15 kWh/m of TS, meaning that energy piles with 6 m spacing can now produce 50 kWh/m at evaporator power 60 W/m.

Recollecting the above results, assuming 50% TS and 6 m pile spacing we obtain the total condenser yield

$$E_{6ts} = 2333\,m \times 50\,kWh/m \sim 117\,MWh, \tag{5}$$

with the required thermal storage amount holding as

$$ET_{6ts} = 2333\,m \times 15\,kWh/m \sim 35\,MWh. \tag{6}$$

Since the resulting condenser yield is 117 MWh < 168 MWh, we still need to increase either pile length or thermal storage.

Consider then 100% thermal storage. From Fig. 12 we find that for 100 W/m with 6 m pile spacing, we require 72 kWh/m TS, giving a condenser yield of ca 83 kWh/m.

Combining this with Fig. 9, we obtain the following energy piles length,

$$L_{6ts2} = \frac{168000\,kWh}{83\,kWh/m} \sim 2024\,m, \tag{7}$$

the according thermal storage amount

$$\dot{Q}E_{6ts2} = 2024\,m \times 72\,kWh/m \sim 146\,MWh, \tag{8}$$

and the maximal heat pump evaporator power

$$\dot{Q}_{condmax_{6}ts2} = 2024\,m \times 100\,W/m = 202.4\,kW. \tag{9}$$

We should also keep in mind that the maximal heat pump evaporator power (202 kW) should be equal to or higher than the initial (140 kW) value. Otherwise, the heat pump will not be sized to 50% and will not be able to cover most of the building heat demand, requiring a more frequent top-up heating correction.

In the case where more thermal storage energy is available, one can decrease the piles length. For 150 W/m at 6 m spacing, the

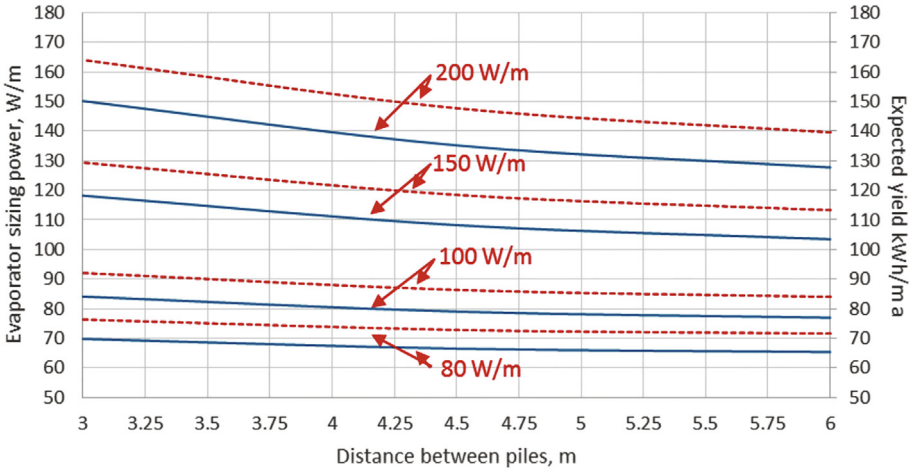

Fig. 9. Power (solid) and yield (dashed) of 30 m-long energy piles in clay, 100% thermal storage.

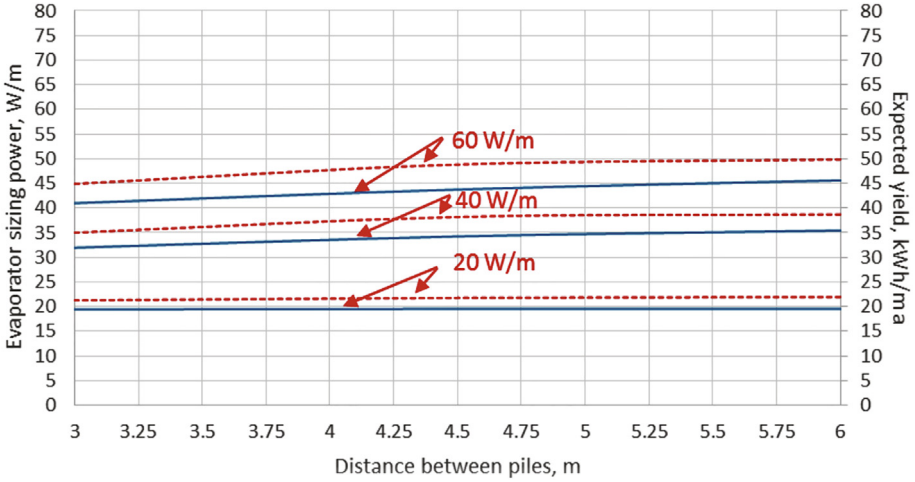

Fig. 10. Power (solid) and yield (dashed) of 30 m-long energy piles in clay, 50% thermal storage.

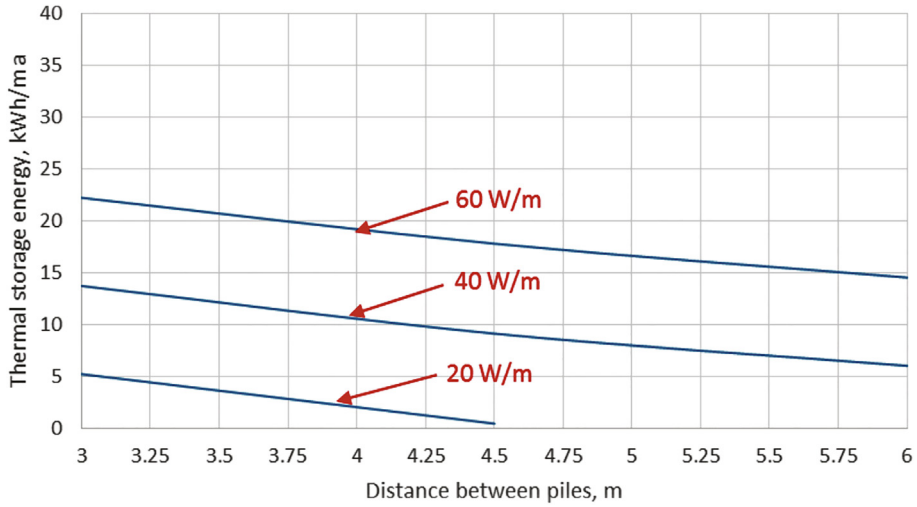

Fig. 11. Thermal storage required to achieve 50% for 30 m-long energy piles in clay.

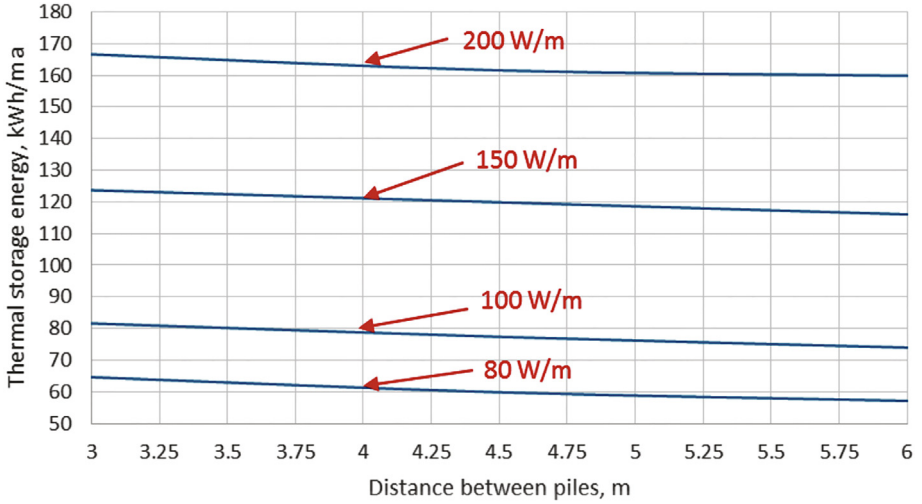

Fig. 12. Thermal storage required to achieve 100% for 30 m-long energy piles in clay.

required TS is about 116 kWh/m, thus the condenser yield would be 112 kWh/m. We accordingly compute the energy piles length that can produce 168 MWh as

$$L_{6ts3} = \frac{168000\,kWh}{112\,kWh/m} = 1500\,m, \tag{10}$$

the required thermal storage energy amount

$$\dot{Q}E_{6ts3} = 1500\,m \times 116\,kWh/m = 174\,MWh, \tag{11}$$

and the maximal heat pump evaporator power

$$\dot{Q}_{condmax_{6}ts3} = 1500\,m \times 150\,W/m = 225\,kW. \tag{12}$$

To recapitulate the above calculations, for our three distinct cases we determined the following energy pile system configurations (L is length, s is spacing):

- No thermal storage: L = 3813 m for s = 6 m, 127 piles;
- 146 MWh thermal storage: L = 2024 m for s = 6 m, 67 piles;
- 174 MWh thermal storage: L = 1500 m for s = 6 m, 50 piles.

5. **Sizing top-up heating**

This can be done very easily by using Table 4. The top-up sizing in clay, for L = 30 m and s = 6 m, amounts to:

- 84% × 360 kW = 302 kW for 60 W/m, no thermal storage;
- 85% × 360 kW = 306 kW for 100 W/m with thermal storage;
- 87% × 360 kW = 313 kW for 150 W/m with thermal storage.

4.1. Application to 16 random building configurations

Here we considered a total of 16 commercial hall-type buildings, using different soils and energy pile lengths, without thermal storage. The results are reported in Table 11. The initial sizing attempt described at point 3. of the guide in the previous section could fulfil both heat pump design load and required annual condenser yield (building heat demand) only in 10 cases out of 64.

Additionally, only 6 cases showed that the sizing almost reached the maximal possible condenser yield at the required evaporator size. In the remaining 48 cases, the energy piles length needed to be increased.

5. Discussion

Our results are listed in table form in Tables 6–11 and plotted in Figs. 13–18. These are valid for a period of 20 years and for a pile field buried in clay or silt, with or without thermal storage.

Table 11
Results of 16 random cases without thermal storage. * labels cases where the initial evaporator power sizing (namely, design load*0.5/60 W/m) produced enough condenser yield.

Case	Design heat load	Annual heat demand	clay 30 m	silt 30 m	clay 15 m	silt 15 m	clay 30 m	silt 30 m	clay 15 m	silt 15 m
nr	kW	kWh/a	required energy piles length, m				maximal evaporator power, %			
1	360	168	3817	2947	3054	2709	164%	126%	131%	116%
2	360	236	5364	4667*	4667*	4667*	115%	100%*	100%*	100%*
3	360	341	7747	5981	6198	5498	166%	128%	133%	118%
4	360	341	7747	5980	6198	5498	166%	128%	133%	118%
5	270	239	5430	4192	4344	3854	155%	120%	124%	110%
6	261	225	5103	3939	4082	3621	151%	116%	121%	107%
7	257	218	4946	3818	3957	3510	148%	115%	119%	105%
8	272	229	5196	4011	4157	3687	147%	114%	118%	105%
9	271	223	5074	3917	4059	3601	144%	111%	116%	103%
10	255	214	4858	3750	3886	3448	147%	113%	118%	104%
11	241	189	4296	3316	3437	3124*	138%	106%	110%	100%*
12	270	239	5430	4191	4344	3853	155%	120%	124%	110%
13	195	151	3439	2655	2751	2528*	136%	105%	109%	100%*
14	195	150	3399	2624	2720	2528*	134%	104%	108%	100%*
15	250	204	4632	3576	3706	3288	143%	110%	114%	101%
16	148	43	1919*	1919*	1919*	1919*	100%*	100%*	100%*	100%*

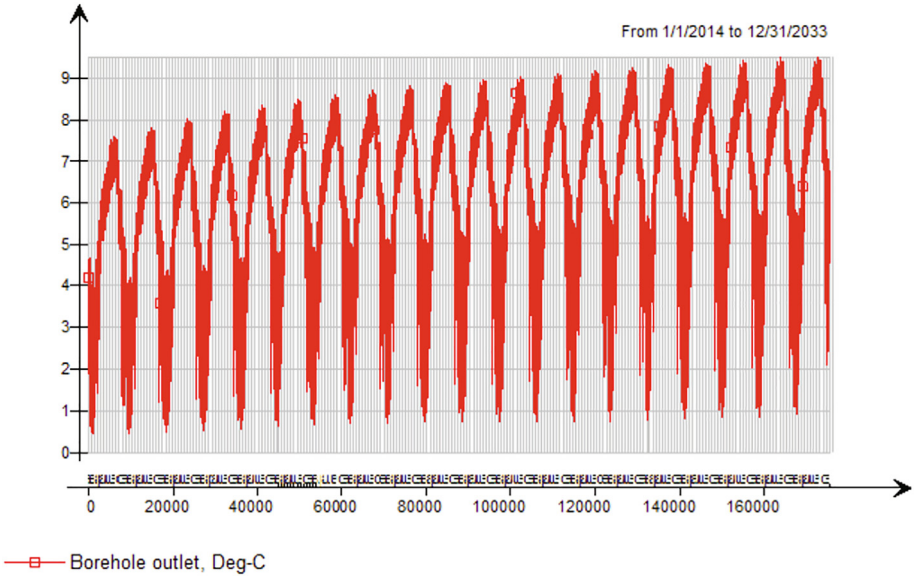

Fig. 13. Borehole outlet temperature for 40 W/m, spacing 3 m, length 30 m, storage 50%, silt.

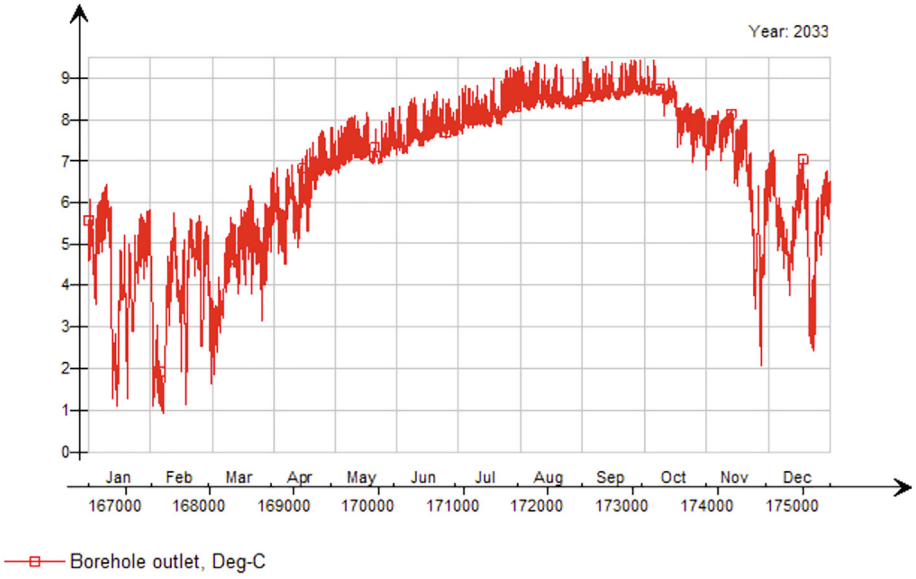

Fig. 14. Borehole outlet temperature for 40 W/m, spacing 3 m, length 30 m, storage 50%, silt, one year.

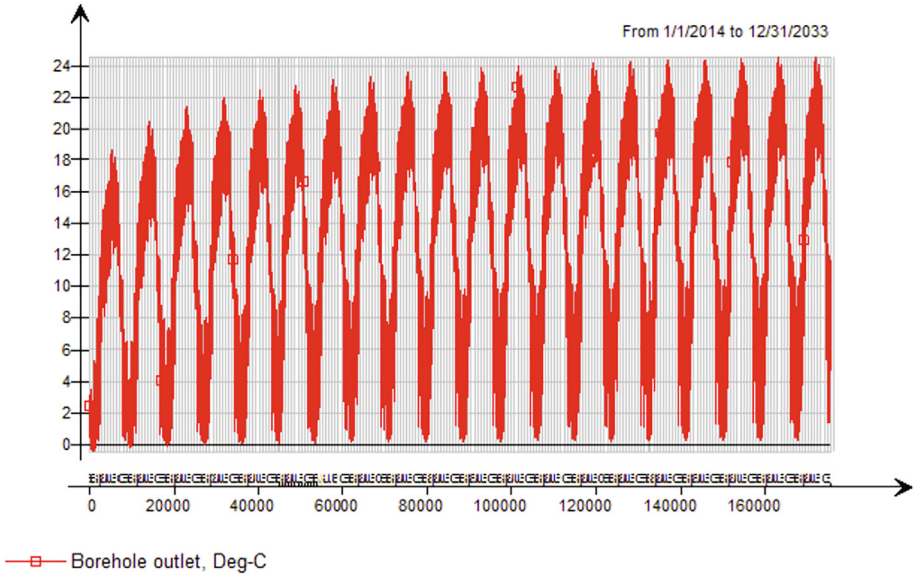

Fig. 15. Borehole outlet temperature for 80 W/m, spacing 3 m, length 30 m, storage 100%, clay.

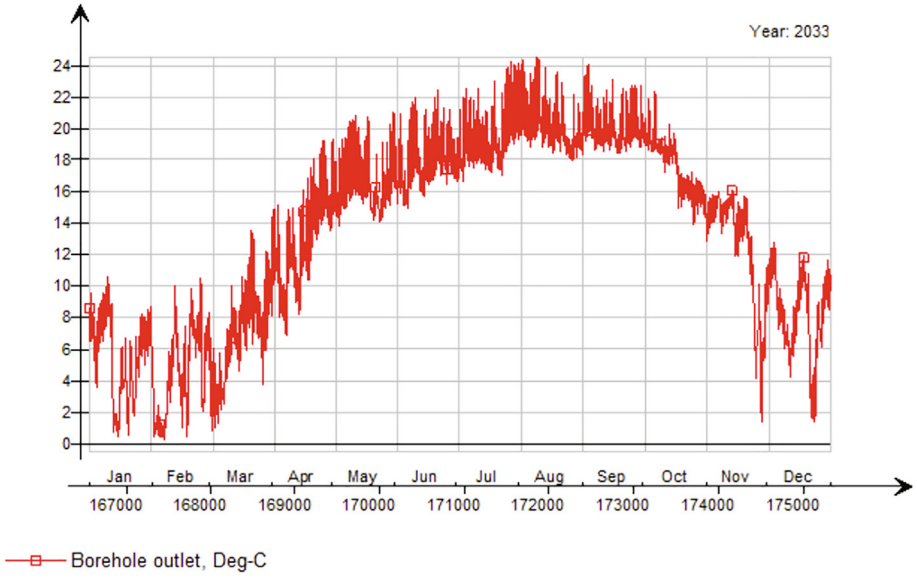

Fig. 16. Borehole outlet temperature for 80 W/m, spacing 3 m, length 30 m, storage 100%, clay, one year.

5.1. Cases with no thermal storage

As it was recently shown in [27], for most simulation hours the energy need for a largely sized heat pump evaporator (200 W/m) is much higher than the geothermal system performance. This finds confirmation in Fig. 8, since comparing the 60 W/m to the 20 W/m curves shows that the power and yield are only doubled and not three times larger.

Concerning the yield per ground surface area, a smaller spacing is instead strongly favoured [27]. A low 20 W/m evaporator power can indeed return more than three times the yield with 3 m vs 6 m spacing. Also, 30 m-long piles return a roughly double yield only for 20 W/m, and pile separation seems not to be critical for *low* initial evaporator heat extraction rates. Fig. 8 shows a hardly linear performance/spacing ratio for piles with same length, since for 20 W/m both evaporator sizing power and expected yield even stay constant although the spacing is doubled.

On the other hand, as it was shown very clearly in [27], a smaller spacing is strongly correlated with a high yield per ground surface area [kWh/m2a]. Compared to a 6 m spacing, a low 20 W/m evaporator power with 3 m spacing can indeed return more than three times the yield.

What matters the most for applications, however, is the demand covered by the heat pump, here calculated as Δ = 100%-(Q required − Q produced)%. The respective values of this quantity for different configurations are reported in Tables 6–10.

A close look at e.g. Table 6 shows that exactly the same demand (97%) is obtained for any pile length and separation. A higher evaporator power induces a moderate decrease in efficiency for 15 m piles, while for 30 m piles the loss is more pronounced. The configuration 60 W/m, 3 m spacing, 30 m length is especially underperforming, with only 59% demand covered by the heat pump.

A smaller extraction power is therefore more performing. Furthermore, shorter 15 m-long piles performed better, since proxim-

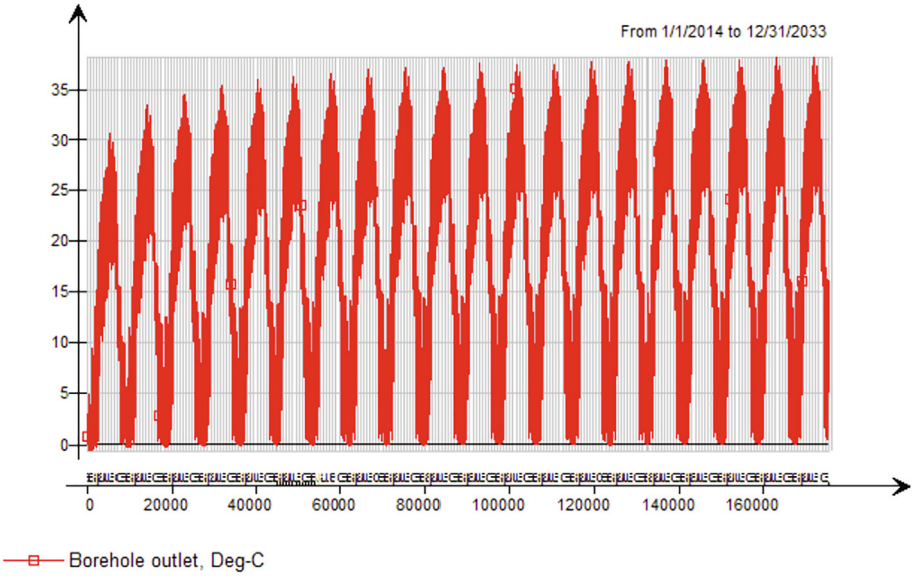

Fig. 17. Borehole outlet temperature for 200 W/m, spacing 3 m, length 30 m, storage 100%, silt.

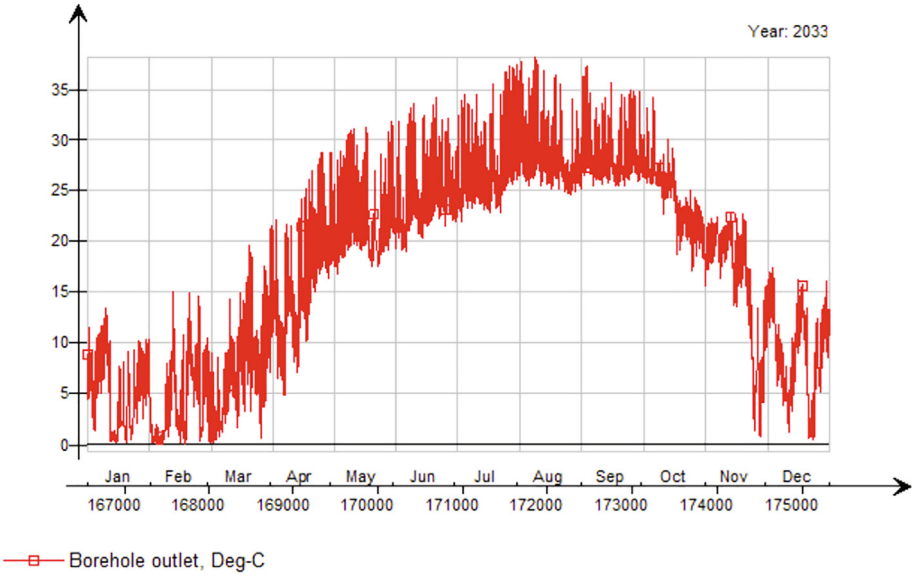

Fig. 18. Borehole outlet temperature for 200 W/m, spacing 3 m, length 30 m, storage 100%, silt, one year.

ity to the building floor boundary for a larger portion of its surface provides free thermal storage via floor heat losses. Additionally, with larger separation the piles are less disturbed and extract more heat without thermal storage (simulated evaporator yield between 20 and 55 kWh/m).

5.2. Impact of thermal storage

According to Table 8, the demand covered by the heat pump decreases roughly linearly with increasing evaporator power, for any pile length. As expected, thermal storage provides a large amount of energy that should not be ignored[3].

Comparing Tables 6 (no thermal storage) and 8 (50% TS), for 3 m spacing and 60 W/m evaporator power the heat pump covers 8% more with 15 m long piles and an impressive 22% more with 30 m piles. This is expected since longer piles dig more into the ground and exploit more thermal mass). This contrasts very clearly with the results obtained without TS.

Interestingly, the impact of pile spacing is here way less relevant than without storage, see Table 6. Yet, this is not surprising, since the thermal inertia of the geothermal system is now enhanced and heat transfer is more uniform.

Assuming 100% thermal storage (e.g. Table 10), the demand covered for higher evaporator powers decreases linearly: for s = 6 m and L = 30 m, 100 W/m cover 85% of demand, while 200 W/m cover only 70% (derivative: −0.15). For 50%TS, the decrease rate is twice as much (derivative: −0.3). Ignoring TS gives a steeper (parabolic) decrease, see Table 6.

The critical role of thermal storage is also very evident in Figs. 13–18, since doubling TS returns a nearly three times larger borehole outlet temperature, which is also very sensitive to the ini-

[3] This is different from the "free" floor energy discussed above since it is applied via solar collector, see Section 2.4.

tial pumping power, see e.g. Figs. 17,18. However, this is not the only determinant factor for the overall system efficiency, as discussed above and illustrated in Tables 6–9.

5.3. Importance of soil material

In general, clay seems to be less performing than silt, especially without thermal storage. This is confirmed in Table 11, where the optimal evaporator power % is reached with silt in most cases[4]

6. Conclusions

In this paper we have introduced a new tabulated method for the early stage design of geothermal installations in buildings, which relies on a parametric study of performance via computer simulations. Considering the specific case of a commercial hall-type building, we were able to determine the performance of the entire heat extraction system connected to the building.

Running simulations pertaining a period of 20 years, including stress tests with very cold periods, we found that the expected yield is not proportional to the evaporator extraction power [W/m], leaning instead in favour of small values (20 or 40 W/m). Moreover, we verified that thermal storage improves the performance dramatically and cannot be ignored. In the sizing example, including TS lead to installing only 50 piles instead of 127, with huge construction savings.

Additionally, we confirmed that for a proper sizing design, long term (20 years) numerical simulations with high detail (i.e. with time steps of max 1 h) are mandatory. This holds especially true when including thermal storage.

As a novel and general outcome, the results could be presented as explicit extraction powers [W/m] and yields [kWh/m] per pile length, for each initial extraction sizing power and energy pile field configuration selected by the user. This was immediately utilized in our estimation tool with a specific sizing guide example.

Although our *quantitative* results are derived from the present case study (commercial-type building in a cold climate), our procedure is fairly general and as such, it can be extended to sizing geothermal systems during the preliminary design stage for *any* building type.

Our study can and should be improved in many ways, such as by relaxing the assumption of an isolated energy piles model that is disjoint from the detailed plant. One could also investigate more into detail the role of soil stratification and other values for the piles length. Nevertheless, we believe to have provided some useful findings as well as a sizing guide that can be applied to a variety of preliminary design studies for the construction of sustainable buildings.

CRediT authorship contribution statement

Andrea Ferrantelli: Conceptualization, Methodology, Investigation, Writing - original draft, Writing - review & editing. **Jevgeni Fadejev:** Conceptualization, Methodology, Software, Investigation. **Jarek Kurnitski:** Conceptualization, Methodology, Writing - review & editing, Supervision, Funding acquisition.

Declaration of Competing Interest

The authors declare that they have no known competing financial interests or personal relationships that could have appeared to influence the work reported in this paper.

[4] More realistically, one should consider at least a mixed soil or some stratification, this however goes beyond the current study.

Acknowledgements

This research was supported by the Estonian Centre of Excellence in Zero Energy and Resource Efficient Smart Buildings and Districts, ZEBE (Grant No. 2014-2020.4.01.15-0016) funded by the European Regional Development Fund, by the programme Mobilitas Pluss (Grant No. – 2014–2020.4.01.16-0024, MOBTP88) and by the European Commission through the H2020 project Finest Twins (Grant No. 856602).

References

[1] European Parliament, Directive 2010/31/EU of the european parliament and of the council of 19 may 2010 on the energy performance of buildings, Off. J. Eur. Union 53 (2010) 13–35..
[2] T. Agemar, J. Weber, I. S. Moeck, Assessment and public reporting of geothermal resources in germany: review and outlook, Energies 11 (2). https://doi.org/10.3390/en11020332..
[3] K. S. Park, S. Kim, Utilising unused energy resources for sustainable heating and cooling system in buildings: a case study of geothermal energy and water sources in a university, Energies 11 (7).https://doi.org/10.3390/en11071836..
[4] J. Spitler, Editorial: ground-source heat pump system research—past, present, and future, HVAC& R Res. 11 (2) (2005) 165–167, https://doi.org/10.1080/10789669.2005.10391132.
[5] E. Guelpa, V. Verda, Thermal energy storage in district heating and cooling systems: a review, Appl. Energy 252 (2019), https://doi.org/10.1016/j.apenergy.2019.113474, 113474.
[6] J. Fadejev, R. Simson, J. Kurnitski, F. Haghighat, A review on energy piles design, sizing and modelling, Energy 122 (Suppl. C) (2017) 390–407.https://doi.org/10.1016/j.energy.2017.01.097..
[7] A.K. Sani, R.M. Singh, T. Amis, I. Cavarretta, A review on the performance of geothermal energy pile foundation, its design process and applications, Renew. Sustain. Energy Rev. 106 (2019) 54–78, https://doi.org/10.1016/j.rser.2019.02.008.
[8] L. Lamarche, S. Kajl, B. Beauchamp, A review of methods to evaluate borehole thermal resistances in geothermal heat-pump systems, Geothermics 39 (2) (2010) 187–200, https://doi.org/10.1016/j.geothermics.2010.03.003.
[9] J. Zhao, Y. Li, J. Wang, A review on heat transfer enhancement of borehole heat exchanger, Energy Procedia 104 (2016) 413–418, clean Energy for Clean City: CUE 2016–Applied Energy Symposium and Forum: Low-Carbon Cities and Urban Energy Systems.https://doi.org/10.1016/j.egypro.2016.12.070..
[10] Q. Zhao, B. Chen, M. Tian, F. Liu, Investigation on the thermal behavior of energy piles and borehole heat exchangers: a case study, Energy 162 (2018) 787–797, https://doi.org/10.1016/j.energy.2018.07.203.
[11] EQUA, IDA ICE – Indoor Climate and Energy, Tech. rep., EQUA, Stockholm, Sweden (2013)..
[12] J. Fadejev, J. Kurnitski, Geothermal energy piles and boreholes design with heat pump in a whole building simulation software, Energy Build. 106 (2015) 23–34, sI: IEA-ECES Annex 31 Special Issue on Thermal Energy Storage.https://doi.org/10.1016/j.enbuild.2015.06.014..
[13] M. Faizal, A. Bouazza, R.M. Singh, Heat transfer enhancement of geothermal energy piles, Renewable and Sustainable, Energy Rev. 57 (Suppl. C) (2016) 16–33, https://doi.org/10.1016/j.rser.2015.12.065.
[14] A. Carotenuto, P. Marotta, N. Massarotti, A. Mauro, G. Normino, Energy piles for ground source heat pump applications: Comparison of heat transfer performance for different design and operating parameters, Appl. Therm. Eng. 124 (2017) 1492–1504, https://doi.org/10.1016/j.applthermaleng.2017.06.038.
[15] A. Ferrantelli, J. Fadejev, J. Kurnitski, Energy pile field simulation in large buildings: validation of surface boundary assumptions, Energies 12 (5) (2019) 770, https://doi.org/10.3390/en12050770.
[16] P. Eskilson, Thermal analysis of heat extraction boreholes (1987)..
[17] H. Yang, P. Cui, Z. Fang, Vertical-borehole ground-coupled heat pumps: a review of models and systems, Appl. Energy 87 (1) (2010) 16–27, https://doi.org/10.1016/j.apenergy.2009.04.038.
[18] J. Claesson, S. Javed, An analytical method to calculate borehole fluid temperatures for time-scales from minutes to decades, ASHRAE Trans. 117 (2011) 279–288.
[19] M. Cimmino, M. Bernier, A semi-analytical method to generate g-functions for geothermal bore fields, Int. J. Heat Mass Transf. 70 (2014) 641–650, https://doi.org/10.1016/j.ijheatmasstransfer.2013.11.037.
[20] L. Lamarche, g-function generation using a piecewise-linear profile applied to ground heat exchangers, Int. J. Heat Mass Transf. 115 (2017) 354–360, https://doi.org/10.1016/j.ijheatmasstransfer.2017.08.051.
[21] F. Dupray, L. Laloui, A. Kazangba, Numerical analysis of seasonal heat storage in an energy pile foundation, Comput. Geotech. 55 (2014) 67–77, https://doi.org/10.1016/j.compgeo.2013.08.004.
[22] F. Cecinato, F.A. Loveridge, Influences on the thermal efficiency of energy piles, Energy 82 (2015) 1021–1033, https://doi.org/10.1016/j.energy.2015.02.001.
[23] R. Caulk, E. Ghazanfari, J.S. McCartney, Parameterization of a calibrated geothermal energy pile model, Geomechanics for Energy and the Environment 5 (2016) 1–15, https://doi.org/10.1016/j.gete.2015.11.001.

[24] J. Fadejev, R. Simson, J. Kurnitski, J. Kesti, T. Mononen, P. Lautso, Geothermal heat pump plant performance in a nearly zero-energy building, Energy Procedia 96 (2016) 489–502, sustainable Built Environment Tallinn and Helsinki Conference SBE16. doi:https://doi.org/10.1016/j.egypro.2016.09.087..
[25] M. Adinolfi, R.M.S. Maiorano, A. Mauro, N. Massarotti, S. Aversa, On the influence of thermal cycles on the yearly performance of an energy pile, Geomech. Energy Environ. 16 (2018) 32–44, https://doi.org/10.1016/j.gete.2018.03.004.
[26] Y. Cui, J. Zhu, Year-round performance assessment of a ground source heat pump with multiple energy piles, Energy Build. 158 (2018) 509–524, https://doi.org/10.1016/j.enbuild.2017.10.033.
[27] F. Loveridge, W. Powrie, 2d thermal resistance of pile heat exchangers, Geothermics 50 (2014) 122–135, https://doi.org/10.1016/j.geothermics.2013.09.015.
[28] Loveridge, Powrie, 2d thermal resistance of pile heat exchangers, Geothermics (2014).

Business, Economy
Art, Design, Architecture
Science, Technology
Crossover
Doctoral Theses

Aalto DT 228/2025

ISBN 978-952-64-2829-1
ISBN 978-952-64-2828-4 (pdf)

Aalto University
School of Engineering
Department of Civil Engineering
aalto.fi